

ORIENTATION, STRUCTURE AND DYNAMICS OF
MAIN CHAIN IN LIQUID CRISTALLINE SIDE-CHAIN
POLYSILOXANES STUDIED BY ^{29}Si NMR



Dissertation

zur Erlangung des akademischen Grades Doktor rerum naturalium
(Dr. rer. nat.)
vorgelegt der

Mathematisch-Naturwissenschaftlich-Technischen Fakultät
der Martin-Luther-Universität Halle-Wittenberg

von Herrn Maxim Terekhov
geb. am: 28. 10. 1973 in Khabarovsk, Rußland

Die Gutachtern:

Prof. Dr. H. Schneider,
Martin-Luther-Universität Halle-Wittenberg, FB Physik.

Frau Prof. Dr. C. Schmidt
Universität Paderborn Department Chemie Physikalische Chemie

Prof. Dr. D. Geschke
Universität Leipzig Fakultät für Physik und Geowissenschaften Institut für Experimentelle
Physik I

Halle (Saale), den 05. 05.2003

verteidigt am 19.11.2003

urn:nbn:de:gbv:3-000006014

[<http://nbn-resolving.de/urn/resolver.pl?urn=nbn%3Ade%3Agbv%3A3-000006014>]

Content

Introduction.

Chapter I. Polymeric Liquid Crystals.....	1
1.1. Polymeric Liquid crystals: general overview.....	1
1.1.1 Liquid crystals, an overview.....	1
1.1.2 Order parameter.....	1
1.1.3 Polymeric Liquid Crystals.....	2
1.2 Liquid-Crystalline Side-chain Polymers. (LCSP).....	3
1.3.Phase transitions and orientational order in LCSP.....	4
1.3.1 Backbone.....	4
1.3.2 Spacer.....	6
1.3.3 Mesogenic unit.....	6
1.3.4 Mutual orientation of the backbone and the mesogenic units.....	7
1.4 Conformation and the orientational order of the main chain in liquid-crystalline side-chain polymers.	
Backbone conformation and anisotropy.....	8
1.4.1. Evaluation of the backbone anisotropy parameters using SANS.....	9
1.4.2. Bilayer model.....	10
1.5. Problem of mutual orientation of the side and main chain in side-chain	
liquid crystalline polysiloxanes.....	12
1.5.1 Chemical constitution of the polysiloxanes. Samples synthesizing.....	13
1.5.2 Physical properties and phase transitions.....	13
1.5.3 Liquid crystalline orientational properties of the polysiloxane samples.....	13
1.5.4. Relation between SANS and NMR results of the backbone conformation investigations in	
polysiloxanes.....	15
Chapter II. Molecular segments orientation study using ²⁹Si NMR methods.....	17
2.1 NMR Spectroscopy, Anisotropic Nuclear Spin Interaction.....	17
2.1.1 Anisotropic chemical shift interaction tensor.....	18
2.2 Orientation Distribution Function.....	21
2.2.1 ODF theoretical background.....	23
2.2.2 Methods of ODF examination by NMR lineshape analysis.....	34
2.2.3 Model Free approaches to ODF estimation using the NMR.....	24
2.2.4 Relationship between NMR-concerned sample coordinate frames.....	27
2.3 Main-chain molecular segments orientation study using ²⁹ Si NMR spectra.....	28
2.3.1 Method of the spectral lineshape analysis based on CS tensor orientation.....	28
2.3.2 ODF ambiguity due to transversal anisotropy, CS -tensor symmetry.....	32
2.3.3 Using direct dipolar interaction of ²⁹ Si pairs for main-chain	
segment orientation study.....	34
Chapter III Callaghan echo combination: theory and application for direct dipolar interaction of rare spin	
pairs detection.....	36
3.1 Callaghan echoes combination: theoretical consideration using density matrix formalism.....	36
3.1.1. Density matrix and spin operators.....	37
3.1.2 Hamiltonians.....	38

3.1.3. Rotation and evolution.....	38
3.1.4. Initial condition.....	38
3.2 General properties of “ β -echo” and “ β -function”.....	41
3.3 The role of spin-spin relaxation.....	42
3.4 Spatial orientation distributions and β -function.....	42
3.4.1 Powder averaging.....	43
3.4.2 Non-isotropic orientation distribution.....	44
3.5 Angular dependence of β -function for non-isotropic ODF.....	45
3.6. ODF parameters evaluation for Legendre series approach using β -function	
angular dependence.....	52
3.7. Determination of the dipolar coupling constant using “ β -spectrum” analysis.....	57
3.7.1. β -echo spectrum for the spin-1/2 pair system.	
Combined influence of the anisotropic chemical shift and dipolar interactions.....	57
3.7.2 β -spectrum lineshape evolution.....	60
Chapter IV. Experimental. Determination of the orientation distribution parameters	
for the polysiloxane PLC samples using β-echo.....	65
4.1 Basic pulse sequences.....	65
4.2 Testing β -echo pulse sequence.....	67
4.3 Pulse length calibration.....	69
4.4 Molecular mobility influence on β -echo.	70
4.4.1 Dipolar interactions averaging and CS inhomogeneity.....	70
4.4.2 Transversal relaxation.....	71
4.5 Dipolar constant determination using « β -spectrum» analysis.	76
4.6 Using FFT filters for the noise factor minimization.....	79
4.7 Determination of the ODF for the M4 sample using the β -function technique.	80
4.7.1 Data normalization procedure.	82
4.8 ODF's moment's determination for the monodomain sample of polysiloxane M6.....	86
4.8.1 Preferable main-chain segments alignment direction determination.	86
4.8.2 Orientation distribution parameters determination.....	87
Chapter V. Results and Discussion.....	91
5.1. Legendre expansion method of the ODF analysis.	91
5.2 Using β -echo properties.....	91
5.3 Simulation of the β -function orientation dependence.....	93
5.4 Dipolar coupling constant evaluation for the ^{29}Si pair in polysiloxanes using β -echo.....	96
5.5 Orientation distribution investigation with β -function Polysiloxane M4 and M6 sample.....	98
5.6 Relaxation measurements.....	101
5.6.1 Additional factors. Intrinsic linewidth relaxation limit.	105

Conclusion.

References

Appendixes I,II,III

Introduction

The end of seventies of the last century brought to the world a new branch of polymer sciences, - the chemistry and physics of polymeric liquid crystals (PLC) [Int.1-7]. The paradox of the situation was, that this field becomes of interest for the polymer researchers nearly after 50 years of progress in the liquid crystalline state theory and practical applications, in the time when the millions of people already used the devices based on the low molecular LC in everyday life. However, the burst of interest in the liquid crystallinity of polymers led to the very fast practical progress in the creation of new materials with extremely valuable properties. The most impressive results were achieved, at first, in development and synthesizing of so-called “armed” fibers (“Nylon”, “Terlon”, “Kevlar”, etc), which immediately become vitally important in aerospace technology [Int.6-10]. The unique properties of the PLC materials are mainly connected with the specific orientational order of the molecules in mesomorphic (i.e. liquid crystalline) state, which combines the structural features of amorphous and crystal phase. That way, the problems of the orientational structure are of great interest when studying the LC polymers. The understanding of the orientational mechanism allows one inquiring the relationship between the structure and properties of the PLC-based materials.

One of the most interesting and promising types of PLC is so-called liquid crystalline side-chain polymers (LCSP). Those are PLC, which contains the mesogenic units in side chains. The attractive properties of this class of compounds are provided by the combination of the low-molecular LC anisotropic properties, originating from the mesogenic units (side-chains), and the potential of persistent macromolecules (main-chain) in creating films and fibers. The phase behaviour of these substances is mainly governed by the mesogenic units, but influenced also by the backbone. Other characteristics, for instance, glass transition, viscous and elastic properties, however, are determined essentially by the main chain. At molecular level, opposite tendencies are expected: While the mesogenic side chains generate some orientational order, the main chains try to maximize the entropy by forming random disoriented coils. The real molecular structure and dynamics are the result of a compromise, which includes a certain orientation of the main-chain segments and, on the other hand, a strong slowing-down of the reorientation process of the mesogenic director in external fields. Thus, investigations of the structure-property relations require the information about the main-chain properties of the LCSP. The particular purpose of the presented work is obtaining the knowledge about the role of main-chain orientation and dynamics. As an object of the investigation, the side-chain polysiloxanes were chosen.

State of preceding work.

Most investigations of the main-chain conformation were done using the small angle neutron scattering (SANS) [Int.11]. The sensitivity length scale of this method lays on the level of the whole molecule shape (either prolate or oblate). However, the orientational order of the main-chain segments of large macromolecules has the sub-molecular character. That is the reason why *Nuclear Magnetic Resonance (NMR)* - the experimental technique which is sensitive to the microstructure and orientational properties on the level of individual atoms or atomic groups may extend our understanding of the main chain structure.

The first investigations of the LC polymers main chain structure in side-chain polymethacrylates using the NMR were done with the selectively deuterated samples [Int.12]. Later the ^{29}Si NMR measurements were performed using the chemical shift anisotropy to probe the orientation [Int.13]. The short review of these and other works on the subject can be found in Chapter I. In the NMR group of *Martin-Luther University of Halle/Wittenberg* the first investigations on the orientation behaviour of side-chain polymers was started in 1994. The series of mesogenic polysiloxane samples were investigated [Int.14]. The information about the ^{29}Si chemical shift tensor axis orientation was obtained (see Chapter I). With this knowledge it becomes possible to calculate the orientation degrees of main chain segments [Int.15]. For the comprehensive interpretation of the results, some proposals about the transversal isotropy/anisotropy of the molecular segments are required [Int.16]. These suggestions cannot be done, however, basing on the only intrinsically one-dimensional information provided by *axially symmetrical chemical shift* spin interaction. Due to this reason, the supplementary information about the main-chain segment orientation needs to be obtained by using an alternative type of orientationally dependent (*anisotropic*) NMR interaction. Most natural solution is to use the angular dependence of the *direct dipolar interaction* to probe the orientation distribution of the vectors, which connect two Si atoms in the LCSP main chain. This vector exactly coincides with the main-chain alignment direction.

However, in the case of the ^{29}Si NMR in polysiloxanes the sufficient difficulties can be foreseen concerned with the relatively low natural abundance of observable spins (4.7%).

This makes the employment of dipolar interaction for the orientation distribution studies quite problematic for two reasons:

- The low natural abundance of ^{29}Si nuclei gives considerably low signal sensitivity ($\approx 0.784\%$ of ^1H spins relative sensitivity), without any possibility to use the enriched samples.

- The low probability, that two neighbored Si both are ^{29}Si , leads to overwhelming part of the NMR signal arising from isolated ^{29}Si and overlapping the weak spin-pair signal of interest.

On the other hand, a low abundance of ^{29}Si ensures us that among the spin pairs nearly no higher-member spin clusters affect the signal. This fact strongly justifies the using of the isolated spin-pair approximation.

To overcome these problems one needs to develop and implement the special ^{29}Si NMR techniques and data processing/interpretation methods. Particularly, the following targets are to be achieved in this work:

1. The features of the polymeric and liquid crystalline structure should be overviewed to get better understanding of their mutual influence as well as the role of both of them on the orientational properties of the LCSP (particularly polysiloxanes). The basic results obtained in the previous investigations of liquid crystalline polysiloxanes with different methods have to be considered [Int.1-7]. The special attention should be paid on methods of orientation distribution function analysis using NMR [Int.14-16].
2. The specific NMR technique called β -echo (proposed in the first time by Callaghan at al.[Int.17]) is to be used for the selective detection of the NMR signal from coupled ^{29}Si spin pairs, with simultaneous suppression of the signal from isolated spins. The design of pulse sequence should be modified to be adapted for using together with cross-polarization NMR technique to increase the signal sensitivity (which is intrinsically low for the ^{29}Si at natural abundance).
3. The relation between the β -echo time evolution behaviour (called β -function) and dipolar interaction strength should be found, using the isolated spin-pair approximation. The consideration needs to be done using the density matrix formalism [Int.18]. Further, the anisotropic character of dipolar interaction should give us the information of how the β -function is influenced by the orientation of Si-Si internuclear vector with respect to NMR laboratory frame. The special attention should be paid on the role of dipolar coupling constant value.
4. On the next stage, the orientation distribution of the silicon-to-silicon (Si-Si) vectors has to be taken into account. The influence of the orientation distribution function (ODF) of «dipolar» Si-Si vectors on β -function behaviour has to be checked using **(i)** Model ODF's (Gaussian-like) and **(ii)** model-free ODFs represented by the Legendre series. The sensitivity of the β -function to the ODF parameters needs to be tested by using the numerical simulations.
5. The sensitivity of the β -function method for the determination of the parameters of orientation distribution supposes to be increased by using the angular dependence. The

changing of the β -function curve when the whole sample is rotating with respect to NMR laboratory frame is to be tested first by simulation. The procedures of the information extraction from several β -function curves have to be developed. The multiparametrical fitting has to be avoided if possible. The linear regression methods are preferable in the case when more than one parameter needs to be found from fitting. The accuracy of dipolar coupling constant determination supposed to be sufficiently increased by analysis of the Fourier transformed β -echo signals (« β -spectrums»).

6. The practical implementation of β -echo sequence has to be done. The critical experimental parameters need to be found as well as a procedure of their optimization. The largest care has to be taken about the calibration of the pulses duration. Because of the compensation character of β -echo technique the errors and imperfection of the pulses suppose to be critical for the whole method accuracy.
7. The role of transversal NMR relaxation has to be investigated in two aspects: (i) influence of T_2 on the β -echo properties and its ability to serve for the orientation distribution estimation and (ii) the interest about the transversal relaxation time T_2 as a sensitive tool for the molecular dynamic investigation [Int.19-23]. The role of temperature as the basic factor which makes influence on the molecular mobility can be investigated. Therefore, the measurements of temperature dependence of the transversal relaxation time need to be done.
8. The experiments using β -function have to be done for two different polysiloxane samples with different mutual orientation of side-chain and main-chain. The polydomain (disoriented) samples supposed to be used in testing experiments as well as in the experiments for dipolar coupling constant determination. Then, the monodomain (oriented) samples should be measured with β -echo technique. The experiments at different orientations of the sample suppose to require the special sensitivity calibration procedures.
9. The obtained experimental results of β -echo measurements have to be processed to extract the information about ODF Legendre moments. The data preprocessing procedures (filtering, smoothing, etc.) suppose to be employed to reduce the noise factor influence. Finally, the orientation distribution function is to be reconstructed using its estimated moments.
10. The temperature dependence of the ^{29}Si transversal relaxation should to be considered and analyzed using the Anderson and Weiss approach to make a suggestion about the mechanisms of the transversal relaxation and to analyze the dynamic properties of the main-chain of polysiloxane samples in glassy and liquid crystalline state [Int.23-24].

Chapter 1. Polymeric Liquid crystals.

1.1. Polymeric Liquid crystals: general overview.

1.1.1 Liquid crystal (LC) a thermodynamic stable phase characterized by anisotropy of properties without the existence of a three-dimensional crystal lattice. Generally, LC is placed in the temperature range between the solid and isotropic liquid phase. Therefore, the term *mesophase* is often used as a synonym of liquid crystalline phase [I.1].

The basic characteristic of mesophase is the tendency of the molecules (*mesogens*) to orient themselves along a common axis, called the *director* (see Fig 1.1). The LC phase creation is more prominent for the substances where the molecules have a strong asymmetry either prolate or oblate. In this case the anisotropy of the properties can originate from the spatial restriction as a consequence of the impossibility to arrange the anisotropic molecules in isotropic manner to fulfill the requirements of the free energy minimization [I.2]. Most of the liquid crystals demonstrate a *polymorphism*, i.e. condition where several "subphases" are observed in the liquid crystalline state. These subphases are formed by changing of the orientational order degree in the sample either by imposing order in one or two dimensions, or by allowing the

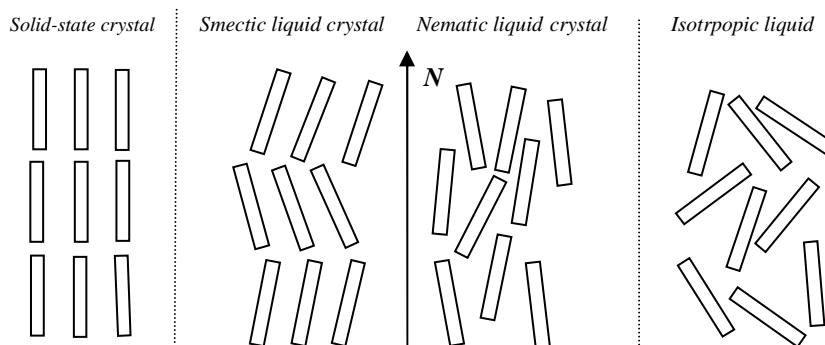


Fig. 1.1 Liquid crystalline state of the substance: no long range order presents (opposite to the solid-state). The molecules axes have preferable orientation given by the local director N (opposite to the random orientation in isotropic liquid). In some subphases the LC exhibits an ordering of the molecules gravity centers (smectic LC).

molecules to have a degree of translational motion. More detailed information about different mesophases and phase transitions can be found in Appendix I (A.I).

1.1.2 Order parameter

To describe the measure of the *orientation order* of the liquid crystal, in general case, the molecular anisotropy tensor, or **order tensor** is to be used. [A.I]. However, in the case of threefold or higher symmetry of the molecules shape, a single number is usually enough for the quantification of the *orientation degree*, which is called order parameter. It is traditionally defined as:

$$S = \left\langle \frac{3}{2} \cos^2 \theta - \frac{1}{2} \right\rangle = \langle P_2(\theta) \rangle_t \quad (1.1)$$

where θ is the angle between long molecular axis and local director, (see **Fig 1.2**) P_2 is the second order Legendre polynomial and brackets means the averaging in time, which occurs because of the thermal motion [AI, I.3]. In some cases, however, the ensemble averaging over all the molecules of the sample can be suggested when speaking about the order parameter or orientation degree. For most of mesophases both definitions, in principle, are equivalent.

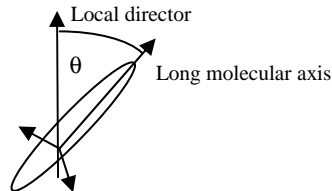


Fig 1.2. LC order parameter S describes the orientational order of liquid crystalline material, allowing for the individual orientational deviation of the molecules axes (denoted as angle θ) from the local director N , averaged either in time or over the collection.

1.1.3. Polymeric Liquid Crystal

Polymer liquid crystals (PLC) are a kind of macromolecular compounds, which combine the properties of polymers with those of liquid crystals. These systems show the anisotropic characteristic of the liquid crystals, and, in the same time, demonstrate a many of useful and versatile properties of polymers. The properties of the PLC mesophases can differ sufficiently from their analogs of the «classical» low molecular LC. In contrast to **Low Molecular Liquid Crystals (LMLC)** a number of PLC have no similarity to the classical liquids even in low ordered subphases and look like a solid glassy samples with melting temperature more than 100°C . However, traditionally, the same terms are used to denote the similar states of the molecular ordering in both LMLC and PLC. In order to polymer molecules demonstrate the ordering properties, the anisotropically shaped rod-like or disk-like elements (called *mesogenic unit*) must present inside. In the same time, for creating the liquid crystalline state of the sample

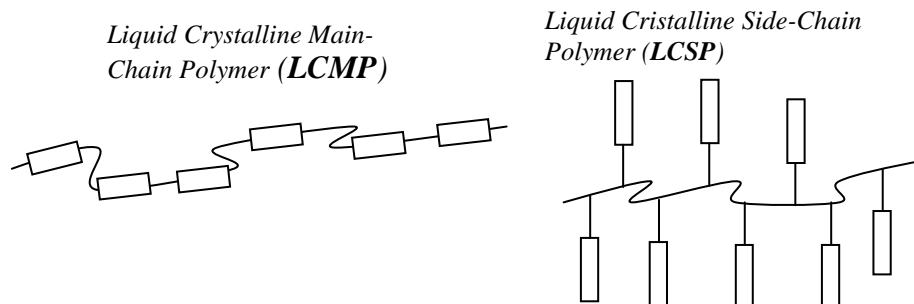


Fig 1.3 Schematic representation of the polymeric liquid crystals with mesogenic units in main (left) and side-chain (right).

these units must be decoupled from each other by the flexible segment of certain length called **spacer**. Additional factors providing the mesomorphic behavior of polymers include the certain polymerization degree, and regular alternation of rigid and flexible units along the main chain.

Depending on the location of the mesogenic moieties the PLC can be separated into *main-chain* and *side-chain*. The first ones have the mesogenic unit as a part of the main-chain of the polymer molecule and for the second the mesophase is formed by the anisotropic molecular segments of the side-chain (see **Fig 1.3**). The origins of the main-chain PLC theory and synthesizing can be found in the classical works of de Gennes [I.4] and Roviello at al.[I.5]. Because the subject of this work concerns the problems of orientation order of the side-chain polymer liquid crystals they will be considered in more details below.

1.2 Liquid-Crystalline Side-chain polymers. (LCSP)

The attempts of synthesizing of the LC polymers with the mesogenic units in side-chain were stimulated by the fast progress of low molecular LC investigations. It seemed to be very attractive to create the polymer systems, which combine in one material the unique properties of the low molecular LC and macromolecular compounds with their ability to create films, tissues and covers. However, the first try to solve this problem by the creation of the polymers with side-chain units directly connected to the main-chain was not quit successful [I.7, I.8]. Finally, it was found that the most convenient matrices for the synthesizing of the PLC with mesogenic

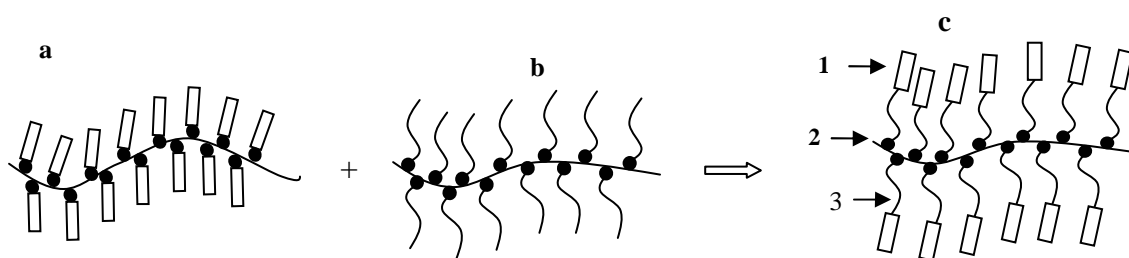


Fig 1.4. Schematic view of the polymer macromolecules with the direct connection of the side-chain to the main chain(a), (b)- comb-like macromolecule with flexible side-chain units, (c)- liquid crystalline side-chain polymer with mesogenic units (1) connected to the backbone (2) via flexible spacer(3).

moieties in side-chain are so called *comb-like polymers*. The main feature of the structure of such a kind of macromolecules is the relatively long (usually aliphatic) side units connected directly to the *backbone* chain (see **Fig 1.4a**). The general approach to creating of the macromolecular systems based on this kind of polymers shown on **Fig 1.4b,c**. Being developed by the different groups [I.8-I.10] it provides the possibility to synthesize the thermotropic LC polymers with the mesogenic units in side-chain.

The most important point of the method is the decoupling of the backbone and mesogenic unit in the side-chain from each other by the flexible *spacer* of methylene chain. This provides the necessary isolation of the backbone and mesogenic groups making possible their cooperation in the creation of the mesophase. The example of the spacer length importance for the mesogenic properties of the side-chain PLC will be discussed later on the particular examples. There are several possibilities of how the side-chain unit can be connected to the spacer. **Fig 1.5** demonstrates the basic type of the rod-like mesogenic fragments, particularly are «end-on», «side-on» and «twin».

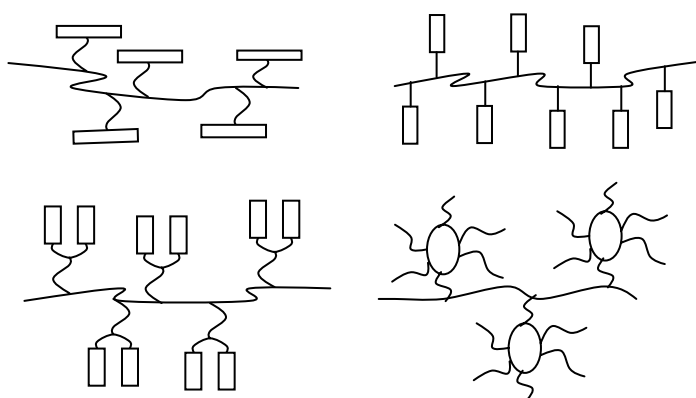


Fig 1.5 Possible structures of the mesogenic unit connections to the backbone in LCSP: (a) –«side-on», (b)–«end-on», (c) «twin-like» (d)-diskotic.

1.3. Phase transitions and orientational order in LCSP. The role of the macromolecular properties.

Independently on the particular structure of the LCSP, their macromolecules generally have the similar design, which includes the rigid side-chain units connected in some way to the main-chain backbone. It is assumed that the side-chain units define the mesogenic properties when the backbone is responsible for the polymeric qualities of the compound. If to take into account the interconnecting flexible spacers both in side- and main chain it is clear that the nature of this kind of objects is quite complicated. The influence of each component on the mesophase state of side-chain PLC will be considered shortly in following.

1.3.1 Backbone

Despite of the fact that mesogenic properties of the LCSP originate from the side-chain mesogenic unit, the polymer «skeleton» of main chain defines the important features of

mesophase forming. Especially important factor is the degree of the polymerization (DP) i.e. the average number of the monomer blocks in the main chain. For instance, it was established in a number of experiments for the *side-chain polysiloxanes* that the temperatures of the subphases transitions are strongly affected by the DP in the regime of oligomers (i.e DP<10) independently on the spacer length. In the same time for 10<DP<100 the transitions temperature changes much

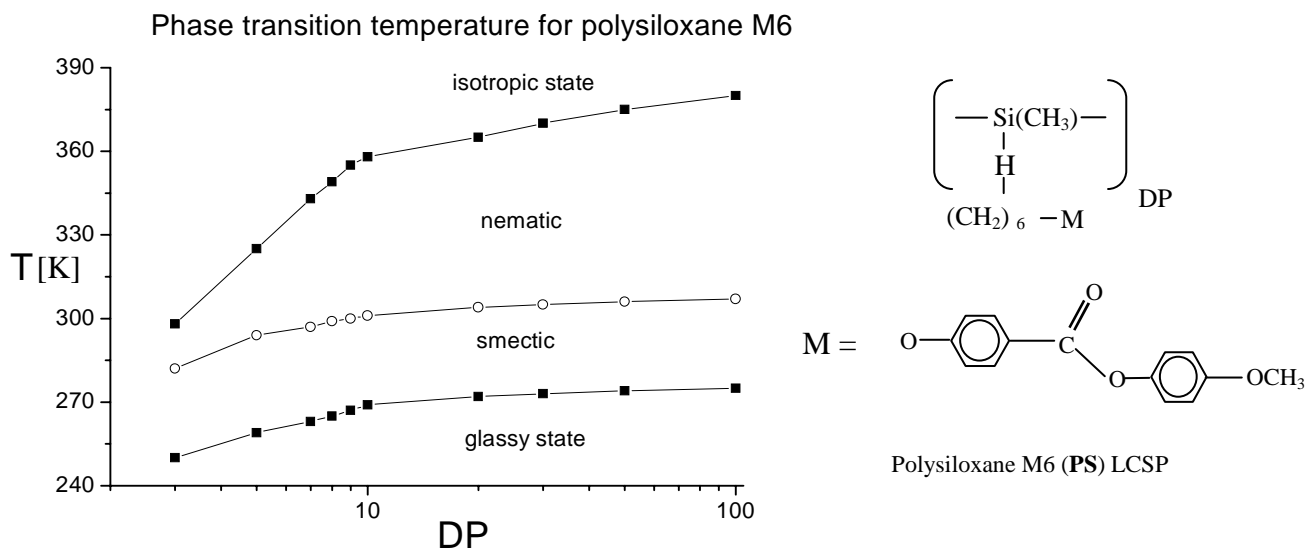


Fig 1.6. Phase transition temperature of the polysiloxanes samples as a function of the polymerization degree.

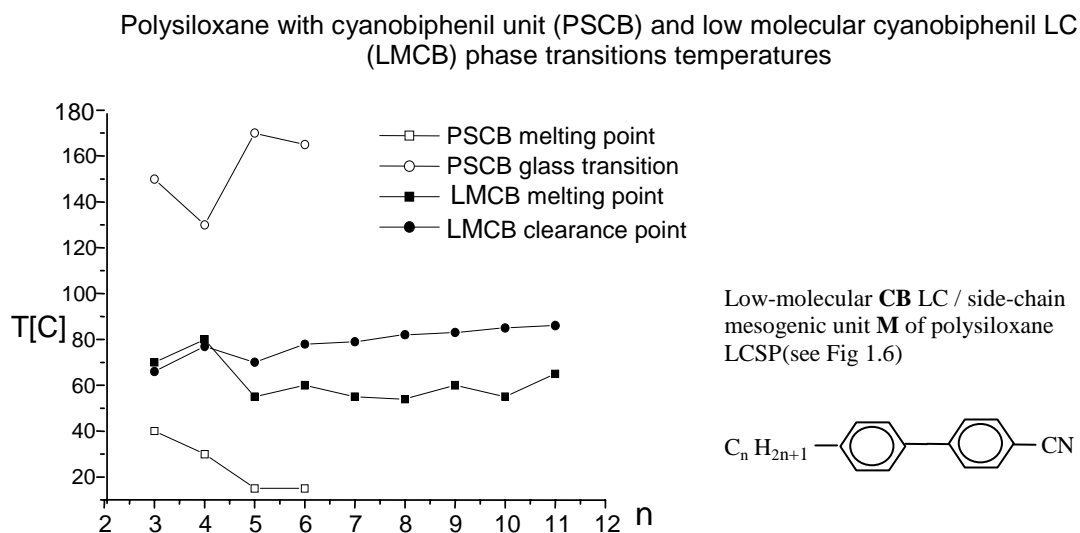


Fig 1.7 Dependence of the phase transition temperatures for the polysiloxane LCSP with cyanobiphenil mesogenic units and its low-molecular analog. The temperature range of the mesophase existence for LCSP is sufficiently broader than for low-molecular **CB** LC.

slowly achieving a plateau for DP>100 value (see Fig 1.6).

Generally, the presence of the main-chain backbone leads to much higher thermostability of the mesophase in comparison to the low-molecular LC. This can be seen when comparing the transition temperatures of the LC of alkocyanbiphenyl type with LCSP having the same mesogenic groups (**Fig 1.7**) in side chain.

1.3.2. Spacer

Spacer or flexible bridge, which connects the side-chain with the backbone, has several functions important for the LC properties. The first one is providing of the independent behavior for mesogenic units that often define the mesophase forming. As it is seen from Table 1, the decrease of the spacer length leads to the narrowing of the temperature range of mesophase existence. Another important function is the plastification influence of the spacer. The increasing of the spacer length leads to decrease of the glassy state transition temperature for the LCSP (Table 1.1). In addition, the number of the methylene units in spacer quite often can define the ability of a polymer to form more than one subphase. Usually, for the other equal parameters, by the increasing the spacer length it is possible to turn from the nematic to smectic state.

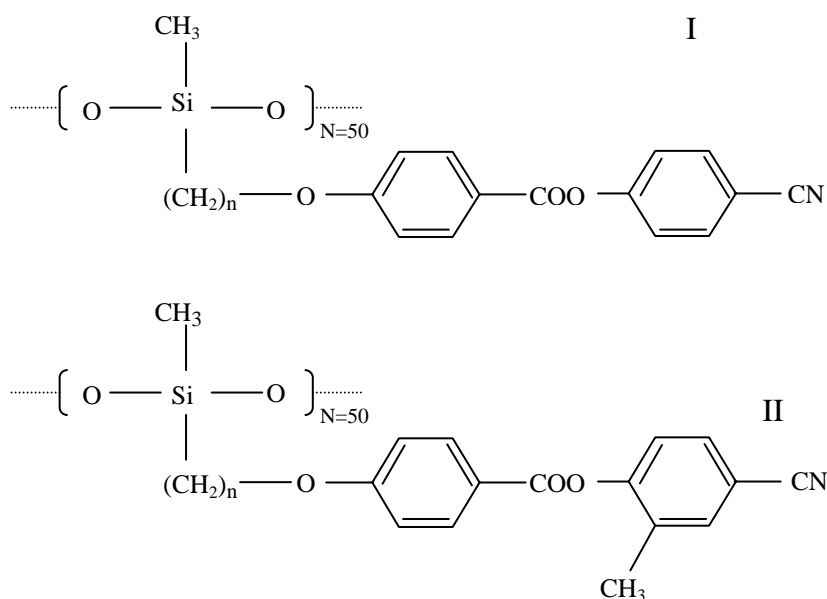
Table 1.1 Phase transition temperature of polysiloxane LCSP's depending on the length of the spacer

$\begin{array}{c} [\sim\text{Si}(\text{CH}_3) - \text{O} \sim]_m \\ \\ (\text{CH}_2)_n - \text{C}_6\text{H}_4 - \text{C}_6\text{H}_4 - \text{CN} \end{array}$	
n=5, m=36	$T_g 14 \rightarrow N_{\text{sub}} 60 \rightarrow I$
n=4, m=50	$T_g 12 \rightarrow S 130 \rightarrow I$
n=3, m=50	$T_g 40 \rightarrow S 152 \rightarrow I$

1.3.3. Mesogenic unit.

Obviously, the side-chain mesogenic unit has the strongest influence on the character of mesophase formed by the particular polymer. For instance, the nematic type of LC structure is characteristic for the homopolymers, which have the short end-groups (**CH₃**, **OCH₃** and **CN**) with 2..6 methylene groups in spacer.

Additionally, the forming of the nematic phase can be promoted by the including of a side substituents into the mesogenic unit. This can be clearly seen by comparison two different series of the polysiloxanes:



All the polymers of type I starting from the $n=3$ form only the smectic phase, while in the LCSP of series II the nematic phase can be observed at $n=5,6$ at clearance temperature $T_N=40-60^{\circ}\text{C}$. The further increase of the spacer length ($n=7-11$) again leads to the smectic ordering $T_S=90^{\circ}$ for $n=7$ and $T_S=130$ for $n=11$. More examples of the phase transition temperature variation depending on the structure of the mesogenic unit can be found in [I.11].

1.3.4. Mutual orientation of the backbone and the mesogenic units

The statistical conformation of the isotropic chain polymers is not consistent with the mesogenic structure [I.2]. This can be confirmed on the example of the mixture of low-molecular LC with linear chain polymers where even if the isotropic phases are completely miscible, the phase separation occurs when the low-molecular system turns to the nematic state. In the case of LCSP no phase separation is possible. That way, the trend of the main chain to form the random coils will conflict with the liquid crystalline ordering of the side-groups. This will makes the side chain to adopt the anisotropic conformation according to the LC phase structure. Generally, it leads to the different orientation character of the mesogenic groups and the backbone that was confirmed in the experiments. This difference seems to be determined by the number of structural features, including the length of the spacer and the flexibility of the main chain. The relation between these two parameters defines the correlation of the side- and main chain behavior under influence of the orientation factors. It is necessary to notice, however, that the effect of the mechanical field (deformation) on the orientation of LCSP is quit different from the

magnetic or electric field. In the later case the orientation more selectively affecting the side-chain, rather than main chain and, that way, a higher orientation degree with *monodomain structure* chain be achieved. In more details the problem of the orientational order in main and side-chain as well will be considered in the next section.

1.4. Conformation and the orientational order of the main chain in liquid-crystalline side-chain polymers. Backbone conformation and anisotropy.

The conformation and ordering of the backbone is the question of great importance for characterization of the structural and dynamical properties of LCSP. The structure of main chain influences both on mechanical and thermodynamic properties, such as viscosity, strength, elastic modules, transition temperatures. During a long time the question of the conformation of the main chain was not discussed in literature. A priori, it was suggested that in the case of the smectic LCSP the main chain is located between the layers of mesogenic units. For nematic state a one-dimensional order of mesogenic groups with disordered conformation of main-chain coils was expected. In the first time the proposition about the anisotropic ordering of the main chain was discussed in [I.12] when studying the orientation of the polysiloxane LCSP by the external magnetic field. Using the neutron scattering for investigation of selectively deuterated side-chain polysiloxanes oriented in the magnetic field, the first information about the conformation of the macromolecules of the side-chain polymers in blocks was obtained.[I.13,14] There are some theoretical approaches to the problem of main-chain conformation. Vasilenko et al [I.15] have used the lattice model. It is based, however, on athermal parameters and can not give the comprehensive explanation of the experimental data, which include a number of temperature dependent results. Another theory developed by Wang and Warner uses the model of cross-coupling between rod-like side-chain and flexible main chain to explain the different structures of the nematic phase in LCSP. The structures are classified by the order parameter of the mesogenic units S_A and backbone S_B . When $S_A > 0$, $S_B < 0$ the shape of the backbone supposed to be the oblate spheroid and the phase is called N_I . The phases with prolate conformation of main-chain with $S_A < 0$, $S_B > 0$, and $S_A, S_B > 0$ are called N_{II} and N_{III} respectively. The segment-segment, segment-mesogen, and mesogen-mesogen interactions in this case are described using the Maier-Saupe theory potentials. Considering the conventional LCSP (with poly(meth)acrylate or polysiloxane main-chain) where in the sense of Maier-Saupe theory the anisotropy of polarizability of the backbone segments is negligible as compared to the mesogens it might be concluded that all mentioned kinds of LCSP have to have the same nematic phase N, that is in contrast to the experimental data. On the other hand, the Warner's theory gives no explanation

about the influence of the spacer length on the orientational properties of the polysiloxanes

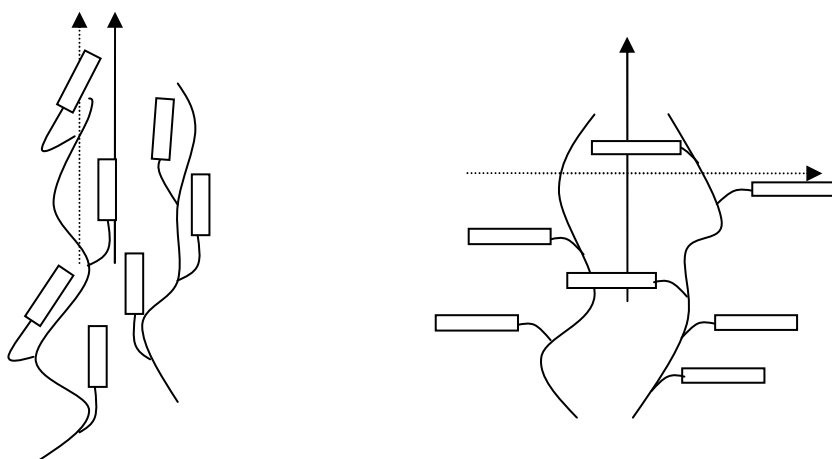


Fig 1.8 Influence of the spacer length on the mesogenic unit orientation. For polysiloxane sample with 4 aliphatic units in spacer the mesogens are aligned parallel to the main chain exhibiting nematic N_{III} phase (uniaxial) (left hand side), when for the number of aliphatic segments 3 and 6 the polymer forms N_I uniaxial nematic phase with orthogonal alignment of mesogenic units with respect to main chain(right hand side).

LCSP. It can be seen on the **Fig 1.8** in the case of the polymer M4 (spacer length $m=4$) the mesogenic units are aligned parallel to the segments of main chain (phase N_{III}), and whole sample is optically uniaxial. The opposite picture is observed for the samples of M3 and M6 ($m=3$, and 6 respectively). The mesogenic units are oriented in the direction perpendicular to the main chain and the sample is biaxial (phase N_I). The cross-coupling model predicts only the perpendicular orientation of the main- and side-chain in both cases for the realistic values of the volume fraction of mesogens.

1.4.1. Evaluation of the backbone anisotropy parameters using SANS.

A number of experimental investigations of the backbone conformations were done using the small angle neutron scattering method (SANS) [I.16] on the samples of polysiloxane and polymethacrylate series (**Fig 1.9**). The samples were mixed from deuterated and hydrogenated molecules to provide the necessary SANS neutron scattering contrast of the molecules to the surroundings. The mesogen induced backbone anisotropy can be described in the terms of the inertia radii R_{\parallel} and R_{\perp} parallel and perpendicular to the local director. The results obtained for deuterated polymethacrylates and polysiloxanes samples exhibit the obvious anisotropy of the macromolecules in mesogenic phase. As it can be seen from the data in the Table 1.2 for the polymethacrylates sample in nematic phase the ratio $R_{\parallel} > R_{\perp}$ is valid, but the anisotropy factor $\eta = R_{\parallel}/R_{\perp}$ is quit low ($\eta=1.1$). Significantly larger anisotropy can be observed in smectic phase. This means the anisotropic conformation of the main chain in the direction perpendicular to the local

director. Based on the results of SANS studies the model of the macromolecular chain allocation within one smectic layer with multiple crossing was proposed [I.14](see **Fig 1.10a**).

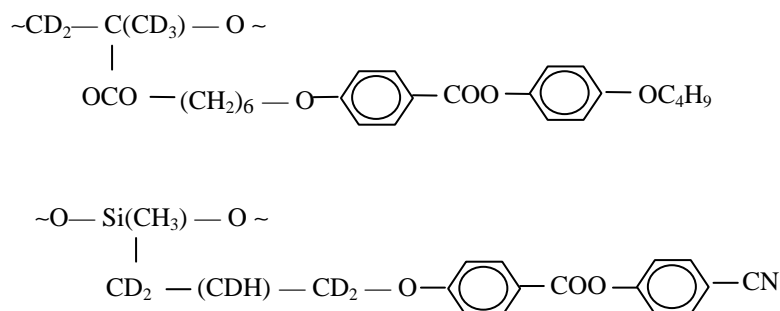


Fig 1.9 Polymethacrylate (top)(PMA) and polysiloxane(bottom)(PS) samples studied by SANS in [I.13] to determine the gyration radii of the macromolecules. The partial deuteration of both main chain (in the case of PMA) and spacer were done to provide the contrast for the neutron scattering. The model of the smectic phase ordering was build basing on the data analysis (see text).

<i>PMA</i>		<i>Phase transition temperature</i>		<i>PS</i>	
	C45→50S110→N116→I				T _g 45→36S _A 146→I
	680		<i>Polymerization degree</i>		63
			<i>Isotropic phase</i>		
R _g	106		<i>Nematic phase</i>		22±2
R	59±5				-
R _⊥	65±5				-
R _⊥ /R	1.1				-
			<i>Smectic phase</i>		
R	22±3				9.9±0.2
R _⊥	65±5				15.8±0.2
R _⊥ /R	4.0±1				1.6

Table 1.2 Gyration radii obtained by SANS for the polymethacrylate (left) and polysiloxane (right) samples (Fig 1.9)

1.4.2. Bilayer model

Another model of the conformation of the backbone in LCSP was proposed in [I.25] with account of data from the work [I.14]. The basic idea of this model introduces the so-called *anisotropy of local rigidity* approach with consideration of the smectic phase like a state with microphase separation of the mesogenic groups and main chains. In this case the backbone is pushed out of the smectic layer and creates the intermediate layer (**Fig 1.10b**). Contrast to the layer crossing model, [I.14] according to this approach, the transition of the backbone through the smectic layers occurs very seldom. The part of the main chain, which tunnels through the mesogenic unit layers (called “tunneling segment”) is located perpendicular to the smectic layer creating a small defect in it. The details of this defect are not known, but the SANS allows one to estimate its density. That way, all the polymeric chain is divided into the separate two-

dimensional coils allocated into the smectic planes. However, despite of the sufficient progress, which gives the application of SANS for the studying of the molecular orientation of LCSP, still there are some problems arises from the necessity of the sample deuteration for the purpose of providing a better contrast. Particularly, this takes place in the polysiloxanes because they are deuterated in different positions in the side groups (see **Fig 1.9**).

That way, the shape of the molecule obtained by the neutron scattering is not necessarily to be a backbone one. The way for making corrections is shown in [I.17], where the apparent molecular shape was estimated for different label distance to the backbone and extrapolated to zero distance. Alternative possibility is given by Noirez et al. [I.18]. Here, another possible problem was also studied: segregation into deuterated and hydrogenated phases could occur in some cases. The sufficient difficulties of both synthesizing the deuterium-labeled substances and neutron scattering experiments, require looking for alternative methods of main-chain conformation studies. X-rays are effective for the smectic phase investigation [I.19]. Although in nematic, the information about main chain obtained from diffraction pattern is relatively poor. ^2H NMR experiments show that in a particular polyacrylate the main chain and also spacer are parallel to the mesogenic unit side groups, while corresponding polymethacrylate demonstrates a perpendicular structure [I.20]. In the same time, SANS experiment demonstrates the oblate

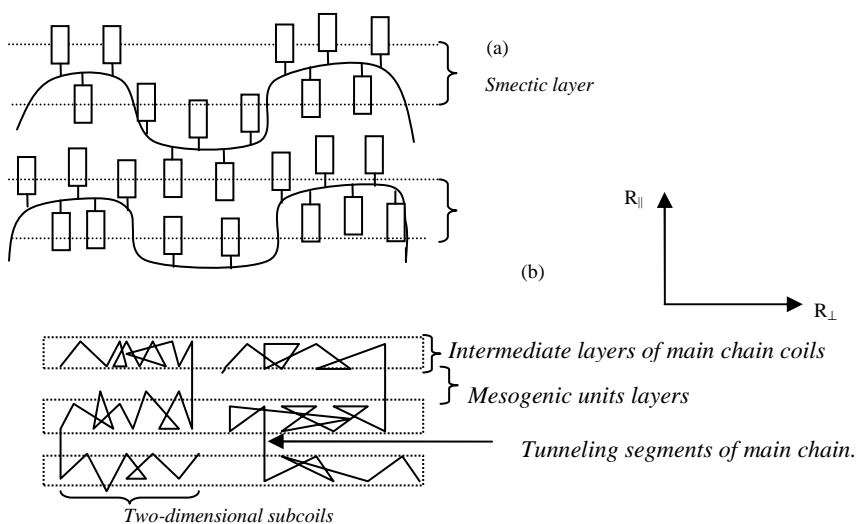


Fig 1.10.a,b The models of the backbone and mesogenic units arrangement for the smectic phase basing on the SANS experiments. (a) - the model proposed in [I.14], - the backbone is placed within one smectic layer with multiple crossing. (b) - microphase separation model [I.26]. The backbone is pushed out of the smectic layers of mesogenic units and creates the own intermediate layer. The tunneling of the backbone through the side-chain layers occurs rather seldom.

backbone conformation [I.18]. This contradiction can arise from the different length scale to which NMR and SANS are sensitive (will be discussed later) and also from the mentioned above problem concerned with molecules deuteration. However, the polysiloxanes give the additional possibilities for the backbone conformation investigation by using the ^{29}Si NMR. This method promises to bring good results because the information about the molecular order is provided by

the silicon atoms, which position in main chain is unambiguous. No special preparation of the samples is required in this case and the problems concerned with the sample deuteration needed for SANS and ^2H NMR can be avoided. That way, in our work the polysiloxanes and ^{29}Si NMR were chosen to find a reliable method of the LCSP main chain conformation study.

1.5 Orientation of the side and main chain in side-chain liquid crystalline polysiloxanes

1.5.1 Chemical constitution of the polysiloxanes. Samples synthesizing.

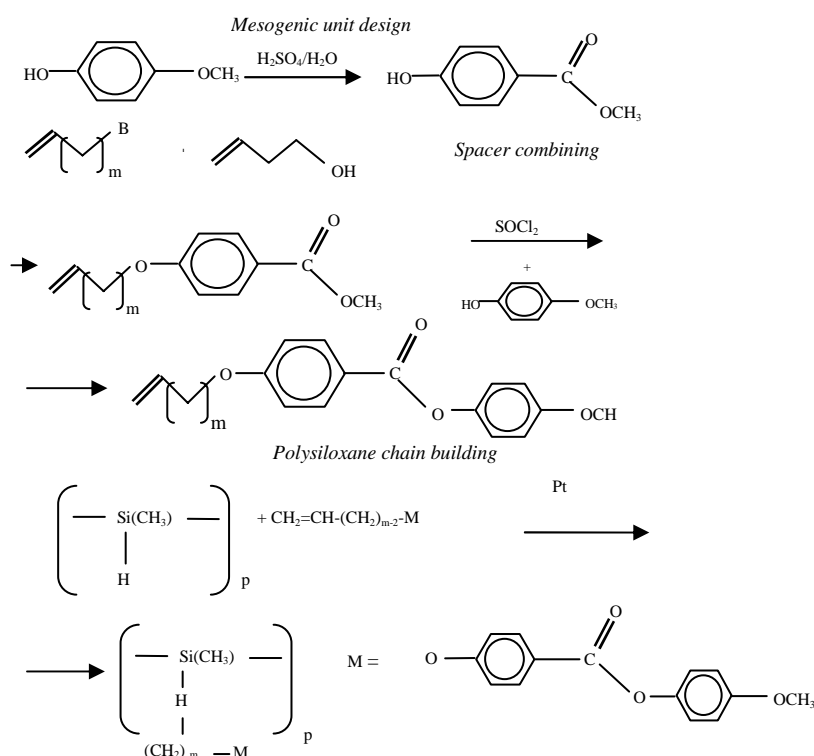


Fig 1.11(top). The stages of the mesogenic unit and spacer synthesis for the liquid crystalline side-chain polysiloxane polymers. (bottom) - The backbone synthesis and assembling of the whole polysiloxane macromolecule

Generally, the method of the polysiloxane-based LCSP synthesis bases on the reaction of the polysiloxanes with the mesogenic monomers of olefin series. The sufficient advantage of this method is that the samples with different polymerization degree can be obtained. Also, the samples with various mesogenic segment structure and desirable spacer length can be obtained. The main stages of the synthesis are shown on Fig 1.11. In our work the samples with spacer length $m=4$ and $m=6$ were used, which will be in the future denoted as **M4** and **M6** respectively.

1.5.2 Physical properties and phase transitions.

The basic thermodynamic properties of the polysiloxane samples chosen for the main-chain conformation investigation measured by DSC are shown in Table 1.3. It should be noticed that the M4 sample has narrower temperature region of the mesophase existence as compared to

M6, but the difference is not too significant (about 5%). However, the nematic to isotropic liquid (NI) transition enthalpy ΔH_{NI} differs on more than 20%. More important is the difference of the heat capacity for the glassy state transition. For the M6 sample it exceeds the ΔC_p of the M4 on more than 35%. This can be easily understood if to look at the DSC diagram, which shows the existence of two different mesophase for M6 sample (smectic-C and nematic $T_g274\pm4 \rightarrow S_C308\pm4 \rightarrow N377\pm2 \rightarrow I$) when M4 sample demonstrates only nematic phase ($T_g280\pm4 \rightarrow N368\pm4 \rightarrow I$). The molar mass distribution parameter $U=M_w/M_n-1$ (where M_n is *number averaged* and M_w is *weight averaged* value of molar mass) obtained by the light scattering (LS) shows that the polymerization degree in M6 sample is sufficiently more homogeneous ($U_{M6}=1.16$) than in the M4 ($U_{M4}=1.57$). The average polymerization degree $\langle p_n \rangle$ of the molecules estimated from the M_n gives also the higher absolute value for M6 ($\langle p_n \rangle=97\pm5$) than for M4 ($\langle p_n \rangle=87\pm5$).

Table 1.3 DSC results for different polysiloxane

PS	T_g [K]	ΔC_p [J/gK]	T_{NI} [K]	ΔH_{NI} [J/g]
M3	287 \pm 4	0.4 \pm 0.1	347 \pm 4	1.2 \pm 0.4
M4	280 \pm 4	0.32 \pm 0.04	368 \pm 4	2.0 \pm 0.3
M6	274 \pm 4	0.5 \pm 0.2	377 \pm 2	2.5 \pm 0.5

1.5.3 Liquid crystalline orientational properties of the polysiloxane samples.

As it was mentioned, the liquid crystalline properties of the LCSP are mainly connected with the anisotropy of the side-chain segments ordering due to their rod-like shape. However, the macroscopic orientation and forming poly- or monodomain LC (see A.I) usually are defined by the external factors, such as electric or magnetic field. Opposite to the case of low-molecular liquid crystals, the homogeneous orientation of the polymers is not always possible even in nematic state. Therefore, the task of separation of the orientation effects on macro and micro level is important. One of the approaches to the macroscopic orientation studying is based on the estimation of the parameters of the local director orientation distribution obtained from analysis of the 1H NMR spectrum [I.21-22]. The orientation distribution of local directors can be characterized by the macroscopic order parameter $S_M=\langle P_{2M} \rangle$ or so-called *orientation degree* defined in a manner similar to the microscopic order parameter S (Eqn. 1.1, for more details see **AI.5-8**) Generally, for LCSP the procedure of the sample macroscopic orientation is the same as for low-molecular liquid crystals. The sample is to be heated to turn into the isotropic state, and then cooled down to the mesophase in presence of the external magnetic field, which provides

the preferable orientation direction for the molecules over the whole sample. However, the specific properties of the polymer samples lead to the strong dependence of the orientation degree S_M from (i) the field strength and (ii) kinetics of the cooling down process. The order parameter in this case can be different for various atomic positions. The selective order parameter estimation for different atomic positions in side-chain polysiloxanes using the ^{13}C NMR is described in [II.23]. Discussing the questions concerning with ^2H NMR studying of the LCSP it is necessary to mention the results obtained in [I.24]. The partial deuteration of the methylene groups and mesogenic units allows estimating the order parameters of the *rigid* and *flexible* parts of the side-chains. Binding the mesogenic units with polymer backbone has *insignificant influence* on the order parameter of the *mesogenic units*. However, the order parameter of the *aliphatic chain* decreases by the *factor of 2* demonstrating the strong mutual perturbation influence of the of the polymer chain and mesogenic segments. Obviously, the orientation of the LCSP in the magnetic field is caused by the anisotropy of the magnetic susceptibility $\Delta\chi$. For the polysiloxane samples M4 and M6 it was in the first time measured in [I.22]. The coincidence of the $\Delta\chi$ values for both samples ($\Delta\chi=(1.5\pm 0.5)\cdot 10^7$ SGSE/g] with known susceptibility values of the analogous low-molecular LC shows some similarity of the structure of LCSP and low-molecular nematics. Therefore, when studying the orientational properties of the LCSP, the question of the mutual influence of the mesogenic units reorientation by the external fields and main chain adopting to the new molecular arrangement becomes quit interesting and important. The first data on elastic constants determination of the polysiloxanes LCSP were obtained in [I.22]. The authors estimated the «splay», «bend», «twist» and elastic deformation coefficient (K_{11}, K_{22} , and K_{33}) (**Fig 1.12**) and their temperature dependence for different samples including M4 and M6 and compared this data with one obtained for low-molecular analogous. The experimental results show that the reducing of spacer length from 6 to

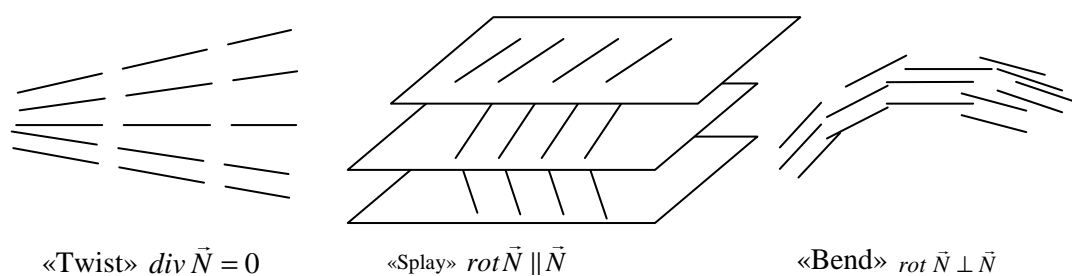


Fig. 1. 12 Schematic representation of the viscoelastic deformations in the nematic LC.

4 units does not make a significant influence on the K_{11} coefficient but changes strongly K_{33} and therefore K_{11}/K_{33} ratio. This can be treated like a confirmation of the backbone contribution to the elastic properties of the side-chain polymer LC phase. However, there was not found any significant influence of the main chain length (polymerization degree) on the «twist» elastic constant K_{22} . In general, basing on the experimental data obtained for the polysiloxane LCSP it

should be noticed that there can not be done any unambiguous conclusion about the influence of the backbone conformation on the elastic and reorientation properties of the LC phase.

1.5.4. Relation between SANS and NMR results of the backbone conformation studies in polysiloxanes.

As it was mentioned above, the conclusions, which could be done concerning the mutual orientation of the main and side-chain in polysiloxanes using the data obtained by different methods are not unambiguous. The extensive investigation of the polysiloxane samples M4 and M6 with the SANS method was done by Siebert in [I.24]. The gyration radii R_{\parallel} and R_{\perp} were determined for different temperatures below the isotropic-to-nematic state transition. **Fig 1.13** demonstrates the variation of the parameter $\eta=R_{\parallel}/R_{\perp}$ with the temperature for the M4 and M6 samples respectively. The obvious conclusion from these data is that for the M4 sample a prolate shape of the molecule is characteristic in the nematic phase for the temperatures below T_{NI} approximately on 10K (where η turns from the values $\eta>1$ to $\eta<1$). In the same time for the M6 sample η goes down continuously with the temperature starting from the value $\eta=0.63$ in nematic state and decreasing by nearly the factor of 2 in smectic phase. However, the information about the shape of the polysiloxane LCSP molecules obtained by SANS does not

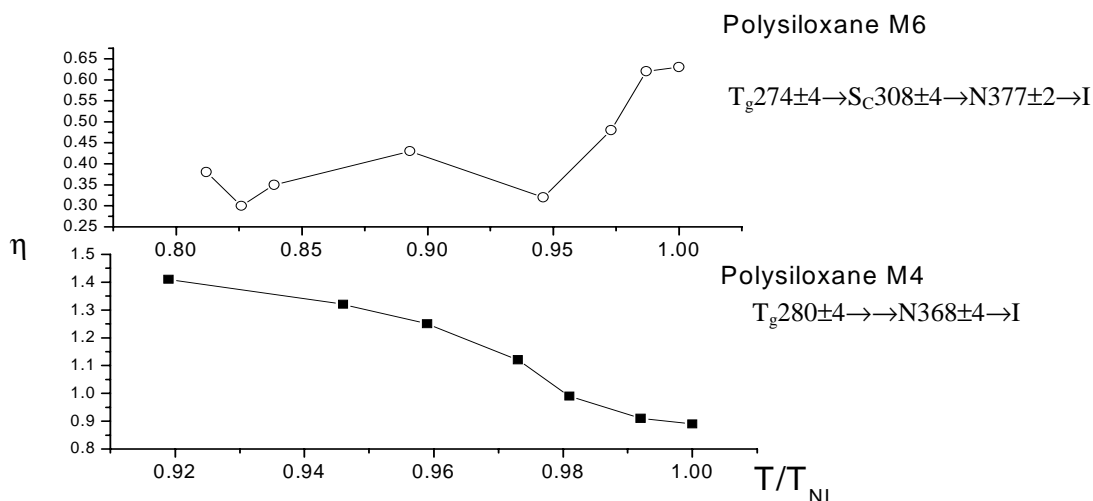


Fig 1.13 The dependence of the gyration radii ratio $\eta=R_{\parallel}/R_{\perp}$ for polysiloxane LCSP M4 and M6 as a function of reduced temperature $T_{red}=T/T_{NI}$. The consequent changing from prolate to oblate conformation occurs for the M4 LCSP (η changes from the value >1 to <1). The M6 sample demonstrates the oblate form in whole temperature range of the LC existence.

allow one making an undisputable suggestion about the orientation of the main-chain there. Moreover, the length scales to which this method is sensitive does not allow to estimate the degree of the backbone orientation and to compare it with the orientation of the mesogenic units. As it was remarked in section 1.2 the information about the orientation properties of the backbone can be also obtained by the NMR. Because the NMR spectroscopy is sensitive to the interactions on the length scale of the chemical bonds, the orientation of the individual segments

of the polysiloxane LCSP main chain can be, in principle, determined using the NMR spectrum of ^{29}Si nuclei. Using the angular dependence of the ^{29}Si NMR spectra the orientation degree of the backbone molecular segments in different polysiloxane samples was estimated in the work of Dr. G. Hempel and colleagues [I.25]. In details the theoretical and practical aspects of the method will be described in the next chapter. Here, it should be mentioned that the main result of the work is the issue that for the M4 sample the orientation degree of the main chain segment with respect to local director has positive value, $\langle P_2 \rangle_S = 0.18$ that means parallel orientation of the main-chain and mesogenic units. In contrast, the orientation degree for the M6 sample is negative $\langle P_2 \rangle_S = -0.23 \pm 0.02$ i.e. the segments of the backbone are oriented preferably orthogonal to the side-chain. That way, the NMR measurements in this case are in qualitative agreement with the SANS data. However, the situation when the *prolate* shape of the molecule (determined by SANS) corresponds to the *perpendicular* orientation of the backbone with respect to the mesogenic units preferable direction (found by the ^{29}Si NMR,) can also take place for the polysiloxane LCSP [I.26]. As it was mentioned already, such a strong contradiction can occur because of the different sensitivity length scales belonging to these methods (NMR: at maximum size of the monomer unit, SANS: size of a macromolecule). **Fig 1.14** demonstrates one of the possible examples of such a backbone conformation. The largest part of the main chain can be compressed between mesogenic layers perpendicular to the local director even if the average

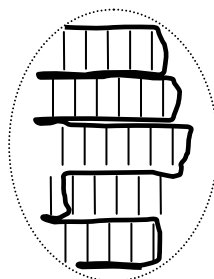


Fig 1.14 Sketch of the possible example of the backbone arrangement. The most part of the molecular segments of the main chain is oriented perpendicular to the mesogenic units, when the averaged shape of the molecule is prolate.

shape of the molecule is prolate. The NMR methods are able to monitor directly the tiny details of the molecular arrangements with possibility to quantify the distribution in the orientation of the backbone individual segments. However, the features of the polysiloxanes structure make difficulties for extraction of the information about molecular ordering of the main-chain directly from NMR spectra. The detailed description of these problems will be done in the next chapter. That way, the task of polysiloxane LCSP backbone conformation investigation requires the development of special ^{29}Si NMR techniques and data interpretation methods. The solving of these problems was chosen to be the main subject of the present work.

Chapter II. Molecular segments orientation study using ^{29}Si NMR methods.

2.1. NMR Spectroscopy, Anisotropic Nuclear Spin Interaction.

The term *Nuclear Magnetic Resonance* (NMR) unifies a big variety of the quantum phenomena based on the interaction of the nuclear spins with magnetic fields and radiofrequency irradiation. Generally, NMR denotes the resonance response of the spin system polarized in the magnetic field on the rf-irradiation. The spectrum of the response signal reflects the picture of the energy levels of the atomic nuclei spins and therefore can be effectively used in many ways for the probing the molecular, structural, dynamical and other properties both on micro and macro level. The basics of the NMR spectroscopy both in theoretical and applied aspects can be found in many textbooks [II.1-3]. Appendix II collects some important information about the NMR theory, which is relevant for current work.

The appearance of a NMR spectrum is determined by the various interactions of the nuclear spins with each other as well as with quantities like local and external magnetic fields, electric field gradient and coupling to the surroundings or lattice. In this section, the most attention will be given to the *anisotropic spin interactions*, which have a great importance for the NMR investigation of the structure and orientational ordering of the systems of our interest.

The most important interaction in the NMR is the coupling of the nucleat spins to the applied external magnetic field. It is Zeeman interaction (see AII.2), which defines the basic (non-perturbed) resonance frequency of the spins system. In reality, this frequency is often changed due to the *chemical shift* and the *indirect couplings*. Both of them depend on the features of the electron shielding in the surroundings of nuclei. They are often used as «portraits» of the molecules chemical properties. Generally, the spin interactions have a vector properties i.e they are quantified with the magnitude and orientation. The interaction of two vectors is described by a *tensor*, which is normally represented by a matrix in Cartesian coordinates. Such kinds of properties have (i) the *direct dipole-dipole coupling*, (ii) *the indirect coupling* between two spins, and (iii) the coupling of the spins with a local magnetic field (*chemical shift*). The similar description has the *quadrupolar coupling*, which is denotes the interaction of the spins with the *tensor of electric field gradient*. In liquids the tensorial properties of the interactions, normally are eliminated by the averaging due to the fast molecular motion, so that only the orientation-independent parts corresponding to the traces of the coupling tensors are effective. From all the interactions mentioned above, only chemical shift and indirect coupling have non-zero traces of tensor matrices. Nevertheless, in solids, the motional averaging is not so effective, and tensorial properties of the interactions lead to the resonance frequency changes, which are orientationally dependent. In this case the description of the interaction Hamiltonian operator in

terms of irreducible spherical tensors instead of Cartesian matrices is helpful [II.4] (see also AII.2).

If the orientation dependence of the resonance line frequency of spin $I=1/2$ is determined only by just one type of the interaction it is possible to use it for measuring the angles of chemical bonds, and other structural characteristic of the molecules. In polycrystalline solid powder, molecular and liquid crystals, polymers and other partially oriented or disoriented samples the angles of the interaction tensor main axes with respect to the external magnetic field and, therefore, the corresponding resonance frequencies are distributed over large range of values. This leads to the broadening of the NMR spectrum to some pattern of the specific shape, so-called *wideline NMR spectrum*. [II.1.2] Generally, the shape of this pattern is, in addition, influenced by the molecular reorientation on the time scale of inverse width of the resonance line. Therefore, the lineshape provides the information on structural, orientational and dynamical properties of the solid sample. [II.5-7]

2.1.1 Anisotropic chemical shift interaction tensor.

The external magnetic field B_0 applied to nuclear spins is always shielded by the surrounding electron clouds. The resulting local field B_{loc} influencing on nuclei in this case is given by

$$\vec{B}_{loc} = (1 - \hat{\sigma}_{CS}) \vec{B}_0 \quad (2.1)$$

where σ_{CS} is the chemical shift tensor. As it was mentioned above, the orientation dependence of the resonance frequencies in the most convenient manner can be treated in terms of irreducible spherical tensors of the second rank. In Appendix II it is shown that the offset of the resonance line due to the anisotropic chemical shift can be separated in isotropic, symmetric and antisymmetric parts. Only *isotropic* and *symmetric* parts influence on NMR spectrum [A2.2, II.4,8]. In principal axes system the tensor is characterized only by the combination of three diagonal elements σ_{xx} , σ_{yy} and σ_{zz} . The resonance frequency offset σ_{zz} caused by the anisotropic chemical shielding can be given as

$$\sigma_{zz} = \sigma_{iso} + \frac{\Delta\sigma}{2} (3 \cos^2(\theta) - 1) - \frac{\Delta\sigma}{2} \eta \sin^2(\theta) \cos^2(\varphi) \quad (2.2)$$

where σ_{iso} is the isotropic part of the frequency shift defined by the tensor trace:

$$\sigma_{iso} = \frac{1}{3} (\sigma_{xx} + \sigma_{yy} + \sigma_{zz}) \quad (2.2a)$$

$\Delta\sigma$ is the tensors anisotropy parameter:

$$\Delta\sigma = \sigma_{zz} - \frac{\sigma_{xx} + \sigma_{yy}}{2} \quad (2.2b)$$

and η is the parameter of asymmetry:

$$\eta = \frac{\sigma_{yy} - \sigma_{xx}}{\sigma_{zz} - \sigma_{iso}} \quad (2.2c)$$

which has non-zero value if the tensor has no axial symmetry. In this case only two main values of tensor $\sigma_{xx}=\sigma_{yy}=\sigma_{\perp}$ and $\sigma_{zz}=\sigma_{\parallel}$ are relevant. Here, θ and φ denote the polar and azimuthal angles between σ_{\parallel} and B_0 , respectively. The tensor properties of chemical shift means that the local field influenced on nuclei differs from the external field B_0 in both magnitude and direction due to the shielding effect of the surrounding electrons. Generally, a connection between external field B_0 and local field B_{loc} can be represented graphically as a second order surface (ovaloid). (see **Fig 2.1**). The perfect detailed explanation of the pictorial representation of CS tensor can be found in [II.9]

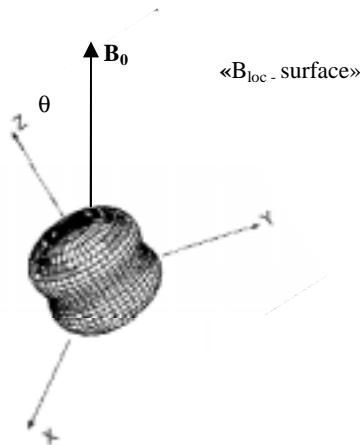


Fig 2.1 Chemical shift tensor (Eqn 2.2) graphical representation. Example for symmetrical CS tensor $\sigma_{11}:\sigma_{22}:\sigma_{33}=1:1:2$; $X=R\cdot\sin(\theta)\cos(\varphi)$, $Y=R\cdot\sin(\theta)\sin(\varphi)$, $Z=R\cdot\cos(\theta)$, $R=(\sigma_{zz})^{-1/2}$, $X^2+Y^2+Z^2=R^2$
 $B_{loc}=(1-\sigma_{zz})B_0$ (See [II.9] for more details.)

More details about the expansion into the irreducible tensors and transformation between laboratory and the principal axes frames using Wigner matrices can be found in (AII.2). Expressions 2.2 allow one finding the lineshape of the NMR spectra determined mainly by chemical shift interaction. For the powder sample, when all the orientations of individual tensors main axis have equal probability the shape of the wideline NMR spectrum can be obtained by the integration over the whole sphere the contributions of corresponding individual resonance lines shifted according to 2.1.

$$S(\sigma) = \iint_{\Omega} f(\sigma - \sigma_{zz}(\theta, \varphi)) \sin \theta d\theta d\varphi \quad (2.3)$$

Here $f(\sigma)$ denotes the shape of the individual lines.

In ideal case for δ -like intrinsic lineshape, i.e. $f(\sigma)=\delta\sigma-\sigma_{zz}(\theta,\varphi)$, for the axially symmetric CS tensor ($\eta=0$) after integration the characteristic spectral density pattern can be obtained:

$$S(\sigma) = \begin{cases} \left(2\sqrt{2\Delta\sigma}\sqrt{\sigma-\sigma_{\perp}}\right)^{-1} & \text{if } \sigma_{\parallel} \leq \sigma \leq \sigma_{\perp} \text{ or } \sigma_{\perp} \leq \sigma \leq \sigma_{\parallel} \\ 0 & \text{for other } \sigma \end{cases} \quad (2.4)$$

Fig 2.2 demonstrates the lineshape pattern, which is built according to Eqn 2.4. The spectral line has a singularity at the frequency $\sigma=\sigma_{\perp}$ corresponding to the angle $\theta=\pi/2$ between the magnetic field B_0 and Z-axis of coupling tensor. For this angle, B_0 lies in XY plane of the principal axes system. The cut-off at σ_{\parallel} corresponds to an orientation of B_0 parallel to Z -axis. Thus, when the orientation of the CS tensor with respect to molecule-fixed coordinate frame is known a *wideline CS spectrum* can be used to determine the molecular orientation. On the other hand, the assumption of δ -like intrinsic lineshape $f(\sigma)$ is, of course, nonrealistic. The inhomogeneity of the CS tensor values distribution and variety of the structural conformation leads to the finite width of the resonance line corresponding to some specific orientation. In this case the CS spectrum is represented by the convolution of the «ideal» pattern corresponding to the δ -like individual lineshape with Gaussian or Lorentz patterns according to **Eqn 2.3** (see **Fig 2.3**)[II.10]. It can be noticed that the formula 2.3 can be reversed and the broadening lineshape function $f(\sigma)$ can be recovered from the experimental powder spectrum. The example of such a deconvolution will be shown in following section.

Distribution of the NMR frequencies due to the anisotropic chemical shift

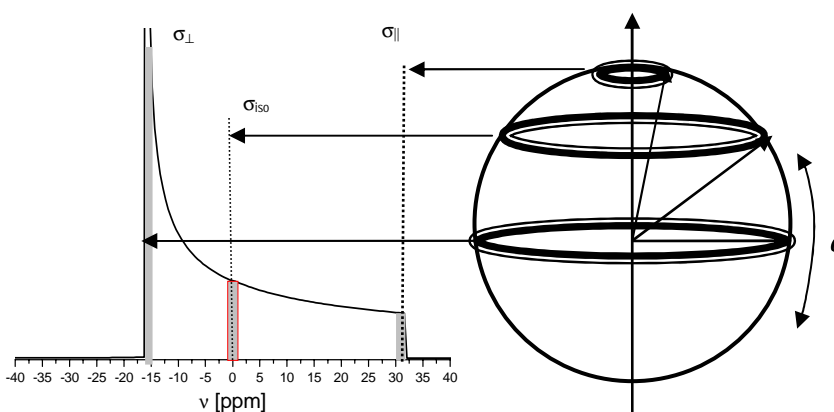


Fig 2.2. Distribution of the resonance frequencies due to the anisotropic chemical shift. Different orientations of the tensor axis with respect to the external field B_0 contribute to the different resonance positions (Eqn 2.2). The example of the powder averaged wideline NMR spectrum for axial symmetric CS tensor is built according to Eqn 2.4.

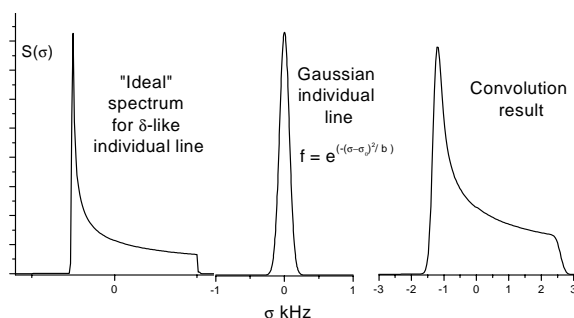


Fig 2.3 Convolution of the «ideal» powder CS pattern with Gaussian broadening function $f(\sigma-\sigma_0)$ for realistic spectrum representation in simulations. The value of broadening factor b reflects the distribution of CS parameters corresponding to the specific tensor axis orientations. This distribution can be caused by a variety of conformations, thermal molecular motion or other reasons.

2.2. Orientation Distribution Function (ODF)

2.2.1 Theoretical background.

The state of orientation of any ordered system can be described in general manner by the **orientation distribution function (ODF)** $W(\theta, \varphi, \psi)$. This function, practically, represents a probability density to find an element of the system in certain orientation with respect to the given coordinate frame. Considering orientation of a partially ordered system (polymers, liquid crystals and others), the most convenient way, usually, is to use the set of **Eulerian angles** [II.2, 4, 6, 11] to describe the probability that the certain element (whole molecule, molecular segment, chemical bond) lays within an infinitesimal interval around angles θ, φ, ψ , with respect to the local director N . (see **Fig 2.4**)

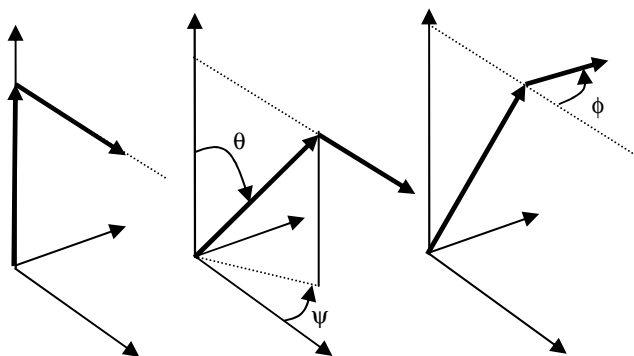


Fig 2.4 Set of Eulerian angles needed for fixing the object's orientation in space. The orientation distribution can be represented like a function of all or some of the angles depending on internal symmetry of the system.

To make further simplification it is comfortable to represent the dependence of ODF W from azimuthal angle θ via its cosine. The advantage of this approach is demonstrated by **Fig 2.5**. Obviously, the amount of elements in direction θ distributed according to some ODF $U(\theta)$ is proportional to the area of the corresponding spherical element $\Delta\theta$. Rings around the sphere with equal $\Delta\theta$ contain more area if they correspond to larger θ . In the same time, rings with equal $\Delta\cos(\theta)$ contain equal area for any value of θ . For the particular case of the isotropic distribution, the cosine representation leads to constant ODF (equal to $1/4\pi^2$), whereas the

representation through θ have to include the factor $d(\cos\theta)=\sin(\theta)d\theta$ to provide a proper normalization.

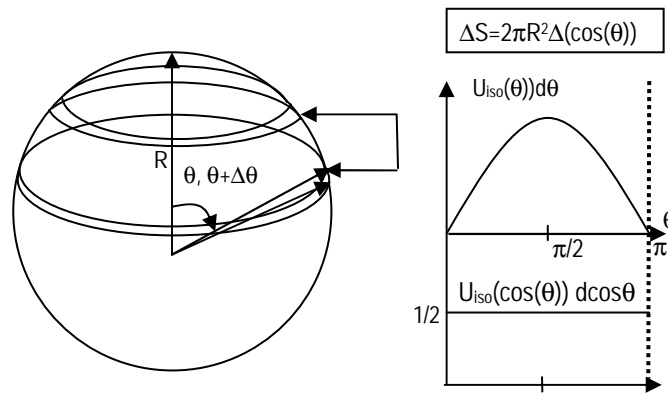


Fig 2.5 Rings around sphere with equal $\Delta\theta$ contain more area if they correspond to larger θ . Rings with equal $\Delta\cos(\theta)$ contain equal area for any θ . The orientation probability for isotropic orientation distribution U is proportional to surface element $\sin\theta\Delta\theta=\Delta\cos(\theta)$ while it is constant if U expressed as a function of $\cos(\theta)$.

It will be shown in the following section that in the case of NMR analysis it is often more convenient to use the representation of the ODF via series of the «moments», for example the generalized spherical harmonics [II.11].

$$W(\theta, \varphi, \psi) = \sum_{n=0}^{\infty} \sum_{m=-1}^{+1} \sum_{k=-1}^{+1} w_{nmk} Y_{nmk}(\cos(\theta)) e^{-im\varphi} e^{-im\psi} \quad (2.5)$$

In many cases, yet, the one or more Eulerian angles are not relevant. For example the bulk polymers in a shape of film or a fiber have overall orthorhombic or hexagonal symmetry, respectively. For different types of liquid crystals, at least an axially symmetrical ordering has to be always assumed. Therefore, depending on the type of system symmetry the dimensionality of the ODF can be reduced to one or two dimensions. Some examples of the ODF's which can be found in real mesogenic and other partially ordered systems are demonstrated on **Fig 2.6** The two-dimensional orientation distribution function is denoted here like a $V(\varphi, \cos(\theta))$. For the particular case when only one (usually azimuthal) angle is relevant the one-dimensional function $U(\cos(\theta))$ will be used.

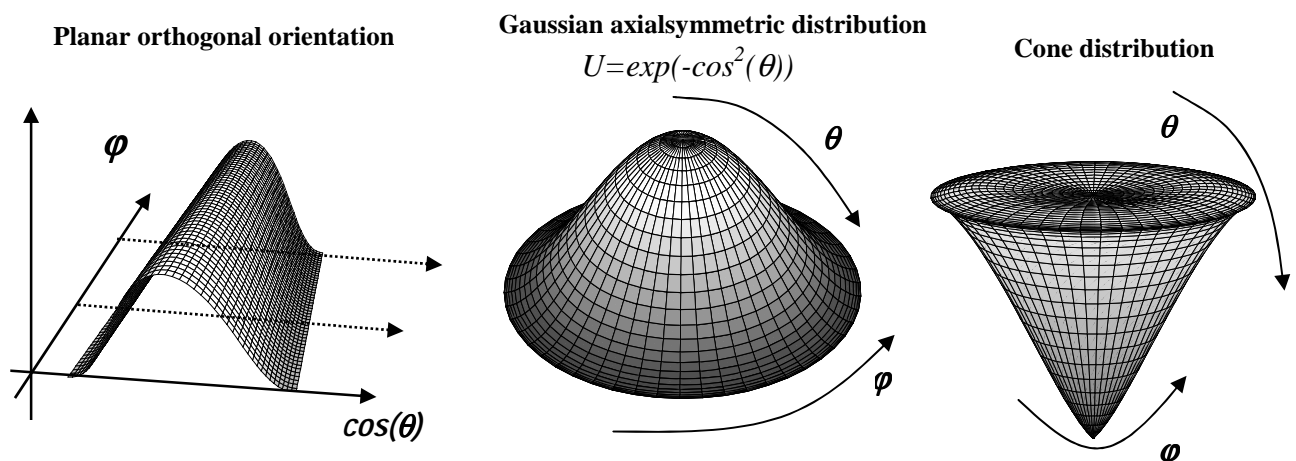


Fig 2.6 The examples of the orientation distribution functions .

2.2.2 Methods of ODF examination by NMR lineshape analysis.

As it was shown in previous section, the anisotropic spin interaction by itself leads to specific pattern of the NMR lineshape. The form of the pattern is different depending on the type and the parameters of the interaction. The orientation distribution function enters the shape of the wideline spectrum in some hidden manner [II.6, 12-14]. The angular dependence of the NMR resonance frequency is given by the Eqn. 2.2 via the orientation of the magnetic field in principal axis system of the spin interaction tensor. Obviously, when some specific orientation distribution is present in the system, some of the angular areas and therefore the corresponding spectral position are more abundant. This leads to the changing of the lineshape function. It is argued that amount of interaction tensor main axes in the interval $\cos(\theta) \dots \cos(\theta)+d(\cos\theta)$, $\varphi, \varphi+d\varphi$ the number of which is $V(\varphi,\cos(\theta))d\cos(\theta)d\varphi$ contribute to the resonance position $\sigma.\sigma+d\sigma$ with intensity $S(\sigma)$.

$$S(\sigma)d\sigma = V(\cos(\theta), \varphi)d\cos(\theta)d\varphi \quad (2.6)$$

The wideline NMR spectrum can be written as the convolution of resonance frequency offset with the orientation distribution function $V(\varphi,\cos(\theta))$.

$$S(\sigma) = \int_0^{2\pi} d\varphi \int_{-1}^1 f(\sigma_0 - \sigma(\cos(\theta), \varphi))V(\cos(\theta), \varphi)d\cos(\theta) \quad (2.7)$$

Here $f(\sigma)$ denotes the intrinsic shape of the individual NMR line. In ideal case $f(\sigma)$ can be considered as δ -function. In practice, different broadening factors leads to the approximately Lorentz or Gaussian pattern for $f(\sigma)$. It was shown in Chapter I that for the uniaxial spin interaction (dipolar, quadrupolar or CS with $\eta=0$) the resonance frequency position depends only on azimuthal angle θ . In this case the information about only the one-dimensional variant of the orientation distribution function $U(\cos(\theta))$ can be extracted from lineshape analysis [II.6,13,14].

One of the frequently used ways of estimation of the ODF is using the specific model function with parameters to be found from the experiments. A number of works are devoted to the developing of the different models of the orientation distribution [II.15-19]. On the other hand, the model approach needs either strong theoretical background to build the realistic sample function with reasonable amount of unknown parameters. Another way round is a “brute force” method of the molecular dynamics simulation which costs a lot of time and computer resources. Therefore, we concentrate in our work on the model free approaches to the orientation distribution, trying to make the experimental results interpretation in the direct way and using only the most common *a priori* suggestions about the system to be studied.

2.2.3 Model Free approaches to ODF estimation using the NMR

There are basically three main “model free” possibilities of the $U(\cos\theta)$ estimation which can be found in literature on this subject:

1. Comparison of the lineshape of oriented and fully disoriented sample.

For one dimension of the ODF, the 2.6 can be rewritten as:

$$S(\sigma)d\sigma = U(\cos(\theta))d\cos(\theta) \quad (2.8)$$

For the isotropic orientation distribution, when $U(\cos(\theta))=1/4\pi$ the isotropic lineshape can be obtained as a «reference spectrum» from the same sample in disordered state.

$$S_{iso}(\sigma) = \frac{1}{4\pi^2} \frac{d\cos(\theta)}{d\sigma} \quad (2.9)$$

Therefore $U(\cos(\theta))$ can be estimated from the corresponding spectral lineshape of oriented sample by dividing it on reference spectrum $S_{iso}(\sigma)$ [II.20-22].

$$U(\cos(\theta)) = 4\pi^2 \frac{S(\sigma)}{S_{iso}(\sigma)} \quad (2.10)$$

The obvious disadvantages of this method are (i) high sensitivity to the unavoidable experimental error (noise, phase distortions) and (ii) necessity to be able to get the spectrum of the isotropic sample (that is not always possible).

2. Deconvolution procedure can be applied to the spectrum lineshape (or, sometimes, the set of lineshape for different sample orientation with respect to external magnetic field) described by Eqn. 2.7 to get the orientation function from the integral. In general, case this leads to the integral equation which solution is the so-called «Fredholm problem of the first kind». In general, it provides only the approximate and often unstable numerical solution for the subintegral function to be found. Nevertheless, using the specially adopted algorithms in some cases it is possible to restore the ODF from spectrum in the form of discrete histogram with reasonable solution stability and error [II.22, 23].
3. Method of the ODF «moments» determination [II.6] extensively developed by Hentschel, Sillescu and Spiess [II.11-14]. For one-dimensional ODF $U(\cos(\theta))$ the spherical harmonics of the expansion series in **Eqn 2.5** becomes Legendre polynomials.

$$U(\cos(\theta)) = \sum_{n=0} u_n P_n(\cos(\theta)) \quad (2.11)$$

The orthogonality of the P_n permits the calculation of the expansion coefficients as

$$u_n = \frac{2n+1}{2} \int_{-1}^1 U(\cos(\theta)) \cdot P_n(\cos(\theta)) d(\cos(\theta)) = \frac{2n+1}{2} \langle P_n \rangle \quad (2.12)$$

and can be treated like the «moments of the n-th order» of the orientation distribution function $U(\cos(\theta))$. For an isotropic distribution $\langle P_0 \rangle = 1$ and $\langle P_n \rangle = 0$ for $n > 1$. For completely ordered sample $\langle P_n \rangle = 1$. Clearly, zero-moment $\langle P_0 \rangle$ quantifies the isotropic part of the orientation distribution. $\langle P_2 \rangle$ is the second moment also known as the *orientation degree* or *macroscopic orientation order parameter*. For weakly ordered samples usually the moments higher than 4 are not relevant for the ODF description. In the same time, with the sample ordering increase the higher moments become more significant. Because the expansion treats molecular order like a perturbation of the isotropic state, it converges for weak order. To achieve converges for high order the ODF may be expanded, for instance, into planar or conical distributions (see **Fig 2.6**).

Because $\cos(\theta)$ enters only by its square into all the types of anisotropic spin interaction tensor constants (see section 2.1) a negative and positive $\cos(\theta)$ which means θ and $\pi - \theta$ cannot be distinguished by this method and $U(\cos(\theta))$ represents the only symmetrical part of the ODF. Therefore, only the coefficients u_n with even power of $\cos(\theta)$ survive in the series (2.11).

Turning to the one-dimensional ODF in expression 2.7 for spectral lineshape and substituting the Legendre series representation for $U(\cos(\theta))$ the Legendre subspectra analysis can be determined:

$$S(\sigma) = \sum_{n=0}^{\infty} \frac{2n+1}{2} S_{2n}(\sigma) \quad (2.13)$$

$$S_{2n}(\sigma) = \langle P_{2n} \rangle \int_0^{\pi} P_{2n}(\cos(\theta)) f(\sigma - \sigma'(\theta)) d \cos(\theta)$$

Here $S_{2n}(\sigma)$ represents the subspectra corresponding to different moments $\langle P_{2n} \rangle$ of the orientation distribution function. Formula 2.13 demonstrates a general approach to the Legendre subspectra analysis. The following steps may depend on many practical aspects of the system to be studied. The application of this approach is restricted by the symmetry requirements mentioned above, that is to cylindrical molecules, macroscopically uniaxial samples and uniaxial tensors of anisotropic spin interactions. For many samples this conditions are fulfilled when using dipolar interaction between protons, deuterons in aliphatic bonds or axially symmetric chemical shift of ^{13}C nuclei [II.7,14, 25]. In simplest variant when the principal axis of the spin interaction tensor is oriented along the molecular segment which orientation is studied, the

determination of the ODF moments according to **2.13** can be performed by direct fitting of the

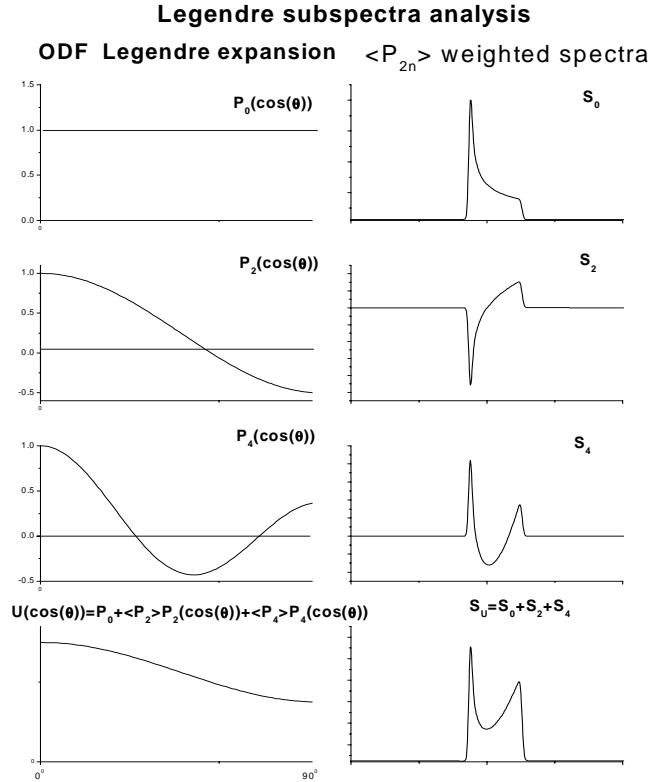


Fig 2.7. Method of the Legendre subspectra analysis for axial symmetric CS tensor. Left column: expansion terms of the ODF $U(\cos\theta)$, Right: corresponding “ P_{2n} – weighted” subspectra. It should be noticed that the roots of the Legendre polynomial are directly reflected as zero-crossing in corresponding subspectra.

experimental spectra with the Legendre subspectra combination varying the $\langle P_{2n} \rangle$ parameters (see **Fig 2.7**). This method can be especially effective for moderate and weak ordering when the higher order moments of the ODF are not relevant.

The examples of Legendre subspectra analysis for the wideline NMR lineshape caused by the uniaxial CS tensor is shown on **Fig 2.7**. The resonance frequency offset due to anisotropic chemical shift with asymmetry parameter $\eta=0$ according to consideration in section 2.1 can be written as:

$$\sigma(\theta) = \sigma_{iso} + \frac{2}{3} \Delta\sigma P_2(\cos(\theta)) \quad (2.14)$$

where $\Delta\sigma$ is CS anisotropy parameter and θ is the angle between the external magnetic field and CS tensor main axis. The intrinsic lineshape function $f(\sigma_0 - \sigma(\theta))$ can be recovered from the spectrum of powder (isotropic) sample:

$$S_0(\sigma) = \int_0^1 f(\sigma - \sigma_{iso} - \frac{2}{3} \Delta\sigma P_2(\cos(\theta))) d \cos(\theta) \quad (2.15)$$

by the deconvolution procedure or using the one-parametrical fitting with some sample function (normally **Gaussian** or Lorentz form) in the manner described in **2.1**. The coefficients $\langle P_{2n} \rangle$

can be chosen to provide the best fit of the analyzed spectra with the result of the Legendre subspectra summation according to 2.13. Fitting may be done «by-eye» or numerically using the appropriate algorithms for minimization of the residuals between calculated and experimental spectrum. The last variant, being more precise, requires a significant amount of the computation recourses, especially for the case of low signal-to-noise ratio in experimental data.

2.2.4. Relationship between NMR-concerned coordinates frames.

In general, , the situation with the angular dependence of spin interactions in NMR is

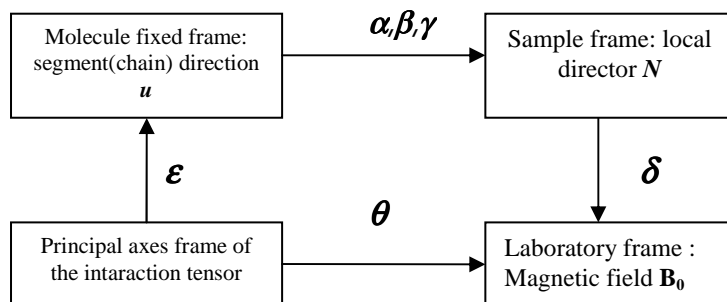


Fig 2.8 The relationship between coordinate frames relevant for the orientation ordering investigation. The transformation of the tensors to express it in terms of different set of angles can be performed using Wigner rotation matrices (see Appendix II).

rather complicated. While the orientation dependence of a resonance line position which enters into 2.13 as $f(\sigma_0 - \sigma(\theta))$ is given via the interaction tensor axes orientation with respect to external magnetic field B_0 , the orientational distribution function specifies a distribution of the preferential direction N in molecule-fixed coordinate frame. Generally, for the description of the orientation distribution of the molecular segments with arbitrary mutual orientation of molecular and spin interaction tensor axes, the one Eulerian angle is not sufficient.

Fig 2.8 shows the relationship between the different coordinate frames and the definitions of the mutual orientation angles. The first Euler angle α describes the azimuthal direction in which segment u is tilted. For the axially symmetric orientation (that is usually assumed for the oriented polymers and mesogenic samples) α is isotropically distributed and can be excluded from consideration by the integration over it. The polar angle β describes the tilt of the segment long axis with respect to the local director N . Angle γ describes the rotation of the segment around its long axis. The main axis of the spin interaction tensor is connected with the orientation of molecular segment by the angle ϵ . The spin interaction intensity, however, depends on the angle between the main tensor axis and the external magnetic field B_0 that gives the laboratory frame in addition to the molecular and spin interaction axes frames. The orientation of the sample (by its local director) in the laboratory frame is described by the angle δ . The general scheme of the frames interconnections is shown on **Fig 2.9** [II.25]

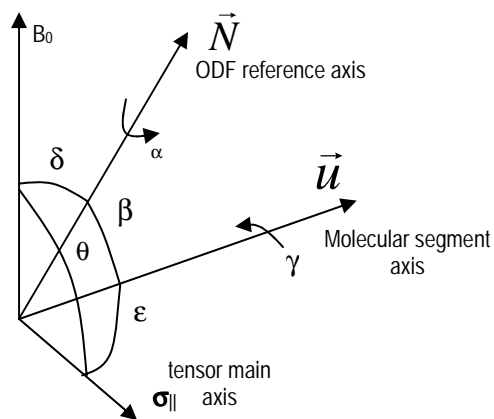


Fig 2.9. The set of angles describing mutual orientation of laboratory (B_0), local director (N) and molecular frames (u , CS). The polar angle β gives the tilt of the segment long axis with respect to the local director N . Angle γ describes the rotation of the segment around its long axis. The main axis of spin interaction tensor is connected with the orientation of the molecular segment by angle ϵ . The dependence on angle α is not relevant in axialsymmetric systems and can be averaged by the integration,

That way, to apply the methods of the Legendre subspectra analysis, it needs to develop the special approach in each specific case depending on the kind of the spin interaction tensor, which is used to probe the orientation distribution and the relationships between the relevant coordinate frames in sample. Basing on the approach described above the NMR spectrum lineshape can be analyzed also in somewhat different manner to get the necessary information. Instead of the expanding into subspectra, the wideline NMR pattern can be decomposed into their moments:

$$M_n = \int_{-\infty}^{\infty} (\sigma - \sigma_0)^n S(\sigma) d\sigma \quad (2.16)$$

It was shown by the Hentschel et al [II.13] that similar to expansion of the lineshape via the Legendre subspectra (2.9), the moments of spectral line can be expressed via the linear combination of the ODF's Legendre polynomial moments $\langle P_n \rangle$. By reversing of this dependence, the moments of the orientation distribution functions can be determined. The application of this procedure for the investigation the orientational order in the side-chain liquid crystalline polysiloxanes using the ^{29}Si NMR will be considered in the following section.

2.3 Main-chain molecular segments orientation investigation using ^{29}Si NMR spectra.

2.3.1. Method of the spectral lineshape analysis based on CS- tensor orientation.

As it was mentioned in Chapter I, the ^{29}Si NMR has significant advantages for investigation of the investigation of the main-chain orientation in polysiloxanes. Particularly, it seems to be quite effective method because the main contribution to the spectrum comes from the main chain silicon nuclei. The only other line, which could be detected, arises from the end group $-\text{Si}-(\text{CH}_3)_3$

with intensity about less than 5% compared to the main resonance. The orientation of siloxane segment can be therefore monitored by means of anisotropy of the chemical shift tensor. It was experimentally established, that for polyalkylsiloxane chains the chemical shift tensor is axially symmetrical with good accuracy, i.e two of three main values has equal shift $\sigma_{\perp}=(-16\pm 1)$ ppm and the third value is shifted by $\sigma_{\parallel}=(32\pm 1)$ ppm with respect to isotropic position $\sigma_{\text{iso}}=(\sigma_{\parallel}+2\sigma_{\perp})/3$. [II.25]. The difference between two positions gives the CS anisotropy value of $\Delta\sigma=(48\pm 1)$ ppm. The mutual orientation of the CS-tensor main axis (σ_{\parallel}), siloxane molecular segment (\mathbf{u}), local director (\mathbf{N}) as well as the relevant angles (particularly, the orientation of tensor axis with respect to external magnetic field \mathbf{B}_0) are shown in **Fig 2.10**

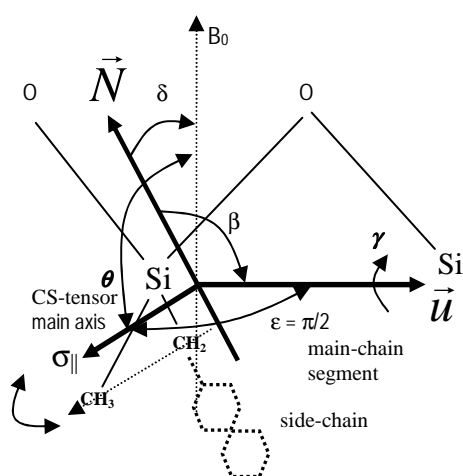


Fig 2.10 Relation between characteristic angles of different coordinate frames applied to the polysiloxane molecular unit. The molecular segment direction \mathbf{u} corresponds to Si-Si interconnection vector. The chemical shift main axis coincides with direction of the $\text{CH}_3\text{-CH}_2$ bond. Local director \mathbf{N} is given by the preferable orientation of side-chain mesogenic units.

The experimental ^{29}Si spectrum of fully disordered polysiloxane sample (**Fig 2.11**) is, of course, somewhat broadened as compared to the theoretically predicted pattern (**Fig 2.2**). The reason is mainly in distribution of CS tensor main values arising from conformational and structural disorder (for instance the distribution of intermolecular distances). The intrinsic lineshape $f(\sigma)$ of the individual resonance line recovered from the experimental spectrum by deconvolution procedure according to Eqn 2.15 can be fitted by the Gaussian function with satisfying accuracy (see **Fig 2.12**). [II.24]

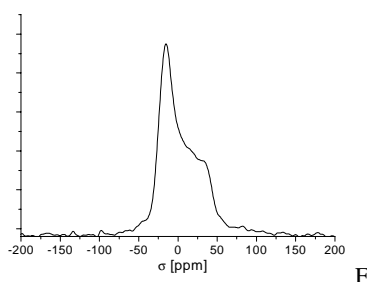


Fig 2.11. Experimental ^1H decoupled ^{29}Si NMR spectrum of disoriented (powder-like) polysiloxane M6 sample. The lineshape is determined by the axially symmetric CS tensor with $\Delta\sigma=48$ ppm.

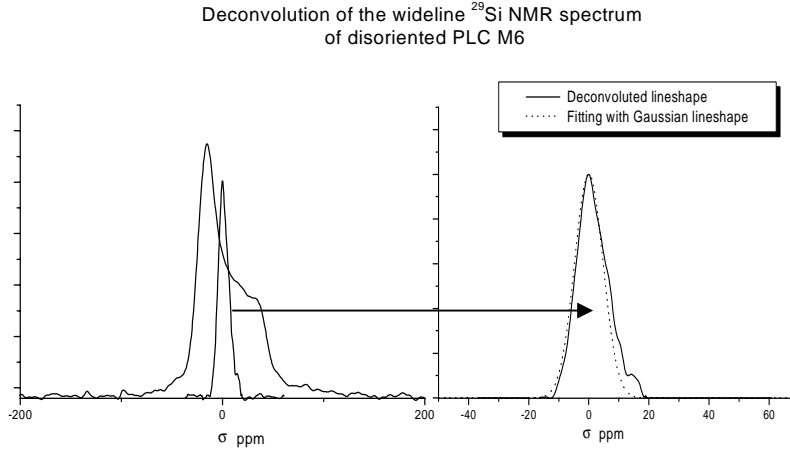


Fig 2.12. The example of the of powder polysiloxane ^{29}Si CS NMR spectral pattern deconvoluting in order to obtain the intrinsic lineshape. Deconvoluted line (right) can be fitted with with the Gaussian function that is typical for the polymer samples. The broadening parameter and the lineshape characterize the thermal motion and tensor parameters variety because of the conformation distribution.

In oriented sample, where some orientations of CS-tensor σ axes is more probable than others, the deformation of the lineshape pattern from the isotropic one takes place according to more or less abundant spectral positions corresponding to specific angular directions. The clear evidence of the non-isotropic ordering of σ main axes in the sample comes when the CS-spectral patterns are recorded with different orientation of the sample local director N with respect to external magnetic field. Varying angle δ the maxima of orientation distribution function $U(\theta)$ and therefore the maxima of the spectral intensity $S(\sigma(\theta))$ (eqn 2.8) can be shifted to different positions (see **Fig 2.13.**)

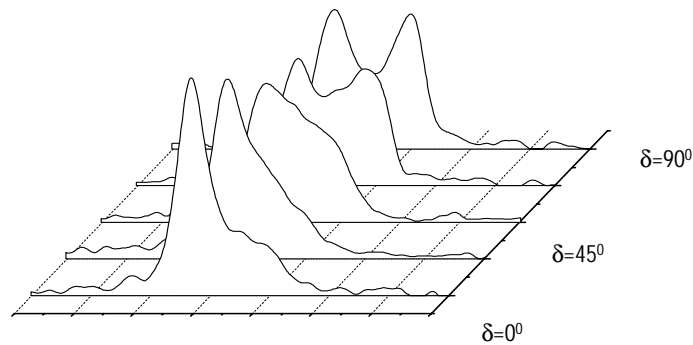


Fig 2.13 ^{29}Si spectra of oriented polysiloxane M6 recorded under different orientation of the local director with respect to magnetic field. With sample rotation the maxima of the CS axes ODF is shifted to the different positions with respect to the external magnetic field. This is reflected in the variation of the spectral density for the same position together with angle δ changing.

In our case we are interested in the distribution of orientations of the main-chain segments u , which have a perpendicular orientation with respect to the CS tensor main axis ($\varepsilon=90^\circ$). Hence, when $\delta=0^\circ$, u can particularly has either parallel or perpendicular orientation to B_0 In first case the σ main axis is preferably perpendicular to B_0 which leads to strong enhancement of $\sigma=\sigma_\perp$ spectral position intensity. In the other case all angles between σ and B_0 are possible. Due to the

axialsymmetry of the ^{29}Si CS-tensor the wideline NMR spectrum provides only one-dimensional information about the distribution of the polar angles of CS main axis orientation θ , denoted as orientation distribution function $U(\theta)$.

In principle, $U(\theta)$ could be obtained by the direct dividing procedure of the spectra of oriented and unoriented samples (2.10) or by the method of Legendre subspectra analysis described in previous section. However, the spectra of polysiloxanes have a strong inhomogeneous broadening of the intrinsic lineshape $f(\sigma)$ and, therefore, the rounding-off of the wideline spectrum $S(\sigma)$. This makes the direct analysis of the spectral pattern very complicated. Therefore, the method of the spectral line moments and their connection to the moments of the $U(\theta)$ Legendre expansion seems to be most appropriate in this case.

Replacing the integrand of Eqn 2.16 by 2.8 and 2.14 we get

$$M_n = (2\Delta\sigma/3)^n \langle P_2^n \rangle \quad (2.17)$$

entering the notation:

$$m_n = \frac{M_n}{(2\Delta\sigma/3)^n} \quad (2.18)$$

The powers of the $P_2(\cos(\theta))$ can be expanded according to (2.12) via the finite sum of the Legendre polynomials of even order.

$$\begin{aligned} m_1 &= \langle P_2 \rangle_{CS} \\ m_2 &= \frac{11}{35} \langle P_4 \rangle_{CS} + \frac{2}{7} \langle P_2 \rangle_{CS} + \frac{1}{5} \langle P_0 \rangle_{CS} \\ m_3 &= \frac{18}{77} \langle P_6 \rangle_{CS} + \frac{108}{385} \langle P_4 \rangle_{CS} + \frac{3}{7} \langle P_2 \rangle_{CS} + \frac{2}{35} \langle P_0 \rangle_{CS} \end{aligned} \quad (2.19)$$

Because of the normalization conditions, $\langle P_0 \rangle_{CS}$ has the value $\frac{1}{2}$ if $\cos(\theta)$ has its full range from -1 to +1 ($\theta = [\pi..0]$) and 1 if the interval is restricted to $[0..1]$ ($\theta = [\pi/2 ..0]$).

$$\begin{aligned} \langle P_2 \rangle_{CS} &= m_1 \\ \text{Relations 2.19 can be inverted as : } \langle P_4 \rangle_{CS} &= \frac{35}{18} m_2 - \frac{10}{18} m_1 - \frac{7}{18} \\ \langle P_6 \rangle_{CS} &= \frac{77}{18} m_3 - \frac{7}{3} m_2 - \frac{7}{6} m_1 + \frac{2}{9} \end{aligned} \quad (2.20)$$

The moments m_n can be obtained directly according to (2.18) and (2.16) using the wideline ^{29}Si spectrum. To get the Legendre moments $\langle P_{2n} \rangle$, unambiguously characterizing the orientation distribution function $U(\theta)$, the equation 2.20 is then applied. In practice, an additional step is required due to the problem of the accuracy of the reference point determination which has to be chosen so that $m_1=0$. Theoretically, m_1 represents the shift of the gravity center between the

spectrum of oriented and disoriented sample. For a weak orientation order degree, which is typical for polysiloxanes, this shift is comparable to the experimental error. Therefore, the wideline ^{29}Si spectrum lineshape was recorded at different values of angle δ which describe the tilting of the sample local director with respect to external magnetic field B_0 (see **Fig 2.13**). Because of the axial symmetry of sample orientation, the angular dependence of the Legendre moments will be given by:

$$\langle P_{2n} \rangle_{CS}(\delta) = \langle P_{2n} \rangle_{CS}(0) \cdot P_{2n}(\cos(\delta)) \quad (2.21)$$

It is now possible to get the $\langle P_{2n} \rangle(0)$ either by fitting of the $\langle P_{2n} \rangle(\delta)$ curve using relations (2.20). The alternative variant is to use the orthogonality conditions of the Legendre polynomials:

$$\int_{-1}^1 P_l(x) P_k(x) dx = \frac{2l+1}{2} \delta_{lk}$$

which allows one to select from the linear combinations (2.19) one by one all the moments $\langle P_{2n} \rangle$ to be found just by the integration with corresponding Legendre polynomial. This can be done with higher accuracy than by using of gravity center shift of the wideline pattern.

2.3.2 ODF ambiguity caused by transversal anisotropy and CS tensor symmetry

It should be recollected that $U(\cos(\theta))$ is still only an intermediate result. The purpose is to get the orientation distribution of the molecular segments \mathbf{u} with respect to local director \mathbf{N} . The determination of latter is only possible using some additional information about the distribution of CS tensor axes in a plane perpendicular to \mathbf{u} . In the case of *transversal isotropy* [II.25] of the CS tensor main axes distribution, (i.e the equal probability for all of their orientations in the plane perpendicular to the segment \mathbf{u}) the estimation of segment orientation degrees $\langle P_n \rangle_S$ will be possible simply by means of the multiplication with the corresponding Legendre polynomial of the cosine of interconnection angle ε .

$$\langle P_n \rangle_{CS} = \langle P_n \rangle_S \cdot P_n(\cos(\varepsilon)) \quad (2.22)$$

Nevertheless, for the backbone segments of LCSP, the essential deviation from transverse isotropy can take place. A rotation of the main-chain segments around own axis requires different conformations of the spacer and different excluded volume space (see **Fig 2.14**)

Therefore, a violation of the transverse isotropy has to be expected leading to the γ -dependent *correction terms*. In extreme cases, it can be not only a minor correction, but also even reversing of the sign of the orientation order degree. Consequently, because of the possible transversal anisotropy of the tensor axes distribution, the comprehensive approach demands

considering a two-dimensional distribution function $V(\cos(\beta), \gamma)$, to determine the orientation of the molecular segment u from the orientation of the CS-tensor. In the same time, the axially symmetric CS-tensor of ^{29}Si in polysiloxanes, in general, provides only one-dimensional information about the own orientation. To overcome this problem some *a priori* suggestions about the type of γ -dependent correction for the $U(\cos(\beta))$, have to involved into consideration. For example, the analysis of two-dimensional ODF $V(\cos(\beta), \gamma)$ and the corresponding moments of the orientation order can done if to suggest that the correction term can be separated on the γ -dependent and independent parts:

$$V(\cos(\beta), \gamma) = 1/2\pi U_0(\cos(\beta)) + U_1(\cos(\beta)) \cdot g(\gamma) \quad (2.23)$$

Where $U_0(\cos(\beta))$ is **transversally independent part of V**, and U_1 represents the amplitude of the γ -dependence. The detailed analysis of this specific case can be found in [II.25]. Thus, to prove

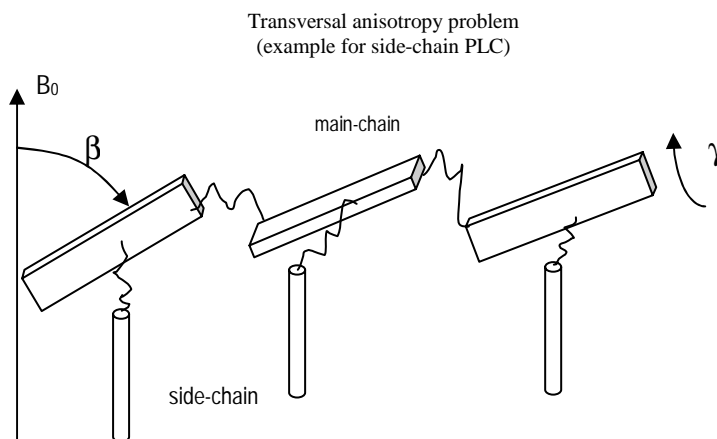


Fig 2.14 An illustration of the transversal anisotropy problem for the main-chain segment orientation in the polysiloxanes. Different angles γ require different conformations even for the same angle β , that leads to the violation of the isotropic distribution for γ (transversal anisotropy)

the correctness of different model approaches and simplifications some independent information about the orientation of the molecular segments is required. Such information can be obtained by using a method directly sensitive to the orientation of the molecular segment. This allows one avoiding the problems of the ambiguity of the data interpretation discussed above. Moreover, if the moments of the segments ODF $\langle P_{2n} \rangle_s$ could be determined directly by the method different from the ^{29}Si CS-spectrum analysis, the correction terms in Eqn 2.23 caused by the transversal anisotropy can be estimated. The possibility for such an alternative method employing will be considered in the following section.

2.3.3 Using direct dipolar interaction of ^{29}Si pairs for main-chain segment orientation study.

To get information about the orientation of the molecular segment independently from the methods of the CS-tensor orientation, some alternative tensor spin interaction should be used.

It can be seen on **Fig 2.10** that the orientation of the segment \mathbf{u} coincides with the interconnection vector of two silicon atoms. Therefore, the most natural decision is to use the angular dependence of direct dipolar interaction to probe the orientation distribution of these vectors. The dipolar interaction leads to the splitting of each energy levels (and therefore the resonance line) on two and the value of the splitting depends on the angle between the vector, which connects the involved nuclei, and the external magnetic field. In time domain NMR signal it appears like amplitude and, generally, the phase modulation of the resonance signal with the *dipolar splitting frequency*. The angular dependence of the dipolar splitting frequency is represented via the second Legendre polynomial that makes natural to perform the analysis of the ODF in terms of the moment expansion, as well as in the case of the CS-tensor spectrum. For example, the method of moment expansion similar to the one described for the ^{29}Si CS-spectrum can be applied to determine the orientation order in low-molecular liquid crystals using the second moment of the wide-line ^1H spectrum mainly determined by the direct dipolar coupling [II.19]. For the polysiloxane LCSP samples the dipolar interaction of the protons in phenyl ring was used to get the information about the ordering of the side-chain mesogenic units which determine the macroscopic orientation of whole sample (local director N)[II.26]. In the case of ^{29}Si NMR in polysiloxanes, yet, a sufficient difficulties can be foreseen, which makes problematic the employing of dipolar interaction for the orientation distribution studies.

The first problem is concerned with natural abundance of the ^{29}Si nuclei that is 4.7% of total amount of the silicon atoms in any sample. The rest of the atoms contain the ^{28}Si nuclei which have zero spin ($\mathbf{I}=\mathbf{0}$) and, therefore, do not contribute to the NMR signal. The enrichment with the ^{29}Si nuclei is technologically very problematic and expensive and applicable not to all the sort of the samples, especially in the case of polymers. That way, the NMR signal from the ^{29}Si is intrinsically low that leads to the essentially long measurement period to get reasonable signal-to-noise ratio in experiment. Situation becomes more difficult when the dipolar interaction between two ^{29}Si nuclei needs to be observed. Obviously, at natural abundance only less than 10% of all the ^{29}Si nuclei (or $\approx 0.005\%$ of total silicon amount) in the sample establish the coupling pairs (see **Fig 2.15**). Thus, the 90% of the NMR signal comes from non-coupled spins and does not give any information about the ^{29}Si - ^{29}Si dipolar interaction. Therefore, the useful signal (i.e. signal of coupled spins) has to be separated, in some way, from the significantly higher signal of non-coupled ^{29}Si . The second problem arises from the low strength of the dipolar interactions between two ^{29}Si as compared to the interaction caused by other anisotropic terms of nuclear Hamiltonian, particularly the chemical shift. From the quantum, chemistry calculations the dipolar splitting frequency for coupled ^{29}Si can be roughly estimated as 200...300 Hz. In the same time, it was shown in previous section that the total width of the CS-

pattern is of the order of CS anisotropy constant value (about 48 ppm for polysiloxanes). For the external magnetic field **9.4T**, using to measure the spectra, this gives the value about 3000Hz, that is on one order of magnitude higher than dipolar splitting. In addition, the intrinsic line (obtained from the ^{29}Si wideline spectrum deconvolution) is broadened up to 500Hz because of the structural conformation inhomogeneity or CS parameters distribution.

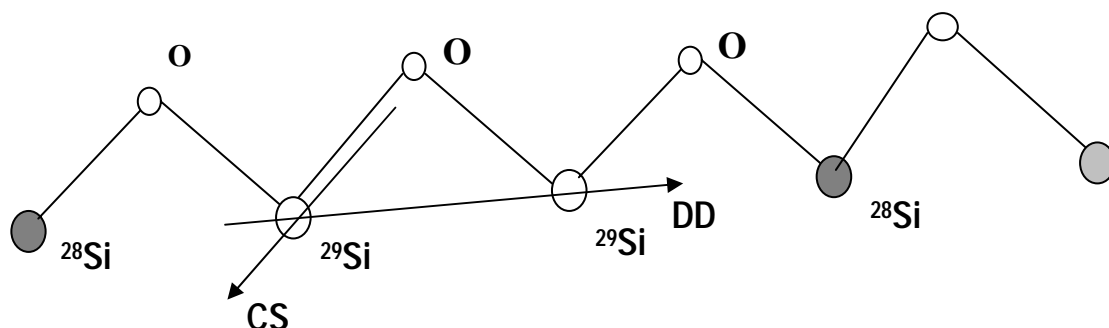


Fig 2.15 Only 5% of nuclei are ^{29}Si spins, which contribute to NMR signal. The rest are ^{28}Si (95% of whole Si in the sample at natural abundance) which give no signal. The non-coupled spins are, therefore, give 90% of whole signal and the coupled ones only 10%.

These factors cover the dipolar splitting in the ^{29}Si NMR spectrum and do not allow observing it directly. For this reason, the special technique has to be developed and applied to *(i)* separate the signal of coupled and non-coupled spins and *(ii)* to get the information about the dipolar coupling in presence of the resonance line inhomogeneous broadening (which may exceed the dipolar coupling in a factor of 10) due to another types of nuclear spin interactions. The solution of the theoretical and practical aspects of the mentioned above problems represents the main subject of current work and will be considered in the following chapters.

Chapter III. Callaghan echo combination: theory and application for direct dipolar interaction of rare spin pair detection.

Recently, Callaghan and Samulski proposed a method of the direct measurement of weak residual dipolar interaction [III.1,2]. The method is based on detection of the differential signal of the combination of three types of spin echoes. The normalized evolution time dependence of the combination of three types of spin echo:

$$\beta(\tau) = (S_1(\tau) - S_2(\tau) - S_3(\tau)) / 3S_0 \quad (3.1)$$

where $S_{0,1,2,3}$ represents the corresponding types of the signal

$$\begin{aligned} S_0 - \left(\frac{\pi}{2} \right)_x & \text{ - FID} \\ S_1(\tau) - \left[\left(\frac{\pi}{2} \right)_x - \tau - \left(\frac{\pi}{2} \right)_y \right] & \text{ - "solid echo"} \\ S_2(\tau) - \left[\left(\frac{\pi}{2} \right)_x - \tau - \left(\frac{\pi}{2} \right)_x \right] & \text{ - "}\frac{\pi}{2}\text{"-Hahn echo"} \\ S_3(\tau) - \left[\left(\frac{\pi}{2} \right)_x - \tau - (\pi)_y \right] & \text{ - "}\pi\text{"-Hahn echo"} \end{aligned} \quad (3.2)$$

is called in [III.1] “ β -function”. The square brackets symbolically denote the type of well-known pulse sequence applied to observe the spin-echo signal [A2.2.7, III.3].

For the purpose of convenience, in future the term “ β -echo” will be also used in this work to denote the full time domain signal of the “threefold echo” combination (3.1-2). In the following section the theoretical consideration of this echo combination will be done using density matrix formalism. It will be shown that “ β -echo” has the effective selective properties for separation of the nuclear spin interaction described by linear and bilinear terms of nuclear Hamiltonian (see **AII.2**). This allows one observing a weak nuclear spin interaction caused by bilinear terms of Hamiltonian, in presence of strong linear interactions such as isotropic and anisotropic chemical shift, magnetic field inhomogeneity, etc).

3.1 Callaghan echoes combination: theoretical consideration using density matrix formalism

In following, we consider the effect of the described above echo combination, using the *ab initio* density operator approach for the case of a homonuclear system of two isolated spins $\mathbf{I} = \mathbf{S} = 1/2$.

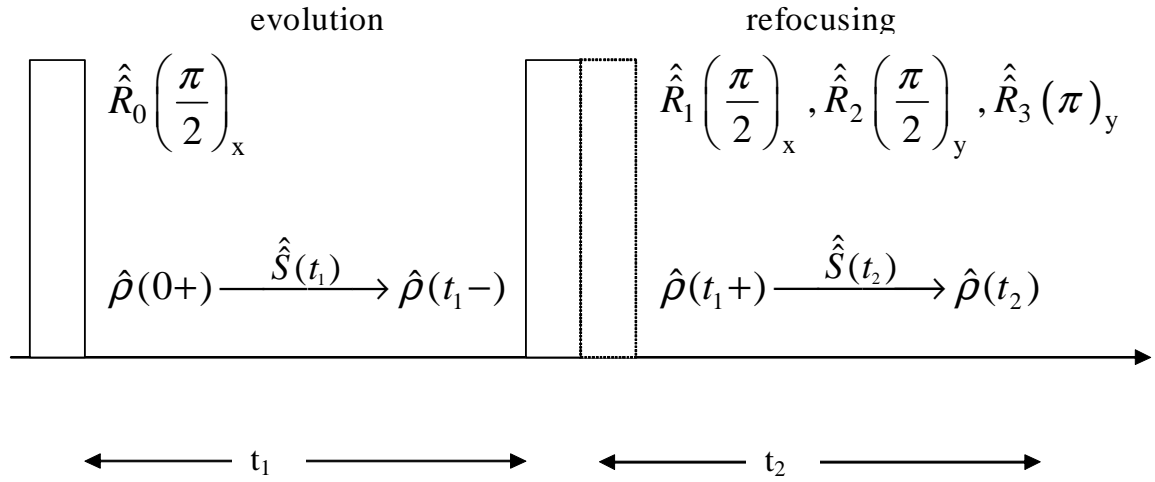


Fig 3.1 Calculation of the “ β -echo” evolution using density matrix formalism. The rotation operator \mathbf{R}_0 creates non-equilibrium coherences $\hat{\rho}(0+)$ (rf $\pi/2$ pulse is phase “x”). On the next stage the propagator S influences on density matrix, to describe its time evolution under the spin Hamiltonian. After application of the second rf-pulse operator for each echo ($\mathbf{R}_1, \mathbf{R}_2, \mathbf{R}_3$) and influencing onto each resulted density matrix $\rho_i(\tau+)$ by the propagator of refocusing period the differential magnetization $M_1-M_2-M_3$, (where $M_i = \text{Tr}[I_i \rho_i]$) can be calculated.

3.1.1 Density matrix and spin operators.

The standard high-temperature approximation for the density operator is used:

$$\rho_0 = \frac{1}{Z} \left(\hat{E} + \frac{\hbar \gamma B_0}{k T} \hat{I}_z + \hat{S}_z \right) \quad (3.3)$$

Where \hat{E} denotes unity matrix (for other notations see **Chapter.II** and **A2.3**) Further, we omit the entire constants and only the behavior of $\hat{I}_z + \hat{S}_z$ will be the subject of interest. The matrices of spin operators can be derived using the standard product operator formalism (see for detailed explanation (**A2.3**), [III.4,5]).

3.1.2.. Hamiltonians.

For the demonstration of the most important properties of “ β -echo” the homonuclear spin system with two kinds of spin interactions will be considered. All the

types interaction linear with respect to the spin operator (that is Zeeman interaction, chemical shift interaction, magnetic field inhomogeneity) can be combined together as:

$$\hat{H}_L = -\Omega \hat{J}_z = -\Omega(\hat{I}_z + \hat{S}_z) \quad (3.4)$$

The *indirect scalar interaction* of nuclear spins does not depend on the orientation of the spin system and therefore is not the subject of interest. The description of quadrupolar interaction for the spins $I=1$ is fully equivalent to the system of two spin $\frac{1}{2}$ [II.2]. The case of $I>1$ should be considered separately and some aspects of quadrupolar “ β -echo” theory will be mentioned later. That way, the only direct dipole-dipole interaction will be included in spin Hamiltonian (see **A2.2**).

$$H_D = -\frac{2}{3} \omega_{0D} (3I_z S_z - \mathbf{IS})$$

$$\omega_D = \frac{3}{4} \frac{\gamma^2 \hbar^2}{r^3} (3 \cos^2(\theta) - 1) = \omega_{0D} P_2(\cos(\theta)); \quad \omega_{0D} = \frac{3}{2} \frac{\gamma^2 \hbar^2}{r^3} \quad (3.5)$$

3.1.3. Rotation and evolution

To express the effect of different r.f-pulses on the density matrix, the rotation operators $\hat{\mathbf{R}}_{\mathbf{a}}(\psi)$ are used, describing the rotation of the magnetisation vector on the angle ψ around axis α . The time evolution of density operator during the period τ under the influence of some Hamiltonian \hat{H} can be expressed by the corresponding evolution operator or so called propagator (see **A2.3**, [III.4,5]).

$$\hat{S}(\tau) = e^{i\hat{H}\tau} \quad (3.6)$$

The influence of the rotation and evolution on density operator can be described with its matrix subjected by the unitary transformation with corresponding operator matrix $\hat{R}_{\alpha}(\psi)$ or $\hat{S}(\tau)$:

$$\hat{\rho}_R = \hat{R}_{\alpha}(\psi) \hat{\rho} \hat{R}_{\alpha}^+(\psi) \quad , \quad \hat{\rho}(\tau) = \hat{S}(\tau) \hat{\rho}(0) \hat{S}^+(\tau), \quad (3.7)$$

To make the expressions shorter the standard Liouville space superoperator notation will be used (**A2.3**):

$$\hat{R}\hat{A}\hat{R}^+ \Rightarrow \hat{R}\hat{A} \quad (3.8)$$

3.1.4. Initial condition

We start from the equilibrium density matrix taken according to (3.3) as $\hat{\rho}_0 = (\hat{I}_z + \hat{S}_z)$. As we deal with the homonuclear case, further we will consider the combined spin operator $\hat{J}_i = \hat{I}_i + \hat{S}_i$, $i = x, y, z$. The first pulse $R_x(\pi/2)$ rotates the magnetization into the direction of the y axis preparing non-equilibrium density matrix $\rho(0+)$:

$$\hat{\rho}(0+) = \hat{R}_x\left(\frac{\pi}{2}\right)\hat{\rho}_0 = \hat{J}_y \quad (3.9)$$

Then the propagator (3.6) has to be applied to find the resulting density matrix in the end of the first evolution period t_1 - (see **Fig 3.1**).

$$\hat{\rho}(t_1-) = \hat{S}(\tau)\hat{\rho}(0+) \quad (3.10)$$

On the next step the corresponding rotation operators $\hat{R}_\alpha^i(\psi)$ (see eqn. (3.7)) should be employed for each component ($i=1,2,3$) of β -echo combination individually to implement the second pulse influence on density matrix.

$$\hat{\rho}_i(t_1+) = \hat{R}_\alpha^i(\psi)\hat{\rho}_i(t_1-) \quad (3.11)$$

Finally, the evolution operator being applied to the new coherence state after the second pulse provide us the picture of all 3 variants of density matrix time development in the refocusing period t_2 . (**Fig 3.1**) Considering moment $t_1=\tau$ and $t_2=\tau+t$ the resulting states of the spin system for each echo pulse sequence can be represented as:

$$\begin{aligned} \hat{\rho}_1(2\tau+t) &= \hat{S}(\tau+t)\hat{R}_y\left(\frac{\pi}{2}\right)\hat{S}(\tau)\hat{\rho}(0+) - \text{"solid echo"} \\ \hat{\rho}_2(2\tau+t) &= \hat{S}(\tau+t)\hat{R}_x\left(\frac{\pi}{2}\right)\hat{S}(\tau)\hat{\rho}(0+) - \text{"}\pi/2\text{-Hahn echo"} \\ \hat{\rho}_3(2\tau+t) &= \hat{S}(\tau+t)\hat{R}_y(\pi)\hat{S}(\tau)\hat{\rho}(0+) - \text{"}\pi\text{-Hahn echo"} \end{aligned} \quad (3.12)$$

The observable transversal magnetization $M_i(2\tau+t)$ is given by:

$$M_\pm^k(2\tau+t) = \langle \hat{M}_\alpha^k \hat{\rho}_k(2\tau) \rangle = Tr[\tilde{M}_\pm^k \tilde{\rho}_k] \quad (3.13)$$

where $\tilde{M}_\pm^k = J_\alpha^k \pm iJ_\alpha^k$; $k = 1, 2, 3$ represents the matrices of the corresponding spin operators (**AII.3,III.6**)

Combining all three terms according to (3.1) the *real component* of the β -echo amplitude dependence on the echo delay time τ can be expressed as:

$$M_x^\beta = \frac{M_x^1 - M_x^2 - M_x^3}{3M_0} \quad (3.14)$$

$$M_x^\beta = \frac{2}{3} \sin(\omega_D \tau) \sin(\omega_D \tau + \omega_D t) = \frac{2}{3} \sin(\omega_D \tau) \cos(\omega_D t - (\frac{\pi}{2} - \omega_D \tau)) \quad (3.15)$$

For the simplicity, the frequency offset Ω is set to 0 in the expression 3.15. The case when it plays a role will be considered in the last sections of this chapter. The “ β -function” introduced by Callaghan can be obtained by substituting in (Eqn 3.15) value $t=0$:

$$\beta(2\tau) = \frac{1}{3} [1 - \cos(2\omega_D \tau)] \quad (3.16)$$

From the first part of 3.15 it is also can be seen why “ β -function” was sometimes named “sine correlation function”. Both *amplitude and phase* of the “ β -echo” signal depends on the correlation of the bilinear (dipolar) interactions in first and second evolution period. This feature as well as the other properties of the β -echo, which make it valuable for the practical application in the present work will be considered in the following section.

3.2 General properties of “ β -echo” and “ β -function”.

Generally, the following interpretation of β -echo can be done: All three types of echo involved into the combination 3.1 are able to “refocus” the linear interaction making the “time reversing” operation for the corresponding terms of Hamiltonian. And only “solid echo” has the same properties also with respect to bilinear terms. Remembering, that for linear terms of Hamiltonian the refocusing pulse flipping angle $\psi = \pi/2$ is exactly by a factor of 2 less effective as compared to the $\psi = \pi$, and combing the signals in the manner shown by (3.1-2) the result influenced only by the bilinear terms of Hamiltonian can be obtained. Considering equation (3.15) the following conclusion about the “ β -echo” signal can be issued:

The differential signal of the three echoes is not symmetrical with respect to the moment $t=0$, which denotes the equal time of evolution and refocusing period for each individual echo. Both amplitude and phase of the “ β -echo” signal depends on the correlation of the bilinear (dipolar) interactions in first and second evolution period. In our case the dipolar interaction modulates the resulted signal following the moment $t=0$ by

amplitude with a factor of $\frac{2}{3} \sin \omega_D \tau$ and by phase with a factor of $\frac{\pi}{2} - \omega_D \tau$. From this fact

originates two practically important consequences concerning β -function properties:

1. The intensity of the β -echo and so the value of β -function is always equal zero if no bilinear interaction terms present in nuclear spin Hamiltonian.
2. The amplitude of “ β -echo” will be zero if there is no opportunity for the spin system to evolve under the bilinear Hamiltonian i.e. evolution period $\tau=0$.

The property (1) means that β -echo has effective selective properties with respect to different type of nuclear interactions. Only the spins undergoing the interactions, which are described by the Hamiltonian containing bilinear terms will contribute to the β -echo. The property (2) is important for the practical implementation of the β -echo in experiment, because, as well as many of other compensation schemes in NMR, it is sensitive to the pulse duration errors. The role of pulse imperfections in β -echo experiment will be discussed in Chapter IV.

The above consideration shows, that combining together three kinds of spin echo it is possible to separate the NMR signals, which originate from the spins involved into different types of spin interactions – linear and bilinear. However, it still does not take into account two important facts:

1. The transversal relaxation, which makes influence on the spin system during the evolution period.

2. The macroscopic distribution of the orientation of internuclear vectors for individual spin pairs with respect to the magnetic field, which leads to distribution of the dipolar coupling strength for different spin pairs (3.5). According to Eqn 3.15 one can expect that the resulting β -echo will be a superposition of the signals modulated by amplitude and phase in different manner. In following sections both these aspects, important for comparison the theory and experimental results of β -echo application, will be considered.

3.3 The role of spin-spin relaxation

In each echo experiment, which contribute to “ β -echo”, both in evolution and refocusing period (Fig 3.1) the spin system is influenced by the random fluctuation of the local magnetic fields. This process irreversibly destroys the coherence (i.e. off-diagonal elements of density matrix) order, leading to the *spin-spin relaxation* and manifest itself as

a decay of transversal components of macroscopic (observable) magnetization. The characteristic time of this decay is defined by the intensity the spin-spin interactions and by the rate of its fluctuation. It is also strongly connected to the parameters of the intra and intermolecular motions [III.8-12]. In more details the questions of spin-spin relaxation theory and its application for the investigation of the parameters of the molecular motion will be considered in Chapter V. Generally, it should be mentioned that transversal relaxation effect in β -function (Eqn 3.16) can be taken into account by multiplication the resulted expression for the transversal magnetization amplitude with a “relaxation function” $R(2\tau)$. The actual expression for this function depends on a number of factors and parameters of the molecular dynamics into which the spins are involved. However, for big amount of practical cases the transversal relaxation leads to the exponential decay and can be characterized with only one parameter - *transversal relaxation time* T_2 :

$$\beta_R(2\tau) = \beta(2\tau)e^{-2\tau/T_2} \quad (3.17),$$

where $\beta(2\tau)$ -“non-relaxed β -function” which comes from (Eqn 3.16).

3.4 Spatial orientation distributions and β -function.

In the previous consideration in was shown that the β -echo intensity time dependence (β -function) in the case of homonuclear two spin $\mathbf{I}=1/2$ system is governed by the intensity of the dipolar interaction, via the magnitude of dipolar coupling constant in (3.16). As it was discussed above the value of the ω_D pre-factor includes the spatial part of dipolar Hamiltonian and depends on both distance between involved spins and the orientation of the interconnection vector of the spin pair with respect to external magnetic field \mathbf{B}_0 (Eqn 3.5). However, in practice the orientation distribution of the internuclear vectors connected to the molecular orientation is never uniform even in macroscopically ordered sample with molecular segments containing perfectly isolated spin pairs. (Fig 2.15). Hence, the orientation distribution function (see Chapter II) $U(\cos(\theta))$ should be included into consideration to take into account the amount of the spin pairs with specific orientation of internuclear vector. Thus, the contribution of the spin pairs for which internuclear vector lies within angular limits $\theta, \theta + d\theta$ can be expressed as:

$$d\beta_\theta = \beta(\omega_D(\theta)) \cdot U(\cos(\theta)) d\cos(\theta) \quad (3.18)$$

To get the resulted expression for the β -function evolution, the eqn (3.18) should be integrated over all possible orientation of the internuclear vectors. Finally, with account of transversal relaxation we come to the following result for the β -function evolution:

$$\beta_{\Sigma}(2\tau) = \frac{1}{3} \left[\int_0^1 (1 - \cos(\omega_D(x)2\tau)) \cdot U(x) dx \right] R(2\tau), \quad x = \cos(\theta) \quad (3.19)$$

For the exponential transversal relaxation function $R(2\tau)$ (which is valid for big amount of cases) we get:

$$\beta_{\Sigma}(2\tau) = \frac{1}{3} \left[\int_0^1 (1 - \cos(\omega_D(x)2\tau)) \cdot U(x) dx \right] e^{-\frac{2\tau}{T_2}}, \quad x = \cos(\theta) \quad (3.20)$$

The influence of the orientation distribution on the β -function evolution behavior will be considered in the following sections.

3.4.1 Powder averaging

One of the most frequent situations, which also have significant practical importance, is the full disorder of the molecular segment orientation leading to the isotropic orientation distribution. In this case the normalized ODF has no angular dependence $U(\cos(\theta))=1/4\pi$. For such an occurrence, the integral **3.20** can be evaluated analytically:

$$\beta_{\Sigma}(2\tau) = e^{-\frac{2\tau}{T_2}} \left[1 - \sqrt{\frac{\pi}{3\omega_{0D}}} C(y) F_c(\sqrt{y}) - S(y) F_s(\sqrt{y}) \right] \quad (3.21)$$

where $y = 2\omega_{0D}\tau$, $C(y) = \cos(y)$, $S(y) = \sin(y)$ and

$$\int_0^1 \cos(ax^2) dx = \sqrt{\frac{\pi}{2a}} F_c(\sqrt{a}), \quad \int_0^1 \sin(ax^2) dx = \sqrt{\frac{\pi}{2a}} F_s(\sqrt{a}) - \text{Fresnel integrals}$$

In this expression, the only parameter which directly depends on the spin interaction properties is the value of *dipolar coupling constant* ω_{0D} (we don't discuss the question concerning T_2 in the moment). This parameter (see Eqn **3.5**) includes the distance between coupled spins and its gyromagnetic ratio. Thus, it gives us a way to estimate the ω_{0D} from experiment just by the one-parametrical fitting with β -function the experimental data obtained from disordered sample. This will be of great importance for the next stage, when the β -function experimental data of the sample with some unknown orientation distribution function needs to be examined. The results of the simulation of the β -function evolution are represented on the **Fig 3.2**. Here, β -function was integrated with isotropic ODF (“powder averaging”) according to equation **3.20**. The value of the dipolar coupling constant $\nu_{0D} = \omega_{0D}/2\pi$ has been varied from 50 to 350Hz, (preliminary estimation for the samples of interest gives $\nu_{0D} \approx 220\text{Hz}$).

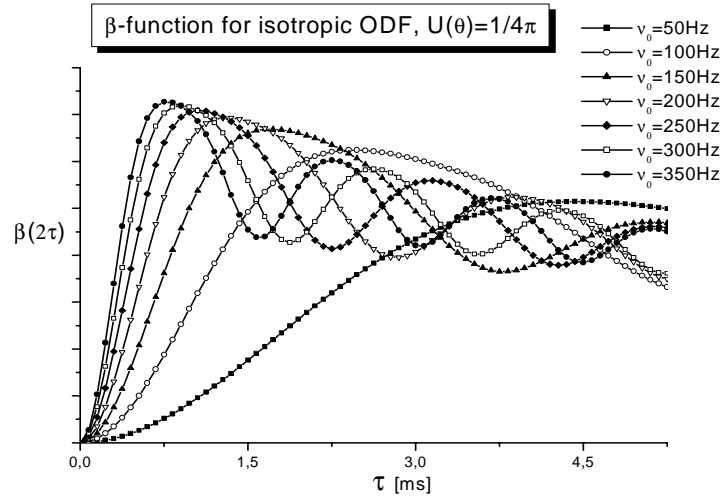


Fig 3.2 The result of simulation of β -function evolution for isotropic orientation distribution $U(\theta)=1/4\pi$ according to (Eqn 3.20). The value of dipolar coupling constant $\omega_D=2\pi\nu_0$ has been varied within frequency range 50-350Hz. Simulations have shown that the value of ω_0 makes considerable effect on the positions of the first and second maxima of the β -function.

Simulation shows that variation of ω_{0D} within 20-30%-provides a considerable effect on the behavior of β -function, which can be identified, visually by the shift of the position of the first and second maxima. That way, the dipolar coupling constant value can be determined from the powder averaged β -function experiment either with “by-eye” fitting or using nonlinear regression (with eqn. 3.21) methods.

3.4.2 Non-isotropic orientation distribution.

The simulation performed for the isotropic orientation distribution shows that the behavior of β -function changes significantly with the variation of the dipolar interaction strength. However, considering eqn. (3.20) it can be shown, that the role of the orientation distribution in the resulted function $\beta_{\Sigma}(2\tau)$ can be also sufficient when the orientation probability density differs for individual spin subsystems. The orientation distribution density $U(\theta)d\theta$ in 3.20 gives us the amount of spin subsystems, which internuclear vectors preferable orientation lay within angular range $\theta - \theta + d\theta$ with respect to magnetic field B_0 . These subsystems contribute to the resulting β -function with own individual frequency component $d\beta_{\theta}(2\omega_D(\theta)\tau)$ (3.18). If any orientation of the molecular segments presents in our system, some angular direction $d\theta$ will be more abundant with the spin subsystems than another. This leads to the variation of the contribution of these components into the shape of the curve $\beta_{\Sigma}(2\tau)$. Thus, the stronger orientation function $U(\theta)$ differs from the isotropic one the stronger resulting curve deviates from the presented in **Fig. 3.2** [III.1,2]. **Fig. 3.3**

represents the result of the simulation of such a “non-isotropic β -function” behavior for the case of the different modeling ODF's.

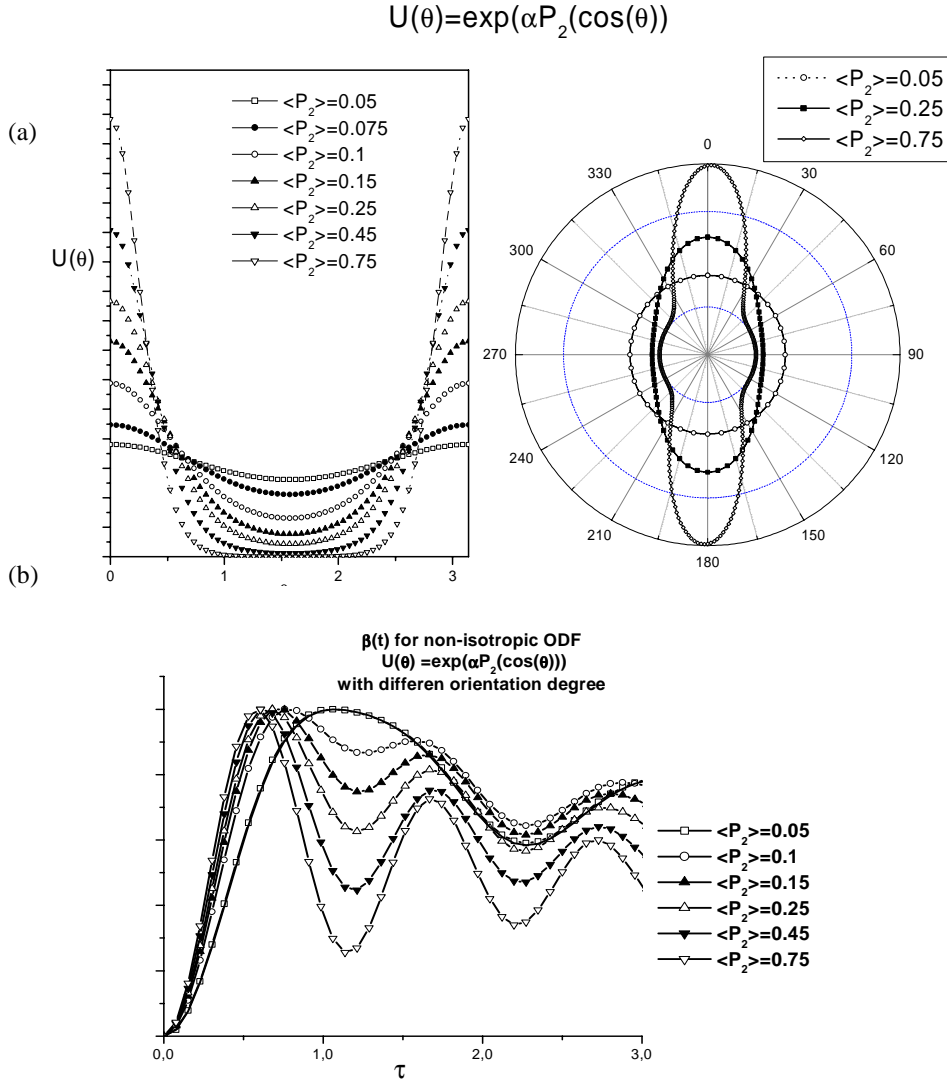


Fig 3.3 (a)-Examples of the orientation distribution for Gaussian-like orientation distribution function (3.22) of the internuclear vectors. The variation of the orientation degree parameter $\langle P_2 \rangle$ describes the different systems ordering state: from nearly isotropic ($\langle P_2 \rangle \approx 0$) to perfectly ordered ($\langle P_2 \rangle \approx 1$).

(b)-Numerical simulation of β -function dependence on the orientation degree parameter of the internuclear vectors distribution. Gaussian-like function $U(\cos(\theta)) = \exp(\alpha P_2(\cos(\theta)))$ (see **Fig 3.3a**) was used for calculations according to (3.20). The orientation degree was varied by manipulation with parameter α . Dipolar coupling constant was set to $\nu_D = 250 \text{ Hz}$. Simulation shows a significant sensitivity of β -function time evolution on the orientation degree parameter.

As an example the Gaussian-like distributions function:

$$U_G(\cos(\theta)) = \exp(\alpha P_2(\cos(\theta))) \quad (3.22)$$

where $P_2(\cos(\theta))$ – is the second order Legendre polynomial, was used in simulations. The form of the $U_G(\cos(\theta))$ both in polar and Cartesian system are represented below on

Fig 3.3a. **Fig. 3.3** shows that the form of the β -function curve evolves remarkably with

changing of the parameter α , which regulates the *orientation degree parameter* $\langle P_2 \rangle$ of the current distribution (see Chapter II about *orientation degree*). For comparison the β -function corresponding to the uniform alignment of the internuclear vectors along the z-axis of the laboratory frame (magnetic field \mathbf{B}_0) and, thus, described by the δ -like orientation distribution function $U(\theta)$, is shown. The results of the numerical simulation show us that “non-isotropic” β -function is sensitive to the variations of the order parameter of the orientation distribution within full range of its possible values from 0 to 1. The non-linear regression methods can not be applied directly to the (3.20), because for the arbitrary form of $U(\cos(\theta))$ the analytical solution of the integral is not always possible. However, for the one or two parametrical ODF model a “by-eye” fitting or minimization procedure can give the approximation of the experimental data with reasonable error. Gaussian-like ODF model in some cases provides a good resemblance of the theoretically predicted and experimental values of different parameters concerned with the orientation properties of liquid crystals and polymers. However, the “fixed-model” approach in each special case requires a strong theoretical background for the model used for interpretation of the experimental data. For the liquid crystalline polymers, which are the subject of our interest, the building of *ab initio* model of the orientation distribution seems to be a difficult task. That way, the «model-free» approach based on Legendre series described in Chapter II, appears to be more effective way to estimate the orientation distribution of our interest. The application of this approach to describe the β -function evolution for the system with arbitrary orientation degree and distribution is demonstrated by the **Fig 3.4**.

$$U(\cos(\theta)) = \sum_{n=0} \langle P_{2n} \rangle P_{2n}(\cos(\theta)) \quad (3.23)$$

Because of the axial symmetry of the orientation distribution $U(\cos(\theta))$ only even terms are relevant (Chapter. II). The expected values of the orientation degrees for the internuclear vectors distribution which can be estimated from the ODF's of the CS tensors main axes allows one restricting the series with maximum 4-order term without significant lost of the generality [III.13]. The normalization requires that the $\langle P_0 \rangle$ has the constant value $\frac{1}{2}$. The region of the values of $\langle P_2 \rangle$ and $\langle P_4 \rangle$ was chosen according the estimation which has been done in [III.13] for our samples and covers the one decade of relative variation. The variations of the ODF form for different values of $\langle P_2 \rangle$ and $\langle P_4 \rangle$ coefficients are shown on (**Fig 3.5**).

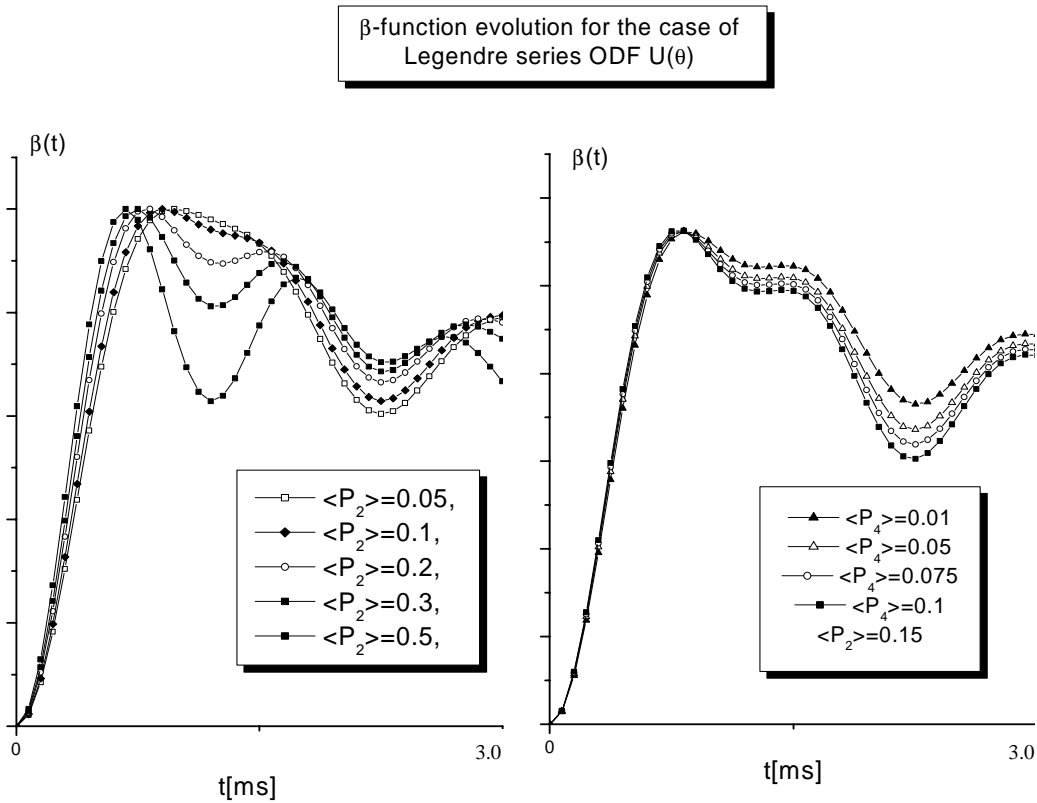


Fig 3.4 Fig 3.4 β -function evolution calculation for Legendre polynomials representation of the ODF $U(\cos(\theta))$ (3.23). The Legendre coefficient $\langle P_2 \rangle$ (left) and $\langle P_4 \rangle$ (right) values were varied within one decade to estimate their roles in the forming of the β -function curve shape.

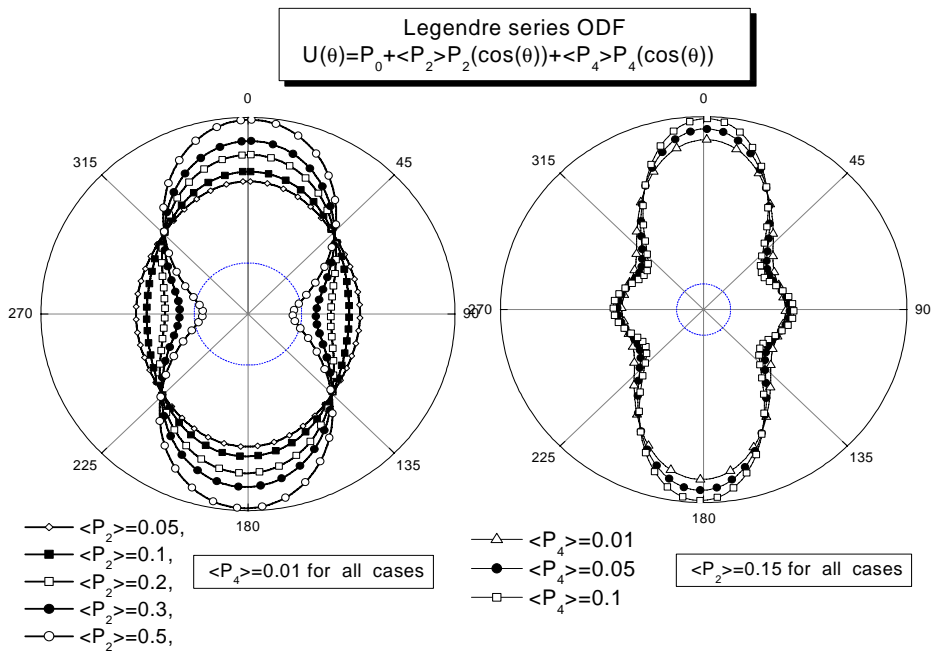


Fig 3.5 Variation of the orientation distribution function $U(\cos(\theta))$ with changing of its Legendre expansion coefficients $\langle P_2 \rangle$ and $\langle P_4 \rangle$. The relative influence of $\langle P_4 \rangle$ on the form of ODF looks insignificant as well as on the β -function (Fig3.4)

To characterize the deviation between the values of $\beta(t)$ corresponding to different orientation parameters the relative residual function (**RRF**)

$$R^{\langle P_{2,4} \rangle}(t) = \frac{|\beta_{\max}^{\langle P_{2,4} \rangle}(t) - \beta_{\min}^{\langle P_{2,4} \rangle}(t)|}{\beta_{\max}^{\langle P_{2,4} \rangle}(t)} \quad (3.24)$$

can be introduced. Here $\beta_{\max,\min}^{\langle P_{2,4} \rangle}(t)$ corresponds to the values of β -function calculated for the maximal and minimal values of the Legendre coefficients $\langle P_2 \rangle_{\max,\min}$ and $\langle P_4 \rangle_{\max,\min}$ in ODF $U(\cos(\theta))$ given by (3.23), respectively. The exceeding by the residual function $R^{\langle P_{2,4} \rangle}(t)$ the level of typical experimental error 0.1 (10%) can be considered like a sufficient criterion of our ability to resolve between parameters $\langle P_{2,4} \rangle_{\max}$ and $\langle P_{2,4} \rangle_{\min}$ related

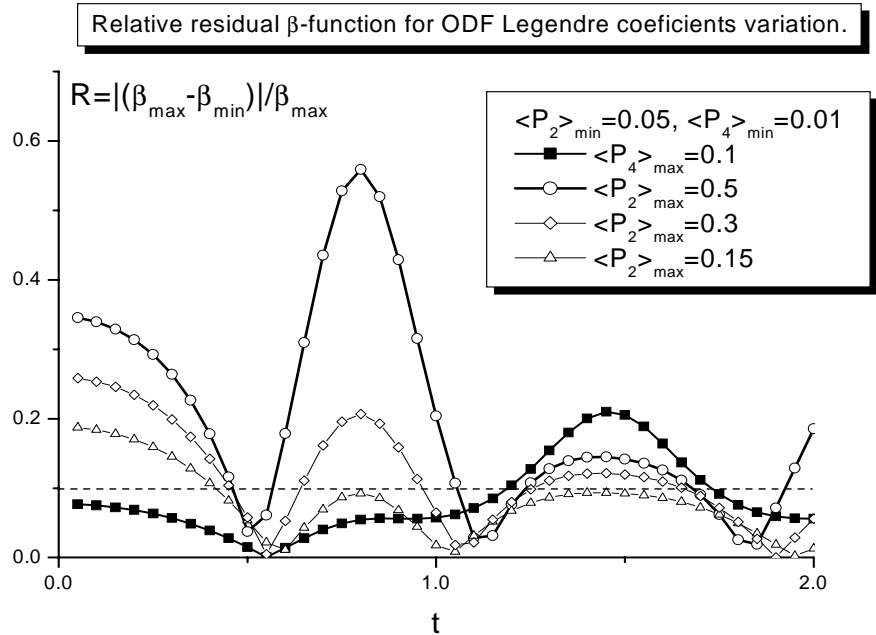


Fig 3.6 Relative residual β -function (3.24) for different values of the ODF Legendre coefficients variation. Acquiring more points in the time regions where $R^{\langle P_2 \rangle}$ is maximal (and exceeds the experimental error), the necessary standard deviation of $\langle P_2 \rangle$ determination can be succeeded rather fast. However, within preliminary estimated range of the $\langle P_2 \rangle$ and $\langle P_4 \rangle$ values, the 10% relative experimental error will prevent to resolve the $\langle P_2 \rangle$ values smaller than 0.1. The situation is even worse for $\langle P_4 \rangle$ values (see «solid square» curve) because the RRF for the whole region of expected values (0.01..0.1) lays nearly completely under 10% level.

with the corresponding curves.

The variation of $\langle P_2 \rangle$ coefficient within one decade shows the sufficient influence on the shape of the β -function (**Fig 3.4** left). For preliminary estimation, the residual function $R^{\langle P_2 \rangle}(t)$ was calculated using $\langle P_2 \rangle_{\min} = 0.05$ in $\beta_{\min}^{\langle P_2 \rangle}(t)$. Calculation shows that for the values of $\langle P_2 \rangle_{\max} > 0.1$, the RRF (3.24) $R^{\langle P_2 \rangle}(t)$ exceeds or at least achieve the level **10%** of maximum during the sufficient part of the evolution period between 0 and 2ms

(**Fig 3.6**). On contrary, the influence of the $\langle P_4 \rangle$ on evolution of $\beta(t)$ in the same time scale, for variation of $\langle P_4 \rangle$ within one decade ($\langle P_4 \rangle_{min}=0.01$, $\langle P_4 \rangle_{max}=0.1$) is nearly negligible. For the evolution period ($t_e < 2ms$) the residual function $R^{\langle P_4 \rangle}(t)$ in its maximum exceeds level $R^{\langle P_4 \rangle}(t) = 0.1$ for only very small period. Practically it means that the only very reliable experimental measurements of β -function allows one estimating independently two coefficients of the $U(\cos(\theta))$ Legendre expansion. The estimation of the typical values of the ODF moments expected for the object of our interest gives $0.35 \geq \langle P_2 \rangle \geq -0.05$. and $0.05 \geq \langle P_4 \rangle \geq 0$, respectively. Therefore, according to the **Fig 3.6** the difficulties of estimation of the orientation degree values smaller than $\langle P_2 \rangle = 0.1$ can be expected already at the moderate experimental signal-to-noise ratio $S/N \approx 0.1$. For the same level of experimental error the $\langle P_4 \rangle$ value can be estimated from fitting of the single β -function curve only by the order of magnitude. However, the situation can be improved if to study the evolution of β -function under rotation of whole sample (and hence whole distribution of spin subsystems inside) with respect to the magnetic field B_0 . It will be shown that this can provide us additional information about the orientation distribution and improve the reliability of the data analysis.

3.5 Angular dependence of β -function for non-isotropic ODF.

Generally, the orientation distribution describes the state of the internal macroscopic orientation of the subsystems the whole macrosystem consists of. The ODF of whole system is defined with respect to some intrinsic principal axes system (“molecular frame”) of the sample (shown like axis N on **Fig 3.7a**). In our previous consideration we suggested for convenience that the principal axis of the orientation distribution and NMR “laboratory frame” axis (external magnetic field B_0) are parallel each other. In such a case the only one angle θ characterize both the (i) probability of some partial orientation of the molecular segment \vec{s} and (ii) the intensity of anisotropic interactions of the nuclear spins of this segment. However, in general, it is not necessary that these two axes are collinear (see **Fig 3.7b**). Moreover, in a number of experiments [III.14, 15], measurements of the parameters of spin interaction with variation of angle between laboratory and molecular frame provide the information about the orientation properties.

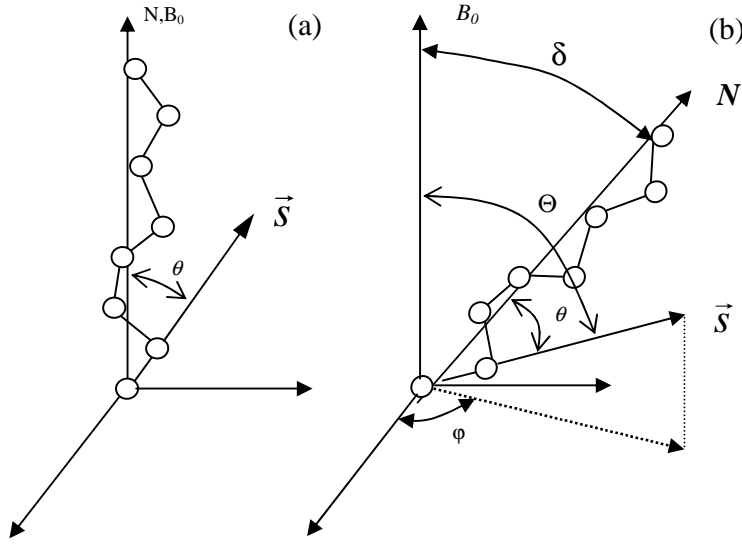


Fig.3.7 Mutual orientation of the coordinate frames for molecular chain. Three coordinate system and angles connecting them are relevant: 1) laboratory frame (defined by external magnetic field B_0), 2) molecular frame (N) defined by molecular segments preferable orientation (ODF reference axis) 3) principal axis of nuclear Hamiltonian (S)

When molecular axis, which is reference one for the orientation distribution (*ODF-axis* in following) is tilted with respect to laboratory frame axis defined by external magnetic field B_0 , another two angles (among ODF angle θ) become relevant for β -function consideration. The first one is the tilting angle δ between molecular frame and ODF axes. The second is the angle Θ between the external magnetic field B_0 and individual molecular segment \vec{s} , which define the intensity of dipolar interaction according to equation (3.5) ($\cos(\theta)$ now should be replaced with $\cos(\Theta)$). For the orientation distribution, function the transformation between “tilted” molecular and reference laboratory frame $U(\cos(\theta)) \rightarrow U'(\cos(\Theta), \delta)$ can be performed using standard Euler rotation matrix formalism:

$$\begin{aligned} \cos(\theta) &\xrightarrow{R(\cos(\delta))} \cos(\Theta); \\ \cos(\theta) &= -\sin(\Theta) \sin(\varphi) \sin(\delta) + \cos(\Theta) \cos(\delta) \end{aligned} \quad (3.25)$$

Because, the azimuthal angle φ is now also sufficient for the averaging over all possible orientation, the surface integration has to be used to calculate “tilted” β -function, which becomes now dependent on the value of δ :

$$\beta_{\Sigma}(2\tau, \delta) = \iint_{\Omega} [1 - \cos(2\omega_D(x)\tau)] R(2\tau) U'(x, \delta) dx d\varphi, \quad x = \cos(\Theta) \quad (3.26)$$

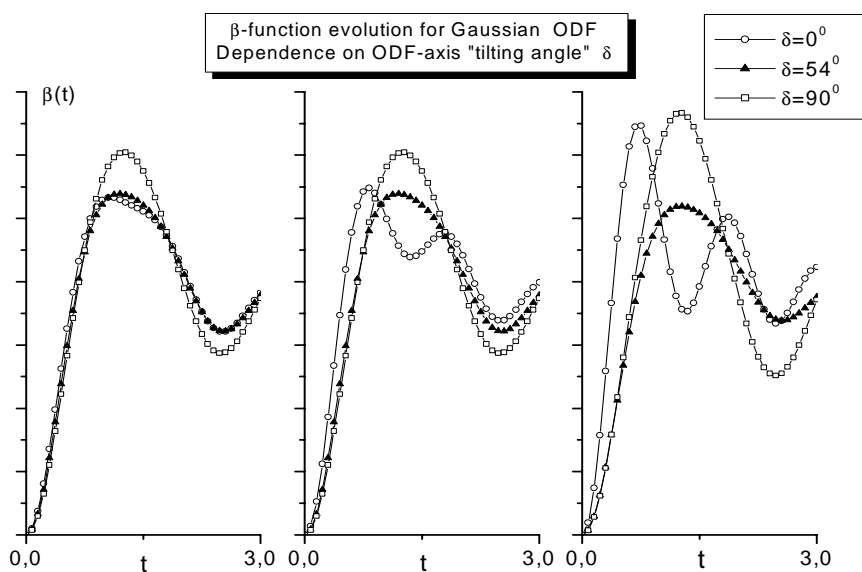


Fig 3.8 Simulation of the angular dependence of β -function evolution for Gaussian ODF with different orientation degree. Parallel, orthogonal, and «magic angle» mutual orientation of laboratory and molecular axes were considered.

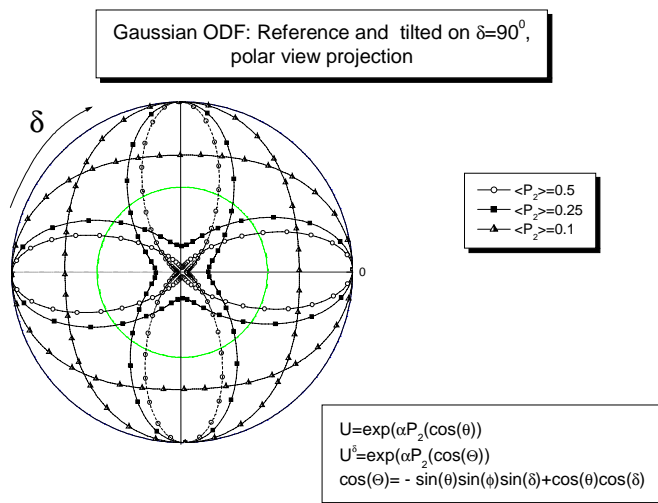


Fig 3.9 Example of polar view of «tilted» ODF's with different orientation degree parameter. Gaussian ODF with orientation degree 0.1, 0.25 and 0.5 have been used. Coordinate angle transformations have been performed according to eqn. (3.25) for tilting angle $\delta=90^\circ$. «Plane projections» for $\phi=0$ are shown.

Fig 3.8 shows the variation of β -function form calculated by formula (3.26) with changing of tilting angle δ . As before, the Gaussian ODF (3.22) with different orientation degree parameter $\langle P_2 \rangle$ (see Fig. 3.9) was used. The relation between referenced $U^t(\cos(\theta), \delta=0) = U(\cos(\theta))$ and «tilted» $U^t(\cos(\theta), \delta=90^\circ)$ is shown on Fig 3.9. Some important conclusions can be done basing on the simulation of the β -function angular dependence using one-parametrical Gaussian ODF:

- (i) «Magic angle» orientation ($\delta=54^0$) of ODF reference axis with respect to laboratory frame gives the same dependence $\beta(t)$ for *any orientation degree* parameter $\langle P_2 \rangle$ (**Fig 3.8**, «solid triangles»).
- (ii) For «orthogonal orientation» ($\delta=90^0$) only maximal amplitude of the β -function curve increases together with orientation degree (**Fig 3.8**, «open squares»). It is remarkable, that the absolute and relative positions of maximums and minimums of the β -function keep constant for any $\langle P_2 \rangle$ value in this case.
- (iii) Collinear orientation ($\delta=0$) of ODF reference axis and laboratory frame leads to considerably strong changes in $\beta(t)$ with variation of the ODF parameters. These facts can be explained if to recollect that the second Legendre polynomial $P_2(\cos(\delta))=(3\cos^2(\delta)-1)/2$, which basically defines the β -function numerical properties (via angular dependence of coupling constant ω_D (3.5) and via the parameters of the ODF) is equal to 0 at $\delta=54^0$, maximal at $\delta=0$ and minimal at $\delta=90^0$.

Finally, the sufficient fact should be noticed: the variation of the ODF parameters has the strongest influence on β -function curve in the region of its first maximum. For the evolution periods which are long in comparison with the τ_{max} , the superposition of many components of different subsystems $\beta_{\theta}(t)$ (Eqn 3.18) leads to averaging and smoothing of the orientation effects.

In the following section it will be shown that, the angular dependence of the β -function (3.26) gives more effective methods of the orientation parameter evaluation in the case of model-free «Legendre series» approach than the direct fitting procedure described in 3.4.2.

3.6. ODF parameters evaluation for Legendre series approach. Using β -function angular dependence

It was shown in 3.4.2, that the coefficients of Legendre representation of the ODF can be estimated by the direct fitting of the β -function time evolution dependence. However, the estimation by means relative residual function (**RRF**) of this method efficiency, under conditions of the real experimental signal-to-noise ratio, shows us, that the only few parts of the β -function curve can be effectively used for the fitting. Moreover, for the low-oriented systems, with $\langle P_2 \rangle < 0.1$ and $\langle P_4 \rangle < 0.05$ the relative error can exceed 50%. The problem

becomes more complex if to take into account that the integral (3.20) does not give an analytical solution even for restricted amount of Legendre series terms to represent $U(\theta)$. Therefore, it is impossible in this case to apply the standard methods of non-linear regression for the β -function curve approximation. Another alternative that is using the methods of the numerical minimization of the difference between model and experimental curves requires a lot of calculation resources even in the case of only two fitting parameters. In addition, the minimization methods quite often give an ambiguous result, especially for oscillating functions.

The situation can be improved by using the β -function angular dependence properties described qualitatively in section 3.5. Using of the “tilted ODF” concept allows one (i) employing more effectively the parts of β -function curve most sensitive to the orientation properties, and (ii) to find faster and more accurate method of the ODF parametrical approximation.

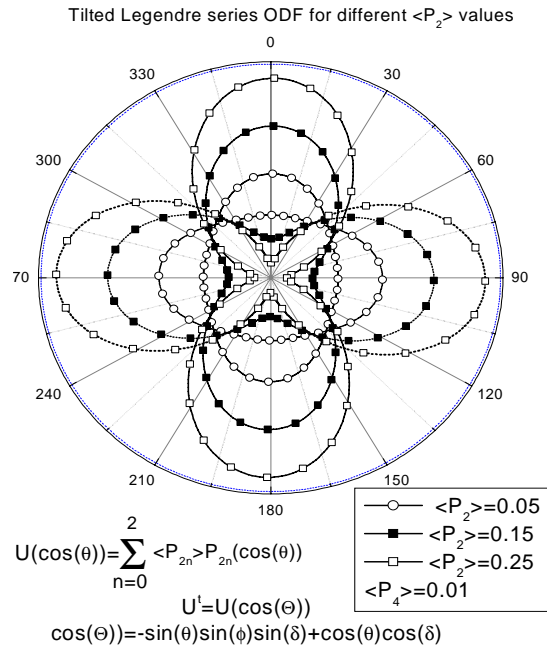


Fig 3.10. Polar view projection of the mutually tilted Legendre series ODF. 0,2,4-order terms were used for calculation of reference (solid line) and 90°-tilted (dotted line) ODF's with different orientation order degree $\langle P_2 \rangle$. The value of $\langle P_4 \rangle$ coefficient was set to 0.01. $\langle P_0 \rangle = 1/4\pi$ because of the normalization requirements

The transformation between two mutually tilted ODF's represented by Legendre series is performed using the approach shown in (3.5). The examples of the polar view projection of the functions characterized with the different orientation degrees $\langle P_2 \rangle$ for the case of mutually orthogonal ODF reference axes are shown on **Fig.3.10**.

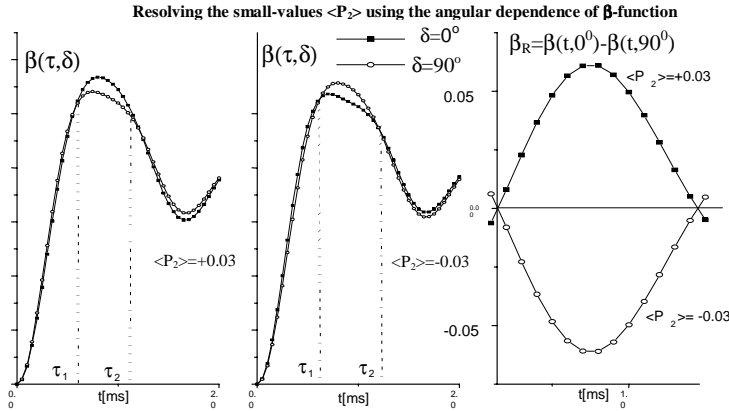


Fig. 3.11 Estimation of the orientation degree for weakly anisotropic ODF. The fact of the anisotropy presence and the sign of the close-to-zero $\langle P_2 \rangle$ parameter can be determined from the comparison of the β -functions evolution, observed with two orthogonal orientation of the ODF reference axis with respect to laboratory frame..

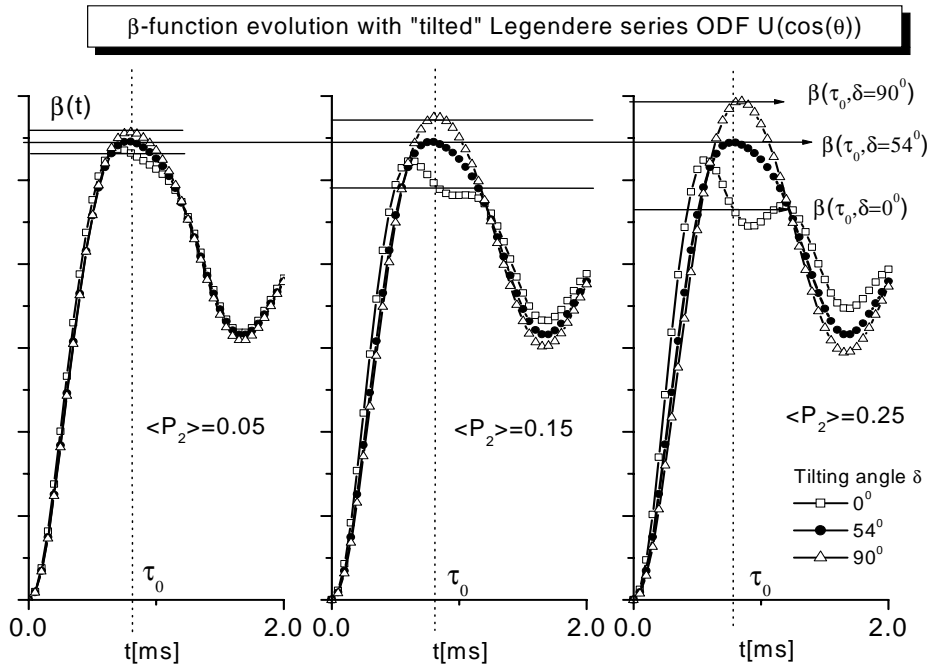


Fig 3.12 Using the β -function angular dependence to increase the effectiveness of ODF parameters determination. The "magic angle" orientation of the ODF main axis provides the same curve for various $\langle P_2 \rangle$ value. The time moment τ_0 when $\beta(\tau_0, \delta=54^\circ)$ achieve its first maximum $\beta_{\max}(\delta=54^\circ)$ can be chosen like a reference point to define the calibration function Δ_β . (see **Fig 3.13-14**).

One of the simplest but important example when the β -function angular dependence employing can be considerably valuable is the case of the «nearly isotropic» ODF. Practically, it means that the orientation degree $\langle P_2 \rangle$ is close to zero by absolute value and it becomes important to know the sign of the anisotropy i.e. if the $\langle P_2 \rangle > 0$ or < 0 . The insignificant relative deference (RRF does not exceed 5%), between the β -functions corresponding to small positive and negative values of $\langle P_2 \rangle$ (less than 0.1) does not allow finding unambiguously the sign of orientation degree. **Fig 3.11** illustrates the comparison of β -function curves $\beta(t, \delta)$ corresponding to the equal by absolute value ($|\langle P_2 \rangle| = 0.03$) but

opposite by sign orientation degrees calculated for the two mutually orthogonal orientation of the ODF reference axis ($\delta=0^0$, and 90^0 respectively). It can be seen that in the region of first maximum (i.e. $\tau_1 < t_m < \tau_2$) the values RRF $\beta_R \equiv (\beta(t_m, 0^0) - \beta(t_m, 90^0))$ have the same sign as the sign of corresponding $\langle P_2 \rangle$. That means $\beta_R > 0$ if $\langle P_2 \rangle > 0$ and vice versa. The difference between «positive» and «negative» β_R exceeds 10% at maximum that gives the criteria for the evaluation of the $\langle P_2 \rangle$ with good reliability using the relatively small amount of experimental data (the only part of the curve between τ_1 and τ_2 is used) at reasonable signal-to-noise ratio.

Fig 3.13

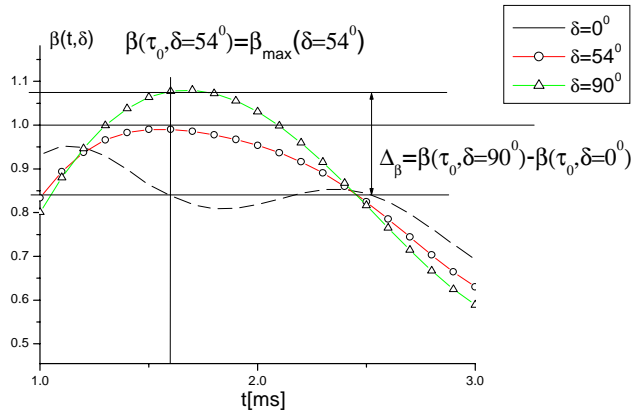


Fig 3.14

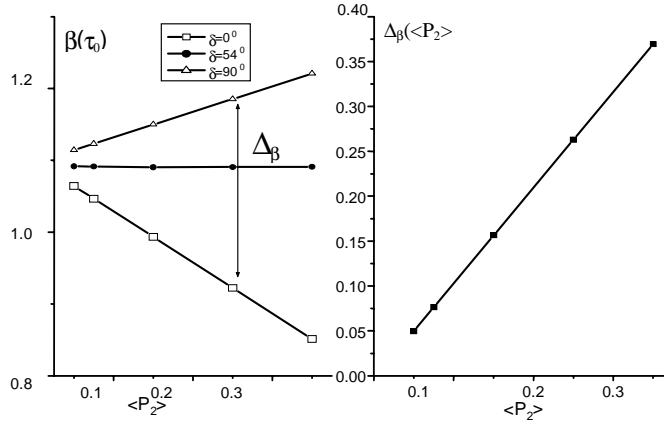


Fig 3.13, 3.14 Calibration function $\Delta_\beta(\langle P_2 \rangle) = \beta(\tau_0, \beta=90^0) - \beta(\tau_0, \beta=0^0)$, gives the convenient way for increasing of the $\langle P_2 \rangle$ values estimation exactness. The dependence is linear within all possible range of the ODF coefficient $\langle P_2 \rangle \in [0..1]$. Choosing τ_0 as the point of first maximum $\beta(t, \delta=54^0)$ provides the maximal tangent of $\Delta_\beta(\langle P_2 \rangle)$, line and, therefore, minimize the relative error of $\langle P_2 \rangle$ estimation.

The similar to the described above idea, with some modifications, can be employed to increase the efficiency and accuracy of the ODF parameters numerical estimation by means the β -function. **Fig 3.12** shows the calculation of the β -function angular dependence for several various $\langle P_2 \rangle$ coefficient used to represent the ODF function with Legendre series. The $\langle P_4 \rangle$ value was set to 0.01 for all the cases (**Fig 3.10**). It can be seen from the

Fig 3.12 that the $\beta(t, \delta)$ curve corresponding to the $\delta=54^0$ has the same form for any value of the ODF orientation degree. This aspect of the $\beta(t, \delta)$ behavior was already shortly discussed above in **3.5** on example of the Gaussian-like ODF. The fact that the values of $\beta(t, \delta=54^0)$ is the same for the curves corresponding to any $\langle P_2 \rangle$ (see **Fig 3.12**) allows one to define the function $\Delta_\beta = \beta(\tau_0, \delta=90^0) - \beta(\tau_0, \delta=0^0)$ (see **Fig 3.13,14**)-which will depend only on the value of $\langle P_2 \rangle$. The calculation shows that the dependence $\Delta_\beta(\langle P_2 \rangle)$ is perfectly linear. Choosing τ_0 like a position of first maxima of $\beta(t, \delta=54^0)$, i. e. $\beta(\tau_0, \delta=54^0) = \beta_{\max}(\delta=54^0)$ one can provide the maximal tangent $d\Delta_\beta/d\langle P_2 \rangle$ and therefore the highest accuracy of the $\langle P_2 \rangle$ determination by this method. Employing this technique gives three basic advantages as compared to the direct fitting procedure (i) the only few amounts of data points needs to be acquired in the region of β -function are the most experimentally reliable (the time period of when it achieves the first maximum), (ii) the method of the $\langle P_2 \rangle$ is purely numerical and does not require either not completely reliable minimization procedures or “by eye” fitting approach.

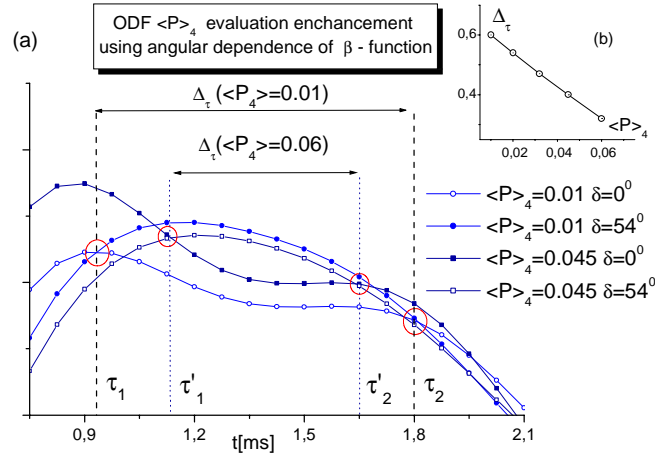


Fig 3.15 The linear correlation for between $\langle P_4 \rangle$ and the parameters of the β -function curves corresponding to “tilted” ODFs. The crossing point of the $\beta(t, \delta=0^0)$ and $\beta(t, \delta=54^0)$ is used to define the linear calibration function for the $\langle P_4 \rangle$ coefficient.

It was shown in the section (3.4) that the procedure of the numerical evaluation of the $\langle P_4 \rangle$ coefficient of the ODF is especially difficult task for the experimentally relevant ranges of signal to noise ration and the expected value of $\langle P_4 \rangle$ within [0.01..0.1]. However, using the angular dependence of β -function the linear correlation can be found between the parameters of the curves corresponding to the different ODF tilting angles and the value of its $\langle P_4 \rangle$ coefficient. In this case the linear dependence can be found if to use the function Δ_τ

defined like a time period which fulfill the “crossing” conditions for the β -function curves corresponding to the angles $\delta=0^0$ and $\delta=54^0$. $\Delta\tau=\tau_1-\tau_2$, where $\beta(\tau_1,\delta=0^0)=\beta(\tau_1,\delta=54^0)$ and $\beta(\tau_2,\delta=0^0)=\beta(\tau_2,\delta=54^0)$. It can be seen from **Fig 3.15** that the distance between the points of crossing of two curves increases linearly with the $\langle P_4 \rangle$ value (**Fig 3.15b**). Similar to the case of the $\langle P_2 \rangle$ coefficient the criteria of $\langle P_4 \rangle$ determination allows one using the most reliable part of the β -function data. It also provides the enhancement of the numerical evaluation procedure efficiency by connection of the parameters of the angularly dependent β -function curves directly with the ODF properties by means the simple and obvious linear dependence.

3.7. Determination of the dipolar coupling constant using “ β -spectrum” analysis.

3.7.1. β -echo spectrum for the spin-1/2 pair system. Combined influence of the anisotropic chemical shift and dipolar interactions.

So far our consideration of the β -echo combination was restricted with the « β -function» i.e. the amplitude of the threefold echo signal at the moment when evolution period is equal to refocusing period (see **Fig 3.1**), $t_1=t_2=\tau$. It was shown in previous sections that the time evolution of function $\beta(2\tau)$ is highly sensitive to the anisotropic bilinear spin interactions and therefore to the spatial orientation of its principal axes. However, the additional information can be obtained by the analysis of the FID signal followed by this moment of the spin system evolution. The β -function evolving in presence of orientation distribution of the principal axes of the bilinear interactions represents the integral sum of the individual harmonics corresponding to the specific interaction intensity defined by the orientation of the interaction axis with respect to external magnetic field (see Eqn 3.18-3.20). The situation is quite analogous to the case of the standard FID following the single excitation pulse—the individual harmonics behavior can be probed by the Fourier transformation of the time-domain signal of the β -echo. Similarly to the case of 2D NMR it can be expected, that the resulted « β -spectrum» will be modulated by amplitude and phase depending on the duration of the preceding echo period $t_e=2\tau$.

The analytical expression for the « β -echo» is given by the eqn 3.13. Combining together all three contributing terms corresponding to the individual echoes, the resulted observable magnetization can be found as:

$$M_{\pm}(2\tau + t) = \left[e^{i(-\Omega - \omega_D)t} + e^{i(-\Omega + \omega_D)t} \right] - \left[e^{i(-\Omega - \omega_D)t - i\omega_D 2\tau} + e^{i(-\Omega + \omega_D)t + i\omega_D 2\tau} \right] \quad (3.27)$$

Here, Ω denotes the frequency offset due to the linear terms of Hamiltonian and ω_D means the coupling factor which characterize the bilinear (for example dipolar) interactions. For the case of the β -function, (the value of M_{\pm} at $t=0$), the value of Ω obviously plays no role and was omitted in previous consideration. However, if the full “ β -echo” signal and the information about the spin system which can be derived from its spectrum are considered, the linear interactions are important factor of the lineshape forming. It was discussed in the chapter II that in solid matters the interactions of the spins with their surroundings has an anisotropic character. The important type of linear interaction - *anisotropic chemical shift* characterizes the asymmetry of the chemical surroundings provide a resonance frequency offset dependent on the orientation of the principal axes of the *CS tensor* with respect external magnetic field (see Chapter II). Therefore analyzing the “ β -echo” signal (3.27) for the case when the probed sample has a particular orientation of the spin subsystems, the angular dependence of both Ω and ω_D has to be taken into account.

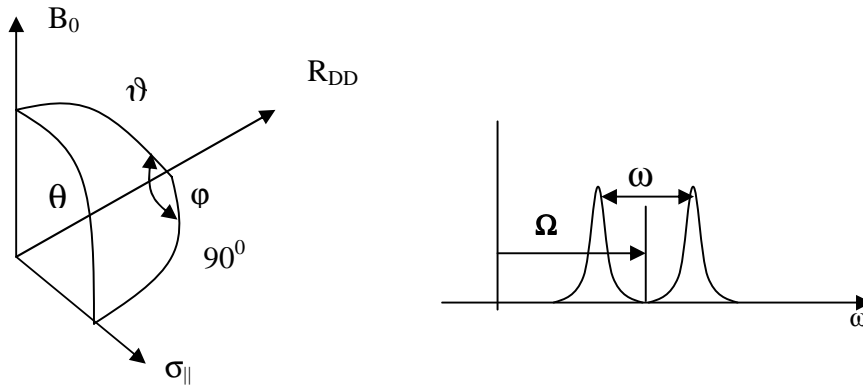


Fig 3.16 Mutual relations between principal axes of the dipolar and chemical shift spin interactions. The 90° angle between σ_{\parallel} and R_{DD} is typical for the polysiloxanes (Si-C and Si-Si bonds in polysiloxanes). The CS interaction leads to the offset of the resonance, when the dipolar one is responsible for splitting of the spectral line in two. Both the offset and splitting depends on the orientation of the principal axis of the interaction with respect to magnetic field B_0 , However, the effect is masked by the inhomogeneous CS-broadening which exceeds the dipolar splitting.

Here, we restrict our examination of the “ β -spectrum” by the case important for particular purposes of our work: (i) the CS tensor is symmetrical, (ii) the value of the chemical shift anisotropy $\Delta\sigma$ is much bigger than the expected dipolar coupling constant

ω_D and (iii) the dipolar interactions takes place between two spins $I=1/2$ so the formula 3.27 is relevant to describe the « β -echo» signal.

To consider the behavior of the spin system under two angularly-dependent types of interactions the mutual orientation of their principal axes has to be taken in to account. **Fig 3.16a** illustrates the relation between the three principal axes of interactions connected with the spin system which define its NMR spectrum. The axis σ_{\parallel} define direction the main axis of symmetrical tensor of *chemical shift* (CS). According to the (Eqn 2.1-5) this interaction leads to the shift of the resonance line Ω dependent on the CS-anisotropy parameter $\Delta\sigma$ and the angle between main axis of the CS tensor and magnetic field (see also A2.2). The vector R_{DD} gives the orientation of the internuclear vector which connects the spin pair involved into dipolar interaction. This leads to splitting of each resonance line into two, separated by the spectral distance ω_D proportional to the dipolar coupling constant ω_D and the second Legendre polynomial of the angle between R_{DD} and B_0 . (**Fig 3.16b**). Generally, the mutual orientation of the dipolar and chemical shift principal axes R_{DD} and σ_{\parallel} depends on the local environment and the structure of the molecular segment. We consider the situation when these axes are preferably *orthogonal* as it takes place in the systems of our interest. Finally, the frequency offset and splitting parameters described by the CS and dipolar interaction with account of the angular dependence can be expressed as:

$$\begin{aligned}\omega_D &= \omega_{0D} P_2(\cos(\vartheta)) \\ \Omega &= \Delta\sigma P_2(\cos(\theta)) = \Delta\sigma P_2(\sin(\vartheta)\cos(\varphi))\end{aligned}\quad (3.28)$$

Substituting the 3.28 into 3.27 and applying the Fourier transformation the subspectra corresponding to the defined orientation can be obtained

$$S_{\beta}^{\ominus}(\omega, 2\tau) = \int_{-\infty}^{+\infty} M_{\pm}(2\tau + t, \Omega(\Theta), \omega_D(\vartheta)) e^{i\omega t} dt \quad (3.29)$$

Here Θ denotes the set of polar and azimuthal space angles $\Theta(\vartheta, \varphi)$. To get the full spectrum the integration over all possible orientation has to be performed with account of the orientation distribution function:

$$S_{\beta}(\omega, 2\tau) = \iint_{\Theta} S_{\beta}^{\ominus}(2\tau, \Omega(\Theta), \omega_D(\vartheta)) U(\Theta) d\Theta, \quad d\Theta = d\cos\vartheta d\varphi \quad (3.30)$$

According to (3.27-3.30) it can be expected that the spectral line shape of β -echo will differ from the spectrum of «normal» FID or single echo. The intensity of individual subspectrum corresponding to the particular orientation of internuclear vector R_{DD} will be modulated

both by amplitude and phase by the β -function (see 3.2). Generally, the position of each subspectrum will be defined by the frequency offset Ω corresponding to the angle ϑ . Because both CS and dipolar interaction are determined by only one angular parameter (ϑ and θ respectively), the contribution of each spin pair with particular ω_D to the spectral position corresponding to the chemical shift offset $\Delta\Omega$ is *not* unambiguous even for the case of *transversal isotropy* of the CS-main axes distribution with respect to dipole-dipole internuclear vectors. Thus, obtaining the information from the “ β -spectrum” is, generally, a more difficult task than the β -function analysis. However, using a combined the time and frequency domain analysis, allows one to estimate the parameters of spin interactions (particularly the dipolar coupling constant ω_{DD}) with higher accuracy than it is possible from pure β -function analysis.

3.7.2 β -spectrum lineshape evolution.

The lineshape of the NMR spectrum of a spin system generally depends on the relation between the properties of the individual Hamiltonians of the spin interactions. The situation which takes place in the system of our interest is characterized by the strong linear interaction (anisotropic CS) which prevails over bilinear (dipole-dipole interaction)). According to the preliminary estimation, the CS-anisotropy $\Delta\sigma$ exceeds dipolar coupling constant ω_{DD} on the order of magnitude in the magnetic field used in our experiments (9.4T). On the other hand, the deconvolution of the experimental spectrum shows that the intrinsic lineshape of the individual subspectra in «CS-pattern» is described with the Gaussian function with the characteristic width about 20% of CSA value (see **Fig 3.17**). Under these conditions, the splitting of the spectral lines caused by dipolar interactions is completely masked by the convolution with CS-broadening line. It was shown above that in the case when the spectrum will be obtained using β -echo technique the individual position defined by the CS-offset will be modulated with the by the dipolar interactions represented in a form of β -function.

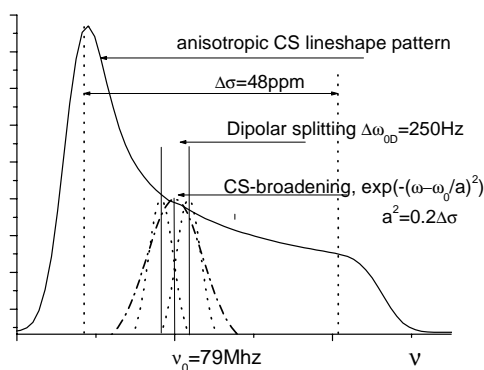


Fig 3.17 Relation between characteristic scales of the spin interactions for the polysiloxanes LCSP. (i) Anisotropic chemical shift pattern with $\Delta\sigma=48\text{ppm}$ (solid line). (ii) Broadening of the intrinsic spectral line because of the CS – inhomogeneity – Gaussian function with broadening factor $\cong 0.2\Delta\sigma$ (dashed line) (iii) Dipolar splitting $\omega_{0D}\cong 250\text{Hz}$

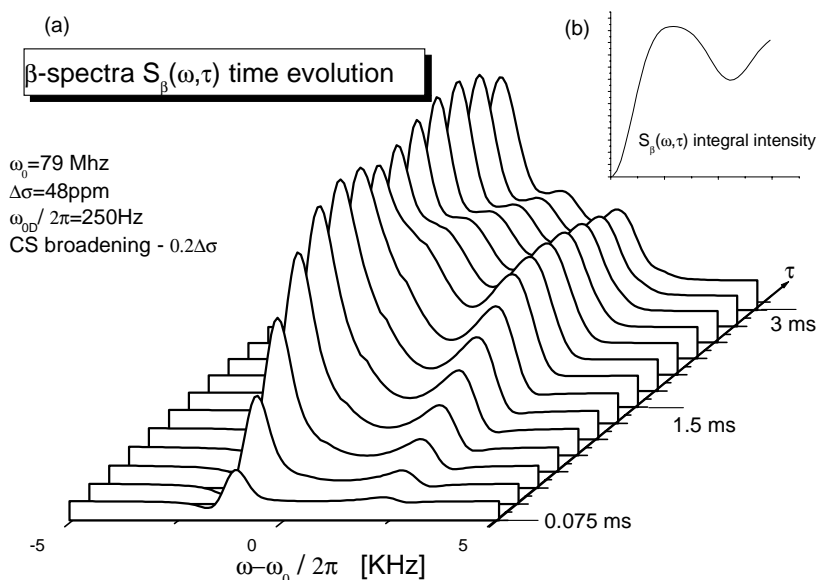


Fig.3.18 Evolution of the β -echo spectrum lineshape depending on the echo delay time. Numerical simulation was done according to eqn.3.27-3.30. The parameters of the chemical shift anisotropy and dipolar coupling constant as well as chemical shift broadening characteristic for the spin systems of interest (polysiloxanes, ^{29}Si nuclei) were used (see Fig 3.17).

Fig 3.18 illustrates evolutions of the spectral line shape with variation of β -echo delay time $t_e = 2\tau$, calculated according to equation (3.27-3.30). The case of the isotropic orientation of CS-tensor axes σ_{ij} and internuclear vectors R_{DD} was considered ($U(\Theta) = 1/4\pi$). The following conclusions can be done based on the analysis of the numerical simulations of the β -echo spectra:

1. The integral intensity of the whole spectrum corresponds to the β -function dependence of the time domain β -echo signal (**Fig 3.18b**).

2. The individual position of the spectrum corresponds to different orientation of CS and dipolar interaction principal axes. Therefore, β -function modulates each individual spectral position in different manner.

3. Because of the axial symmetry of both CS and dipolar interaction, more than one orientation ϑ of dipolar vector R_{DD} is possible for specific orientation of CS main axis θ . (see **Fig 3.16**) Thus, the amount of β -function harmonics $\beta(\omega_D(\vartheta), 2\tau)$ which contributes to the evolution of the spectral lineshape are different for each subpectra $S_\beta(\Omega(\theta), \tau)$. (**Fig 3.19a**) Here $\Omega(\theta) = \alpha(\theta) - \omega_0$ denotes the resonance offset caused by anisotropic CS interaction. More remarks can be done concerning with the last item. It can be expected, that because of the mutual orthogonality of the CS and main axis and dipolar vector the position $\Omega(\pi/2) = \sigma_\perp$ is always more abundant with “fast” β -function harmonics corresponding to the $\omega_D(\vartheta=0) = \omega_{0D}$. On contrary, for the spectral positions corresponding to $\sigma_\parallel > \Omega(\theta) > 0$ ($0 < \theta < 54^\circ$) the contribution of the β -function harmonics with maximal value of $\omega_D(\vartheta)$ are very small or completely excluded.

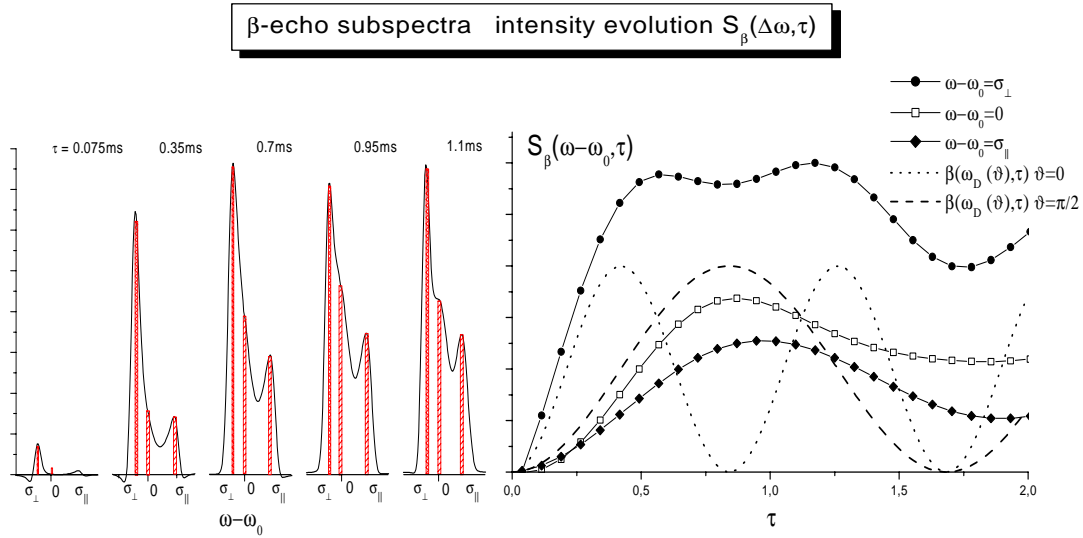


Fig 3.19 β -echo subpectra analysis. The intensities of the spectral components in CS-pattern are modulated by β -function. (see 3.27-3.29). Because of the arbitrary distribution of the CS main axes around dipolar vector, different spectral positions are abundant with superposition of β -function harmonics in different manner (see details in text). The β -function harmonics corresponding to values of $\omega_D(\vartheta)$ at $\vartheta=0$ and $\pi/2$ are shown for the illustration.

Fig 3.19 demonstrates the behavior of the individual β -echo spectrum components at three character positions mentioned above, depending on the echo time delay. It can be seen that the spectral component with the offset value σ_\perp includes a multiple β -function harmonics corresponding to the wide range of dipolar vector orientation ($\omega_{0D} > \omega_D(\vartheta) > 0$). In the same time, the evolution of the spectral positions $\omega - \omega_0 = 0$ and $\omega - \omega_0 = \sigma_\parallel$ can be described with more limited amount of the β -function components with the value of $\omega_D(\vartheta)$ from 0

($\vartheta=54.7^\circ$) to $\frac{1}{2} \omega_{0D}$ ($\vartheta=\pi/2$). The contribution of the “slow” harmonics in all the cases can be minimized by the restricting of the consideration of the spectral components evolution with time period preceding the first maximum of the corresponding component S_β .

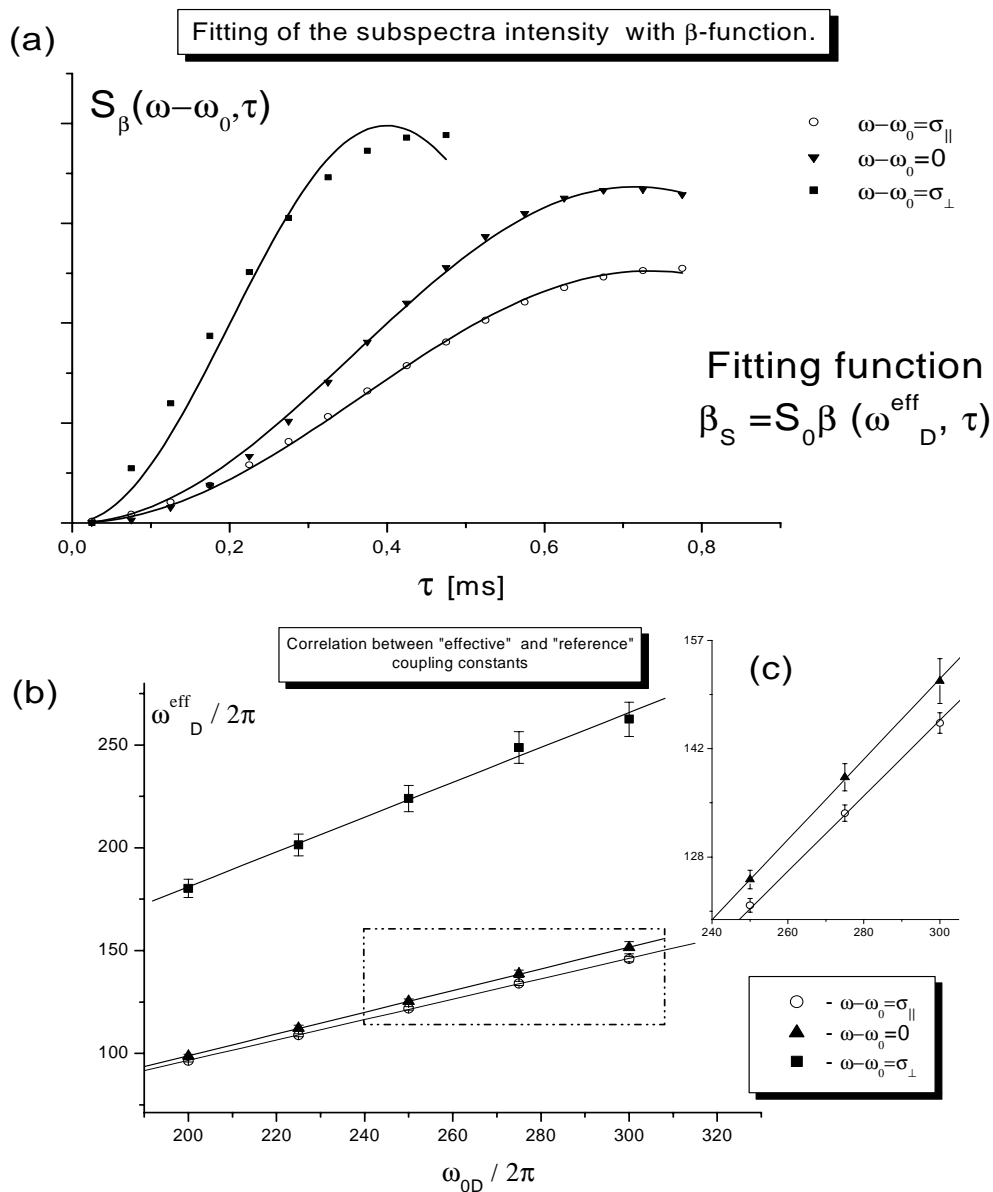


Fig 3.20 (a)- Fitting of the subspectra intensities with β -function «harmonics» for the short β -echo evolution time τ . The deviation from the « β -like» dependence is relatively small for spectral components $0 < \omega - \omega_0 < \sigma_{\parallel}$, and maximal for $\omega - \omega_0 = \sigma_{\perp}$. (**Fig b,c**) For the first case, perfectly linear (with relative error within 1%) correlation between «reference» parameter ω_{0D} and value ω_{eff} , shows that one-parametrical β -function approximation of the spectral components allows the sufficient increasing of the accuracy of the dipolar coupling constant determination in comparison to the β -echo FID amplitude analysis.

Under these conditions the individual spectral components can be fitted by the single β -function harmonic with defined value of the ω_{eff} proportional to the dipolar coupling

constant ω_{0D} . **Fig 3.20a** represents the example of such a one-parameter non-linear fitting of each β -echo spectra intensities at three characteristic positions. (The amplitude S_0 was defined for the minimal value of “referenced” ω_{0D} used in calculation for each spectral position and was fixed for the other values). It can be noticed that the mean square deviation (and therefore relative error of the fitting parameter determination) is minimal for the spectral position $\omega - \omega_0 = \sigma_{||}$ and increases slowly for the S_β at $\omega - \omega_0 = 0$. In the same time the evolution of the β -echo spectral components for the frequency values around $\omega - \omega_0 = \sigma_{\perp}$ obviously is characterized by the contribution of multiple β -function harmonics also with ω_D close to the ω_{0D} , and therefore the one-parameter fitting is not so successful. The mean square deviation for the last case is nearly on the one order of magnitude higher than for single β -function harmonic fitting of the spectral components $S_\beta(\omega - \omega_0, \tau)$ at $\sigma_{||} > \omega - \omega_0 > 0$. The correlation between the reference parameter ω_{0D} (used in the simulation of the β -echo spectra according to the eqn. (3.27-3.30)) corresponding to “fastest” β -function harmonic and the “effective” β -function harmonic frequency values ω_D^{eff} is demonstrated by the **Fig 3.20b,c**. It can be seen, that the relation between ω_D^{eff} and ω_{0D} can be characterized by linear dependence with the relative error less than 1% for the spectral positions $\sigma_{||} > \omega - \omega_0 > 0$ and within 5% for the $\omega - \omega_0 = \sigma_{\perp}$. In the same time, because of the geometry factors the amplitude of the spectral components at the position σ_{\perp} is in 2-3 times larger than for the $\sigma_{||} > \omega - \omega_0 > 0$, which leads to the larger relative accuracy of the spectral intensities determination and therefore better fitting accuracy when the signal-to-noise factor is taken into account. Therefore, for the experimental data processing the reasonable compromise should be found between experimental and methodological errors to choose the set of the spectral components for the fitting procedure.

That way the value of the dipolar coupling constant ω_{0D} , which plays the basic role for the determination of the orientation parameters by the β -function, can be evaluated from the analysis of the β -spectra of the disordered samples with sufficiently better accuracy than it is possible from the pure time domain β -function analysis.

Chapter IV. Experimental. Determination of the orientation distribution parameters for the polysiloxane PLC samples using β -echo.

All the NMR experiments were performed using the **VARIAN™** solid-state spectrometer («Unity-400» console) with superconductive magnet, providing a magnetic field of 9.4T that corresponds to 400MHz and 79MHz NMR working frequency for ^1H and ^{29}Si nuclei respectively. The $\pi/2$ pulse had a duration of about $4\mu\text{s}$ for ^1H channel at maximal available r.f. power. The $\pi/2$ pulse length for the ^{29}Si channel was adjusted depending on the particular r.f. probe tuning (see description below). The FID was digitized with the time interval $2.5\mu\text{s}$ for ^1H signal and $25\mu\text{s}$ for ^{29}Si spectrum that corresponds to a spectral width 400 KHz and 40 KHz respectively. About 2500 (for ^1H) and from 256 to 360 (for ^{29}Si) complex FID data points were acquired, using the quadrature detection.

The sample temperature manipulation during experiment was performed using the «coldfinger» device in combination with standard temperature control unit providing the temperature stability within 0.1°C during 24-48 hours. For the NMR signal recording at different orientation of the sample with respect to external magnetic field the stepper motor controlled by the spectrometer computer was used.

4.1 Basic pulse sequences.

To observe the β -echo within single experiment the specific pulse sequence was used.[IV.1] Basically, the necessary combination of the NMR signals can be obtained using the

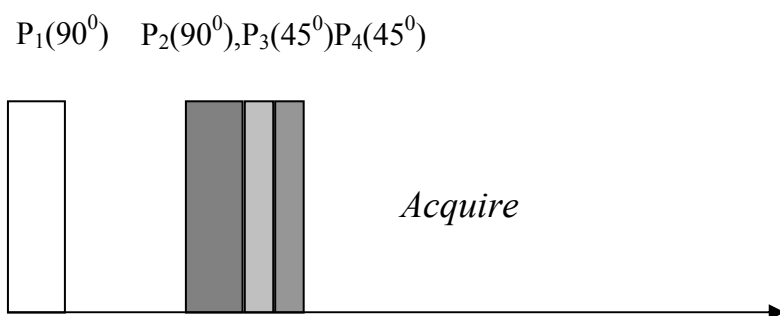


Fig. 4.1 Composite pulse sequence for β -echo signal generation. The combination of one 90°_α and two 45°_β pulses can be used to produce «zero», 90° and 180° pulse depending on the phases α and β .

appropriate phase cycle both for the receiver and transmitter. An efficient pulse sequence, which generates the β -echo is shown on (**Fig 4.1**). The composition of one 90°_α and two 45°_β pulses can be used to generate «zero», 90° and 180° pulse depending on the phases α and β . The appropriate

phase cycle is shown in Table 4.1. The triple units of the β -echo pulses are incorporated into the eight-step **CYCLOPS** sequence of Hoult and Richards [IV.2]. That way, it is possible to

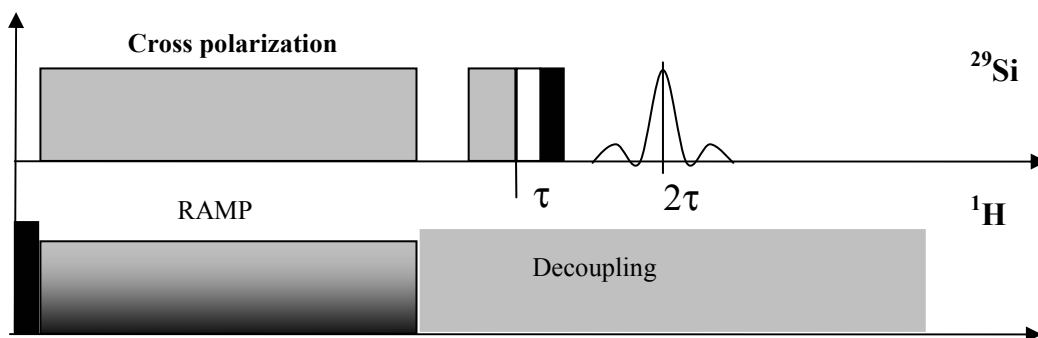


Fig 4.2. Pulse sequence scheme for Callaghan echo combination combined with **RAMP**ed cross polarization for the experiment sensitivity enhancement.

generate the necessary echo superposition using a single pulse sequence in one experiment. This allows one minimizing possible errors due to variation of the hardware parameters. Such an implementation of the pulse sequence for the β -echo generation has obvious advantage in the case of ^{29}Si NMR signal acquiring, which requires sufficiently longer total experiment time in comparison to the ^1H NMR (see the discussion of the sensitivity problems in the Chapter II). To increase the experiment sensitivity the ^{29}Si NMR signal is generated by the **RAMP**-ed cross-polarization transfer from the protons (see **Fig 4.2**).[IV.3]

The Hartman-Hahn [IV.4] contact is established for 3 ms under rf. field strengths in ^{29}Si channel of about $\gamma_{^{29}\text{Si}}B_1^{^{29}\text{Si}} \approx 40$ KHz. For ^1H channel the r.f. irradiation strength was varied with the modulation depth of about 15% (≈ 6 KHz) to compensate the r.f. field distribution inhomogeneity and provide the maximal coverage with the Hartmann-Hahn conditions ($\gamma_{^{29}\text{Si}}B_1^{^{29}\text{Si}} = \gamma_{^1\text{H}}B_1^{^1\text{H}}$) for the whole sample volume. During the echo-signal excitation and acquisition in ^{29}Si channel, the ^1H spins were decoupled from the ^{29}Si ones by the strong CW irradiation in the proton channel to avoid the additional line broadening due to ^1H - ^{29}Si dipolar interaction. The intensity of the decoupling pulse was set according to $\gamma_{^1\text{H}}H_1 \approx 60$ KHz that significantly overcome the strength of the dipolar coupling between the ^{29}Si and ^1H spins [IV.5].

Table 4.1

Phase cycling scheme

P_1	0,	0,	0	0	0	0	2	2	2	2	2	2	1	1	1	1	1	1	3	3	3	3	3	3
P_2	1,	0,	1	3	2	3	1	0	1	3	2	3	2	1	2	0	3	0	2	1	2	0	3	0
P_3	1,	1,	1	3	3	3	1	1	1	3	3	3	2	2	2	0	0	0	2	2	2	0	0	0
P_4	3,	3,	1	1	1	3	3	3	1	1	1	3	0	0	2	2	2	0	0	0	2	2	2	0
P_A	0,	2,	2	0	2	2	2,	0,	0	2	0	0	1	3	3	1	3	3	1	1	3	1	1	3

24 step «CYCLOPS»{ $P_1 = 0, 2, 1, 3$ } Phases notation is standard, i.e {0=x, 1=y, 2=-x, 3=-y}

The detailed consideration of the CP and “ramped” CP processes as well as ^1H decoupling procedure can be found elsewhere [IV.5-11].

Example of the pulses “unit” generating β -echo:

Step 1 $P_1=(90)_x$ $P_2+P_3+P_4=\{(90^0)_y+(45^0)_y+(45^0)_{-y}\}=(90^0)_y$ - «Solid echo» acquired as $(+x) \rightarrow S_1$
 Step 2 $P_1=(90)_x$ $P_2+P_3+P_4=\{(90^0)_x+(45^0)_y+(45^0)_{-y}\}=(90^0)_x$ - «Hahn echo -1» acquired as $(-x) \rightarrow -S_2$
 Step 3 $P_1=(90)_x$ $P_2+P_3+P_4=\{(90^0)_y+(45^0)_y+(45^0)_y\}=(180^0)_x$ - «Hahn echo -2» acquired as $(-x) \rightarrow -S_3$

$$S_\beta=S_1+(-S_2)+(-S_3)$$

4.2 Testing β -echo pulse sequence.

In the first stage of the experiments on β -echo some testing measurement were performed with the intention to confirm the correctness of the β -echo generation by implementing of the threefold pulse scheme described above. For the demonstration purposes the experiment was

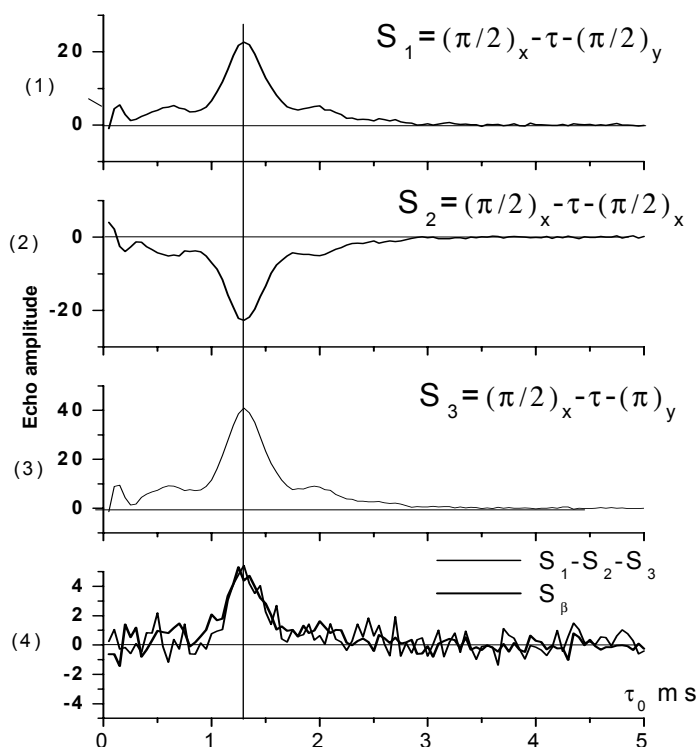


Fig. 4.3a. Comparison of β -echo generated in three independent experiments (plot 1-3) and, single “composite” (plot 4) respectively. Plot 4 shows that threefold composite pulse combination (thick line) gives the same result as numerical combining of the individual echoes obtained in separate experiments (thin line). The magnitude of the β -echo signal (10% of “normal Hahn echo”) is in agreement with estimation for the relative share of the coupled spin pairs.

setup so that 3 echoes contributing to the β -echo combination can be acquired subsequently together with the «threefold pulse» experiment. To be able making a comparison of the signal intensities, the number of signal scan averaging blocks was set for the β -echo combination in 3

times larger than for the individual echoes ($5 \times 24 = 120$ and $5 \times 8 = 40$ respectively). The echo delays time was set to (i) $\tau \rightarrow 0$ and (ii) $\tau \approx \tau_{\max}$, where $\beta(\tau_{\max}) = \beta_{\max}$ i.e. according to the estimation of possible β -echo maximum for the expected ^{29}Si pairs dipolar coupling intensity (see **Chapter. III**) in the polysiloxanes. The result of the experiment is shown on **Fig 4.3 a,b**.

It can be seen (**Fig 4.3a**), that the signal shape and intensity of β -echo at $\tau \approx \tau_{\max}$ obtained numerically from the signals of the contributing echoes S_1, S_2, S_3 are the same as for the β -echo generated by the pulse sequence (taking into account the noise level).

For echo delay time $\tau_0 \rightarrow 0$ ($\tau_0 = 25 \mu\text{s}$) (**Fig 4.3b**) the β -echo generates the signal which is in 50 times lower than an FID (or S_3 echo)[IV.1]. This value differs insignificantly from the noise level and corresponds to the error residual signal coming from the rf-pulse imperfections (see details below and in Appendix III).

The absolute intensity of the β -echo signal for the $\tau_0 = \tau_{\max} \approx 1.2\text{ms}$ is approximately 10% of the Hahn echo S_3 ($\pi/2 - \tau - \pi$) amplitude [IV.12]. This corresponds to the theoretically expected

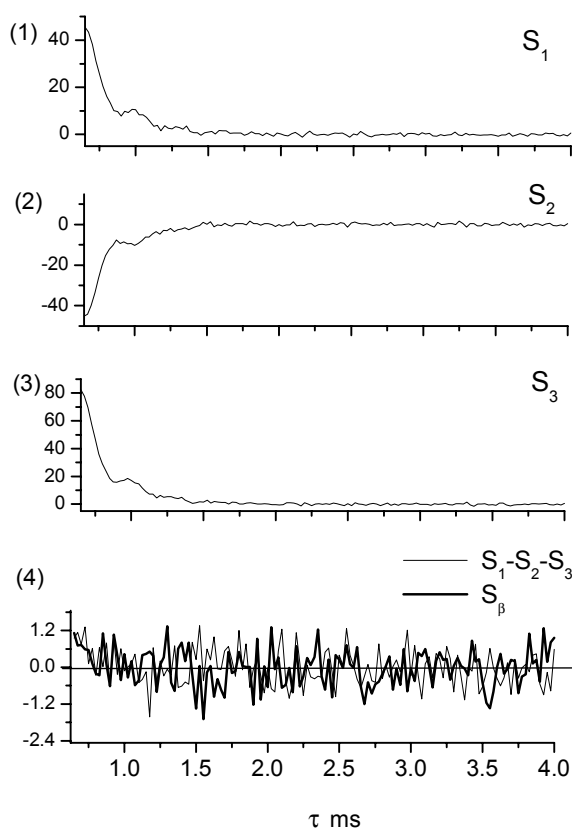


Fig 4.3b. Both combined and separate β -echo experiments demonstrates echo signal mutual compensation when β -echo evolution period goes to 0. The residual signal comes from the magnetization flip angles deviation from the theoretically required (AIII)

share of the ^{29}Si pairs in the polysiloxane sample in comparison with the total amount of ^{29}Si nuclei at natural abundance (see **3.3**). That way, it is confirmed experimentally that β -echo

sequence are able to select the signal of spin pairs coupled with the dipolar mechanism suppressing the signal from non-coupled spins [IV.1].

4.3 Pulse length calibration

It is shown in Appendix III that the uncertainties of the magnetization flip angle produced by the r.f. pulse leads to the appearance of the residual signal of β -echo even for the case when no bilinear terms present in the spin Hamiltonian. Therefore, the combination cannot perform its *filtering function* completely and the signal evolving under linear terms of the Hamiltonian brings an error signal distorting the β -function behavior. Particularly, a clear evidence of the non-complete compensation of the linear spin interactions due to the pulses errors is the presence of **(i)** non-zero real component for the evolution time $\tau=0$ and **(ii)** non-zero imaginary component of the β -echo for any other value of τ (see Appendix III). That way, the process of calibration of

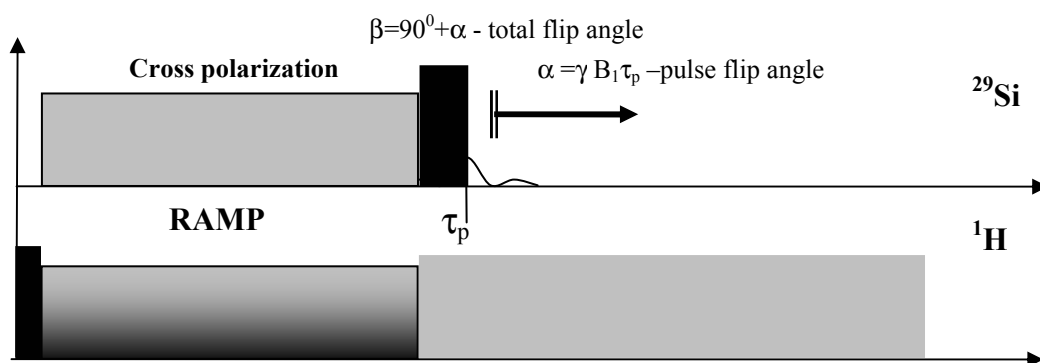


Fig 4.4 Pulse duration coarse calibration for β -echo experiment. At $\alpha=90^\circ$ a total flip angle of the CP+pulse supposed to be 180° producing the minimal (in ideal case zero) signal in comparison with the «pure CP signal» S_0 ($\tau_p=0$)

the pulse sequence parameters can be separated into «coarse» and «fine» tuning stages:

For the coarse tuning the combination of cross-polarization with immediately followed 90° -pulse is used. Such a r.f-pulses group, demonstrated on **Fig 4.4**, in ideal case is equivalent to the 180° -pulse and therefore should not produce any observable transversal magnetization. However, the spectral line broadening (due to the anisotropic CS) leads to the different effective length of the pulses for different resonance frequency offset (see Appendix III) and therefore brings some amount of transversal magnetization discovering itself as an observable NMR signal. That way, the duration τ_p of the «effective 90° -pulse» is determined by the minimization of the «residual» signal $S(\alpha)$, varying $\alpha=\gamma B_1 \tau_p$ - the flip angle corresponding to τ_p . The

dependence of the residual signal magnitude (absolute value) as a function of pulse length τ_p is shown on **Fig 4.5a**.

The signal intensity $S_{abs}(\alpha)$ was normalized on the maximal FID absolute value detected without the second pulse ($\tau_p=0$). Using the absolute value of the signal $S_{abs}(\alpha) = \sqrt{\{\text{Re}[S(\alpha)]\}^2 + \{\text{Im}[S(\alpha)]\}^2}$ allows one avoiding the problems concerned with choosing of the proper FID phasing. When the region of the pulse length corresponding to the minimum of the observable signal is roughly localized, the fine calibration of the pulse duration can be done.

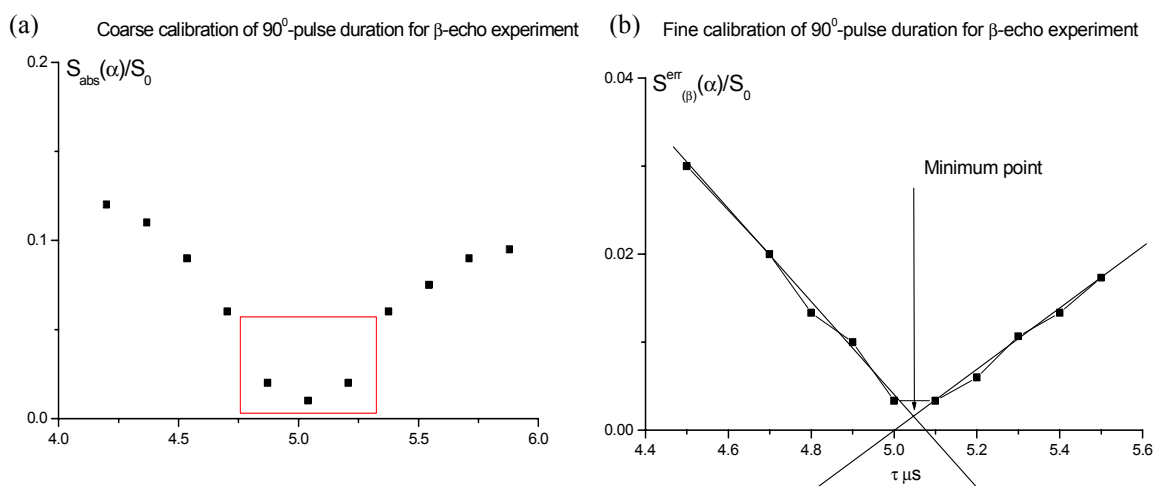


Fig. 4.5(a) Coarse calibration of 90°-pulse for β -function measurements. The compensation of the signal generated by cross-polarization (equivalent to 90° pulse) by an additional pulse with the variable flip angle α is used. The maximal signal suppression corresponds to flip angle $\beta=180^\circ$ and therefore to $\alpha=90^\circ$. **(b)** Fine tuning of the 90° pulse for the β -echo measurements by minimization of the “error signal” for the β -echo evolution time equal $\tau=0$ (see also **Fig. 4.2b**)

In turn, the fine tuning of the 90° pulse is performed using the β -echo properties. It was shown in *Appendix III* that the small r.f-pulses imperfections lead to linear dependence of the non-compensated magnetization from the tilting angle (and therefore from the rf-pulse duration) error. For the echo time $\tau=0$ the only «residual» β -echo signal resulted from the pulse length error will be observed. Similarly to the first stage, the absolute value of the FID is used to find the pulse duration bringing the minimal «error signal». Due to the linear dependence of $S_{\beta}^{err}(\alpha)$ the linear regression can be applied to provide the maximal exactness for the pulse calibration. An example of the pulse fine-tuning procedure, using the β -echo signal at zero echo time τ is shown on **Fig 4.5b**.

4.4 Molecular mobility influence on β -echo.

4.4.1 Dipolar interactions averaging and CS inhomogeneity.

The important factor influencing on the effectiveness of the β -echo experiment in the

case of polysiloxanes is a dynamics of the spin system, particularly the molecular mobility. The strength of dipolar interactions, which determine the β -function behavior is strongly dependent on the character of its averaging by the thermal motion of the molecules [IV.13-18]. For the case of the polysiloxane LCSP, it becomes especially important because of the intrinsically weak dipolar coupling between the ^{29}Si nuclei and significant difference in the character of the molecular dynamics in different LC subphases.

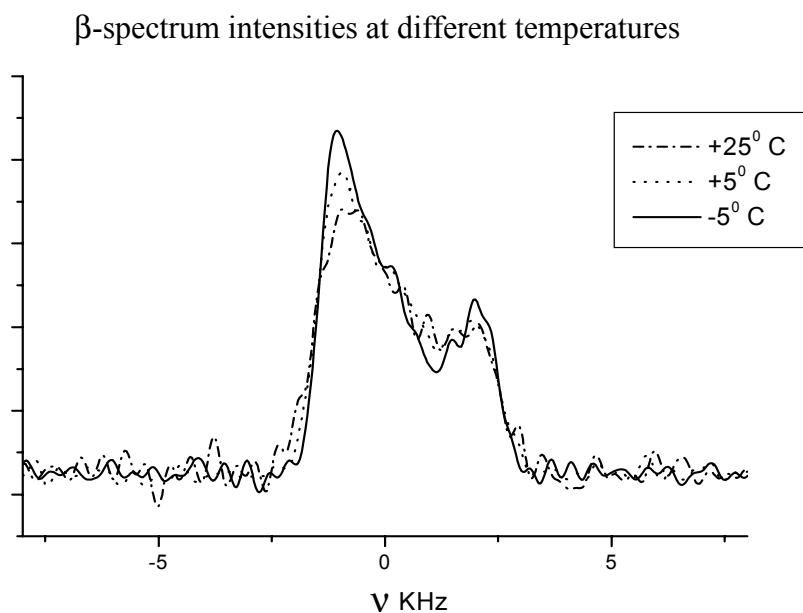


Fig 4.6 Temperature dependence of the Fourier transformed β -echo signal (β -spectrum). The thermal motion leads to the averaging of the dipolar interaction that effectively corresponds to the smaller dipolar coupling constant ω_{0D} and therefore, to decrease of the β -signal intensity (see Chapter III).

Fig 4.6 demonstrates a difference of the intensities of β -echo signals acquired at various sample temperatures. It can be expected that the freezing of the sample down to the glassy state leads to restriction of the molecular mobility and, therefore, increasing of the effective dipolar coupling constant. This can be observed on **Fig 4.6** as an increase of the relative intensities of β -echo spectra (taken with respect to the noise level). Moreover, the decrease of the spectral line broadening due to smaller effective CS distribution at slower molecular motion brings additional contribution to the β -echo signal intensity.

4.4.2 Transversal relaxation

Another important aspect of the thermal motion influence on the β -echo is a *transversal relaxation* factor. It was already mentioned in the Chapter III that to reproduce the realistic picture of β -echo evolution, the decay of transversal magnetization due to the spin-spin relaxation should be taken into account. In our consideration this have been done in quite simple

manner by introducing the exponential relaxation factor $R = \exp(-\tau_0/T_2)$ into β -function, where T_2 is the transversal (or spin-spin) relaxation time and τ_0 is the echo time. This simplification can be done if to suggest that all three components of β -echo subdue the same transversal relaxation behavior, namely, – the exponential decay with one characteristic relaxation time T_2 . It is known from literature that for the polymer samples and especially for the liquid crystalline ones the transversal relaxation behavior can depend strongly on the intensity of molecular thermal motion [IV.19-22]. That way, the detailed transversal relaxation measurements have been done for the samples of our interest with three main purposes:

- (i) determination the transversal relaxation time T_2 which is required for the proper comparison of the β -function simulation results with the experimental data,
- (ii) finding the temperature range where the single exponential description of the transverse relaxation is valid and,
- (iii) the last but not least - where the relaxation disturbing of β -function behavior still allows the extraction of the necessary information from it.

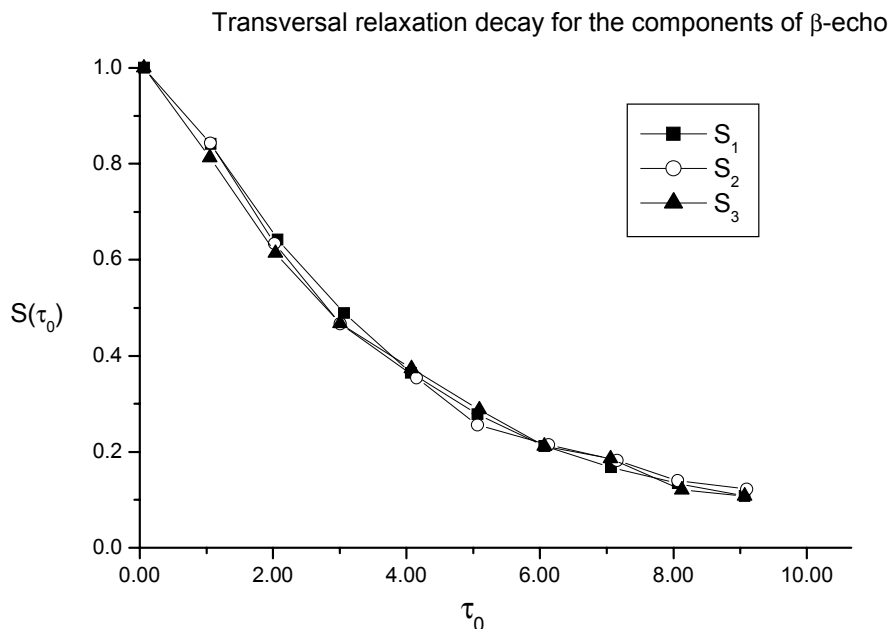


Fig 4.7. Transversal magnetization decay for each component of β -echo at low temperature. Monoexponential relaxation is demonstrated. Echo amplitude was normalized on maximal value.

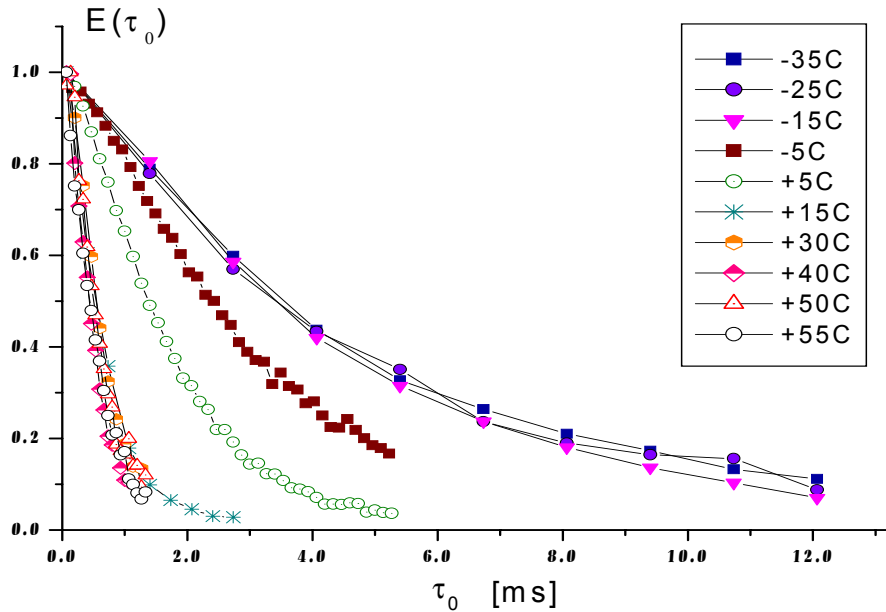


Fig 4.8a Transversal relaxation time temperature dependence for the polysiloxane M4 PLC sample. Three different characteristic temperature ranges can be selected corresponding to different regimes of thermal motion.

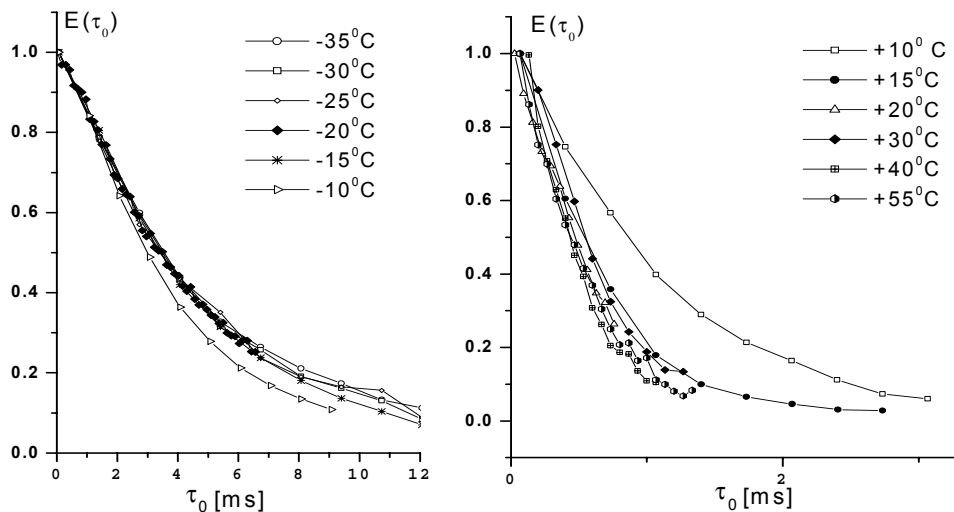


Fig 4.8b At both utmost ends of the probed temperature area ($T=-35..+55\text{C}$) the relaxation decay curves have an asymptotic limit where $T_2(T)$ dependence is very weak as compared to the relatively narrow central region ($-5..+15\text{C}$) with fast T_2 changing by the temperature

For this purposes, the transversal relaxation was measured by a standard spin-echo technique, (i.e. by measuring the time evolution of spin-echo denoted as the component S_3 of β -echo). In practice, this was done using the same pulse sequence that was described above for the β -echo, with the threefold pulse combination replaced by the single π_y pulse. However, one can notice that using both other components of the β -echo with the pair of 90^0 pulse would lead to exactly the same results for the relaxation dependence (see **Fig 4.7**) The relaxation experiments have covered the temperature range from $+55^0\text{ C}$ to -35^0 C . The resulted experimental curves are

presented on (Fig 4.8a,b) It can be seen that the transversal relaxation time changes dramatically decreasing in temperature range from 0⁰ C to +25⁰ C in a factor of 4.

The increase of the temperature from 25⁰ to 55⁰ C makes practically no further influence on the relaxation time, which keeps the constant value $T_2=0.8\text{ms}$. Similarly, the lowering temperature from -15⁰ C to -35⁰ C also shows an asymptotic dependence where the relaxation ratio remains nearly constant ($T_2=6.5\text{ms}$). An intermediate case is represented by the temperature region 0⁰ .. -15⁰ C within which the relaxation time T_2 increases by a factor of 1.5.

That way, one can conclude that at least three regimes of the molecular motion can be selected in the probed region of temperatures for the polysiloxane sample. More details on the interpretation of the transversal relaxation measurements results can be found in Chapter V. Here, it is only necessary to pay attention that for the temperatures over +10⁰ C the transversal relaxation time is shorter or comparable with the characteristic time of the dipolar correlations for the ²⁹Si pairs (estimated as the evolution period preceding the first maximum of β -function in absence of the transversal relaxation Fig 4.9a). This means that the information about the low

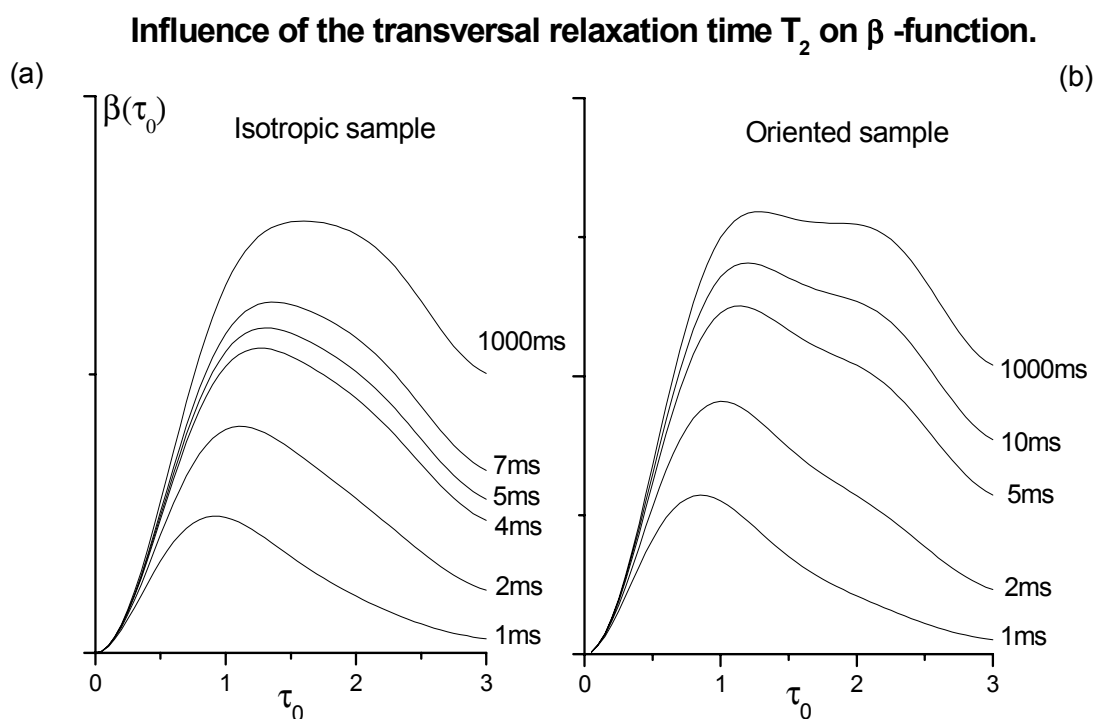


Fig 4.9.a. Influence of the transversal relaxation on the β -function maximal amplitude and time position of first maximum. It can be seen, that for the T_2 shorter than the certain characteristic time of the dipolar correlations (approximately equal to the time position of the β -function first maximum in the case of infinitely long T_2) the maximal β -function intensity decrease rather quickly. For the dipolar coupling, constant equal to 200-250Hz the T_2 should be longer than 2-2.5 ms that in the case of M4 sample corresponds to the temperature of $T \approx +5^0$ C.

(b) Influence of the transversal relaxation on the possibility to differentiate the β -functions corresponding to different orientations. Obviously, for the T_2 value shorter than the characteristic dipolar correlations time, the orientation features of β -function degenerate and the curves becomes indistinguishable from the ones corresponding to the isotropic sample orientation.

frequency β -function harmonics (i.e. with long evolution period) will be lost due to the relaxation decay. Due to the same reason the sufficient decrease of the available signal intensity will occur. These two factors make very difficult or nearly unsolvable the problem of distinguishing and analysis of β -function curves corresponding to the different orientation parameters in the case of short transversal relaxation time (see **Fig 4.9b**).

Summarizing, one can say, that the temperature range above 0°C was found inappropriate for the β -echo investigation in the available polysiloxane LCSP samples because of the irrecoverable losses of the observable magnetization. These losses come from the molecular thermal motion, which produces the dephasing effect on dipolar coherences via the (i) dipolar interaction averaging and (ii) spin-spin relaxation.

Additionally, the transversal magnetization decay for the temperatures $T > +15^{\circ}\text{C}$ becomes non-exponential, that makes the task of β -function analysis much more complicated than under the exponential relaxation conditions perfectly fulfilled for the low-temperatures. Therefore, it would be optimal to perform measurements in the temperature range of -25°C – -35°C providing the maximal achievable transversal relaxation time. However, due to the technical reason the supporting of such a low temperatures during the 48-72 hours, which is required for the β -echo experiments, could be problematic. That way, the regular measurements with polysiloxanes LCSP were performed at the temperature from -5°C to -10°C depending on the duration and particular purposes of the measurements. More detailed discussion of the transversal relaxation measurements results will be done in Chapter V.

4.5 Dipolar constant determination using « β -spectrum» analysis.

It can be seen from the theoretical consideration of β -function properties that the initial point of a way, which, brings us from the nuclear spin interactions to the parameters of the orientation distribution of the molecules, is the value of dipolar coupling constant ω_{0D} . Obviously, due to the large number of intermediate steps the accuracy of this parameter estimation is of critical importance for all the subsequent calculations. In the section (3.3) it was shown that the most reliable results of the ω_{0D} evaluation can bring the complex analysis of the β -echo subspectra evolution. The corresponding β -echo experiments were performed on the sample of polysiloxane M4 with polydomain (unoriented) structure. Initially, for the rough estimation of the maximum of β -function from 10 to 20 signals of β -echo were acquired varying the echo delay time τ_0 from 0 to 3-4 ms with the step 100..500 μs . The longitudinal relaxation time of the ^{29}Si ($T_1 \approx 1$ sec) requires the relatively long magnetization recovery delays (pause between the subsequent averages had to be set to 4 sec in our measurements). To estimate roughly the β -

function maximum the number of averages of each echo signal was varied from 480 to 720 that

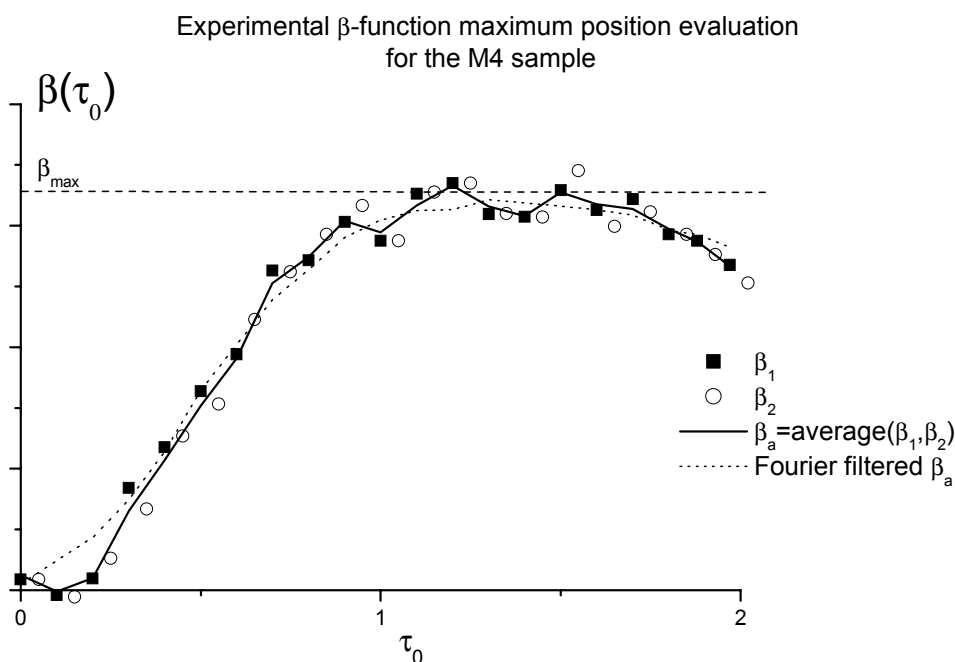


Fig 4.10. Experimental results on β -function maximum rough estimation for the M4 sample. The result of the experiments using different sets of the evolution time τ_0 are then combined by the averaging. Finally, the low-pass Fourier filtration can be applied to reduce the noise factor influence (see below)

Fourier transformed ^{29}Si NMR β -echo evolution for the disoriented PLC sample.
(polysiloxane M4)

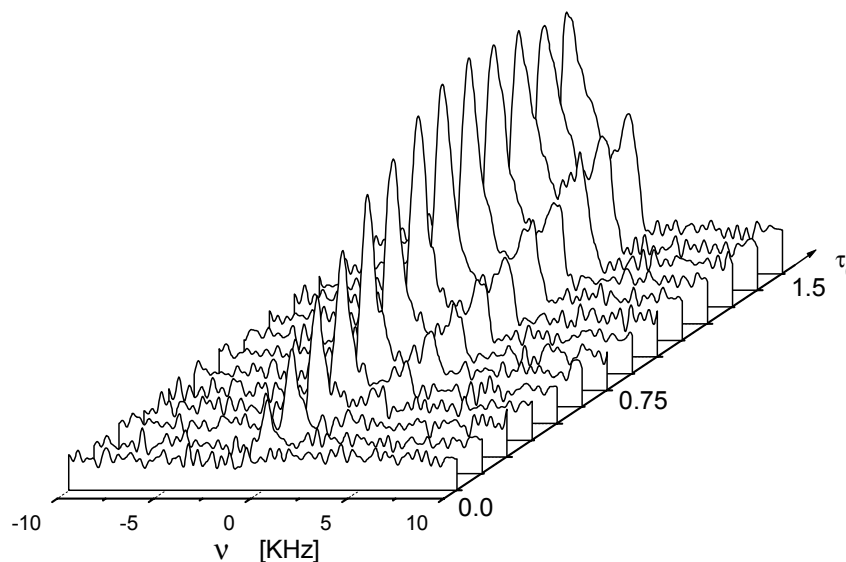


Fig 4.11. Fourier transformed β -echo signals (“ β -spectra”) acquired for the polysiloxane M4 sample. The evolution of the lineshape is observed due to the different position in spectrum defined by the anisotropic chemical shift corresponds to the different dipolar coupling intensity related with the different orientation of the internuclear vector (see Chapter 3 for more details).

lead to the total experiment duration of about 5-8 hours providing moderate signal-to-noise ratio (S/N=3..5). The β -function, in principle, might be established in dependence on chemical shift position for each point of the spectrum. However, because of the spectral broadening (see 3.7.2

and **Fig 2.12**, **Fig 3.17**) it is reasonable to use the spectral intervals of the order of intrinsic line broadening width (**Fig 2.12**). This also gives the additional advantage of certain improvement of S/N ratio.

The evolution of the β -spectrum intensity at the the characteristic positions.

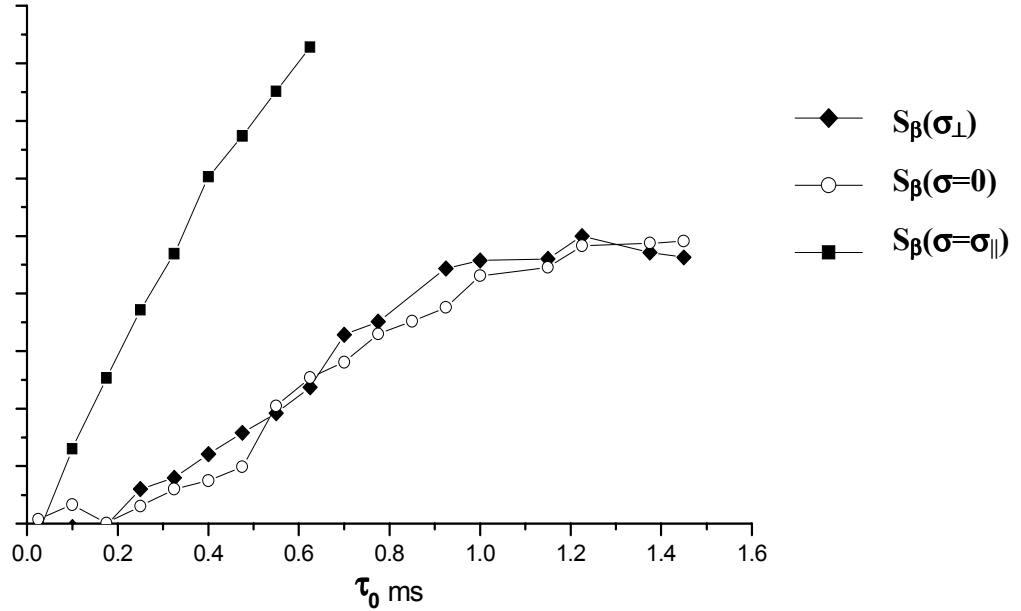


Fig 4.12. The evolution of the spectral density of the β -echo signal at the characteristic positions corresponding to the main values of the CS tensor. The points represent the integral $S_\beta^{(i)}$ (see text) for each position.

An example of the results of β -function maximum search experiments is presented by the **Fig 4.10**. Function $\beta(\tau_0)$ represents amplitude of the time domain β -echo signal in the moment τ_0 . To make sure about the results reproducibility, the experiments were repeated using different arrays of the values for the evolution time τ_0 (denoted as β_1 and β_2 on **Fig 4.10**). The curves of the several measurements then can be then combined together by deriving an averaged curve. Finally, the low-pass Fourier filter can be applied to reduce the noise influence (see below). By comparison of these experimental data with the β -function simulation results from Chapter III the dipolar coupling constants can be estimated roughly within value of 200..250Hz, that is in agreement with a priori theoretical estimation. That way, according to the consideration has been done in (3.7.2) for the optimal β -spectra analysis the β -echo evolution time period of $\tau_0=0...1.5$ ms was chosen (see **Fig 4.10**).

The following measurements, with final aim of the ω_{0D} estimation from the β -spectrum, requires higher accuracy and, therefore, were done acquiring from 1920 to 2400 scans for each

echo signal that increases the signal-to-noise ratio approximately by the factor of 2 ($S/N \sim N_a^{1/2}$, where N_a is the number of averaging of the signal).

Afterwards, obtained β -spectra $S_\beta(\sigma, \tau_0)$ (**Fig 4.11**) were integrated over the limits $\sigma_i \pm \delta$, where σ_i are the characteristic positions of CS spectrum ($\sigma = \sigma_{\parallel}$, $\sigma = 0$, $\sigma = \sigma_{\perp}$) and $\delta = 0.1 \Delta\sigma$ (taken from the estimation of broadening factor by the CS spectrum deconvolution (see **Fig 2.12a,b**).

$$\text{The obtained integral values } S_{\beta}^{(i)}(\sigma_i, \tau_0) = \int_{\sigma_i - \delta}^{\sigma_i + \delta} \Omega_{\beta}(\sigma', \tau_0) d\sigma', \text{ where } \Omega_{\beta}$$

denotes β -spectrum, are presented on (**Fig 4.12**). The curves $S_{\beta}^{(i)}$ then were fitted with the corresponding β -function harmonics (see **3.7.2**) to get the effective dipolar coupling constants $\omega_{eff}^{(i)}$. The results of this procedure for all three characteristic spectrum positions are

presented on the (**Fig 4.13**). Finally, the coupling constant $\omega_{0D}^{av} = \frac{1}{3} \sum_{i=1}^3 \omega_{0D}^{(i)}$ determined, where $\omega_{0D}^{(i)}$ values were taken from linear «calibration» dependence $\omega_{0D}^{(i)} = a_i \omega_{D,eff}^{(i)} + b_i$ for each of three spectral positions have been used (see **3.7.2** and **Fig 3.20** for explanation). The results of the ω_{0D} evaluations are presented in the Table 4.2

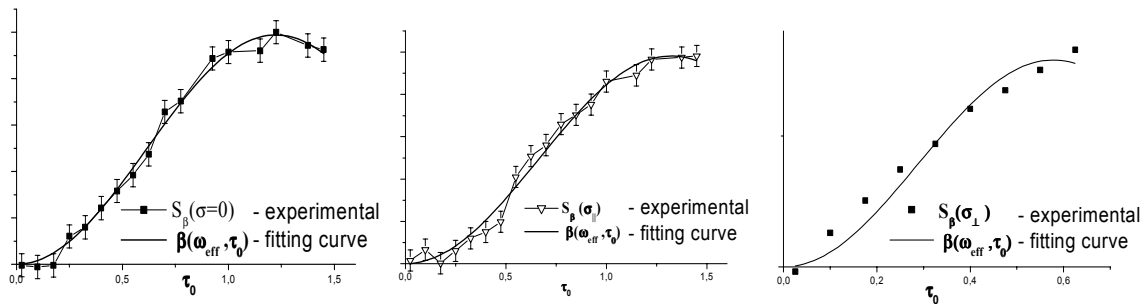


Fig 4.13. The experimental curves, obtained by the integration of β -spectrum for the characteristic values of CS tensor (**Fig 4.12**), are fitted with the β -function parametrically dependent on the effective dipolar coupling constant ω_{eff} .

Table 4.2 Dipolar coupling constant evaluation results

-----	$\sigma = \sigma_{\parallel}$	$\sigma = 0$	$\sigma = \sigma_{\perp}$
$\omega_{eff}/2\pi$	110	115	210
$\omega_{0D}/2\pi$	225	222	230
$\Delta\omega_{eff}/2\pi$ (fitting)	8	9	14
$\Delta\omega_{0D}/2\pi$			
(calibration)	6	7	10
$\omega_{0D}^{av}/2\pi = (225 \pm 10) \text{ Hz}$			

Here, $\Delta\omega_{eff}$ means the error of the experimental data fitting with β -functions. The value $\Delta\omega_{0D}$ represents an error introduced by the intrinsic calibration curve $\omega_{0D}(\omega_{eff})$, uncertainty, which arises from the fact that small but finite region of spectral density of β -echo signal is treated as a corresponding to the single β -function harmonic described with single parameter ω_{0D} . However, the error of calibration does not exceed a fitting procedure error, which includes also the experimental noise contribution.

4.6 Using FFT filters for the noise factor minimization.

The methods of the ODF moments determination described in (3.7) allows one reducing the influence of the noise factor by using the specific properties of β -function orientation dependence. Practically, it means that the characteristics of the β -function curves used for the orientation parameters analysis, provide the sensitivity, which exceeds the experimentally relevant signal-to-noise ratio. However, these methods, being based on the evaluation of the β -functions maximums and crossing points, needs rather accurate interpolation to obtain the continuous curves from the discrete experimental data points. The “brought-in” distortion due to the incorrect experimental smoothing can eliminate all advantages of the curves comparison

Application of FFT low-band filtering for interpolation and noise factor reducing in β -function

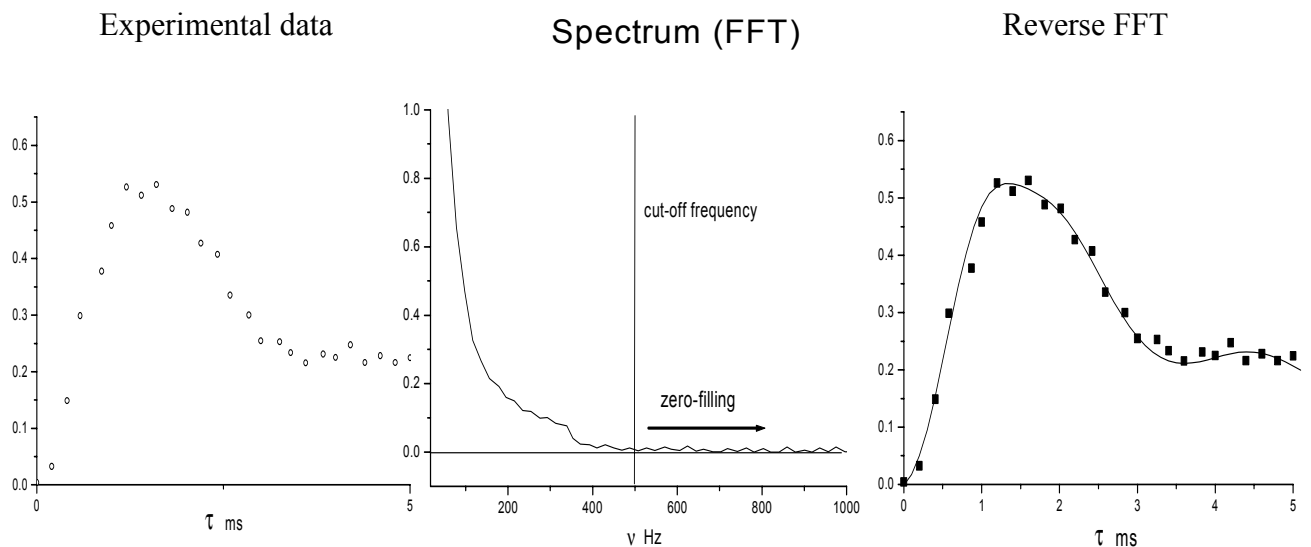


Fig 4.14. Application of the low-band Fourier filtration for the controllable data smoothing and noise factor reducing. The experimental β -function data passes the FFT procedure with subsequent cutting-off the high-frequency part of the spectrum which is supposed to does not contain the useful signal due to the absence of higher frequencies in the dipolar interaction spectrum for the ^{29}Si pairs.

analysis. In contrast, the proper methods of the data pre-processing allow one to increase the accuracy of the targeting parameters determination. Two factors are important when choosing the interpolation procedure for the data point:

1. Exact knowledge about the part of information, which can be lost from data set after procedure performing. (and the possibility of its control)
2. The procedure should be as much as possible selective for the separation the noise and “useful” signal.

Both these criteria are well satisfied by employing of the low-band FFT filter [IV.23-25] for the data pre-processing. The useful information in this case can be selected from the signal (and then separated from the noise) using the knowledge about a highest possible harmonic of β -function. An example of the low-band FFT filtering/interpolation procedure of β -function data is demonstrated on **Fig 4.14**.

As it can be expected the intensity of β -function spectrum (should not be confused with “ β -spectrum”) decreases rather fast for the frequencies higher than dipolar coupling constant $\omega_{\eta D}$. That way, the higher frequency harmonics will contain only the noise signal, which can be cut off. The interpolation of the data curve in the case of FFT filtration procedure can be done by zero-filing in the frequency domain (fully analogous to the zero-filing of the time domain FID signal to get the spectrum smoothed)

4.7 Determination of the Orientation Distribution Function for the polysiloxane M4 sample using the β -function technique.

It was shown in Chapter III, that the shape of β -function curves is determined by 3 basic factors: (i) the intensity of bilinear interaction (expressed via the dipolar coupling constant value $\omega_{\eta D}$), (ii) microscopic orientation distribution of the principal axes of these interactions (internuclear vectors for the ^{29}Si nuclei coupling) and (iii) macroscopic orientation of the sample with respect to the NMR laboratory frame (external magnetic field). The value of $\omega_{\eta D}$ can be determined independently using the sample in disoriented (multidomain) state and then can be used in the analysis of the data of β -function experiments over the oriented samples as the known fixed value. According to consideration has been done in (3.6), the comparison of β -function curves obtained for the different sample macroscopic orientation with respect to the NMR laboratory frame allows one estimating its microscopic ordering parameters. Particularly, the characteristic of β -function curves corresponding to the zero, right and “magic” tilting angles can be directly connected with the 2-nd and 4-th Legendre expansion moments of the sample

ODF. However, the methods used for the $\langle P_2 \rangle$ and $\langle P_4 \rangle$ determination requires the analysis of the slightly different parts of the β -function curves (corresponding to the different periods of β -echo evolution respectively). Moreover, the $\langle P_4 \rangle$ evaluation requires a higher accuracy of the experimental data treating because the sensitivity of β -function to the orientation distribution features decreasing strongly with the signal-to-noise ratio (see 3.6). Particularly, the $\langle P_4 \rangle$ evaluation needs rather precise determination of the crossing points of the different β -function curves, that in turn requires the sufficient amount of experimental data points for correct and unambiguous curve interpolation. On the other hand, the intrinsically low intensity of β -echo for ^{29}Si dipolar coupling requires the relatively large amount of signal averaging. That way, to fit the reasonable duration, the experiments on β -function orientation dependence were done in two steps. At first the “region of interest” (ROI) for the β -function curves is to be found. This particularly means, that the time positions of the β -function curves, which are important for the $\langle P_2 \rangle$ and $\langle P_4 \rangle$ evaluation should be roughly estimated by the scanning of relatively large period of β -echo evolution. On this stage, a moderate amount of the averaging can be used for each point. The value of $\langle P_2 \rangle$ can be then roughly estimated from the amplitude of the curves corresponding to characteristic sample orientations. On the second stage the selected ROI for each orientation have to be explored in details acquiring the β -echo amplitude through the minimal periods and using the maximal (possible within the reasonable experimental timeframe) amount of scans for each point. For the first measurements, the sample of oriented polysiloxane LCSP M4 was chosen. As it was mentioned in Chapter I, this LCSP has preferably parallel orientation of main chain and local director (given by the side-chain). This allows one evaluating

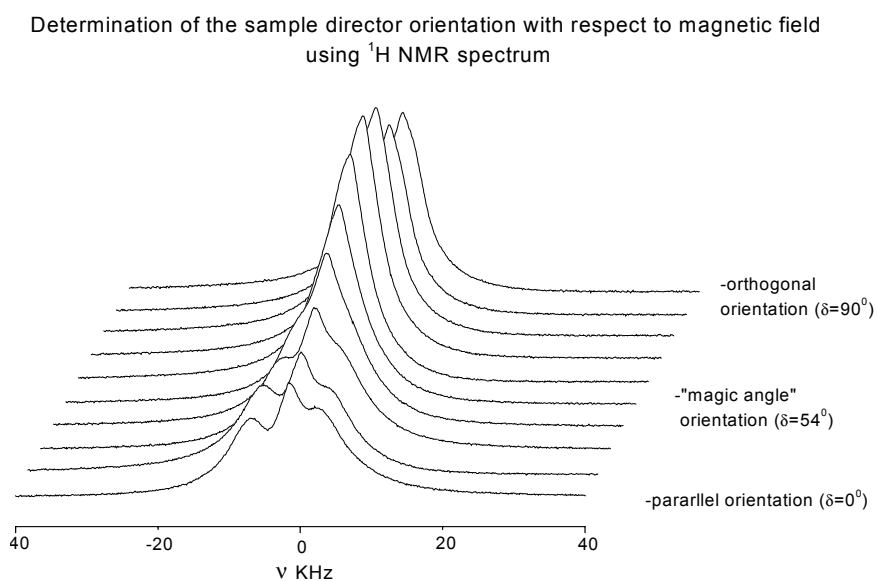


Fig. 4.15. Determination of the monodomain M4 sample local director orientation using ^1H NMR wideline spectra orientation dependence. The maximal line splitting caused by dipolar interactions of aliphatic protons corresponds to the parallel orientation of the mesogenic unit with respect to magnetic field.

this orientation direction considerably quickly and accurately using the ^1H spectrum determined mainly by the coupling of the aliphatic protons in the side-chain [IV.26-27]. In practice, the reference orientation at which the sample local director is parallel to the external magnetic field H_0 was found by the angular dependence of ^1H spectrum second moment. The dipolar coupling, similarly to the axial symmetric CS interaction is proportional to the $P_2(\cos(\beta))$, where β is angle between interaction axis and magnetic field. Recollecting the consideration has been done for the ^{29}Si spectra angular dependence in Chapter I,II one can conclude that the lineshape second moment angular dependence maximum (arising from the maximal NMR linewidth, see Fig 4.15) corresponds to the parallel orientation of dipolar interaction axis (corresponding in turn to the orientation of sample local director).

4.7.1 Data normalization procedure.

Another problem arising from the long time needed for measurements with β -function is that the curves corresponding to the different orientation cannot be recorded during the one

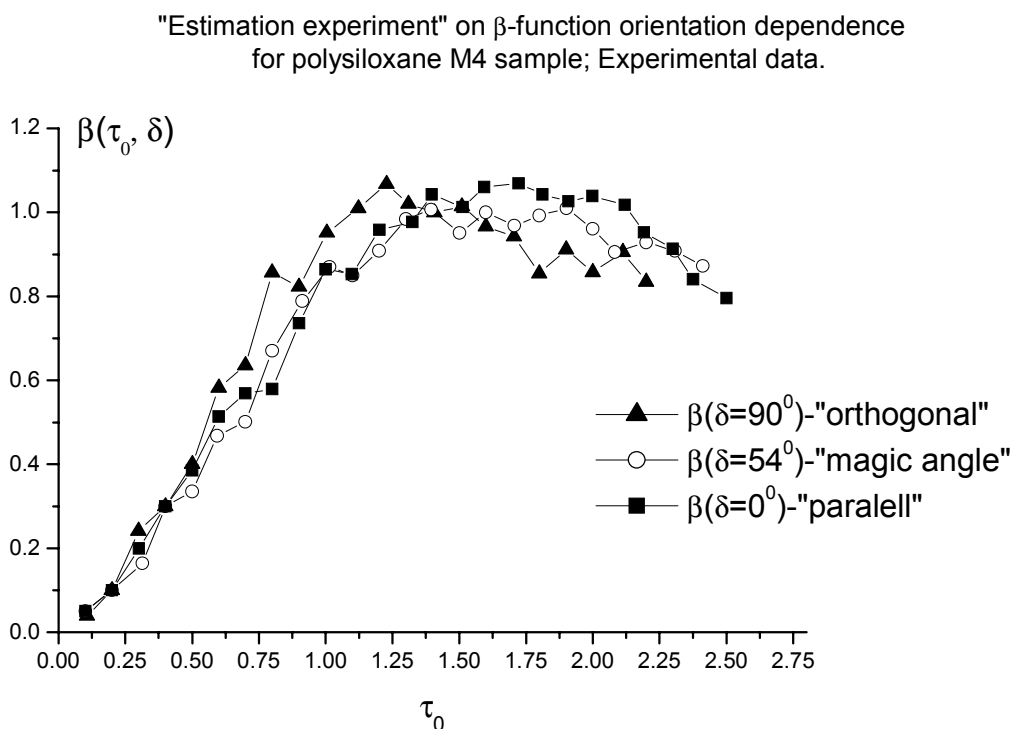


Fig 4.16. The results of the estimation stage of the experiments over the β -function orientation dependence in monodomain M4 sample. Three characteristic orientations of the sample local director with respect to the magnetic field were probed.

experiment session. This means that for comparison of the curves from different measurements some normalization or reference is needed. For this purposes each angle-dependent experiment

was started with recording of some amount of data points for the parallel orientation of the sample on the initial (prior β -function maximum) part of the β -echo evolution. The normalization coefficient can be found by the averaging of the ratios of the corresponding elements of two sets:

$$R = \frac{\sum_{k=1}^N \beta'(\tau_k)}{\sum_{k=1}^N \beta''(\tau_k)}$$

where $\beta'(\tau_k), \beta''(\tau_k)$ denotes β -function values defined in two different experiments at the same moment of evolution time τ_k and N – the amount of points used for the averaging. The resulted coefficient \mathbf{R} has been used to bring the dataset of two different experiments to the same relative intensities.

The results of the “estimation stage” of the experiments of beta-function orientation dependence are shown on **(Fig 4.16)**. Three characteristic orientation of the local LC-director with tilting angles of $\delta=0^0$, 54^0 (“magic angle”) and 90^0 with respect to the external magnetic field were measured. The 600 scans were acquired for each point leading to the 16 hours of experiment time for each orientation of the sample. In the presented plot the β -function curve recorded at the “magic angle” orientation was used as the referencing i.e. all the curves were normalized to get the maximum of $\beta(\tau_0, \delta=54^0)$ equal 1. It can be seen that the relation between the curves obtained at characteristic orientations of the sample LC-director with respect to the magnetic field B_0 qualitatively reproduces the theoretically predicted picture (see Chapter **III**). In the same time, due to the moderate amount of signal averaging scans used in the estimation stage of the experiment, the signal-to-noise ratio does not exceeded 5 (i.e. noise level is about 20% of total signal). This allows one only quite rough estimating of the curves parameters required for the orientation parameters evaluation (particularly, the position of the $\beta(\tau_0, \delta=54^0)$ curve maximum which is needed to determine the $\langle P_2 \rangle$ value). The situation is improved after application of the described above FFT low-band data filtering. The results of this procedure for different cut-off frequencies of FFT-filter are shown on **(Fig 4.17)**.

As it can be expected when considering the simulation results (Fig 4.14), the best effect

Noise influence reducing by the low - band FFT-filters;
the cut-off frequency adjustment for the β -function experimental data

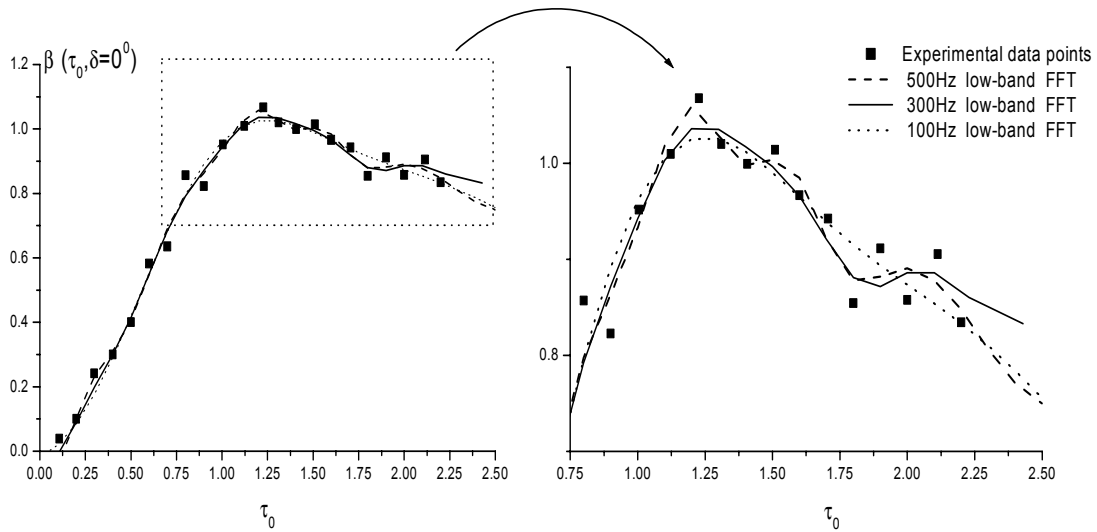


Fig. 4.17. Application of the low-pass Fourier filtration to the β -function data for curve smoothing and reducing of the noise factor. The cut-off frequency has to be adjusted according the maximal observed harmonic in β -function spectrum to make the filtration procedure the most effective.

"Estimation experiment" on β -function orientation dependence
for monodomain polysiloxane M4 sample; Fourier filtered β -function curves.

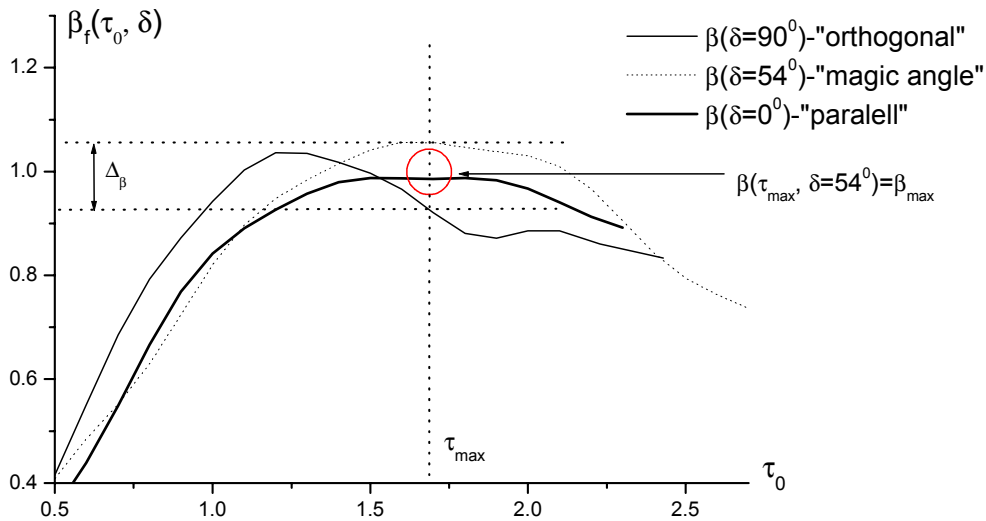


Fig 4.18. Fourier filtered data of the «estimation experiment» for the β -function or orientation dependence (see Fig 4.16). The cut-off frequency for low-pass filtration was set to $\nu_c=300\text{Hz}$.

for data interpolation with simultaneous smoothing (and therefore reducing of the noise effect) gives the filtration with the cut-off frequency which is close to the frequency of the highest signal harmonic contributed to the total β -function ($f_{max} \approx \omega_{0D} / 2\pi$). For the higher and lower cut-off frequencies, the noise suppression and data interpolation are not effective respectively. For

the “evaluation” stage the number of scans used for NMR signal averaging was increased in 4 times ($N_{av}=2880$) that gives increasing the signal-to-noise ratio approximately in the factor of 2 in comparison to the evaluation stage. The β -echoes were probed within the β -function ROI evolution period found in the estimation measurement stage. Twenty β -echo signals were acquired for each sample orientation that gives the total experiment time duration of about 48 hours. On the preprocessing stage, all the data sets were normalized using the preceding reference β -function measurements (see the method described above). Afterwards, the low-band FFT filtration with cut-off frequency $\nu_c=300\text{Hz}$ were applied to reduce the noise factor influence.

The ODF's moments were estimated by the comparison of the curves parameters according to the method described in (3.6). The maximum value of $\beta(\delta=54^\circ)$ is achieved at the moment $\tau_{max}=1.7\text{ms}$.

For the subsequent analysis, the following iteration scheme was used:

1. The difference of the β -function values of parallel and orthogonal sample orientation $\Delta\beta(\tau_{max})=\beta(\tau_{max}, \delta=90^\circ)-\beta(\tau_{max}, \delta=0^\circ)$ is determined from the β -function curves plot.
2. The ODF's second moment value $\langle P_2 \rangle$ is estimated from the calibration dependence $\Delta\beta(\langle P_2 \rangle)$ (see 3.6). To build the calibration dependence in zero approximation the value $\langle P_4 \rangle$ was taken equal to $\langle P_4 \rangle = 0.01$.
3. The period $\Delta\tau=\tau_1-\tau_2$ is determined (see **Fig 4.18**). Here τ_1 and τ_2 denotes the time moments which fulfill the condition $\Delta\beta(\tau_1)=\Delta\beta(\tau_2)=0$, (i.e. the time moments corresponding to the crossing of the β -function curves with parallel and orthogonal sample orientation).
4. The value of the ODF 4-th moment $\langle P_4 \rangle$ is evaluated from the calibration dependence **3.14**. $\Delta\tau(\langle P_4 \rangle)$, calculated using the $\langle P_2 \rangle$ value determined on stage 2.
5. Returning to stage 2. The obtained $\langle P_4 \rangle$ value is used to build the next approximation of the calibration dependence $\Delta\beta(\langle P_2 \rangle)$.

The described iteration cycle is performed until the achieving of the pre-chosen convergence condition for the $\langle P_2 \rangle$ and $\langle P_4 \rangle$. Particularly, in our case the process was stopped when the relative error of the iteration step became smaller than the relative noise level of β -echo signal:

$$\Delta P_{2,4} = \frac{|\langle P_{2,4} \rangle_{i+1} - \langle P_{2,4} \rangle_i|}{\langle P_{2,4} \rangle_{i+1}} \leq \left(\frac{S}{N}\right)^{-1},$$

The linear dependence which has been found for the calibration functions $\Delta\beta(\langle P_2 \rangle)$ and $\Delta\tau(\langle P_4 \rangle)$ (see Chapter III) allows one to recalculate it rather fast for each iteration step (obviously the only 2 points are needed to determine the linear dependence equation and to find the new value of the $\langle P_2 \rangle$ from it).

Table 4.3 shows the results of the iteration procedure performed for the β -function orientation dependence. It can be seen that both $\langle P_2 \rangle$ and $\langle P_4 \rangle$ iteration sequences converge to get the predefined limit of the error already after 3 steps. The $\langle P_2 \rangle$ and $\langle P_4 \rangle$ obtained in steps number 4 and 5 can be considered as a demonstration of the iteration process convergence trend (the estimated values remains within the experimental error «gap» defined by the noise level).

Table 4.3 Iteration procedure results for the orientation distribution function moments estimation using β -function orientation dependence. (M4 sample)

N	$\langle P_2 \rangle$	$\langle P_4 \rangle$	ΔP_2	ΔP_4
1	0.097	-	-	-
2	0.087	0.0032	0.04598	-
3	0.083	0.0035	0.00723	0.05714
4	0.0824	0.0037	0.00485	0.05405
5	0.082	0.0039	0.00488	0.05128

4.8 Determination ODF moments for the monodomain sample of polysiloxane M6.

On the next stage of the work, the technique of the ODF's evaluation tested on the polysiloxane PLC M4 was applied for the investigation of the main-chain orientation parameters of the sample denoted in Chapter I as **M6**. This **LCSP** has both the backbone and side-chain molecular structure, which are identical to the M4 sample. The structural difference concluded into the spacer length (two more CH_2 groups are present). This, however, leads to the dramatic changing of the preferable orientation of the side-chain with respect to the backbone from parallel (M4) to the orthogonal (M6) that is confirmed by the analysis of the CS spectrum orientation dependence (see Chapter II). This structural feature makes the LCSP M6 a very interesting object for the investigation of the orientation distribution using the β -echo and β -function.

4.8.1 Preferable main-chain segments alignment direction determination.

Most of the technical procedures of the measurements with M6 sample were the same as for the M4 sample. However, because the orientation of the main-chain segments was not known a-priori, a preliminary search of the characteristic angular positions has been needed for the β -function analysis. It was already mentioned, that for the moderate orientation degree $\langle P_2 \rangle \gg \langle P_4 \rangle$ the simulation shows that the β -function corresponding to the parallel orientation of the preferable segment's alignment direction (also was referred as “segment’s ODF reference axis”) with respect to magnetic field, has the biggest derivation in the initial evolution period in

comparison to all others sample orientations (see Chapter III). Using this circumstance, a sample position corresponding to the perpendicular orientation of the main-chain segments with respect to the magnetic field can be found by comparison of the grow up ratios of β -echo amplitude for different tilting angles δ using 4-5 points of the initial evolution period. The tilting angles region for this search was chosen using the ^{29}Si CS spectral lineshape orientation dependence data (see Chapter II). Particularly, the orientation of the ^{29}Si CS tensor main axis perpendicular to the magnetic field can be used as the starting point to find the preferably parallel orientation of chain-segment alignment (of course, if to take into account the suggestions concerning the transversal anisotropy).

To avoid the problems concerned with the different probe sensitivity calibration for different sample orientations the processing of the results of the orientation estimation measurements were done in following manner:

1. The angular region preliminary estimated as parallel orientation of main-chain segments with respect to the external magnetic field (using ^{29}Si CS tensor axis orientation) was chosen.
2. 5-6 points of the initial period of β -echo evolution $\tau = \tau_{min} \dots \tau_{max}$ were recorded for several different sample orientations δ_i within above-mentioned angular region.
3. Each curve were normalized on the maximal value so that $\beta(\delta_i, \tau_{max})=1$. Then, the derivation $D(\delta_i, \tau_0) = d\beta(\delta_i, \tau_0)/dt$ of each curve was calculated in the time moments τ_{min} and τ_{max} .
4. The curve providing the maximal value of the parameter $\Delta D(\delta_i) = D(\delta_i, \tau_{max}) - D(\delta_i, \tau_{min})$ is considered like the one corresponding to the parallel alignment of main-chain segments with respect to the magnetic field. ($\delta_i=0$).

An example of this process demonstrated on **Fig 4.19 a,b**. The experimental β -echo data points corresponding to several different sample-tilting angles δ_i are plotted on **Fig 4.19a**. Due to the artificial normalization the difference between the curves are not apparent. However, the derivation curves (**Fig 4.19b**) show the clear difference in the β -functions corresponding to different orientations δ_i . Particularly, the curve $\beta(\delta_2, \tau_0)$ with fastest grow up ratio in the probed evolution period can be easily identified.

4.8.2 Orientation distribution parameters determination

The coincided structure of the most of molecular fragments allows one using the experimental results obtained for the LCSP M4 in analysis of β -echo experiments on the LCSP M6. Particularly, the value of dipolar coupling constant $\omega_{\theta D}$ determined for the M4 suppose to be

the same for the LCSP M6 (due to the identical backbone structure). That way, the β -echo experiments with the latter sample were started directly from the orientation dependence investigation. Due to the less amount of the substance available, the number of signal averaging scans (and therefore the duration of the experiment) for the M6 sample had to be increased in comparison to M4 to get the same signal-to-noise ratio. However, the β -echo measurements of the orientation dependence of the M4 sample allowed one saving the experimental time and to concentrate directly on the β -function ROI for the corresponding experiments on the M6.

The initial point of the measurements with β -function orientation dependence for the M6 sample were described in previous section. When the sample orientation, corresponding to the parallel alignment of main-chain segments and magnetic field, were found, the regular measurements of β -function have been performed in the same manner as it was described for the “evaluation” stage of the experiments with M4 sample. Three characteristic orientations “parallel”, “orthogonal” and “magic angle” were probed acquiring 20 β -echo points in each case. From 2880 to 3200, signals averaging were used for each point. Additionally, the conventional ^{29}Si and ^1H spectra were recorded during the orientation search measurements to be able to relate the orientation parameters of main-chain with the orientation of local director (determined by mesogenic units of side-chain). The procedures of the data preprocessing (normalization, filtering, etc) were performed according to the procedures described for the M4 sample in previous sections.

The results of the measurements on β -function orientation dependence for the M6 LCSP polysiloxane is shown on **Fig 4.20a,b**. It can be seen even qualitatively that M6 sample demonstrates stronger orientation character than the M4. Particularly, it can be seen by appearance of the additional features in the β -function curve corresponding to “parallel” orientation which was not observed in the case of M4. The results of the data processing with the aim of determination of the ODF’s Legendre expansion moments by the iteration procedure (see description above) are summarized in **Table 4.4**

The supplementary data of the ^1H and ^{29}Si spectra and its relation with the β -function “orientation search” results are shown in **Fig. 4.21**. Being evaluated in previous experiments (see Chapter II), the values of the ODF's second moments, as well as the spectral lineshapes of ^{29}Si and ^1H spectra, allows one determining perfectly well a current angular position of the sample with respect to magnetic field. For this purpose, the values of the first moment of ^{29}Si spectra $M_1(\delta_i)$ recorded at corresponding angular positions δ_i during the orientation search with β -function was fitted with the calibration curve $f(\delta) = \langle P_2 \rangle_{CS} P_2(\delta)$, where $\langle P_2 \rangle_{CS}$ is the second moment of the CS main axis ODF. That way, the preferable alignment of the CS main axis

(defined from $M_I(\delta)$) can be correlated with the main-chain segment orientation (defined from $\beta(\delta)$ derivation).

Additionally, the acquired ^1H spectra allow one relating the backbone segments orientation straightforwardly with the sample local director (see above). For the calculation of

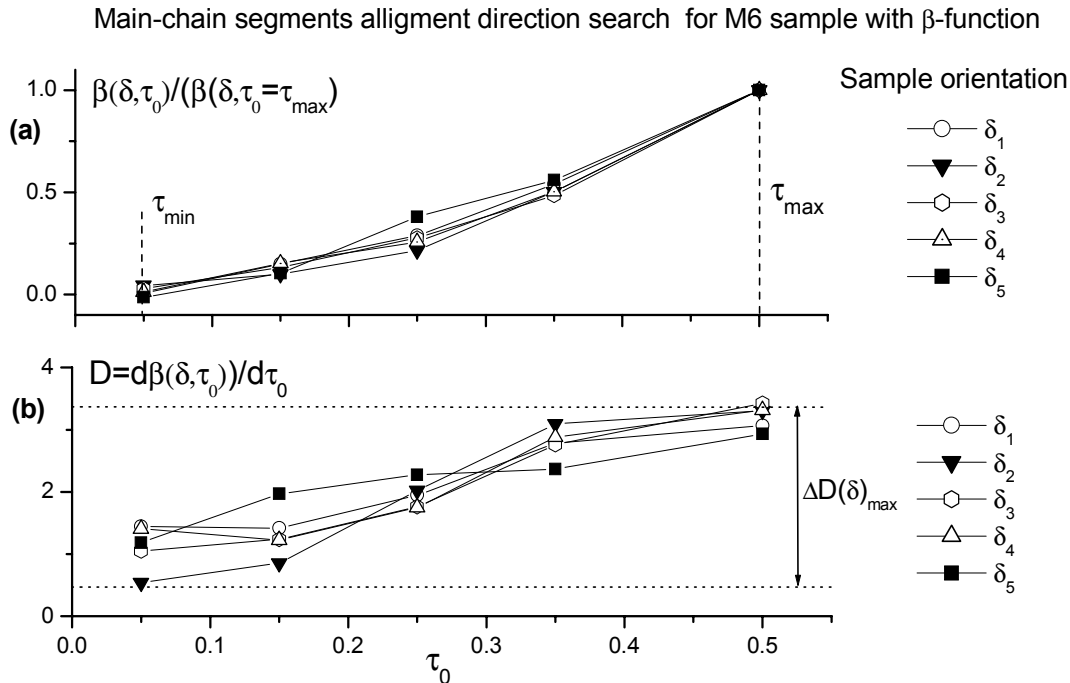


Fig 4.19. Determination of the main-chain segments alignment orientation with respect to the magnetic field for the M6 monodomain sample using β -function orientational properties. Particularly, the β -function curve corresponding to the searched parallel segment orientation has to provide the maximal grow up ratio of the β -echo amplitude in the initial evolution period (due to the maximal contribution of the high frequency β -function harmonics, see (3.5-3.7)). The β -echo signal amplitudes were normalized on its maximal values (Fig a) for each orientation. As the characteristic of the β -echo amplitude grow up ratio, the β -function curvature in the initial evolution period had been used. The curvature evaluation has been done, in turn, by the estimation of the β -function first derivation changes (Fig b)

Experiments on β -function orientation dependence for the monodomain M6 LCSP

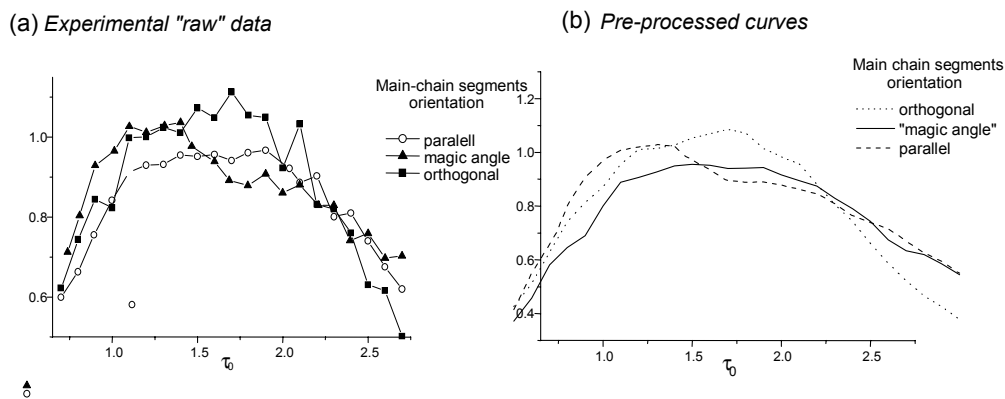


Fig 4.20. Evaluation of the ODF moments for the monodomain oriented M6 PLC using β -function orientation dependence. Raw β -echo signal contains more noise than in the case of M4 sample measurements due to less sample's mass available. The number of signal averaging had to be increased up to $N_{\text{av}}=3200$ for each point. The main chain segment alignment has been estimated in separate experiment and correlated with the ^{29}Si CS main axis and sample local director orientation. The β -function curves particularly show that the orientation degree of M6 sample is significantly higher than for M4.

the second moment orientation dependence $M_2(\delta)$ of the ^1H absolute (power) spectrum were used. This allows one avoiding the phasing problem and increases the accuracy sufficiently (the details about the possibility of using the power spectrum instead of real one in the case of M_2 estimation can be found in [IV.27]). As the $M_2(\delta)$ of ^1H spectrum has the local maximum at $\delta=90^\circ$, the scaled values of $|M_2(0)-M_2(\delta)|$ are plotted to make the convenient comparison with $M_1(\delta)$ of ^{29}Si spectrum dependence, which has the minimum there.

Table 4.4 Orientation distribution function moments determination for the monodomain M6 sample

N	$\langle P_2 \rangle$	$\langle P_4 \rangle$	ΔP_2	ΔP_4
I	0.285	-	-	-
2	0.245	0.0055	0.16	-
3	0.233	0.0067	0.051	0.17
4	0.224	0.0071	0.04	0.056
5	0.221	0.0072	0.03	0.0042

That way, the results of the main-chain segments orientation distribution evaluation, performed by using of the ^{29}Si - ^{29}Si dipolar coupling and β -echo can be combined together with the results of the conventional ^{29}Si spectrum orientation dependence studying. This provides us the information about the ^{29}Si chemical shift tensor main axis orientation. Additionally, the orientation distribution functions of mentioned above molecular frames can be correlated with the sample local director orientation. The latter can be estimated from the orientation dependence of the ^1H spectrum.

In the conclusion chapter the results of the described above β -function experiments will be discussed and summarized.

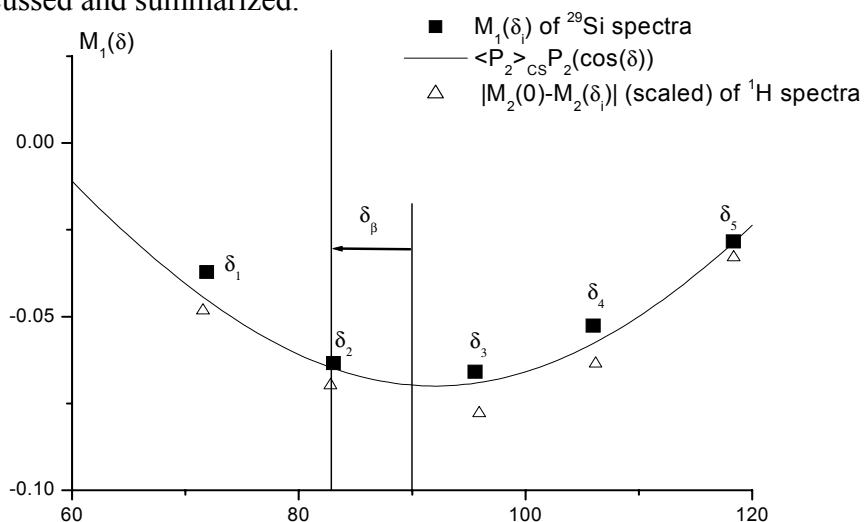


Fig 4.21. Finding the mutual relation between the characteristic orientations of the different molecular frames of the M6 LCSP. Supplementary to the β -echo recording for the angular positions δ_1, δ_5 the conventional ^{29}Si and ^1H spectra were acquired. This allows one obtaining the information about the orientation of the ^{29}Si CS tensor axis and local director orientation for these positions using the preliminary known angular dependence of the lineshape first moment. (see Chapter II). The angular shift δ_β shows that main-chain «parallel» alignment position found using β -function

Chapter V. Results and Discussion.

5.1. Legendre expansion method of the ODF analysis.

The model-free approach to the orientation parameters evaluation leads us to the expansion of the orientation distribution function (ODF) in to the Legendre series. Due to the symmetry principles only even order of Legendre polynomial and corresponding coefficients are relevant for the ODF description (by probing the anisotropic spin interactions with NMR methods it is not possible to distinguish between angle θ and its complement i.e. θ and $(\pi-\theta)$). These coefficients called “moments” of the 2-nd, 4-th, etc order, in principle, provide full information about the orientation distribution. [V.1,2] The advantage of such an approach is that no *a priori* knowledge and assumptions about the character of the ODF are required. That way, the estimated ODF suppose to be more “honest” in comparison with the one based on specific model which parameters have to be found. Another positive side of this method becomes obvious when the connection between the moments of NMR wideline spectrum (*determined by the anisotropic CS interactions*) and the moments of the ODF are demonstrated. Particularly, it is shown that the moments of the spectrum can be represented by the linear combination of the Legendre moments [V.3] (see Chapter II). The application of the moment-analysis method makes possible the subsequent estimation of the ODF moments by using one-parametrical fitting on each stage of the analysis. This makes the results more stable and reliable in comparison with the situation when two or more parameters have to be fitted simultaneously in “model-specific” cases. The corresponding approach has been applied to estimate the parameters of the ODF for the CS main axis of the ^{29}Si nuclei in the polysiloxane samples.

Unfortunately, the transversal anisotropy problem does not allow making unambiguous conclusion about the main chain orientation using the simplest one-dimensional ODF analysis. To describe the orientation distribution in this case two angles are needed (the direction of axis and rotation around it, see 2.3.2 and Fig 2.15). However, in the case of polysiloxane the symmetrical CS tensor provides only one-dimensional data about its main axis orientation. To get the information about the second dimension the dipolar coupling of the ^{29}Si pairs can be used. This angle-dependent spin interaction characterizes the orientation distribution of the internuclear vectors and, therefore, the main chain molecular segments with respect to the NMR laboratory frame. However, to be able to detect the dipolar coupling at low natural abundance of ^{29}Si the specific technique called β -echo needs to be employed [V.4].

5.2 Using β -echo properties.

It was shown in Chapter III that the Callaghan echo combination generates the NMR signal, which has two important properties:

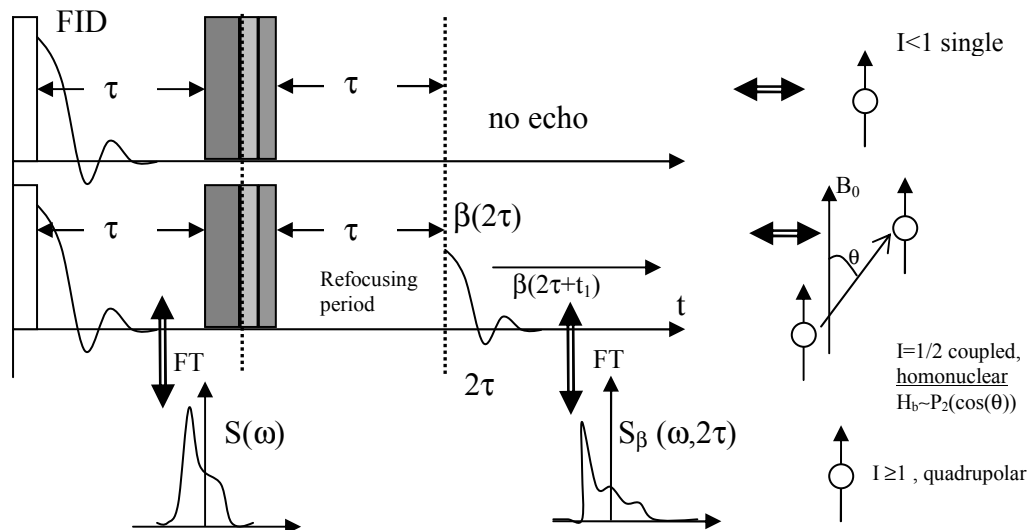


Fig 5.1 Important properties of β -echo employed for the purposes of the presented investigation.

1. Bilinear interaction selective – the only coherences which evolved under the bilinear spin Hamiltonian survive in the generated signal
2. Linear interaction refocusing – in the time moment $t=2\tau$ where τ is the delay, between excitation and refocusing pulses the linear interactions are «time-reversed» completely to the state $t=0$ (if not to take into account the transversal relaxation) (see **Fig 5.1**).

The testing measurements were performed on the polysiloxanes samples to probe the dipolar interactions of ^{29}Si pairs at natural abundance. The mentioned above properties of β -echo were demonstrated in practice both qualitatively and quantitatively (see **4.2**). The specific calibration procedure, however, has to precede each experiment to determine the duration of 90° -pulse due to the high sensitivity of the β -echo effectiveness to the deviations of r.f. pulses length from required values.

Thus, using the first property we select the part of the NMR signal which contains the information about bilinear interaction H_b and, therefore, about the orientation of the corresponding principal axes (see **Fig 5.1** right). In our particular case, the information about angular dependence brings the ^{29}Si nuclei involved into dipolar coupling with the neighbor spin. This interaction strength depends on the orientation of the internuclear vector in the NMR laboratory frame. The signal from “single” ^{29}Si nuclei is suppressed that vitally is important due to the low share of the coupled spins among its total amount. That way, the influence of the dipolar interactions can be observed even in presence of much stronger anisotropic interactions (namely – anisotropic chemical shift) in a form of spectral line shape specific modulations (see “ β -spectrum”). On the other hand the CS interaction influence can be excluded completely if to

use the “refocusing property» of β -echo. Due the fact that the moment $t=2\tau$ is equivalent to the $t=0$ for the linear spin interactions the dependence $\beta(2\tau)$ called « β -function» contains the information only about the bilinear part of spin Hamiltonian. Therefore, there are three principal ways of using β -echo combination:

- «Pure» β -function evolution analysis.
- « β -spectrum» evolution analysis.
- « β -spectrum» orientation analysis.

5.3 Simulation of the β -function orientation dependence.

Unfortunately, the applicability of the spectral lineshape analysis in the case of β -echo is limited. When the spectral positions intensities become dependent on two ODF’s simultaneously (namely, of the CS tensor main axis and the Si-Si internuclear vector) the two-dimensional spherical harmonics have to be used for the adequate description of the spectral lineshape form dependence on the orientation parameters. In this case the analysis become rather complicated and will require three-dimensional experiment (in the case of one-dimensional ODF two dimensions - one spectral and one angular were to be used). That way, it is worthwhile to use the Fourier transformed β -echo only for the isotropic orientation distribution to determine the dipolar coupling constant. In this case, the ω_{0D} value will be fixed for the subsequent analysis of the oriented sample making β -function dependent only on the orientation parameters to be determined. Because the information about the orientation distribution of Si-Si vectors is contained in the intensity of dipolar interactions of the ^{29}Si pairs, it is reasonable not to include other anisotropic interactions (the CS tensor orientation) into consideration. That means, in practice, using the «pure» β -function, i.e. evolution dependence $\beta(2\tau)$.

There are three circumstances however which have to be taken into account in our case.

- Dipolar coupling for the ^{29}Si - ^{29}Si pair in polysiloxanes is expected to be at least on the order of magnitude weaker than the anisotropic CS interaction.
- The orientation degree of the main-chain is lower than the LC order parameter in the same sample (related to the side-chain orientation).
- A low natural abundance of ^{29}Si leads to a small amount of coupled spin pairs. The signal-to-noise ratio will of about 10-20 (5-10% noise level) for the reasonable experiment time.

Generally, for the arbitrary oriented sample with ODF of the internuclear vectors described by $U(\cos(\theta))$, β -function will be represented by an integral sum of the individual harmonics β_{θ} :

$$\beta_{\Sigma}(2\tau) = \left[\int_0^1 \beta_{\theta}(2\tau) U(\cos(\theta)) d \cos(\theta) \right] R(2\tau), \quad (5.1),$$

$$\beta_{\theta}(2\tau) = (1 - \cos(\omega_D(\theta))) 2\tau, \quad \omega_D(\theta) = \omega_{0D} \cdot P_2(\cos(\theta))$$

where $R(\tau)$ is the function, which describes the transversal relaxation (see Eqn. 3.20). There are obvious methodological difficulties to analyze a function under the integral. Even in the case of isotropic sample the analytical solution of (3.20), include the Fresnel integrals. For the $U(\theta)$ which differs from isotropic it becomes much more complicated and the non-linear regression method will certainly fail to get even single fitting parameter. To test the character of the β -function dependence on the orientation distribution a detailed simulations for the relatively simple case of one-parametrical Gaussian-like ODF $U(\theta)$ have been performed. It was shown that for the strong orientation (i.e. high orientation degree) even «by-eye» fitting might be effective. In addition, good results could be obtained by using different minimization procedures. However, the sensitivity of β -function to the orientation distribution decreases non-linearly with the orientation degree (3.4.2, 3.5). For weak orientation, the diversity between curves is smaller than the fluctuations due to the noise level (10 to 20%) even if corresponding orientation degrees differing in more than 2 times by absolute value. The minimization methods are usually also not stable in the case when more than one parameter needs to be adjusted. Especially, the question of stability is critical for the case when more than one parameter is responsible for the orientation. Therefore, applying a model free approach based on the Legendre polynomial expansion to the orientation distribution function one should take care about the sensitivity of the β -function to the variation of the expansion coefficients (i.e. “ODF moments” $\langle P_n \rangle$). It is also important to have the method, which gives the reliable and stable results of estimation of these parameters. For this purposes the analysis of the β -function dependence on the coefficients of the Legendre expansion of the ODF was done using the concept of relative residual function (**RRF**) (see 3.4). It was shown that using just plain β -function data when estimating the orientation degree values $\langle P_2 \rangle < 0.15$ for any fitting procedure the significant difficulties can be expected already at the moderate experimental signal-to-noise ratio $S/N \approx 0.1$. For the same level of experimental error the expected $\langle P_4 \rangle$ value can be directly estimated from fitting of the single β -function curve only by the order of magnitude^a.

Moreover, the procedure of non-linear fitting/minimization of simultaneously two parameters is rather unstable. Assuming the 10% error due to the noise fluctuations leads us to the possible deviation about 50% for $\langle P_2 \rangle$ and up to 100% for $\langle P_4 \rangle$ (3.4). The situation is

^a Obviously, for the higher ODF moments, the situation is much worse. However, for a moderately ordered polysiloxane samples the contribution of the highest moments $n > 4$ into ODF is negligible, their influence on β -function were not considered at all.

improved by the considering the behaviour of the β -function under the reorientation of the whole sample (and therefore the ODF's reference axis) with respect to the NMR laboratory frame. The simulation shows that in this case it is possible to achieve much higher resolution of the ODF moments estimation by comparison of the curves corresponding to different sample tilting angles. Particularly, for the constant value of $\langle P_2 \rangle$ the largest absolute difference shows the β -function curves corresponding to parallel and orthogonal orientation of the ODF's reference axis with respect to the laboratory frame (external magnetic field). On the other hand, β -function curve corresponding to the tilting of the sample on “magic angle” ($\delta_m \approx 54^\circ$) is, practically, insensitive to the variation of $\langle P_2 \rangle$ due to the fact that $P_2(\delta_m) = 0$. This automatically provides us a reference for the comparison of two other curves. Particularly, this allows one finding the linear correlation between the difference of two β -function's curves (corresponding to “parallel” and “orthogonal” orientation) and related values of the $\langle P_2 \rangle$. In similar manner the linear parameter, which connects the period between the crossings of two β -functions (in this case for “parallel” and “magic angle” orientation) and the value of the $\langle P_4 \rangle$ was found. That way, there are three critically important aspects, which allow one proposing the improvement of the ODF parameters estimation effectiveness by using the orientation dependence methods.

They are:

- The specified parameters of β -functions has linear relation with the ODF moments to be estimated.
- The pairs of β -functions which are used in the procedures are different for the $\langle P_2 \rangle$ and $\langle P_4 \rangle$ estimations
- The ODF's moments are “decoupled” with respect to the parameters used for their evaluation. This means that a variation of $\langle P_4 \rangle$ has very insignificant influence on the parameter which is used for the $\langle P_2 \rangle$ estimation (if the latter one is fixed) and vice versa.

These three aspects make possible to implement a quite simple and intuitively clear iteration procedure of the $\langle P_2 \rangle$ and $\langle P_4 \rangle$ estimation. It has the sufficient advantages in comparison with the other possible methods (for example non-linear, “by-eye” or other “direct” fitting methods):

- Requires reasonable amount of data points to be acquired in the experiment.
- In each approximation step only one parameter needs to be adjusted.
- Bases on linear dependences and therefore provide a good stability of the results even under condition of a significant noise factor

- Being transparent on each step allows the control over the errors. Does not require the sophisticated calculation procedures and therefore makes possible the fast achieving of necessary convergence of the results.

The proposed technique was tested and the effectiveness was proved on the example of two polysiloxane samples with different character of the orientation distribution functions (see below).

5.4 Determination of the dipolar coupling constant for ^{29}Si pair in polysiloxanes using β -echo.

The results of the measurements using the β -echo using the isotropic polysiloxane sample allows one to determine the value of static dipolar coupling constant of for the ^{29}Si pairs ω_{D} . The procedure is based on the analysis of the time evolution of the “ β -spectrum” i.e. Fourier

transformed β -echo signal, $S_{\beta}(\omega, 2\tau) = \int_{-\infty}^{+\infty} \beta(2\tau + t_1) e^{-i\omega t_1} dt_1$ (**Fig 5.1**). Particularly, the evolution

behavior of the spectral density at some characteristic spectral positions, determined by the anisotropic chemical shift is used. The individual position of the ^{29}Si NMR spectrum corresponds to the different orientation of CS and dipolar interaction principal axes. Therefore β -function modulates each individual spectral position in different manner. This allows one minimizing the amount of the harmonics with different dipolar correlation frequencies which have to be taken into account in the β -function curve analysis.

Practically it becomes possible to make the one-parametrical fitting of the behavior of each component using the β -function corresponding to the one particular frequency. The systematic error caused by the contribution of more than one β -function harmonic will depend on the spectrum position, which is analyzed. Particularly, the simulation shows that the time evolution of ^{29}Si CS spectrum positions corresponding to the $\sigma=0$ and $\sigma=\sigma_{\parallel}$ due to the dipolar correlations generated by the β -echo can be described by the single “effective” β -function harmonic. The correlation between “effective” and real coupling constant values is linear with less than 5% systematic fitting error (see Chapter 3) that confirms the methodological correctness of the proposed method. Analysis of the spectral density at $\sigma=\sigma_{\perp}$ leads to the larger systematic error caused by the intrinsically higher amount of the β -function harmonics which may contribute at this spectral position. However, the absolute intensity of the β -spectrum at $\sigma=\sigma_{\perp}$ due to the geometry factors is more than in 3 times higher than for the other two position under consideration. Therefore, better signal-to-noise ratio makes reasonable to include this

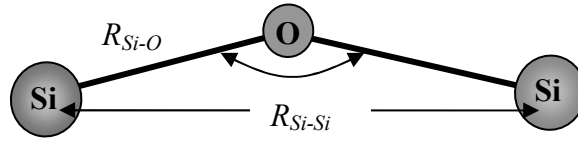


Fig 5.2 Geometry of the Si-O-Si group in polysiloxane. The dipolar coupling constant ω_{0D} obtained in β -functions experiment allows estimating the R_{SiSi} distance and therefore the angle of the Si-O-Si bond.

position into the analysis of the spectral data to make the results more stable with respect to the noise perturbations.

The experimental data obtained from the β -spectrum analysis of the isotropic M4 sample confirms a good functionality of the proposed technique of the dipolar coupling constant determination, even in the case of low signal-to-noise ratio caused by low natural abundance of ^{29}Si nuclei. Estimation of the dipolar coupling constant for the ^{29}Si spin pairs in the polysiloxane M4 sample gives us the value $\omega_{0D}/2\pi = \nu_{0D} = (225 \pm 10)\text{Hz}$ that is in on the order of magnitude smaller than the CS anisotropy ($\Delta = 48.4\text{ppm} \approx 3.2\text{KHz}$ at 9.4T). The obtained value of ω_{0D} can be used to estimate the geometrical parameters of the Si-O-Si chemical group configuration in polysiloxanes (see Fig 5.2).

Using the Eqn. 3.5 the internuclear distance R_{Si-Si} can be estimated as.

$$R_{Si-Si} = \sqrt[3]{7101\text{Hz} \cdot \text{\AA}^3 \cdot \nu_{0D}} = (3.15 \pm 0.15) \cdot 10^{-10}\text{m} . \quad (5.2)$$

Taking into account the cosine theorem:

$$\cos(\sphericalangle \text{Si-O-Si}) = 1 - \frac{r_{SiSi}^2}{2r_{SiO}^2} , \quad (5.3)$$

Using the known from literature value for $R_{Si-O} = 1,619 \cdot 10^{-10}\text{m}$ one can find the value of $\sphericalangle \text{Si-O-Si} = (155^\circ \pm 2^\circ)$. This number is in a perfect agreement with the estimations obtained from quantum chemistry calculations ($\sphericalangle \text{Si-O-Si} = 156.9^\circ$).

The alternative suggestions had been discussed, predicted the tetragonal symmetry of the Si-O-Si bond (i.e $\sphericalangle \text{Si-O-Si} = 109.28^\circ$), leading us to the dipolar coupling constant $\nu_{0D} = 384,2\text{Hz}$ that is far out from the experimentally found with β -function measurements.

That way, the method of the dipolar coupling constant estimation using the analysis of the Fourier transformed spectrum of the β -echo signal shows a good effectiveness being applied in the case of ^{29}Si nuclei at natural abundance. The method allows one overcoming the difficulties concerned with both dominating of the CS interaction in the NMR spectrum (as well as other types of linear interactions) and the low relative fraction (about 10%) of the observable coherences, which contains the information about the dipolar coupling. The obtained value of

v_{0D} has been used in all following calculations concerned with the determination of orientation distribution parameters using the β -function, where it plays the critically important role.

5.5 Orientation distribution investigation with β -function. Polysiloxane M4 and M6 sample.

To test the methods developed for the estimation of the ODF parameters with β -function, the monodomain polysiloxane M4 sample has been used. The *a priori* knowledge about the preferable orientation of the main-chain segments allows one avoiding the preliminary measurements needed for this direction estimation (see 4.5.1). The orientation degree expected for the main-chain orientation in M4 sample is rather small and all the procedures of its estimation, therefore, required as small as possible experimental and methodological error. The separation of the measurements into two stages was done to obtain the maximal possible signal-to-noise ratio for the region important for the orientation parameters estimation (see region of interest= ROI in Chapter IV). The special calibration procedure should precede each experiment with orientation dependence to make a comparison of the absolute signal intensities for the measurements with various sample orientation and different hardware settings.

Additionally, the low-pass Fourier filtering procedure was implemented and tested to reduce the noise influence and to provide the controllable experimental data smoothing and interpolation required for the $\langle P_2 \rangle$ and $\langle P_4 \rangle$ evaluation procedure. The filtration is based on the knowledge about the highest possible β -function harmonic frequency which is equal to the

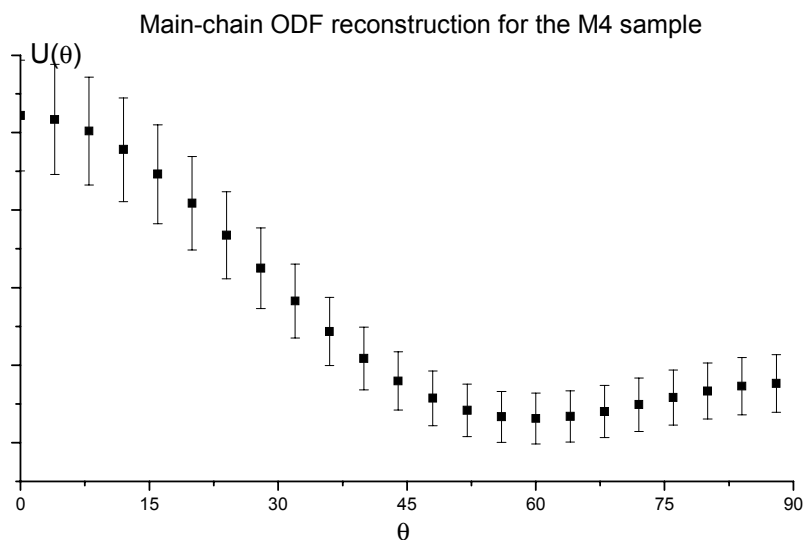


Fig. 5.3 Reconstruction of the main-chain orientation distribution function using the values of the moments $\langle P_2 \rangle$ and $\langle P_4 \rangle$ obtained by the β -function measurements. Error bars includes both uncertainty of the iteration procedures and experimental error due to the noise factor.

dipolar coupling constant value. Using the developed experimental and calculation procedures the orientation dependence of β -function curves has been measured and the parameters of orientation distribution function were evaluated.

It was found that the values of the ODF moments evaluated by the iteration procedure converge considerably fast. The approximation error of 5% is achieved in only 3 steps both for $\langle P_2 \rangle$ and $\langle P_4 \rangle$. The reconstruction of the ODF using the obtained values for polysiloxane M4 is shown on **Fig 5.3**. The maximal error is estimated to be about 10% that includes the experimental noise factor (reduced however by filtering) and methodological error of the calculation procedure. It should be noticed that in the reconstructed ODF the contribution of highest Legendre expansion coefficients ($n > 4$) is omitted. Therefore, the increase of $U(\theta)$ near the angular position $\theta = 90^\circ$ most probably does not reflect the reality and with account of higher degree moments would be smoothed. However, despite of intrinsic imperfections, the representation of the ODF with only two Legendre moments provides valuable information about the main-chain orientation character in polysiloxanes.

Preparing the experiments on the ODF analysis of the polysiloxane M6 sample some data obtained in the β -function measurements of M4 was used. Due to the equivalent chemical structure of the main chains, the ^{29}Si dipolar coupling constant is the same for both samples. The β -function **ROI** was extended in both directions of the time scale on 10% in comparison with the M4 sample measurements. The preliminary stage, however, required the orientation evaluation experiment in order to determine the preferable direction of main chain alignment. This was done by using the procedure based on the β -function behaviour in the initial period of its evolution. For the preferably parallel orientation of the main-chain segments (and therefore internuclear vectors) the contribution of the β -function harmonics with the frequency close to ν_{0D} is maximal (obvious from the fact that dipolar frequency $\nu_D = \nu_{0D} \cdot P_2(\cos(\theta)) \rightarrow \nu_{0D}$, when $\theta \rightarrow 0$). Therefore, the β -function curve with maximal grow up ratio at the initial evolution period will correspond to searched parallel orientation. In practice, the absolute increase of the β -function derivation in the initial evolution period ($t_e < (2/3)\nu^{-1}_{0D}$) is used as the measure of maximal fast harmonics contribution. In parallel, the measurements of the conventional ^1H and ^{29}Si NMR spectra were done. That way, the mutual orientation of the CS tensor main axis (^{29}Si CS spectrum), main-chain segment (via Si-Si «dipolar vector») and side-chain mesogenic units (by the ^1H spectrum determined by dipolar interactions of the aliphatic protons) becomes obvious. It can be seen on the (**Fig 4.21**) that the parallel alignment of the main-chain with respect to magnetic field differs slightly both from the orthogonal orientation of the ^{29}Si CS main axis and the local director (mesogenic units orientation). This deviation can be estimated as

$\delta_\beta=7^0\pm 2^0$. After establishing the «parallel» orientation direction of the main-chain segments with respect to laboratory frame, the procedure of ODF moments evaluation repeats completely the one used for the polysiloxane M4 sample. The resulting reconstruction of the ODF using obtained values of the Legendre moments can be seen on **Fig 5.4**.

As it was expected from the experiments with ^{29}Si CS spectra orientation dependence, the orientation degree of the main-chain segments for the M6 polysiloxane is obviously higher than for the M4. The value of second ODF moment differs in nearly 3 times for this samples (see **Table 4.3,4.4**). On the other hand, the value of $\langle P_2 \rangle$ for the M6 sample obtained using the β -function deviates from the one estimated from the CS main axis ODF evaluation (see Chapter I). The last fact brings an additional evidence of the transversal anisotropy characteristic for the main chain segments orientation in polysiloxanes.

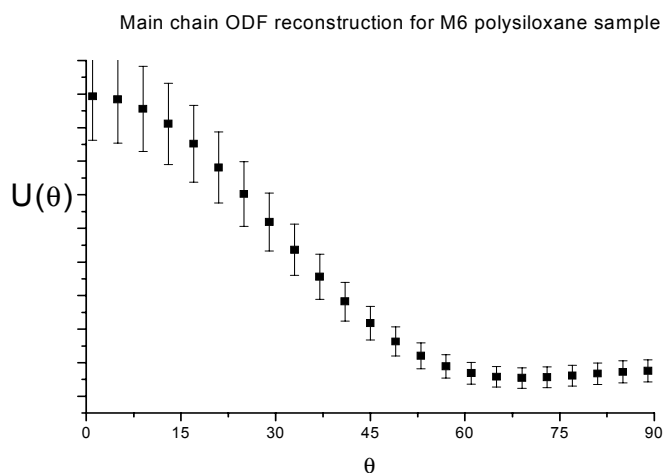


Fig 5.4. The reconstruction of the ODF using the $\langle P_2 \rangle$ and $\langle P_4 \rangle$ values estimated by β -function orientation dependence for the polysiloxane M6 sample.

5.6.1 Relaxation measurements and simulations.

The results of the spin-spin (transversal) relaxation experiments were shortly discussed in Chapter IV as much as they are relevant for the β -function measurements of the orientation distribution of the main chain segments in polysiloxanes. From this point of view, it was only important to find the temperature range where (i) the relaxation behavior has an exponential character which can be easily taken into account in the simulation procedures [V.4,5] and (ii) where the relaxation time is long enough as compared to the characteristic time of dipolar correlations to make possible the analysis of the orientation specific features of the β -function. These conditions are well fulfilled below the temperatures of the glass transition for the polysiloxane LCSP.

However, the temperature dependence of the transversal relaxation found in the experiments with M4 sample themselves represents the separate interesting topic for the investigation. Particularly, as it could be seen from the data showed in Chapter IV, the transversal *relaxation rate increases* with the temperature at least when the last one varies from -10^0C to $+45-50^0\text{C}$. For the temperatures below -10^0C the relaxation ratio changes very slowly with obvious trend for the transversal magnetization decay come to some limiting curve described by the typical *monoexponential* function. In the same time, for the higher temperatures the relaxation curve has more complicated character. Therefore, it is not completely correct in this case, to speak about the “relaxation time” that refers to the exponential function. Moreover, for the temperatures *above 45^0C* the slow *decrease* of the relaxation rate is observed. Such a picture is not typical for liquid or low-molecular LC, where the transversal relaxation rate is normally more or less monotonously *decreases* with the temperature.

The explanation for these features of the transversal relaxation behavior can be done if to use the Anderson-Weiss approach [V.6] to describe the transversal relaxation processes caused by the slow molecular motion modulating the spin interactions [V.7-14].

The starting points of the consideration of the molecular system behavior which leads to the relaxation processes of the transversal nuclear magnetization in this case are:

1. The system consists of a continuous distribution of oscillators which oscillate at any frequency ω in the interval $\omega_l \leq \omega \leq \omega_u$. The static (“instantaneous”) spectrum is denoted by $S(\omega)$, i.e. the probability to find an oscillator in $\omega \dots \omega+d\omega$ is $S(\omega)d\omega$.
2. The time interval $0 \dots t$ is divided into N sub-intervals which have the length Δt . All frequency changes caused by thermal motion take place as jumps only at the ends of these intervals. The conditioned probability that an oscillator is at ω_2 if it was at ω_1 in the preceding interval is denoted by $P(\omega_1, \omega_2)$.
3. The system is stationary, that means $S(\omega)$ as well as $P(\omega_1, \omega_2)$ do not depend on time and on the number of the interval.

The decay of the transversal magnetization in this case is described by the accumulating of phase shift by each oscillator with the time:

$$F(t) = \left\langle \exp \left\{ i \int_0^t \omega(t') dt' \right\} \right\rangle = \int_{-\infty}^{+\infty} Q(\Phi) e^{i\Phi} d\Phi \quad (5.4.1)$$

with $\Phi = \int_0^t \omega(t') dt'$ (accumulated phase); $Q(\Phi)$ is its probability distribution.

The essential part of Anderson-Weiss approach is the assumption of Gaussian-like probability distribution, i.e. :

$$Q(\Phi) = \frac{1}{\sqrt{2\pi\langle\Phi^2\rangle}} \exp\left\{\frac{-2\Phi^2}{2\langle\Phi^2\rangle}\right\} \quad (5.4.2)$$

Integration corresponding to Eq. (5.1) gives

$$F(t) = \exp\left\{-\frac{1}{2}\langle\Phi^2\rangle\right\} \quad (5.4.3)$$

The general solution is now coming after the calculating of the time dependence of $\langle\Phi^2\rangle$. This leads to the autocorrelation function of $\omega(t)$:

$$K(\tau) = \langle\omega(t)\omega(t+\tau)\rangle \quad ; \quad \tau_c \doteq \int_0^\infty K(\tau)d\tau \quad (5.4.4)$$

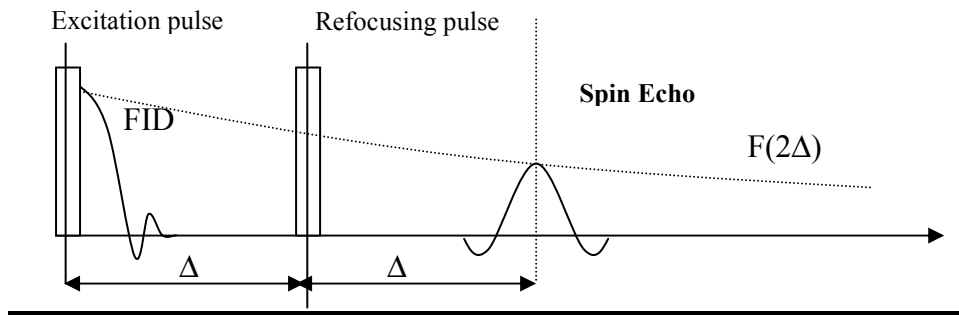


Fig 5.5. Transversal magnetization decay measuring by Hahn echo. The decrease of the transversal magnetization $F(2\Delta)$ after the refocusing of the linear spin interaction dephasing factors (offset/chemical shifts, heteronuclear dipolar couplings) among bilinear factors as homonuclear dipolar comes also from the cumulating phase shift of different spin subsystems caused by the slow molecular motion/diffusion during the period 2Δ .

Application to FID

$$\langle\Phi^2\rangle = \left\langle \left(\int_0^t \omega(t')dt' \right)^2 \right\rangle = 2 \int_0^t (t-\tau)K(\tau)d\tau \quad F(t) = \exp\left\{-\int_0^t (t-\tau)K(\tau)d\tau\right\} \quad (5.4.5)$$

Application to Spin Echo

A refocusing pulse following at moment Δ after initializing the FID corresponds to a flip angle of π (with 0 or 90° phase shift with respect to excitation pulse) for offset/chemical shifts/heteronuclear dipolar couplings. For bilinear (homonuclear dipolar or quadrupolar) interactions the refocusing pulse flip angle should be $\pi/2$ (with 90° phase shift). The target, therefore, is to determine the echo amplitude after the time-reversing period i.e. the value of $F(2\Delta)$. (see **Fig 5.5**)

Expectations:

- Weak correlation: The echo amplitude will not differ from the normal FID signal.(Eqn 5.4.5)
- Strong correlation: The initial dephasing will be refocused completely $\rightarrow F(2\Delta)=1$.
- Intermediate case: $\tau_c \approx \Delta$: Minimum of $F(2\Delta)$.

Calculation:

In Eq. (5.4), ω has to be replaced by another function, which changes at $t = \Delta$ its sign:

$$\hat{\omega} = \begin{cases} \omega(t) & \text{for } 0 \leq t \leq \Delta \\ -\omega(t) & \text{for } \Delta \leq t \leq 2\Delta \end{cases} \quad (5.4.6)$$

where ω exhibits the normal correlation behaviour. Then it follows

$$\begin{aligned} \langle \Phi^2 \rangle &= \left\langle \left(\int_0^{2\Delta} \hat{\omega}(t') dt' \right)^2 \right\rangle = \left\langle \left(\int_0^{2\Delta} \omega(t') dt' - \int_{\Delta}^{2\Delta} \omega(t') dt' \right)^2 \right\rangle = \\ &= \left\langle \left(\int_0^{2\Delta} \omega(t') dt' \right)^2 \right\rangle + \left\langle \left(\int_{\Delta}^{2\Delta} \omega(t') dt' \right)^2 \right\rangle - 2 \left\langle \int_0^{2\Delta} dt' \int_0^{2\Delta} dt'' \omega(t') \omega(t'') \right\rangle \end{aligned} \quad (5.4.7)$$

The evaluation of the expression is omitted for shortage. Finally, the echo amplitude is given by

$$\begin{aligned} F(2\Delta) &= \exp \left\{ - \int_0^{\Delta} (2\Delta - 3\tau) K(\tau) d\tau + \int_{\Delta}^{2\Delta} (2\Delta - \tau) K(\tau) d\tau \right\} \\ &= \exp \{ -2I_1 + 3J_1 + 2I_2 - J_2 \} \end{aligned} \quad (5.4.8)$$

With the definitions

$$I_n \doteq \int_{(n-1)\Delta}^{n\Delta} K(\tau) d\tau \quad ; \quad J_n \doteq \int_{(n-1)\Delta}^{n\Delta} \tau \cdot K(\tau) d\tau \quad (5.4.9)$$

Limiting cases:

- Very shortly decaying $K(\tau)$:

$$I_1 = \langle \omega^2 \rangle \tau_c \Delta \quad ; \quad I_n = 0 \text{ for } n \geq 2 \quad ; \quad J_n = 0 \text{ for all } n \quad (5.4.10)$$

- Constant K :

$$K \equiv \langle \omega^2 \rangle \quad : \quad I_n = \langle \omega^2 \rangle \Delta^2 \quad ; \quad J_n = \langle \omega^2 \rangle \left(n - \frac{1}{2} \right) \Delta^2 \quad (5.4.11)$$

Particular cases:

- **Weak correlation**

K decays already when $\tau \ll \Delta \rightarrow \Delta - \tau \approx \Delta$. Together with (Eqn 5.4.4) it follows

$$F(2\Delta) = \exp \left\{ - \langle \omega^2 \rangle \tau_c \cdot (2\Delta) \right\} \quad (5.4.12)$$

For short τ_c this is quite close to unity.

- **Strong correlation**

$$(\tau_c \gg \Delta): \text{Dependence on third power of time. } F(2\Delta) = \exp \left\{ \frac{1}{12} K'(0) \cdot (2\Delta)^3 \right\} \quad (5.4.13)$$

- **Very Strong correlation**

K remains constant. Then both integrals have the amount $(5/2)\Delta^2$ and thus cancel another.

$$\rightarrow F(2\Delta) = 1$$

- **Exponential correlation**

$$F(2\Delta) = \exp \left\{ - \langle \omega^2 \rangle \tau_c \left[(2\Delta) - \tau_c \left(3 - 4e^{-\Delta/\tau_c} + e^{-2\Delta/\tau_c} \right) \right] \right\} \quad (5.4.14)$$

Discussion:

- For **Weak correlation** Eq. (5.14) follows immediately.

- For **strong correlation** ($\tau_c \gg \Delta$) the echo amplitude contains the time to third power in the exponent. (Similarity to description of the relaxation caused diffusion)

$$F(2\Delta) \approx \exp\left\{-\frac{1}{12} \frac{\langle \omega^2 \rangle}{\tau_c} (2\Delta)^3\right\} \quad (5.4.15)$$

- For **very strong correlation** the exponent vanishes. That means $F(2\Delta)=1$ is indeed fulfilled.
- **Minimum:** This is that τ_c for which the exponent without the factor $-\langle \omega^2 \rangle$ has a maximum

$$\tau_{c \min} = \frac{\Delta}{1.89262} = 0.5284\Delta \quad (5.4.16)$$

Thus, the relaxation curves around the temperature providing the correlation time of the molecular motion equal to $\tau_{c \min}$ must cross one another (see Fig 5.6).

Relaxation mechanism

The practical issues and simulations based on the consideration shown above require some suggestion about the spin interactions, which dominates in the transversal relaxation mechanism. That means, it is important to know which spin interactions are modulated by the slow molecular motion, leading to the accumulation of the dephasing effect and, therefore, to incomplete refocusing of the transversal magnetization in Hahn-echo or CPMG experiments. To make the reasonable suggestion, the following factors are to be taken into account:

1. The spin-echo experiment is performed under the ^1H decoupling. Therefore, the dipolar interaction between the ^1H and ^{29}Si plays no role in relaxation (at least in the first order perturbation theory).
2. The dipolar interaction between ^{29}Si nuclei is relatively weak and only about 10% of all ^{29}Si nuclei are coupled (see Chapter I, and IV).
3. The chemical shift interaction, which dominates in the NMR spectrum of ^{29}Si in polysiloxanes, is anisotropic with $\Delta\sigma \approx 48\text{ppm}$ that gives about 3.2 KHz in the magnetic field of 9.4 T and exceeds sufficiently the dipolar interactions.

This means that most realistic suggestion about the transversal relaxation mechanism would be the *reorientation of the ^{29}Si CS tensor main axis* caused by the slow molecular motion. This process leads to the modulation of the CS interaction intensity due to its dependence on the orientation of the CS principal axes system in the laboratory coordinate frame.

The simulation of the transversal magnetization behavior according to the model approach described above is shown on (Fig 5.6). The values of the chemical shift anisotropy $\Delta\sigma=48.3\text{ppm}$ was used for estimation of the second moment of polysiloxane ^{29}Si spectrum to be substituted in Eqn 5.14.

$$|\sigma_{\parallel} - \sigma_{\perp}| = 48.3 \cdot 10^{-6} ; \omega_0 = 2\pi \cdot 79.4 \cdot 10^6 \text{s}^{-1} \rightarrow \langle \omega^2 \rangle = 1.16 \cdot 10^8 \text{s}^{-2} \quad (5.4.17)$$

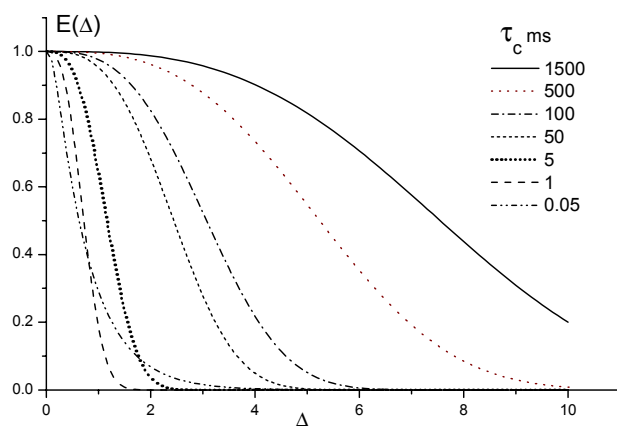


Fig 5.6 Results of the transversal magnetization decay simulation for the anisotropic CS interaction dominated in the transversal relaxation mechanism.

5.6.2 Additional factors: intrinsic linewidth relaxation limit.

The comparison of the simulated and experimental data of the transversal magnetization decay shows that they are in well agreement for the high and moderate temperatures. In this case

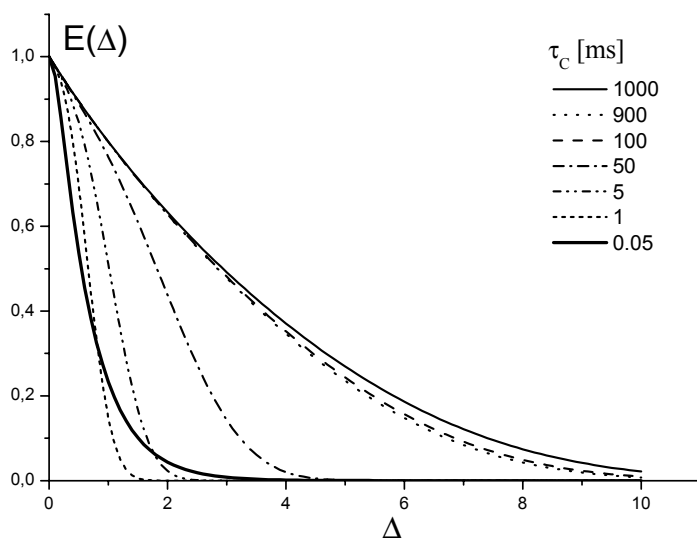


Fig 5.7. Simulation of transversal magnetization relaxation in the M4 PLC sample caused by CS tensor reorientation with account of the dipolar coupling in ^{29}Si - ^{29}Si and ^{29}Si - ^{13}C pairs. The magnetization decay curve tends to the monoexponential curve in strong correlation (i.e. slow motion) limit achieved at the low temperatures of the sample.

the “weak” and “exponential” correlation regimes of the molecular motion are expected and observed in practice (see Eqn 5.4.12-5.4.14) for the polysiloxane sample. The “returning back” of the relaxation curve (than means a decrease of the relaxation ratios after passing a minimum predicted by Eqn 5.4.16) is observed at the end of the probed temperature range ($T \approx 50^\circ\text{C}$). Unfortunately, the effectiveness of the cross-polarization decreases strongly with the temperature (again, due to intensive molecular reorientation) and, therefore, it became technically problematic to perform the further measurements with higher temperature being restricted in the available experimental time. On the other hand, at low temperatures, due to the turning the

sample from LC to glassy state and, the **strong correlation** motional regime ($\tau_c \gg \Delta$) is expected. However, the behaviour of the transversal magnetization does not show agreement with the simulation results, which predict the extremely long or infinite transversal relaxation period in this case (Eqn. 5.13). In the same time, the experimental data shows that there is an obvious limit of the elongation of the transversal relaxation time. This means that the relaxation curves do not change any more, becoming the same fair monoexponential function with $T_2 \approx 7$ ms for all the temperatures below -15°C . This shows, that another mechanism presents being responsible for the transversal relaxation when the CS tensor reorientations become too slow and not effective. This mechanism appears in strong correlation motional regime achieved at low temperatures for the polysiloxane sample. The role of this additional mechanism can play the *dipolar interaction* between (i) ^{29}Si and (ii) between the ^{13}C and ^{29}Si spins. The so-called intrinsic ^{29}Si spectrum line broadening caused by the coupling of these nuclei can be expressed according to [V.15]

$$\Delta\nu = \frac{\pi\mu_0}{6\sqrt{3}} \hbar\gamma_{\text{Si}}^2 n_{\text{Si}} \text{-for } ^{29}\text{Si} \text{-}^{29}\text{Si} \text{ coupling}$$

$$\Delta\nu = \frac{2\pi\mu_0}{18\sqrt{3}} \hbar\gamma_{\text{Si}}\gamma_{\text{C}} n_{\text{C}} \text{-for } ^{13}\text{C}\text{-}^{29}\text{Si} \text{ coupling} \quad (5.5)$$

where $\gamma_{\text{Si,C}}$ is the gyromagnetic ratio of ^{29}Si and ^{13}C spins respectively, \hbar -is a Plank constant and $n_{\text{C,Si}}$ are the spin density for the ^{29}Si and ^{13}C nuclei. The M4 polysiloxane sample with brutto-formula $(\text{SiC}_{19}\text{H}_{22}\text{O}_5)_p$ has the density of 1.12 g/cm^3 that leads to: $n_{\text{Si}}=(7.8..9.422)*10^{25}$ for ^{29}Si (4.7% natural abundance) and $n_{\text{C}}=(3.492 ..4.190)*10^{25}$ for ^{13}C (1.1% natural abundance) spins per m^3 . This brings us the intrinsic linewidth of the ^{29}Si resonance $\Delta\nu_{\text{CSi}}=(33...40)\text{KHz}$ and $\Delta\nu_{\text{SiSi}}=(9..11)\text{KHz}$. Totally, this gives the linewidth $\Delta\nu=40..50\text{Hz}$ that corresponds to the transversal relaxation time $T_2=1/(\pi\Delta\nu)=6.3..7.9\text{ms}$ being in perfect agreement with the experimental data at low temperatures (see Chapter 4). The results of the simulations of the relaxation curves, which have been performed with account of the dipolar coupling mechanism, are shown on **Fig (5.7)**. Obviously, a nearly complete agreement with the experimental data is achieved.

Summarizing the aspects concerned with the topic of transversal relaxation the following issues can be done:

- The transversal relaxation of the ^{29}Si nuclei in the polysiloxane M4 sample is mainly determined by the reorientation of the ^{29}Si CS tensor axes due to the molecular motions.
- The system behavior leading to transversal relaxation can be described in the frame of Anderson-Weiss approach using the «cumulant» theory.

- The fast, moderate and slow relaxation decay of the magnetization can be related with the corresponding «weak», «exponential» and «strong» correlations of the molecular motions that in turn refers to the fast, moderate and slow regimes of the molecular dynamics.
- The «exponential» correlation regime dominates in the temperature range from 0⁰ C to +40⁰C. Turning to the «weak» correlations is to be expected for the temperatures above 50⁰C.
- For the temperature far below glass transition $T < -15^0\text{C}$ the relaxation curve does not have any temperature dependence and its monoexponential behavior can not be explained by the strong correlations of the CS tensor orientation fluctuations.
- The transversal relaxation behaviour at low temperatures can be described properly by taking into account the dipolar interactions of ²⁹Si spins as well as the interactions between ²⁹Si and ¹³C nuclei. A perfect agreement between the experimental and simulation results can be achieved in this case. The details about the relaxation limit caused by dipolar interactions can be found in the classic description of Abragam [V.15].

Conclusion and Summary

In conclusion the following basic items and «milestones» of the presented work can be summarized:

- The outline of basic aspects of the liquid crystallinity in polymers has been made. The main attention was paid to the features of the orientation structure in side-chain LC polymers and particularly to the determination of the Orientation Distribution Function (ODF) of main-chain segments. The basic models proposed to explain the results of SANS, X-ray and NMR investigation were overviewed. The special interest was concentrated on the investigation of the side-chain polysiloxanes [C.1].
- The survey of the NMR techniques, which makes possible estimating of the ODF, has been done. The basic anisotropic spin interactions, which make the NMR sensitive to the molecular orientation both in micro and macro levels, were overviewed (Appendix II, Chapter II). The methods of the lineshape analysis, proposed by Spiess at al., which relate the moments of the spectral density function to the Legendre polynomial expansion moments of the ODF [C.2], were considered.
- The previous stages of the work on the project of liquid crystalline side-chain polysiloxanes investigation in NMR group of University Halle/Wittenberg performed by Günter Hempel and colleagues were analyzed [C.3]. The method of ODF Legendre moments estimation based on the lineshape orientation dependence of the ^{29}Si spectrum determined by the anisotropic CS was discussed in detail. The main advantages of the method are relatively simple experimental and calculation techniques. However, the sufficient disadvantage is an ambiguity of the results caused by (i) intrinsically one-dimensional information provided by the axially symmetrical ^{29}Si CS tensor and (ii) the uncertain factor of the *transversal anisotropy* of the main-chain segments orientation distribution. To uncover this ambiguity it was proposed to probe the orientation of the Si nuclei interconnection vector (coincided with the segment of main chain), using the direct dipolar interaction between the ^{29}Si spins.

However, due to the low natural abundance of ^{29}Si in polysiloxanes (4.7%) the essential signal sensitivity problems can be anticipated. The small amount of the observable spins makes the detection of the dipolar interaction for the orientation distribution studies quite problematic basically because of two reasons:

1. The 4.7% of natural abundance of ^{29}Si nuclei give considerably low signal absolute sensitivity ($\approx 3.7 \cdot 10^{-4}$). There are nearly no possibilities to use the enriched samples in the case of ^{29}Si .
2. The low probability that two-neighbored Si are both ^{29}Si leads to the overwhelming part of the signal arising from isolated ^{29}Si overlapping the weak spin-pair signal of interest.

On the other hand, the low abundance of ^{29}Si has a positive consequence, providing the possibility to consider only isolated spin pairs without taking into account higher-member spin clusters. This simplifies significantly the approach to the experimental data interpretation.

To overcome the problems originating from low natural abundance, the special ^{29}Si NMR technique proposed by Callaghan et al. [C.4] has been used. The implementation of the β -echo combination for the detecting of dipolar interaction between ^{29}Si spins in polysiloxanes required solving a significant amount of both theoretical and practical problems. The body of the work on employing of β -echo for the purposes of the work consisted of the following tasks:

1. The theoretical consideration of the β -echo in the case of the homonuclear system of isolated spins $I=1/2$ has been done using the density matrix formalism. The relation between the β -echo evolution behaviour (called β -function) and the homonuclear dipolar interaction intensity was found. The selective property with respect to bilinear part of spin Hamiltonian was confirmed. The special attention was paid on role of the dipolar coupling constant value.
2. The effect of the non-isotropic orientation distribution function of dipolar vectors on the β -function was taken into account on the next stage. Both model (Gaussian) and model-free (Legendre series representation) approaches to the ODF were considered. The effect of the ODF parameters on the character of the β -function evolution was tested with numerical simulation. The special efforts were applied for testing of the possible accuracy of the ODF Legendre moments estimation using the β -function.
3. The procedure of the β -function sensitivity enhancement with respect to the ODF parameters was developed using the rotation of whole sample with respect to NMR laboratory frame. The method allows one avoiding the non-reliable multiparametrical fitting procedures for the extraction of the ODF parameters. The linear regression can be used in combination with the iteration procedure. Each approximation step allows estimating the $\langle P_2 \rangle$ and $\langle P_4 \rangle$ moments individually, making the whole technique much more stable with respect to the input data noisiness and uncertainties.
4. Due to the critical influence of the dipolar coupling constant value on the β -function the special method of evaluation accuracy increasing was proposed. The Fourier transformed β -echo (“ β -spectrum”) has been used for this purpose. The selective analysis of the spectral components evolution allows one applying the one-parametrical fitting with single β -function harmonic that makes the dipolar coupling constant evaluation procedure much more transparent and precise. In our knowledge, the method of Fourier transformation and spectrum analysis has been never applied so far in combination with β -function.

5. The β -echo pulse sequence was implemented in combination with the cross-polarization from ^1H to ^{29}Si which is used to increase the signal sensitivity (intrinsically low for the ^{29}Si at natural abundance). The selective detection of the signal NMR from the coupled ^{29}Si spin pairs, with suppression of the signal from non-coupled spins was successfully realized. The test measurements demonstrated both qualitative and quantitative agreement with theory.
6. The essential influence of the imperfection of the experimental parameters on the β -function, (particularly the errors in duration of the rf-pulses) was found (Appendix III). The special procedures of the 90° pulse calibration have been implemented to minimize the errors originated from the improper pulse length.
7. The role of transversal NMR relaxation has been investigated in two aspects:
 - (i) influence of transversal relaxation time T_2 on the β -echo properties and its ability to serve for the orientation distribution estimation and
 - (ii) the interest about the transversal relaxation time T_2 as a sensitive tool for the molecular dynamics investigation [C.5-8].

The role of temperature as the basic factor, which has influence on the molecular mobility has been investigated. Measurements of the temperature dependence of transversal relaxation time have been done in wide temperature range. Three characteristic temperature regions of the relaxation time behaviour have been found. Particularly, the transversal *relaxation rate* increases for the temperatures from -10°C to $+45$ - 50°C . For the temperatures below -10°C the relaxation ratio changes very slowly and the transversal magnetization decay tends to the typical *monoexponential* curve. For the higher temperatures the relaxation curve has non-exponential character. For the temperatures *above 45°C* the slow *decrease* of the relaxation rate is observed. Such a picture is not typical for liquids or low-molecular LC, where the transversal relaxation rate normally *decreases* more or less monotonously with the temperature. The analysis of the relaxation data was done in a frame of Anderson-Weiss [C.8] approach supposing the ^{29}Si CS tensor axis reorientation as the primary relaxation mechanism. It was found that different behaviour of the transversal relaxation at different temperatures can be explained using the strong, exponential and weak model of the molecular motion correlations. Additionally, the influence of the ^{29}Si - ^{29}Si and ^{29}Si - ^{13}C dipolar interactions has to be taken into account to explain the relaxation behaviour at temperatures far low than glass transition point. This conclusion was additionally supported with the relaxation experiments using Curr-Purcell-Meiboom-Gill pulse sequence (CPMG) [C.9,10]

However, this is the topic of the separate work to be published as an independent research.

It was shown, that for the β -function experiments the low temperatures, which provides a relatively slow transversal relaxation, are most appropriate when studying the polysiloxane LCSP samples because of the following reasons:

- (i) Fast transversal relaxation destroys the most part of the signal before β -function achieves its maximum and, therefore, the experimental data suffers from low signal-to-noise ratio.
 - (ii) When the relaxation time is shorter than the characteristic time of dipolar correlations the β -function loses its features corresponding to the orientation effects. The reason is that in this case the most part of the low frequency β -function harmonics, which contain the orientational information are destroyed before they can produce a detectable contribution to the β -function.
 - (iii) The relaxation behaviour at low temperatures has the monoexponential behaviour that can be taking into account in the easiest manner in theoretical consideration.
8. The experiments on a disordered (polydomain) sample of polysiloxane M4 have been done with purpose to estimate the value of dipolar coupling constant $\omega_{\theta D}$. The method of the β -spectra analysis has been applied. The obtained value of $\omega_{\theta D}$ was employed for the data analysis of the experiments with oriented (monodomain) samples. Additionally, the obtained value has been used to determine the angle at oxygen atom in Si-O-Si bonds, which was found to be in perfect agreement with the results of quantum chemistry calculations.
9. The experiments on orientation dependence of β -function were done on monodomain polysiloxane M4. The special procedures of the signal intensity calibration had to be used to make possible the comparison of the β -functions recorded at different sample orientation. The low-passing Fourier filtering has been applied (with preliminary tests and simulations) to reduce the noise factor influence and performing a curve smoothing, that is important for the orientation parameters estimation with minimal error. The parameters of the ODF Legendre expansion were extracted from the 3 characteristic β -function orientation dependences. The iteration procedure of the subsequent approximation has shown a good convergence. The total error of the ODF reconstruction using the obtained value of $\langle P_2 \rangle$ and $\langle P_4 \rangle$ does not exceed 10% if not to take into account the systematic error originating from the omitting of the higher ODF moments influence.
10. The β -function experiments on the polysiloxane M6 required an additional measurements in order to find such an orientation of the sample at which the main chain segments are aligned preferably parallel to the magnetic field (NMR laboratory frame). This was done using the initial stage of β -echo evolution when the highest frequency β -function components dominate. The

following procedure of the $\langle P_2 \rangle$ and $\langle P_4 \rangle$ ODF moments estimation was completely analogous to the one used for the M4 sample. Due to the less amount of substance available and, therefore, worse signal sensitivity in the experiments, the error of the ODF reconstruction in the case of M6 is higher for the M4 sample. However, the orientation degree ($\langle P_2 \rangle$) is higher (in a factor of ≈ 2.5) for the M6 as well, so the ODF reconstruction quality is more or less equal in both cases. Simultaneously, the conventional ^{29}Si and ^1H spectra were recorded. This allows one finding the mutual relation between basic molecular frames of the sample. Particularly, the preferable orientation of the main-chain segments in the M6 sample was found to be orthogonal to the local director (side-chain). In addition, the small difference was found between the orientation of main chain obtained by from ^{29}Si CS spectrum angular dependence and from the β -function.

The sufficient novelty of the presented work, by our knowledge, is the application of β -echo for the case of non-enriched, low-abundant spins as ^{29}Si in the case when weak bilinear anisotropic spin interaction are masked by presence of the strong linear ones. It can be concluded that β -echo can be considered as an effective selective method for the NMR signal of the spins coupled via homonuclear dipolar interaction, providing the suppression of the signal from non-coupled spins. Equally, this technique can be employed for the detection of the quadrupolar interaction. The theoretical consideration of β -echo evolution for quadrupolar interaction with spin $\mathbf{I}=1$ will be equivalent to the case of two spins $\mathbf{I}=1/2$.

Most of the similar techniques used for weak dipolar interaction detection are based on double quantum filtering (INADEQUATE, C7, DRAMA, etc) [C.11-13]. The sufficient advantage of the β -echo is that single quantum coherence is detected and therefore the double quantum filter losses are avoided. Also, the β -echo does not require the MAS rotation which is used in most of the double quantum (including the «r.f. dipolar recoupling») methods to overcome the line broadening due to CS anisotropy. [C.14-16]. That way, it can be applied for the ODF estimation using the sample reorientation with respect to magnetic field that would be not possible together with MAS. A relatively long experimental time, which were required for the measurements have been done in the present work is not an intrinsic property of β -echo technique itself, but concerned with the low-natural abundance of the ^{29}Si spins.

The simplicity of the β -echo pulse sequence allows one, in principle, implementing a number of different extensions of the basic experimental technique. Particularly, the combination of the β -echo signal selection with the further detection of dipolar interaction by the Carr-Purcell echo track was tested. The results of these measurements have shown that a rough estimation of dipolar coupling constant can be done rather fast with this technique. However, this method faces with a number of experimental and theoretical problems, which have to be solved before its application in practice.

References to:

Introduction

- Int.1 Ciferri A., Krigbaum W.R., Meyer R.B. (ed.), *Polymer Liquid Crystals*, 1982, Academic Press.
- Int.2 Ciferri A., *Liquid Crystallinity in Polymers; Principles and Fundamental Properties*, 1991, VHC, Weinheim,
- Int.3 Mc Ardle (ed), *Liquid-Crystalline Side Group Polymers*, 1998, Blackie, Glasgow.
- Int.4 Plate N. A., Shibaev V. P., *Comb-like Polymers and Liquid Crystals*, 1987, New York-London: Plenum Press.
- Int.5 Donald A. M.,; Windle A. H., *Liquid crystalline polymers*, 1992, Cambridge Univ. Press, Cambridge.
- Int.6 Griffing A. C., *New liquid crystalline materials*, 1994, Philadelphia : Gordon and Breach.
- Int.7 Jeu, W. H., de, *Physical properties of liquid crystalline materials*, 1980, New York : Gordon & Breach.
- Int.8 Bovey F.A., *Chain Structure and Conformation of Macromolecules*, 1982, Academic Press, New York.
- Int.9 Kroschwitz J.I., (ed.) *Concise Encyclopedia of Polymer Science and Technology*, 1982, Wiley, New York.
- Int.10 Astronautics a. Aeronautics 1982, **20**, N.6 32-36.
- Int.11 Hardouin F., L. Noirez, P. Keller, J.P. Cotton, *Liq Cryst.* 1985, **18**, 129.
- Int.12 Böffel C., Spiess H. W., Higsen B., Ringsdorf H., Ohm, H.R., Kirste, *Makromol. Chem., Rapid Comm.* 1986, **7**, 777.
- Int.13 Titman J.J., Tzou D-L., Feaux de Lacroix S., Böffel C., Spiess H.W., *Acta Polymer.* 1994, **45**, 204.
- Int.14 Griebel M., Dissertation, 1996, MLU Halle/Wittenberg, FB Physik.
- Int.15 Hempel G., Griebel M., Wolf R., to be published.
- Int.16 Hempel G., Jacobi A., Weissflog W., Griebel M., Reichert D., *Macromol. Chem., Phys.*, 1999, **200**, 1608-1618
- Int.17 Callaghan P. T., Samulski E.T., *Macromolecules* 1997, **30**, 113-122
- Int.18 Ernst R.R., Bodenhausen G., and Wokaun A. *Principle of nuclear magnetic resonance in one and two dimensions*, 1987 Clarendon Press, Oxford.
- Int.19 Ball R.C., Callaghan P. T., Samulski E.T., *J. Chem. Phys.*, 1997, **106** (17), 7352-7358
- Int.20 Kimmich R., Schnur G., Köpf M., *Progress NMR Spectr.*, 1988, **20**, 385
- Int.21 Doi M., Edwards S.F., *The Theory of Polymer Dynamics*, 1986, Clarendon, Oxford.
- Int.22 Gennes de P.-G., *J.Chem.,Phys.* 1972, **55**, 572
- Int.23 Abragam A. *Principles of nuclear magnetism*, 1961, Clarendon Press, Oxford.
- Int.24 Anderson P.W. Weiss P.R., *Rev. Mod. Phys.* 1953, **25**, 269

Chapter I

- I.1 Chandrasekhar S., *Liquid crystals*, 1992, Cambridge : Cambridge Univ. Press.
- I.2 Gennes de P. G, *The physics of liquid crystals*, 1974, Oxford : Clarendon Press.
- I.3 Gennes de P.G., *Compt. Rend Ser. B*, 1975, **281**, 101.
- I.4 Roviello A., Sirigu A., *J. Polym Sci., Polym. Lett.*, 1975, **13**, 455
- I.5 Finkelmann H., Ringsdorf H., Wendorff J., *Macromol. Chem.* 1978, **179**, 273-278.
- I.6 Plate N. A., Shibaev V. P., *Comb-like Polymers and Liquid Crystals*, 1987, New York-London: Plenum Press.
- I.7 Plate N. A., Shibaev V. P., *J. Polym Sci.,-Macromol. Rev.*, 1974, **8**, 117-253.
- I.8 Finkelmann H, Rehage G., *Advances in polymer Science*, 1984, **60/61**, 99-171
- I.9 Ringsdorf H., Sneller A., *British Polym. J.*, 1981, **13**, 43-49.
- I.10 Shibaev V.P. *Liquid crystalline polymers*, edited by Plate, N. A., 1980, Moscow, «Khimiya» 190-242.
- I.11 Casagrande C., Veyssie M, Weill C., Finkelmann H., *Polym. Prepr.*, 1983, **23**. N 2 273-274.
- I.12 Kirste R., Ohm H., *Macromol. Chem., Rapid Comm.*, 1985. **6** 179-185
- I.13 Keller P., Carvalho B., Cotton J. e.a *J Physique Lett.*, 1985, **46** L1065-1071
- I.14 Vasilenko S., Khohlov A.R., Shibaev V. P., *Makromol. Chem.*, 1985, **186** 1951.
- I.15 Hardouin F., L. Noirez, P. Keller, J.P. Cotton, *Liq Cryst.*, 1985, **18**, 129.
- I.16 Causquih J.P., Volino F., *Mol. Cryst. Liq. Cryst.*, 1990, **180B**, 357.
- I.17 Noirez L., Cotton J.P., Hardouin F., Keller P., Moussa F., Pepy G., Strazielle C., *Macromolecules.*, **1988**, 21, 2891.
- I.18 Davidson P., Levetut A.M., *Liq. Cryst.*, 1992., **11** 469.
- I.19 Böffel C., Spiess H. W., Higsen B., Ringsdorf H., Ohm H., R. Kirste, *Makromol. Chem., Rapid Comm.* 1986, **7**, 777
- I.20 Böffel Ch., Higsen B., Pschorn U., e. a., *Israel Chem. J.*, 1983, **23**

- I.21 Archard M. F., Sigaud G., Hardouin F., Weill G., Finkelmann H., *Mol. Cryst, Liq. Cryst Lett.*, 1983, **82**, 3 111-118
- I.22 Casagrande C., Veyssie M., Weill C., Finkelmann H., *Mol Cryst, Liq. Cryst. Let.*, 1983, **92**, No ½
- I.23 Hempel G., Wobst M., Israel G., Schneider H., *Makromol. Chem.*, *Makromol. Symp.*, 1993, **72**, 161-189
- I.24 Siebert H., Dissertation, 1999, Universität Freiburg
- I.25 Hempel G., Jacobi A., Weissflog W., Griebel M., Reichert D., 1999, *Macromol. Chem., Phys.*, **200**, 1608-1618
- I.26 Kunchenko A.B. Svetogorsky., Preprints of Joint Institute for Nuclear Research, Dubna, 1986, E 14-86-89, 1-7

Chapter II

- II.1 Abragam A., *Principles of nuclear magnetism*, 1961, Claredon Press, Oxford,
- II.2 Slichter C.P., *Principle of magnetic resonance*, 1963, Harper and Row, New York,
- II.3 Ernst R.R., Bodenhausen G., and Wokaun A. *Principle of nuclear magnetic resonance in one and two dimensions*, 1987, Claredon Press, Oxford.
- II.4 Mehring M., *High resolution NMR in Solids*, 1982, Springer (2nd edn.)
- II.5 Van Vleck J.H., *Phys Rev*, 1948, **74**, 1168
- McBrierty V. J., Parker K. J., *Nuclear Magnetic Resonance of Solid Polymers*, 1993, Cambridge University Press, Cambridge,
- II.6 Schmidt-Rohr K., Spiess H.W., *Multidimensional Solid-state NMR and Polymers* Academic Press, New York, 1994.
- II.7 Anet F.A.L., and O'Leary D.J.O, *Concept Magn. Reson.* 1991, **3**.
- II.8 Radeaglia R., *Solid State NMR*, 1995, **4**, 317-321.
- II.9 Brandolini A.J., Apple T.M., Dybowski C., Pembleton R.G., *Polymer Vol. 23*, 1982, **23**, 39.
- II.10 Jarvis D.A., Hutchinson I.J., Bower D.I., Ward I.M, *Polymer*, 1980, **21**, 41.
- II.11 Hentschel R., Sillescu H., Spiess H.W., *Polymer*, 1981, **22**, 1517.
- II.12 Spiess H.W. in „Development in Oriented Polymers“ ed. by Ward I.M., 1982, Applied Science Publ., Barking.
- II.13 Hentschel R., Schlitter J., Sillescu H., Spiess H.W., *J. Chem Phys.*, 1978, **68**, 56.
- II.14 Ward I. M., “Structure and Properties of Oriented Polymers” 1975, Applied Science Publ. London.
- II.15 Miura H., Hirschinger J., English A. D., *Macromolecules* 1990, **23**, 2169.
- II.16 Hirschinger, J., Miura, H., Gardner, K. H., English A. D., *Macromolecules* 1990, **23**, 2153.
- II.17 Sandström D., Nygren J M., Zimmermann H. and Maliniakt A., *J. Phys. Chem.* 1995, **99**, 6661-6669
- II.18 Molchanov Yu.V., Borodin P.M., Privalov A., *Advances in Liquid Crystal Research and Applications*, ed. by L. Bata. Oxford, Pergamon Press, 1980, **1**, 33-339.
- II.19 Hempel G., Schneider H., *Pure Appl. Chem.* 1982, **54**, 635.
- II.20 Fedotov V. D., Schneider H., *Structure and dynamics of bulk polymers by NMR-methods*, 1989, Springer, Berlin,
- II.21 Roth K-H., Keller F., Schneider H., *Hochfrequenzspektroskopie in der Polymerforschung*, 1984, Akademie-Verl., Berlin.
- II.22 Molchanov Yu.V., Dvinskikh S.V., Komolkin A.V., Abstr. IX-th AMPERE Summer School, Novosibirsk. 1987, p.118.
- II.23 Sapozhnikov Ya. N., Dvinskikh S.V., Komolkin A.V., *Chemical Physics(in Russian)*, 1996, **10**, 101-103.
- II.24 Wiesner U., Schmidt-Rohr K., Böffel C., Pawelzik U., Spiess H.W., *Advanced Materials* 1990, **2**, 484,
- II.25 Hempel G., Jacobi A., Weissflog W., Griebel M., Reichert D., *Macromol. Chem., Phys.*, 1999, **200**, 1608-1618
- II.26 Hempel G., and Schmeisser U., *Journal of Magn. Res. Series A.*, 1996, **121**, 50-55.

Chapter III

- III.1 Callaghan P. T., Samulski E.T., *Macromolecules* 1997, **30**, 113-122
- III.2 Ball R.C., Callaghan P. T., Samulski E.T., *J. Chem. Phys.*, 1997, **106** (17), 7352-7358
- III.3 Hahn E.L. *Phys. Rev.*, 1950, **80**, 580.
- III.4 Ernst R.R., Bodenhausen G., and Wokaun A. *Principle of nuclear magnetic resonance in one and two dimensions*, 1987 Claredon Press, Oxford.
- III.5 Farrar T.C, Harriman J.E., *Density matrix theory and its application to NMR spectroscopy*, 1991, The Farrgaut Press, Madison,.
- III.6 Edmonds A.R. *Angular momentum in quantum mechanics* (2-nd edn) 1974, Princeton University Press

- III.7 Abragam A. *Principles of nuclear magnetism*, 1961, Clarendon Press, Oxford.
- III.8 Slichter C.P., *Principle of magnetic resonance*, 1963, Harper and Row, New York.
- III.9 Wolf D., *Spin temperature and nuclear magnetic relaxation in matter*, 1979, Clarendon Press, Oxford.
- III.10 Pines A., Slichter C.P., Phys. Rev. 1955, **100**, 1014.
- III.11 Blombergen N., Purcell E.M., Pound R.V., Phys. Rev. 1948, **73**, 679.
- III.12 Redfield Adv. Mag.Res. 1965, **1**, 1.
- III.13 Hempel G., Jacobi A., Weissflog W., Griebel M., Reichert D., Macromol. Chem., Phys., 1999, **200**(7), 1608-1618.
- III.14 McBrierty V. J., Parker K. J., *Nuclear Magnetic Resonance of Solid Polymers*, 1993, Cambridge University Press, Cambridge,
- III.15 Schmidt-Rohr K., Spiess H.W., *Multidimensional Solid-state NMR and Polymers*, 1994, Academic Press, New York.

Chapter IV

- IV.1 Callaghan P. T., Samulski E.T., Macromolecules 1997, **30**, 113-122
- IV.2 Hoult D.I., Richards R.E., 1975, Proc. Roy. Soc. (London) **A344**, 311
- IV.3 Pines A., Gibby M.G., Waugh J.S., J. Chem.Phys 1972, **56**, ibid 1973, **59**
- IV.4 Hartmann S.R., Hahn E.L., Phys. Rev. 1962, **128** 2042
- IV.5 Slichter C.P., *Principle of magnetic resonance*, 1963, Harper and Row, New York.
- IV.6 Mehring M., *High resolution NMR in Solids*, Springer (2nd edn.) (1982)
- IV.7 Engelhardt G., Michel D., *High Resolution Solid State NMR of Silicates and Zeolites*, 1987, Willey, New York.
- IV.8 Voekel R., Angew. Chem. Int. Ed. Eng. 1988, **27**, 1468
- IV.9 Levitt M, Sutter D., Ernst R.R., J. Chem.Phys 1986, **84**, 4243
- IV.10 Tegenfeldt J., Haeberlen U., J.Magn.Res., 1979, **36**, 453
- IV.11 VanderHart D.L., McFadden G.B., Solid State Magn. Res., 1996, **7**, 45
- IV.12 Hahn E.L. Phys. Rev., 1950, **80**, 580.
- IV.13 Abragam A. *Principles of nuclear magnetism*, 1961, Clarendon Press, Oxford.
- IV.14 Spiess H. W., Rotation of molecules and nuclear spin relaxation, NMR-Basic Principles and Progress, **15**, 55, 1978
- IV.15 Wolf D., *Spin temperature and nuclear magnetic relaxation in matter*, 1979, Clarendon Press, Oxford.
- IV.16 Anderson P.W. Weiss P.R., Rev. Mod. Phys. 1953, **25**, 269
- IV.17 Blombergen N., Purcell E.M., Pound R.V., Phys. Rev. 1948, **73**, 679.
- IV.18 Redfield A.G., Adv. Magn. Reson., 1965, **1**, 1
- IV.19 Doi M., Edwards S.F., *The Theory of Polymer Dynamics*, 1986, Clarendon, Oxford.
- IV.20 Ball R.C., Callaghan P. T., Samulski E.T., J. Chem. Phys., 1997, **106** (17), 7352-7358
- IV.21 Cohen-Addad J-P. Chem. Phys., 1974, **21**, 1272.
- IV.22 Gennes de P.-G., J.Chem.,Phys. 1972, **55**, **572**
- IV.23 Howell, Kenneth B. *Principles of Fourier analysis*, 2001, Chapman & Hall/CRC
- IV.24 Brémaud P., *Mathematical principles of signal processing: Fourier and wavelet analysis*, 2002, New York ; Berlin ; Heidelberg : Springer.
- IV.25 Nussbaumer, H.J., *Fast Fourier transform and convolution algorithms.*, 1982, Berlin ; Heidelberg : Springer.
- IV.26 Hempel G., Jacobi A., Weissflog W., Griebel M., Reichert D., 1999, Macromol. Chem., Phys., **200**, 1608-1618
- IV.27 Hempel G., Schmeisser U., J. Magn. Res. A, 1996, **121**, 50-55

Chapter V

- V.1 Hentschel R., Sillescu H., Spiess H.W., Polymer, 1981, **22**, 1517.
- V.2 McBrierty V. J., Parker K. J., *Nuclear Magnetic Resonance of Solid Polymers*, 1993, Cambridge University Press, Cambridge,
- V.3 Hempel G., Jacobi A., Weissflog W., Griebel M., Reichert D., 1999, Macromol. Chem., Phys., **200**, 1608-1618
- V.4 Callaghan P. T., Samulski E.T., Macromolecules 1997, **30**, 113-122
- V.5 Ball R.C., Callaghan P. T., Samulski E.T., J. Chem. Phys., 1997, **106** (17), 7352-7358.
- V.6 Anderson P.W. Weiss P.R., Rev. Mod. Phys. 1953, **25**, 269
- V.7 Kimmich R., Schnur G., Köpf M., Progress NMR Spectr., 1988, **20**, 385
- V.8 Collington, Sillescu H., Spiess H.W., Colloid Polym. Sci. 1981, **259**, 220
- V.9 Spiess H. W., Rotation of molecules and nuclear spin relaxation, NMR-Basic Principles and Progress, **15**, 55, 1978

- V.10 Wolf D., *Spin temperature and nuclear magnetic relaxation in matter*, 1979, Clarendon Press, Oxford.
- V.11 Brereton M. G., *Macromolecules*, 1989, **22**, 3667
- V.12 Klein P. G., Adams, C. H., Brereton, M. G., Ries, M. E., Nicholson, T., Hutchings M., Richards L. R., *Macromolecules*, 1998 **31**, 8871
- V.13 Ries, M. E.; Brereton, M. G.; Klein, P. G.; Ward, I. M.; Ekanayake, P.; Menge, H.; Schneider, H. (1999) *Macromolecules*
- V.14 Klinkenberg M., Blümmler, P., Blümich B., (1997) *Macromolecules*, **30**, 1038
- V.15 Abragam A. *Principles of nuclear magnetism*, 1961, Clarendon Press, Oxford.

References to Conclusion

- C.1 H. Siebert, Dissertation, 1999, Universität Freiburg
- Ciferri A., *Liquid Crystallinity in Polymers; Principles and Fundamental Properties*, 1991, VHC, Weinheim
- C.2 Schmidt-Rohr K., Spiess H.W., *Multidimensional Solid-state NMR and Polymers* Academic Press, New York, 1994.
- C.3 Hempel G., Jacobi A., Weissflog W., Griebel M., Reichert D., 1999, *Macromol. Chem., Phys.*, **200**, 1608-1618
- C.4 Callaghan P. T., Samulski E.T., *Macromolecules* 1997, **30**, 113-122
- C.5 Brereton M. G., *Macromolecules*, 1989, **22**, 3667
- C.6 Doi M., Edwards S.F., *The Theory of Polymer Dynamics*, 1986, Clarendon, Oxford.
- C.7 Kimmich R., Schnur G., Köpf M., *Progress NMR Spectr.*, 1988, **20**, 385
- C.8 Anderson P.W. Weiss P.R., *Rev. Mod. Phys.* 1953, **25**, 269
- C.9 Carr H.Y., Purcell E.M., *Phys.Rev.* 1954, **94**, 630
- C.10 Meiboom S., Gill D., *Rev. Sci. Instrum.*, 1958, **29** 688
- C.11 Fyfe C.A., Grondey H., Feng, Y and Kokotalio G.T. *J. Am. Chem. Soc.* 1990, **112**, 8812-8820
- C.12 Hong M., *J. Magn.Res.*, 1999, **136**, 86-91
- C.13 Lessage A., Bardet M., Emsley L., *J. Am. Chem. Soc.*, 1999, **121**, 10897-10993
- C.14 Bechmann M., Helluy X., Sebald A, *J. Magn.Res.*, 2001, **152**, 14-25.
- C.15 Caravetta m., Eden M., Zhao X., Brinkmann A., Levitt M.H, *Chem. Phys. Lett.* 2000. **321**, 205-215
- C.16 Gregory D.M., Mitchell D.J., Stringer J.A., Kiihne S., Shiels J.C., Callahan J., Mehta M.A., Dronby G.P., *Chem. Phys. Lett.*, 1995, 246, 654-663.

References to Appendix I

- A1.1 Chandrasekhar S., *Liquid crystals*, 1992, Cambridge: Cambridge Univ. Press.
- A1.2 Maier W., Saupe A., *Z. Naturforsch.*, 1958, **13A**, 564
- A1.3 Gennes de P. G, *The physics of liquid crystals*, 1974, Oxford: Clarendon Press.
- A1.4 Straley J.P., *Mol. Cryst.Liq. Cryst.* 1973, **24**, 7-20
- A1.5 Straley J.P., *Mol. Cryst.Liq. Cryst.* 1973, **22**, 333-357
- A1.6 Molchanov Yu.V., Borodin P.M., Privalov A., *Advances in Liquid Crystal Research and Applications*, ed. by L. Bata. Oxford, Pergamon Press, 1980, **1**, 33-339.
- A1.7 Molchanov Yu.V., Dvinskikh S.V., Komolkin A.V., *Abstr. IX-th AMPERE Summer School, Novosibirsk.* 1987, p.118.
- A1.8 Sapozhnikov Ya. N., Dvinskikh S.V., Komolkin A.V., *Chemical Physics(in Russian)*, 1996, **10**, 101-103.

Fig. 1,4,5,6 “Polymers and Liquid Crystals, Virtual Textbook” © [Case Western Reserve University](http://plc.cwru.edu/), <http://plc.cwru.edu/>

Fig 9,12 – Reproduced according to A1.6

Appendix II

- A2.1 Bloch F., *Phys. Rev.* 1946, **70**, 460.
- A2.2 Purcell E.M, Torrey H.C., Pound R.V., *Phys Rev*, 1946, **69**, 37.
- A2.3 Abragam A. *Principles of nuclear magnetism*, 1961, Clarendon Press, Oxford.
- A2.4 Slichter C.P., *Principle of magnetic resonance*, 1963, Harper and Row, New York.
- A2.5 Farrar T.C., Becker E. D., *Pulse and Fourier Transform NMR*, 1971 Academic Press, New York.
- A2.6 Ernst R.R, Bodenhausen G., and Wokaun A. *Principle of nuclear magnetic resonance in one and two dimensions*, 1987, Clarendon Press, Oxford.
- A2.7 Farrar T.C, Harriman J.E., *Density matrix theory and its application to NMR spectroscopy*, 1991, The Farrgaut Press, Madison.
- A2.8 Schiff L. I, *Qantum mechanics*, 1968, Mc-Graw-Hill, New-York.
- A2.9 Soren O.W., Eich G.W., Levitt M., Bodenhausen G. and Ernst R.R, *Progr. Mag. Res. Spectroscopy*, 1983, **16**, 163.

- A2.10 Blombergen N., Purcell E.M., Pound R.V., Phys. Rev. 1948, **73**, 679.
- A2.11 Anet F.A.L., and O'Leary D.J.O, Concept magn Reson, 1991, **3**.
- A2.12 Mehring M., *High resolution NMR in Solids*, Springer, 1982 (2 edn).
- A2.13 Duncan T.M., *A compilation of Chemical Shift Anisotropies*, 1990, The Farrgaut, Chicago.
- A2.14 Herzfeld J., Berger J., J. Chem. Phys. 1980, **73**, 6021
- A2.15 Veeman, Progr NMR spectroscopy, 1984, **16**.
- A2.16 Kalinovski H.-O, Berger S., Braun S., *¹³C-NMR-Spektroskopie*, 1984, Chemie, Stuttgart.
- A2.17 Edmonds A.R. *Angular momentum in quantum mechanics* (2-nd edn) Princeton University Press
- A2.18 Rose M.E., *Elementary theory of angular momentum*, 1957, Willey, New York.
- A2.19 Spiess H. W., Rotation of molecules and nuclear spin relaxation, NMR-Basic Principles and Progress, **15**, 55, 1978
- A2.20 Häberlen U., *High Resolution NMR in Solids: Selectiv Averaging*, Adv. Magn. Res. Suppl 1, 1976, Academic Press, New York.
- A2.21 Schmidt-Rohr K., Spiess H.W., *Multidimensional Solid-state NMR and Polymers*, 1994Academic Press, New York.
- A2.22 Blümich B., Spiess H.W., Angew. Chem. Int. Ed. Engl. 1988, **27**, 1655.
- A2.23 Hahn E. L., Phys. Rev., 1950, **80**, 580.

Appendix I. Liquid Crystals

A1.1 Liquid Crystals. General Overview.

The properties of the substance in the liquid crystalline state are intermediate between the properties of the isotropic liquid and solid state crystal. As in liquid state there is no long-range *translational order* in the liquid crystals. In the same time the molecules still keep the *long-range orientational order* i.e. similarly to the solid-state, the liquid crystals demonstrate the anisotropy of the optical, electrical, magnetic and other properties.[A1.1]

Generally, the trend to create a LC phase is inherent to those substances the molecules of which have the anisotropy of the shape like rods, disks, etc. In this case the anisotropy of the properties can follow from the sterical reasons—there is no possibility to allocate spatially the relatively dense system of the anisotropic particles in the isotropic manner. The characteristic orientational order of the liquid crystal state is between the «normal» solid and liquid phases and this is the origin of the term *mesogenic state* (or *mesophase*), used synonymously with liquid crystal state.

A1.2 Characterizing Liquid Crystals

The following parameters describe the liquid crystalline structure: (1) Positional Order, (2)Orientational Order, (3)Bond Orientational Order

Each of these parameters describes the extent to which the liquid crystal sample is ordered. *Positional order* refers to the extent to which an average molecule or group of molecules shows translational symmetry (as crystalline material shows). *Orientational order*, represents a measure of the tendency of the molecules to align along some preferable direction on a long-range basis. *Bond Orientational Order*

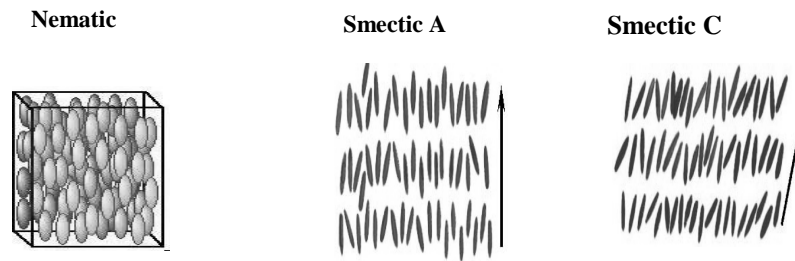


Fig A1.1. The examples of different LC phases. (a)-nematic: the long molecular axes have the preferred orientation along the local director. The phase exhibits no translational order for the centers of gravity of the molecules. (b)Smectics: the molecules are arranged in layers demonstrating orientational and translational ordering inside of them. Normally no correlation in the ordering of two different layers can be found.

describes a line joining the centers of nearest-neighbor molecules without requiring a regular spacing along that line [A1.1].

A1.3 Orientational order tensor and order parameter.

The distinguishing characteristic of the liquid crystalline state is the tendency of the molecules axes to point along a common axis, called the *director*. This is in contrast to molecules in the liquid phase, which have no long distance order. Due to the intrinsic anisotropy of the liquid crystalline state it is natural to characterize the ordering of the molecules with some tensor. In the first time it was done in the Mayer-Saupe theory of the liquid crystalline state [A1.2] and in the works of Landau. The most common approach to the orientational order tensor was developed later in de Gennes treatment [A1.3]. The tensor description gives the orientation of the macroscopic local director (usually it is the optical axis of the LC) with respect to molecular frame axes (see **Fig A.1**). In Mayer-Saupe approach the order tensor is given as:

$$S_{ij} = \frac{3}{2} \langle \cos \theta_i \cos \theta_j - 1 \rangle - \frac{1}{2} \delta_{ij} \quad (\text{A1.1})$$

where θ_i $i=x,y,z$ denotes the angle between the local director and the corresponding axis of the molecular frame. The brackets mean thermal motion averaging in time. For the threefold or higher symmetry of the molecule the only one angle remains relevant. In this case the order tensor \hat{S} has no off diagonal elements:

$$\hat{S} = S \begin{bmatrix} -\frac{1}{2} & 0 & 0 \\ 0 & -\frac{1}{2} & 0 \\ 0 & 0 & 1 \end{bmatrix}, \text{ with } S = \frac{3}{2} \langle \cos^2 \theta \rangle - \frac{1}{2} = \langle P_2 \rangle, \quad (\text{A1.2})$$

where $P_2(\cos(\theta))$ means the second order Legendre polynomial. The scalar factor S usually is called the **order parameter** of the liquid crystalline phase. $S=1$ corresponds to the absolutely ordered system where all the long molecular axes are parallel to the local director. $S=0$ means fully disordered isotropic state. Typical value of the order parameter of the LC varies from 0.4 to 0.9.

A1.4 Polymorphism. Liquid crystalline subphases.

The significant part of the mesomorphic substances demonstrates the ability to exist in more than one liquid crystal structure i.e. the shows the LC phase polymorphism. The subphases of the LC state differs by the type of the both orientational and positional orders of the molecules. Usually the following main types of the LC can be distinguished:

A. Nematic Phases The nematic liquid crystal phase is characterized by molecules that have no positional order but tend to point in the same direction (along the director). In the Fig A1.1, it can be noticed that the molecules point vertically but are arranged with no particular order. The nematic state is the most low-ordered possible state of the LC and is characterized with the order parameter from 0.4 to 0.7 for low molecular LC.

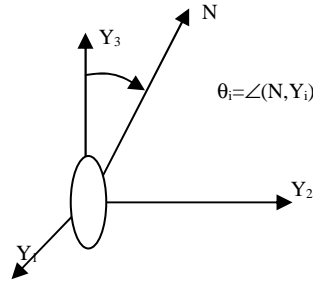


Fig A1.2 Representation of the relationship between the molecular and local director frame to introduce the LC order parameter tensor.

B. Smectic Phases The smectic state is another distinct mesophase of liquid crystal substances. Molecules in this phase show a degree of *translational order* not present in the nematic. In the smectic state, the molecules maintain the general orientational order of nematics, but also tend to align themselves in layers or planes. The smectic state is more ordered than the nematic with order parameter achieving the value $S=0.9$. Many LC compounds are observed to form more than one type of smectic phase. As many as 12 of these variations have been identified, however only the most distinct phases are discussed here. In the *smectic-A* mesophase, the director is perpendicular to the smectic plane, and there is no particular positional order in the layer. The *smectic-B* mesophase orients with the director perpendicular to the smectic plane, but the molecules are arranged into a network of hexagons within the layer. In the *smectic-C* phase, molecules are arranged as in the smectic-A, but the director is tilted at a constant angle to the smectic plane. In some smectic mesophases, the molecules are affected by the various layers above and below them. Therefore, some three dimensional order is observed. *Smectic-G* is an example demonstrating this type of arrangement.

A1.5. Macroscopic ordering of LC. Monodomain and polydomain samples.

As it was mentioned above the local director gives the preferable orientation of the molecules of the liquid crystals. However, the director orientation itself is not necessary to be the same within whole LC sample. Usually, the part of the LC sample where the local director field is homogeneous (i.e the director orientation does not fluctuate significantly from point to point) is called the LC-*domain*. If the director field orientation is homogeneous within the whole sample it is called «homogeneously oriented» or *monodomain*. In other case, when the orientation of the director fluctuates significantly within the sample it is named *polydomain*. To describe the probability of the director orientations distribution function $P(\alpha)$ can be used. One of the frequently used in different works model of $P(\alpha)$ based on so called Mayer-Saupe potential approach is shown on **Fig A1.3** [A1.6]. Similarly to the microscopic order parameter S which quantify the ordering of the molecular axes with respect to the director, the ordering of the director field itself can be described in the term of the orientation degree represented by the second Legendre polynomial averaged with the orientation distribution function $P(\alpha)$. To distinguish this

orientation parameter of the macroscopic domains from the local molecular *order parameter* it is usually called the **orientation degree** :

$$S_M = \int_0^\pi P(\alpha) \cdot \frac{1}{2} (3 \cos^2(\alpha) - 1) d\alpha \quad (\text{A1.3})$$

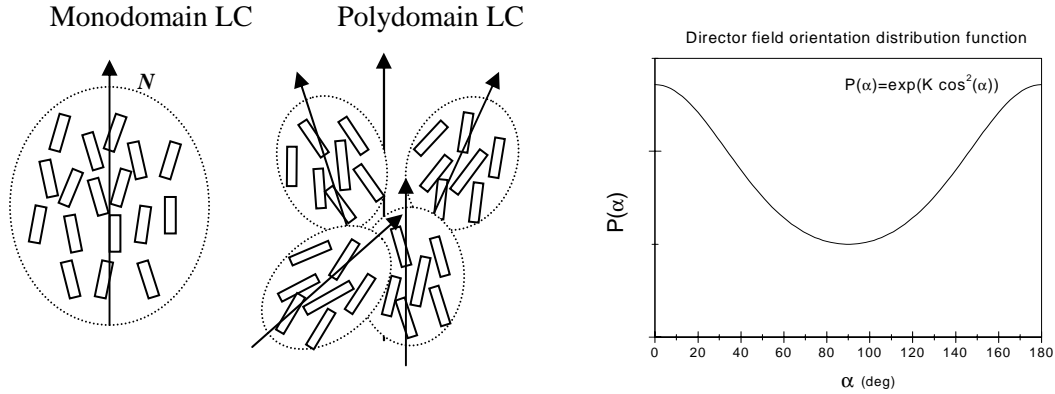


Fig A1.3. The domain structure in liquid crystals. Monodomain sample (left) exhibits the homogeneous orientation of the director field within entire sample volume, while polydomain (right) sample demonstrates the distribution of the directors orientation of different sample regions.

A1.6 Influence of the external electric and magnetic fields on the orientation and structural properties of liquid crystals.

One of the specific and important properties of the LC state of the substance is the ability to change the structure and the molecular ordering under influence of the electric and magnetic fields. The background of the most of the known electric and magnetic effects in the LC is the reorientation of the director of the LC domains under the influence of the external field or the flow caused by it. The direct reason of the reorientation lies in the anisotropy of the electric and magnetic properties of the LC (electric and magnetic anisotropy $\Delta\epsilon = \epsilon_{\parallel} - \epsilon_{\perp}$ and $\Delta\chi = \chi_{\parallel} - \chi_{\perp}$ denoting the difference of the corresponded magnetic and electric constants in parallel and transversal direction with respect to local director). The processes of the molecular rearrangement depend on the initial orientation of the molecules as well as the from the viscoelastic properties of the LC. [A1.1]. The process of the reorientation has the step character. The corresponding values of the barrier voltage and magnetic field strength can be expressed as:

$$U_0 = \sqrt{4\pi K_{ii} / \Delta\epsilon} \quad H_0 = \pi / d \sqrt{4\pi K_{ii} / \Delta\chi}, \quad (\text{A1.4})$$

where K_{ii} the elastic constants of the corresponded deformation type, d is the liquid crystalline layer.

A1.7 Obtaining the monodomain LC samples with external magnetic field. Determination of the LC orientation degree by means of NMR.

The orientational influence of the external fields on the LC can be used to obtain the samples with monodomain structure. When the electric or magnetic field is applied to the LC sample, all the domains will get the same orientation of the local director forming the monodomain sample. However, the fulfilling of the conditions A1.4 can require the extremely large magnitude of the electric or magnetic field for the highly viscous LC subphases like smectic. That way in practice, to be oriented, the sample have to be turned by heating into low viscous nematic phase or the state of isotropic liquid and then cooled down (or quenched) to the high viscous state in presence of the external orientation field. In this case the orientation achieved into the low-viscous case will be fixed and remains unchanged even if to switch off the external orientation field. For the low-molecular LC normally the nematic state is low-viscous enough to obtain the homogeneous orientation of the entire sample. However, for the part of polymer LC the orientation by the external field is not possible even in the nematic state. In this case the orientation degree achievable by the cooling down the sample from isotropic state can sufficiently low than the (molecular) microscopic order parameter S_M . The situation is more entangled in the case of side-chain polymers where the ordering of main chain is quite different from the order of mesogenic units (see Chapter I).

A1.8 Macroscopic orientation degree estimation using the scaling of the NMR interaction by the molecular ordering.

One of the approaches to the estimation of the macroscopic orientation characteristic of the LC is based on the analysis of the angular dependence of the NMR spectra of the completely or partially oriented LC sample [A1.6]. According to Appendix II the parameters of the NMR wideline spectrum (particularly the second moment M_2) depends on the orientation of the sample director with respect to the external magnetic field in which the spectrum is recorded. For the case of the monodomain sample the local (microscopic) and macroscopic order parameters are the same, so the *orientation degree* can be estimated by the analysis of the angular dependence of the NMR spectrum. The corresponded NMR experiment is only possible in the case when the LC has the high-viscous state in which the orientation structure created in the initial position remains unperturbed when the sample is turned on some angle in the magnetic field. For the partially oriented sample (polydomain) the directors orientation distribution $P(\alpha)$ have to be taken into account. The NMR spectrum $S(\omega)$ in this case represents the superposition of the subspectra $S_\alpha(\omega)$ from the domains with different orientation of the local director scaled according to its local tilting angle α :

$$S(\omega) = \int_0^\pi P(\alpha) S_\alpha(\omega(\alpha)) d\alpha \quad (\text{A1.5})$$

The orientation degree can be found using (i) some model function (see A1.7) or (ii) by the deconvolution of the NMR spectral density function (A1.7) to extract the numerical (usually) representation of $\mathbf{P}(\alpha)$ by the special calculation procedure. The example of the orientation degree estimation based on the Gaussian-like model function $P(\alpha) = A \exp(K \cdot \cos^2(\alpha))$ is shown on (Fig A1.3). The orientation “quality” factor K was estimated using the angular dependence of the second moment of the NMR wideline ^1H spectrum $M_2(\beta)$ (Fig. A1.5). The orientation quality was estimated for the polyacrylate LC sample oriented in the magnetic field of different magnitude. As it was expected, the orientation degree increases with the field strength. The plateau of the $K(H_0)$ dependence is achieved at $H_0 = 1.4\text{T}$. However, the orientation quality depends strongly on the ratio of the sample cooling down from the melting point. The smaller temperature decrease speed the better orientation can be achieved. This can be obviously seen by the Fig 1.5 where most prominent angular dependence of $M_2(\beta)$ corresponds to the lowest sample cooling ratio.

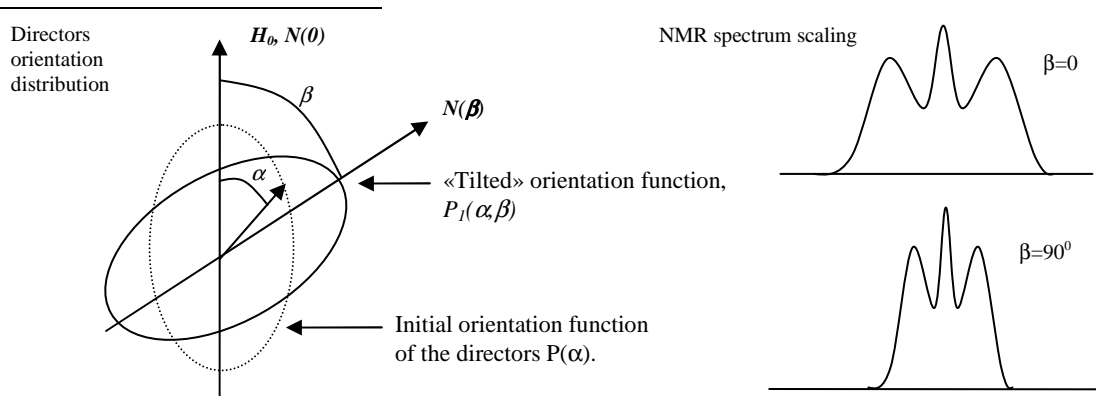


Fig A1.4. NMR experiment on orientation degree evaluation. The NMR spectrum is recorded at different orientations of the sample director $N(\beta)$ (defined by the initial sample orientation $N(0)$) with respect to the magnetic field H_0). The directors' reorientation scales the corresponded nuclear spin interaction leading to the corresponded changes in the NMR spectrum lineshape (right).

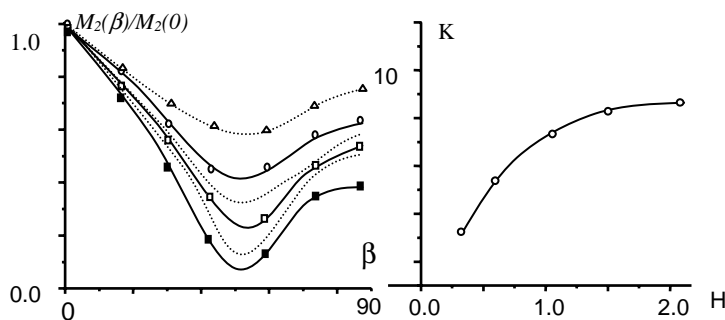


Fig A1.5. Angular dependence of the NMR wideline spectrum cooled down at different intensity of the external orientation field and with different temperature decrease ratio.

Appendix II

A2.1. NMR basics.

The phenomenon of Nuclear Magnetic Resonance (NMR) [A2.1,A2.2] is widely used in a great amount of the researches of a various class of objects. It is employed for the dynamical and structural investigation, qualitative and quantitative analysis both on micro and macro levels. Each special branch of the NMR applications has a great number of features and requires the individual description, which, of course, has been done in many textbooks [A2.3-6]. However, basic principles of the NMR are common for all kinds of its applications. These principles can be considered in two different manners. The dynamic of the isolated nuclear spins can be understood in terms of classical motion of the magnetization vector. To describe the coupled spins, however, it is necessary to have recourse to the quantum mechanical formalism where the state of the system is expressed in terms of wave functions or more generally by a density operator [A2.6,7]. In following section some theoretical foundation of both approaches will be introduced.

A2.1.1 Nuclear magnetization

To understand the origins of the nuclear magnetization the one should refer to the basics of quantum mechanics [A2.8], particularly the property named angular momentum or *spin*. The spin is quantum mechanical operator which eigenvalues can be integer or half-integer. Often the spin quantum number I is referred as to spin. For example, ^1H , ^{13}C , ^{29}Si are often called «spin $1/2$ nuclei». Almost for all elements in the periodic table has isotope with non-zero spin. The magnetic moment is proportional to the spin I of the nucleus: $\mu_I = \gamma \hbar I$, where \hbar is Plank constant and γ defines the gyromagnetic ratio of the nucleus, and can assume both positive and negative values.

A2.1.2 Bloch equations

In the case of independent spin $I=1/2$ nuclei the motion of the ensemble of nuclear spins may be described in terms of the precession of the **spin magnetization vector** that is the macroscopic sum of the individual nuclear magnetic momentum:

$$M = \sum_{k=1}^N \mu_k, \quad (\text{A2.1.1})$$

Equating the magnetic torque for the angular momentum γM connected with macroscopic magnetization we obtain:

$$d\mathbf{M}/dt = \gamma \mathbf{M} \times \mathbf{B}, \quad (\text{A2.1.2})$$

The solution to eqn. A2.1.2 where the B_0 corresponds to a precession of the magnetization about the external field direction at the rate called the *Larmour frequency* $=\gamma B_0$ [A2.1] The resonant phenomenon arises from the application of the oscillated r.f. field on frequency ω_0 . To obtain the expression for the spin evolution we need the circularly polarized component of the oscillating transverse field:

$$B_1(t) = k_x \cdot B_1 \cos \omega_0 t + k_y \sin \omega_0 t \quad (\text{A2.1.3})$$

where k_x, k_y, k_z denotes the unit ort of the coordinate frame. Under the initial condition $M(t)=M_0 k_z$ the solution of A2.1.2 can be written as :

$$M_x = M_0 \sin \omega_1 t \sin \omega_0 t \quad M_y = M_0 \sin \omega_1 t \cos \omega_0 t \quad M_z = M_0 \cos \omega_1 t \quad (\text{A2.1.4})$$

where $\omega_1 = \gamma B_1$. The expression A2.1.4 describes the simultaneous nutation about the stationary field B_0 at the Larmour frequency ω_0 and precession around the field B_1 at the frequency $\omega_1 = \gamma B_1$. For the purposes of illustration it is convenient to turn into the rotating frame, which coordinated axis \mathbf{x} and \mathbf{y} rotates with the frequency ω_R about z direction.

In this case the magnetization vector “feels” the effective longitudinal field $\mathbf{B}_{eff} = \mathbf{B}_0 - \omega/\gamma$. obviously, at resonance conditions $\omega = \omega_0$, the \mathbf{B}_1 field is also stationary and only the precession around \mathbf{B}_1 field is apparent. It is now easy to visualize the influence of the of a short burst pulse of the

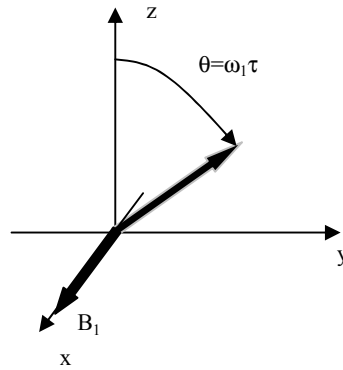


Fig A2.1.1 In the rotating frame where B_1 is stationary the effective longitudinal field is zero on resonance and only the precession about B_1 is apparent.

resonant field \mathbf{B}_1 known in NMR as “rf-pulse” (Fig A2.1.2).. If the duration of the pulse is τ the rotation angle of the magnetization vector will be $\omega_1 \tau = \gamma \mathbf{B}_1 \tau$. It is also important that the initial phase of the r.f. field \mathbf{B}_1 establish the direction of the magnetization vector rotation. The significance of the initial phase angle becomes important when the second pulse is applied after the first one. If to denote the initial direction of the magnetization tilting as X -axis then the r.f. pulse is usually called $\theta_{\pm y}$, where θ means turning angle and index “y” labels the axis about which the rotation is performed. Obviously, if the next r.f.-pulse is phase shifted on 90° it corresponds to the rotation in the direction of y-axis and will be called $\theta_{\pm x}$.

A2.1.3 Relaxation

The effect of the resonant r.f. pulse is to disturb the spin system from its thermal equilibrium state. Then, the equilibrium will be restored by a process called NMR relaxation. This process involves the exchange of the energy both inside the spin system and between spins and external thermal reservoir known as “lattice”. The phenomenological description of this process is given by equation:

$$dM_z/dt = -(M_z - M_0)/T_1, \quad (\text{A2.1.5})$$

where T_1 is known as the spin-lattice (or “longitudinal”) relaxation. Similarly, the transverse magnetization, being disturbed by the r.f. resonant excitation, returns to the equilibrium state (equal to 0) with characterized time T_2 called *spin-spin* (or **transversal**) relaxation time. Despite of the apparent similarity, the nature of transversal and longitudinal relaxation is different. As indicates the name the spin-spin relaxation leads to the establishment of the thermal equilibrium within the spin system and corresponds to the dephasing of the *coherent quantum state* [A2.6]. The phenomenological description of the transverse relaxation subdues the equation similar to the eqn (A2.1.5), namely:

$$dM_{x,y}/dt = -M_{x,y}/T_2 \quad (\text{A2.1.6})$$

This is expression is valid in Blombergen Purcell and Pound (BPP)[A2.10] theory approach which works well for spins residing in liquid state molecules.

Combining the equations A2.1.6 and A2.1.7 we obtain the complete view of **Bloch equations**:

$$\begin{aligned}
dM_x/dt &= \gamma M_y (B_0 - \omega/\gamma) - M_x/T_2 \\
dM_y/dt &= \gamma M_z B_1 - \gamma M_x (B_0 - \omega/\gamma) - M_y/T_2 \\
dM_z/dt &= -\gamma M_y B_1 - (M_z - M_0)/T_1
\end{aligned}
\tag{A2.1.7}$$

which provides the classical description of the many phenomena important in NMR applications.

A2.1.4 Signal detection.

Suppose the coil of the r.f. resonant circuit tuned on the Larmour frequency is placed around the sample with the symmetry axis transverse to the polarizing external field \mathbf{B}_0 . In laboratory frame the transverse magnetizations precessing around \mathbf{B}_0 will induce an oscillatory e.m.f. at Larmour frequency ω_0 . The transversal magnetization following the excitation r.f. pulse can be found as the solution of Bloch equations:

$$\mathbf{M}(t) = [\mathbf{k}_x M_0 \cos \omega_0 t + \mathbf{k}_y M_0 \sin \omega_0 t] \cdot \exp(-t/T_2)
\tag{A2.1.8}$$

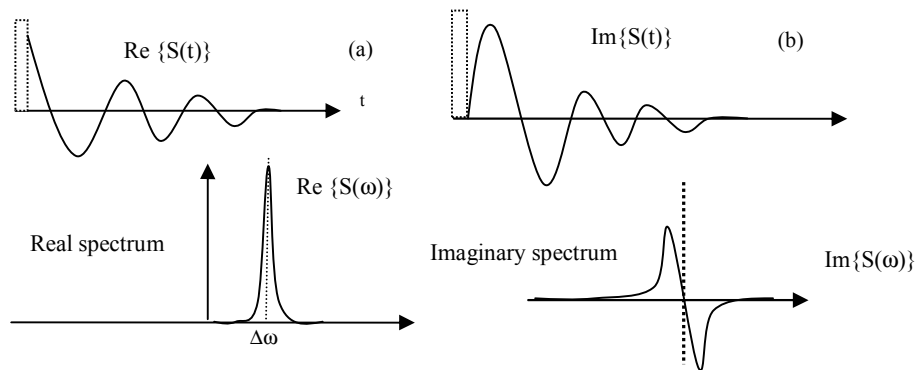
To be observed the high-frequency NMR signal is mixed with heterodyne signal with frequency offset $\Delta\omega$. As the result we get an output signal (in complex form):

$$S(t) = S_0 \exp(i\Delta\omega t) \cdot \exp(i\phi) \cdot \exp(-t/T_2),
\tag{A2.1.9}$$

where ϕ is absolute receiver phase (adjustable parameter) and S_0 is the initial signal amplitude immediately following the r.f. pulse. The NMR signal measured as decaying voltage is therefore, known as Free Induction Decay (FID). With the Fourier transformation the signal can be represented in frequency domain. The real part of the Fourier image of $S(\omega)$ is usually called *absorption line*. At phase $\phi=0$ the *absorption* represents the Lorenz line with width at half-maximum equal to $1/\pi T_2$. The imaginary part called *dispersion* at $\phi=0$ is symmetrical with respect to the $\Delta\omega=0$ (See Fig A2.1.5).

A2.1.5. Simple (Hahn) spin echo.

The inhomogeneity of the external magnetic field as well as local fields leads to the differing of the precession frequency for different locations in the sample. The frequency spread leads causes the dephasing of the FID following the 90° pulse. The transverse magnetization coherence state,



A2.1.5 FID following the excitation r.f. pulse. The real and imaginary phase correspond to receiver-phase ($\phi=0$). The complex Fourier transformation gives absorption and dispersion components at heterodyne offset frequency $\Delta\omega$.

therefore, has the lifetime $T_2^* = (\gamma\Delta B_0)^{-1}$ which is smaller than the “true T_2 ”

originated from the spin-spin interactions. Here ΔB_0 denotes the maximal external field inhomogeneity (of all the types). However, already in the first years of NMR development Hahn[A2.23] shown that the losses of coherences are reversible. By applying the 180° after the time delay $t=\tau$, one can obtain the signal of “spin-echo” in the moment of $t=2\tau$ after the first

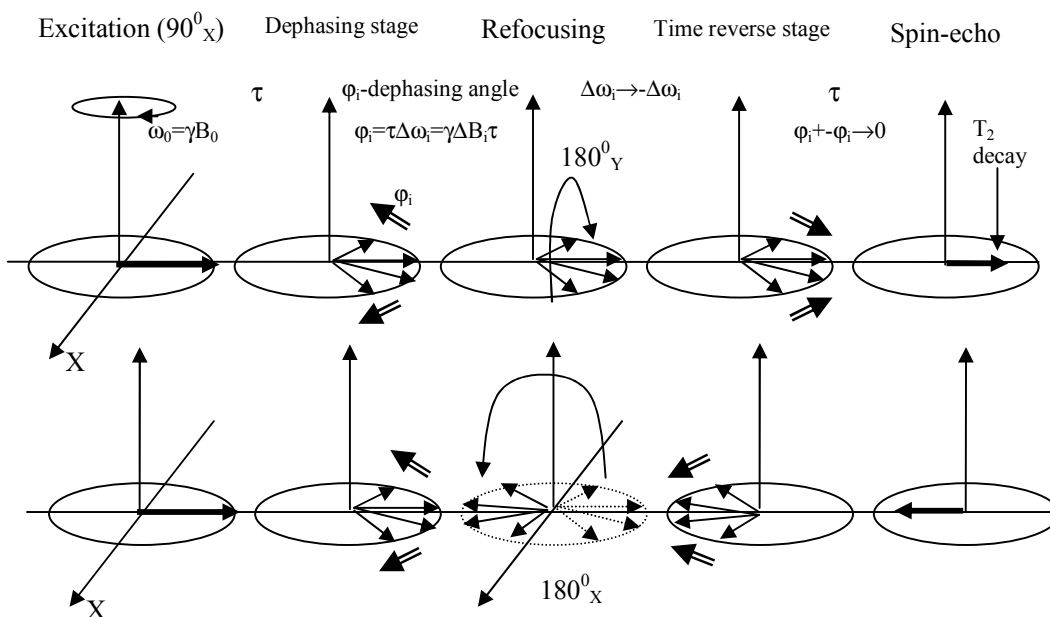


Fig A2.1.6 Spin echo classical illustration in the rotating frame system. The excitation by 90_x pulse turn the magnetization along y-axis. The inhomogeneity of the magnetic field makes different components (isochromats) of the magnetization rotate with different frequencies (either faster or slower than rotating frame depending on the local field offset) leading to dephasing. The 180° pulse turns magnetization depending on its phase around x, or y axis. In both case the direction of the isochromats rotation changes on opposite. Therefore, after the time period exactly equal to the dephasing one all the isochromats will concentrate in one vector producing the spin-echo-signal. (see Fig A2.1.7)

pulse 90° pulse sequence is shown on Fig A2.1.6.

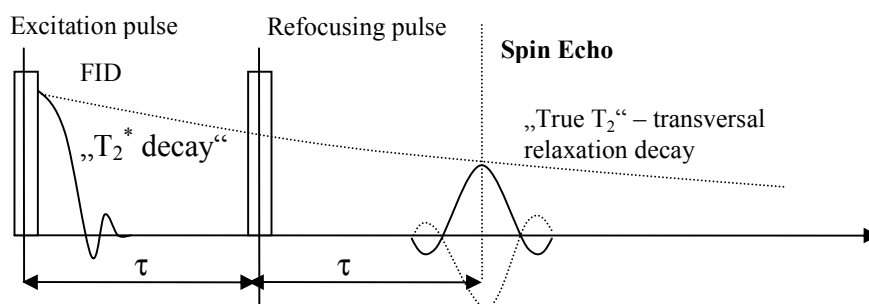


Fig A2.1.7 Spin-echo signal. The transverse magnetization after the 90° pulse falls down with the characteristic time T_2^* being dephased in isochromats, (Fig A2.1.6) The refocusing pulse perform “time reversing” and brings all the components back excepting loses due to spin-spin (transversal) relaxation. The sign and amplitude of echo depend on phase and duration of the refocusing pulse.

It is important to notice that the phase and duration of refocusing pulse can be set more or less arbitrary. The first echo observed by Hahn was obtained using the pair of 90° pulses. However, in such a case the refocusing will be incomplete and echo amplitude will be only $1/2$ of maximal possible achieved by the 180° refocusing pulse. Particularly, this property is used in the β -echo to provide the compensation scheme. The precise consideration using the classical approach is done in Appendix III and with density matrix formalism in Chapter III.

A2.2 Spin interactions

The intensity of the nuclear spins interaction determines the separation of the energy levels of the spin system and, therefore, the corresponding resonance frequencies. The full Hamiltonian of the spin system is the sum of the individual contributions responsible for the specific kind of the interaction of spins inside the system or with surrounding (“lattice”). In the following the individual spin interactions which are the most important for the solid-state NMR and especially for the investigation of the orientation of the molecular order will be considered.

A2.2.1 Zeeman interaction.

Zeeman interaction, i.e. interaction of the spins with external magnetic field is usually a largest one in NMR spin system Hamiltonian. It is essentially defines the level of the nuclear polarization (see A2.1).

$$H_z = C^z I_z B_0 \quad (\text{A2.2.1})$$

Here I_z denotes the matrix of the z-projection of spin operator. B_0 – the external magnetic field. The prefactor C^z can be found in table A2.2.1. The energy level splitting resulting from H_z defines the NMR Larmour frequency (see Eqn A2.1.2). It is important to notice that the other nuclear spin interactions in NMR are normally considered like a mere perturbation of the Zeeman interaction. The first-order perturbation theory is usually used in NMR to calculate the frequency shift arising from other types of interactions excepting the case of strong *quadrupolar* coupling.

A2.2.2 Quadrupole interaction

The second largest interaction in NMR Hamiltonian is usually the quadrupolar¹ that is the interaction of the electric *quadrupolar momentum* of nuclei and local *electric field gradient* established by the electron surrounding. It is important, that only the spins with $I \geq 1$ exhibit the quadrupolar momentum and therefore it plays no role for the ^1H , ^{29}Si , ^{13}C and other nuclei with spin $I=1/2$. The quadrupolar Hamiltonian is expressed by the operator:

$$\hat{H}_q = C^q \hat{I} \hat{Q} \hat{I} \quad (\text{A2.2.2})$$

Where I is the matrix of full spin operator Q is the quadrupolar coupling tensor. Obviously, the quadrupolar Hamiltonian is *bilinear* with respect to the nuclear spin operator. The tensor Q is proportional to the tensor of electric field gradient. The quadrupole interaction can not be observed in the case of the averaging by the fast molecular motion which takes place in liquids. The quantity C^q is a proportionality factor defined in Table A2.2.1.

A2.2.3 The direct dipole-dipole interaction

The dipole-dipole interaction describes the through-space coupling of magnetic moments (Fig A2.2.1b). The Hamiltonian for the homonuclear dipole-dipole coupling of two spins $I=1/2$ looks similar that one for the quadrupole coupling for the spin $I=1$, because in both cases the total spin number of the system is equal 1. However the energy levels perturbation for the dipolar interactions is sufficiently smaller than the quadrupolar and usually varies from 10 to 100 KHz for ^1H in solids but can be significantly smaller for other nuclei. The Hamiltonian operator for the coupling between two spins can be written as:

$$H_d = C^d \hat{I} \hat{D} \hat{S} \quad (\text{A2.2.3})$$

where I and S are the spin vector operators of the coupled nuclei. The prefactors displayed in Table A2.2.1 shows that the coupling energy is reverse proportional to the cube of the distance between nuclei. This dependence provides highly valuable information about internuclear distances in solids. Similarly to the quadrupolar tensor the trace of the dipolar is zero. So the dipolar coupling places no role in liquids under fast motional averaging conditions.

A2.2.4 Magnetic shielding (Chemical shift)

The externally applied magnetic field is shielded at the site of the nucleus by the surrounding electrons. As the result *local fields* influenced on nuclei differs from the external both in magnitude and direction can be written as:

$$B_{loc} = (1 - \hat{\sigma})B_0 \quad (\text{A2.2.4})$$

where σ is chemical shift (CS) tensor [A2.11]. Differently from the quadrupole and the dipole-dipole interactions, the shielding is dependent on the strength of magnetic field B_0 . It is also linear interaction with respect to spin operator contrary to the bilinear dipolar and quadrupolar:

$$\hat{H}_\sigma = C^\sigma \hat{I} \hat{\sigma} B_0 \quad (\text{A2.2.5})$$

The principal values of the CS tensor are established for a great number of compounds and can be found in literature [A2.12-14]. The averaging of tensor gives isotropic chemical shift constant:

$$\sigma_{iso} = \frac{1}{3} Sp\{\hat{\sigma}\} \quad (\text{A2.2.6})$$

Practically σ_{iso} shows the difference between the Larmour frequency of shielded and non-shielded nuclei. Because of the sensitivity to the properties of the electron clouds of atom and features of the chemical bonds the chemical shift is the standard tool used for structure elucidation, qualitative and quantitative analysis and many other chemical applications. Because of the dependence on the magnitude of the applied external field it is convenient to measure the chemical shift value in relative units with respect to some standard NMR frequency:

$$\delta = \frac{\omega_0 - \omega_L}{\omega_0} \quad (\text{A2.2.7})$$

Here δ denotes the relative chemical shift, ω_L – observed resonance Larmour frequency and ω_0 is the reference standard frequency. In literature the value of relative chemical shift is usually given in ppm (*parts per million*). For example, the range of chemical shift for ^1H nuclei in different substances covers 13ppm, while that of ^{13}C achieve 250ppm [A2.15]. The highest known chemical shift has the ^{129}Xe nuclei which can extend up to 8000 ppm.

A2.2.5 General formalism

The important point making the consideration of all kinds of anisotropic spin interaction very similar is that the corresponded Hamiltonian can be separated in spin depended and spatial (angular) depended part [A2.16,17]. First, the common properties of the spatial part will be considered as the most important for the aims of our work. For each type of the interaction mentioned above the spatial part of Hamiltonian expressed by the corresponded tensor \mathbf{P}_λ (where λ indexes the specific type of the interaction) can be expanded in isotropic part $\mathbf{P}_\lambda^{(0)}$, antisymmetric part $\mathbf{P}^{(1)}_\lambda$ and symmetric part $\mathbf{P}^{(2)}_\lambda$, with zero trace. Omitting in following index λ for simplicity the tensor components can be written in principal axes system XYZ of the symmetric part as:

$$\hat{P} = R \begin{bmatrix} 1 & 0 & 0 \\ 0 & 1 & 0 \\ 0 & 0 & 1 \end{bmatrix} + \begin{bmatrix} 0 & P_{xy} & P_{xz} \\ -P_{xy} & 0 & P_{yz} \\ -P_{xz} & -P_{yz} & 0 \end{bmatrix} + \delta \begin{bmatrix} -\frac{1}{2}(1+\eta) & 0 & 0 \\ 0 & -\frac{1}{2}(1-\eta) & 0 \\ 0 & 0 & 1 \end{bmatrix} \quad (\text{A2.2.8})$$

$P^{(0)} \quad + \quad P^{(1)} \quad + \quad P^{(2)}$

Because angular representation of the spin interaction anisotropic character is more convenient, the spherical coordinates instead of Cartesian is preferred [A2.18]. The expression (A2.2.8) will represent the sum of the second rank irreducible tensors with corresponded components $\{P_{lm}\}$:

$$P_{00} = R, \quad P_{10} = -i\sqrt{2}P_{xy}; \quad P_{1\pm 1} = P_{xy} + P_{yz}, \quad P_{20} = \sqrt{\frac{3}{2}}\delta; \quad P_{2\pm 1} = 0; \quad P_{2\pm 2} = -\frac{1}{2}\delta\eta \quad (\text{A2.2.9})$$

The isotropic part which is always observable even in fast motional averaging regime is defined as:

$$R = \frac{1}{3}(P_{xx} + P_{yy} + P_{zz}) = \frac{1}{3}Sp\{\hat{P}\} \quad (\text{A2.2.10})$$

In first order of the perturbation theory the NMR frequency is determined by the only **isotropic** and **symmetric** terms. The effect of antisymmetric is not observable [A2.11]. Two parameters are sufficient in symmetric parts which defines the anisotropic part of the frequency changes due to the spin interactions. These are the principal value of the anisotropy δ or Δ :

$$\delta = P_{zz}^{(2)} = \frac{2\Delta}{3} = \frac{2}{3}\left[P_{zz} - \frac{P_{xx} + P_{yy}}{2}\right] \quad (\text{A2.2.11})$$

and the asymmetry parameter η :

$$\eta = \frac{P_{yy} - P_{xx}}{\delta} = \frac{P_{yy} - P_{xx}}{P_{zz} - R} \quad (\text{A2.2.12})$$

where the principal values are ordered according to Haebleren [A2.19].

For different interaction λ the expressions for R , δ and η are listed in Table A2.2.1 [A2.18,20]. Using the tensor representing the different interactions λ , the generic Hamiltonian can be expressed in terms of the irreducible spherical tensors:

$$\hat{H}_\lambda = C^\lambda \sum_{l=0}^2 \sum_{m=-l}^l (-1)^m T_{lm}^\lambda \sum_{k=-l}^l P_{lk}^\lambda D_{k,-m}^{(l)}(\varphi, \theta, \psi) \quad (\text{A2.2.14})$$

Here P_{lm} and T_{lm} describe the space- and spin-dependent parts of the Hamiltonian respectively. The components of T_{lm} can be found in table A2.2.2. Equation A2.2.14 is valid in laboratory frame system connected with external magnetic field \mathbf{B}_0 . However, the principal values of the spin interaction tensors R , δ , η , are expressed in the principal axes frame. To recalculate the tensors component of two systems connected with the set of Eulerian angles φ, θ, ψ , the Wigner matrices $D_{km}^{(l)}(\varphi, \theta, \psi)$ are used. The elements of the matrices of different order can be found in literature [A2.12].

A2.2.6. Strong magnetic field approximation.

In strong magnetic field the resonance frequencies are determined mostly by the Zeeman term of the NMR Hamiltonianⁱⁱ. All other terms can be considered as a perturbation of the energy levels. In **secular approximation** of the perturbation theory only the terms of interaction Hamiltonian which are diagonal in eigenbasis of the Zeeman Hamiltonian are relevant. These are the components of T_{00} and T_{20} [A2.12, A2.21]. The anisotropic part of the Hamiltonian can be then written as:

$$H_\lambda = C^\lambda T_{20}^\lambda \frac{1}{2} \sqrt{\frac{3}{2}} \delta_\lambda \left[3 \cos^2 \theta - 1 - \eta_\lambda \sin^2 \theta \cos(2\varphi) \right] \quad (\text{A2.2.15})$$

The Euler angles θ and φ are the polar angles which determine the orientation of the magnetic field B_0 in principal axes system of tensor P . (see Fig A2.2.1).

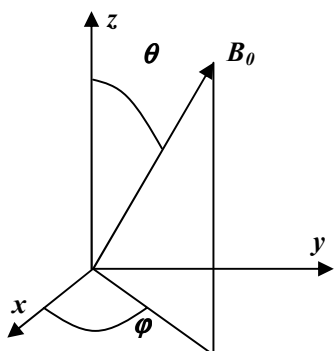


Fig A2.2.1 Polar Euler angles θ and φ defined via the orientation of the magnetic field B_0 in principal axes of coupling tensor P .

Within first order perturbation theory the only transitions between levels with difference of magnetic quantum number $m = \pm 1$ are allowed. This gives $2I+1$ lines for the interaction of a spin I nucleus. Therefore, dipolar (for 2 spins $I=1/2$) and quadrupolar couplings (for $I=1$) appears like a splitting of the resonance line in two. For CS interaction of $I=1/2$ the only one line is observed shifted at the position defined by the perturbation Hamiltonian H_σ . The coupling tensor of the dipolar interaction is always axially symmetric. The symmetry of the quadrupolar tensor and the tensor of chemical shift depends on the electron density configuration in the surroundings of the nuclei. The summary of the frequency and lineshape changes due to the different spin interactions are shown in Table A2.2.3.

Table A2.2.1 Factors and constants of the couplings Hamiltonian

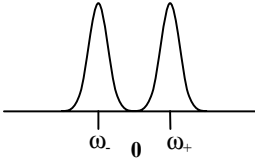
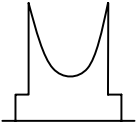
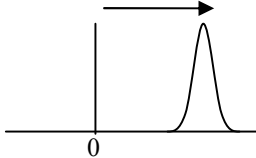
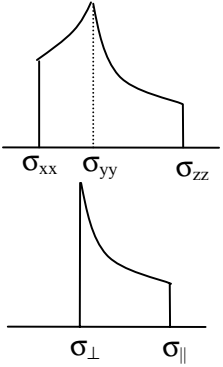
	C_λ	R	δ	δ	η
Zeeman	Z	$-\gamma$	1	-	-
Quadrupolar	Q	$eQ / [2I(2I-1)]$	0	eq	η_Q
Dipolar	D	$-\mu_0 \gamma_I \gamma_S / 4\pi$	0	$1 / r^3 IS$	-
CS	σ	γ	σ	$2\Delta_\sigma/3$	η_σ

γ – gyromagnetic ratio, r – distance between coupled spins I and S , eq and eQ – electric field gradients and

Table A2.2.2 Spin operators T_{lm}^λ in laboratory frame diagonal in the eigenbasis of Zeeman Hamiltonian (relevant for secular approximation) The full table of T_{lm} can be found elsewhere [A2.12, A2.21]

λ	T_{00}	T_{20}
Z	$I_z B_0$	-
Q	-	$6^{-1/2} [3I_z^2 - I(I+1)]$
D	-	$6^{-1/2} [3I_z S_z - IS]$
σ	$I_z B_0$	$(2/3)^{1/2} I_z B_0$

Table A2.2.3 NMR lineshape and frequency changes due to the anisotropic spin interaction summary. [A2.22]

Perturbation from Zeeman frequency	Individual lineshape	Powder averaging
<p>Dipolar coupling of to two spins $I=S=1/2$ (homonuclear case)</p> $\omega_{\pm} = \frac{\Delta_D}{2} (3 \cos^2 \theta - 1) = \frac{3}{2} \frac{\gamma^2 \hbar}{r^3} P_2(\cos(\theta))$ <p>Here $P_2(\cos(\theta))$ – second order Legendre polynomial</p>		
<p>Chemical shift</p> $\sigma = \frac{\Delta_{\sigma}}{2} (3 \cos^2 \theta - 1 - \eta_{\sigma} \sin^2 \theta \cos 2\alpha)$ $\Delta \sigma = (\sigma_{zz} - \frac{\sigma_{xx} + \sigma_{yy}}{2}) \quad \text{CS - anisotropy}$ $R_{\sigma} = \sigma_{iso} = \frac{1}{3} (\sigma_{xx} + \sigma_{yy} + \sigma_{zz}) \quad \text{isotropic CS}$ $\eta_{\sigma} = \frac{\sigma_{xx} - \sigma_{yy}}{\sigma_{zz} - \sigma_{iso}} \quad \text{CS - asymmetry}$ $\sigma = \sigma_{iso} + \frac{2}{3} \Delta \sigma P_2(\cos \theta) \quad \text{for } \sigma_{xx} = \sigma_{yy} = \sigma_{\perp} \text{ and } \sigma_{zz} = \sigma_{\parallel}$		

A2.3 Density operator formalism

A2.3.1 Density operator

The **density operator** [A2.7] permits the most convenient and general description of the quantum mechanical system dynamics. The extensive treatment of this question is widely presented in literature. Here, the only basic properties of this approach to the QM description of the system will be done. We start with the time- independent Schrödinger equation of the wave function $\psi(t)$.

$$\frac{d}{dt} |\psi(t)\rangle = -i\hbar H(t) |\psi(t)\rangle \quad (\text{A2.3.1})$$

where $H(t)$ is the Hamiltonian or total energy operator of the system. The Plank constant \hbar in following consideration will be omitted for convenience and the energy will be measured in circular frequency units. The state function can be expanded in terms of the full orthonormal basis

$$\text{as: } |\psi(t)\rangle = \sum_{i=1}^N c_i(t) |i\rangle \quad (\text{A2.3.2})$$

where the time-dependence of $|\psi(t)\rangle$ is expressed in terms of time dependent coefficients $|c(t)\rangle$ and N is the dimension of the vector space or of all admissible functions called *Hilbert space* (H-space). Two cases can be distinguished for the quantum system:

1. Pure state: all spins of the ensemble are described with the same wave-function The corresponding density operator ρ is defined as a product of the ket and bra vectors

$$\rho(t) = |\psi(t)\rangle \langle \psi(t)| = \sum_{i,j} c_i(t) c_j(t) |i\rangle \langle j| \quad (\text{A2.3.3})$$

2. Mixed state (ensemble in thermal equilibrium). The density operator is then understood as an average over the all-possible state of the ensemble with corresponding probabilities weighting:

$$\rho(t) = \sum_k p_k \sum_{i,j} c_i^k(t) c_j^{k*}(t) |i\rangle\langle j| = \sum_{i,j} \overline{c_i(t) c_j^*(t)} |i\rangle\langle j| \quad (\text{A2.3.4})$$

For the pure state we obtain:

$$\langle r | \rho(t) | s \rangle = c_r(t) c_s^*(t) \quad (\text{A2.3.5})$$

whereas for the mixed states we find

$$\langle r | \rho(t) | s \rangle = \sum_k p^k c_r^k(t) c_s^{k*}(t) = \overline{c_r(t) c_s^*(t)} \quad (\text{A2.3.6})$$

The interpretation of the density matrix is possible in the eigenbasis of the Hamiltonian H . The diagonal element ρ_{rr} is to be treated as the probability to find system in the eigenstate $|r\rangle$ i.e $\rho_{rr} = P_r$ is the *population of the energy level* of state $|r\rangle$. The off-diagonal element

$$\rho_{rs} = \langle r | \rho(t) | s \rangle = \overline{c_r(t) c_s^*(t)} \quad (\text{A2.3.7})$$

Indicates a “coherent superposition” of eigenstates $c_r(t) |r\rangle + c_s(t) |s\rangle$ in $\psi(t)$ that means that the phase of various members of the ensemble are correlated with respect to $|r\rangle$ and $|s\rangle$. Such a coherent superposition, or simply “*coherence*”, can be associated with the *transition between two eigenstates* $|r\rangle$ and $|s\rangle$. Particularly, if two states span an allowed transition with a difference in magnetic quantum numbers $\Delta M_{rs} = M_r - M_s = \pm 1$, the coherence ρ_{rs} is related to the transverse magnetization components $M_{rs}^\pm = M_{rs}^{(rs)} - i M_{rs}^{(rs)}$.

A2.3.2 Density operator equation.

From the time-dependent Schrödinger equation the equation of motion for the density operator can be derived.

$$\frac{d}{dt} \rho(t) = -i [H(t), \rho(t)], \quad (\text{A2.3.8})$$

This differential equation called Liouville-von Neumann equation has the formal solution in form of:

$$\rho(t) = U(t) \rho(0) U(t)^{-1}, \quad U(t) = T \cdot \exp \left\{ -i \int_0^t H(t') dt' \right\} \quad (\text{A2.3.9})$$

where the Dyson time-ordering operator T prescript the evaluating of the exponents in cases when the Hamiltonians at different time moments do not commute $[H(t'), H(t'')] \neq 0$.

A2.3.3 Expectation values

For normalized wave function the expectation value $\langle A \rangle$ of an operator A :

$$\langle A \rangle = \sum_k p_k(t) \langle \psi_k(t) | A | \psi_k^*(t) \rangle \quad (\text{A2.3.10})$$

with account of eqn A2.3.7 for $\rho(t)$, the expectation value of an operator can be found by evaluating the trace of its matrix representation product with matrix of density operator:

$$\langle A \rangle = Tr \{ A \cdot \rho(t) \} \quad (\text{A2.3.11})$$

A2.3.4 Reduced spin density operator.

The previous consideration has been done for the entire quantum mechanical system. The basis wave functions of H-space depend both on spatial and spin variables. However for the most of NMR application it is usually sufficient to evaluate the restricted amount of operators acting

separately on nuclear and electron spins. The rest of the freedom degrees can be referred to as the “lattice” reservoir.

$$\sigma(t)_{ss'} = \sum_f \langle s'f | \rho(t) | fs \rangle = Tr_f \{ \rho(t) \}. \quad (\text{A2.3.12})$$

Where s and f -denotes the spin and spatial wave functions respectively. The full Hamiltonian will be reduced to H^s which is the spin part acting only on spin variables, (obtained by the averaging of the full Hamiltonian over the spatial coordinates)

$$H^s = \sum_f \langle f | H | f \rangle = Tr_f \{ H \}. \quad (\text{A2.3.13})$$

A2.3.5 Explicit matrix representation of the master equation.

The direct way of solving the master equation is to follow the explicit matrix representation of the density operator.

$$\frac{d}{dt} \sigma_{rs} = -i \sum_k (H_{rk} \sigma_{ks} - \sigma_{rk} H_{ks}) \quad (\text{A2.3.14})$$

The terms originating from the commutator with Hamiltonian H may be expressed by *supermatrix* element H_{rstu} of the commutator *superoperator* \hat{H} (see following section).

If the elements of density operator are arranged in the form of a column vector σ , eqn A2.3.14 can be written as

$$\frac{d}{dt} \sigma = -i \hat{H} \sigma \text{ with the formal solution: } \sigma(t) = \exp\left\{ \left(-i \hat{H} \right) t \right\} \sigma(0) \quad (\text{A2.3.15})$$

where $\sigma(0)$ denotes the initial state of density operator. The H-space form of the solution can be obtained immediately as:

$$\sigma(t) = R(t) \sigma(0) R^{-1}(t) \text{ with } R(t) = \exp\{-iHt\}. \quad (\text{A2.3.16})$$

Schematically the unitary transformation A2.3.16 can be replaced with the multiplication on matrix of dimension $n^2 \times n^2$ with column vector $\sigma(0)$

$$\sigma(t) = \hat{R}(t) \sigma(0) \quad (\text{A2.3.17})$$

The supermatrix \hat{R} can be built according (A2.3.27)

A2.3.6. Liouville operator space

From previous analysis of the master equation solution it can be noticed that the commutator or unitary transformation influencing on density operator has the strong analogy with the transformations which Hilbert space operators make over its elements i.e. wave-functions on vectors of the state. The analogy can be preceded by introducing the superoperator space called Liouville space (L-space) over the space of Hilbert (H-space) operators. An example of such an operator relation is the commutator:

$[H, \sigma] = H \cdot \sigma - \sigma \cdot H$ it can be written in the abbreviated superoperator notation

$$\hat{H} \sigma \equiv [H, \sigma]. \quad (\text{A2.3.18})$$

An operator acting on the operators is called superoperator when: 1. $\hat{S}A \in L$ and 2. $\hat{S}(aA + bB) = \hat{S}aA + \hat{S}bB$ We denote supeoperators by capital letters with a double hat.

Important classes of the superoperators.

1. Commutator

For each operator C a commutator superoperator \hat{C} may be defined by $\hat{C}A = CA - AC = [C, A]$.

When C is hermitian operator the \hat{C} is hermitiant as well.

2. Unitary transformation superoperator.

The unitary transformation RAR^{-1} with $R = \exp\{-iHt\}$ may be expressed by the unitary superoperator $\hat{R} : \hat{R}(\tau) = \exp(-i\hat{H}\tau)$

Therefore,

$$\hat{R}(\tau)\sigma(t) = \exp(-i\hat{H}\tau)\sigma(t) = \exp(-iH\tau)\sigma(t)\exp(+iH\tau) = \sigma(t+\tau) \quad (\text{A2.3.21})$$

Shortly it can be written schematically as: $\sigma(t) \xrightarrow{H\tau} \sigma(t+\tau)$ In this notation the series of transformation can be written chronologically:

$$\sigma(t) \xrightarrow{H\tau_1} \sigma(t+\tau_1) \xrightarrow{H\tau_2} \sigma(t+\tau_2) \quad (\text{A2.3.22})$$

A2.3.7. Matrix representation of the superoperators

By giving the complete operator basis $\{B_s, s=1..n^2\}$ it is possible to represent any superoperator \hat{S} influencing operator A in the form

$$\left(\hat{S}A\right)_{pq} = \sum_{lm} \sum_{jk} S_{jk} B_{j,pl} B_{k,mq} = \sum_{lm} S_{pq,lm} A_{lm} \quad (\text{A2.3.23})$$

where B_j and B_k is left and right translation basis superoperators, with the supermatrix elements

$$S_{pq,lm} = \sum_{jk} S_{jk} B_{j,pl} B_{k,mq} = \sum_{jk} S_{jk} (B_j \otimes B_k^t)_{pq,lm}, \quad (\text{A2.3.24})$$

where \otimes means the direct outer product of two matrices. This representation can be used to calculate the supermatrices for any superoperator. For example for the commutator we obtain:

$$\hat{C}A = CAE - EAC, \quad (\text{A2.3.25})$$

where E represents the unity matrix. This leads to the following expression for the supermatrix:

$$(\hat{C}) = (C) \otimes (E) - (E) \otimes (C^t). \quad (\text{A2.3.26})$$

The matrix representation of the unitary transformation $\hat{R}A = RAR^{-1}$, is obtained in form :

$$\left(\hat{R}\right) = (R) \otimes (R) \quad (\text{A2.3.27})$$

A2.3.8. Application of the superoperator algebra for the spin system density matrix evolution calculation in the NMR experiments. Rotation in spin space.

The unitary transformation A2.3.26-27. can be used to describe the rotation of the density operator in three-dimensional spin space. For example the evolution under *chemical shift* or *rf-pulses* is described by the linear combination of the Cartesian spin operators (I_x, I_y, I_z). Thus the transformation:

$$I_{k\beta} \xrightarrow{\phi I_{k\alpha}} I_{k\beta} \cos \phi + I_{k\gamma} \sin \phi, \quad (\text{A2.3.28})$$

where $\alpha, \beta, \gamma = x, y, z$ and cyclic permutations, express a rotation through an angle $\phi = -\gamma B_{\alpha} \tau$ in physical space around α -axis. Rotation about tilted axes can be decomposed: for example the effect of an rf-pulse with arbitrary phase angle ϕ (defined as an excursion from the x - towards the y -axis of the rotating frame) is described by the three steps:

$$\sigma(t_-) \xrightarrow{-\varphi \sum_k I_{kz}} \xrightarrow{\beta \sum_k I_{kz}} \xrightarrow{+\varphi \sum_k I_{kz}} \sigma(t_+) \quad (\text{A2.3.29})$$

i. In some cases the quadrupolar coupling can be stronger than Zeeman. It is pure quadrupolar resonance (NQR) when the extremely high quadrupolar coupling constant (up to hundreds MHz) allows to observe the transitions in spin system without external magnetic field.

ⁱⁱ Excepting the case of NQR (see (i))

Appendix III β -echo classical illustration

Here, we consider the important properties of the β -echo combination basing on the classical vector model. For the demonstration purposes, only the case when no bilinear terms are present in spin Hamiltonian will be analyzed. The full consideration using density matrix formalism is done in Chapter III. Initial state of the magnetization vector \mathbf{M} supposed to be the thermal equilibrium value $M_z=M_0$, $M_x=0$, $M_y=0$, with z-axis corresponding to the magnetic field direction \mathbf{B}_0 . (Fig A3.1.)

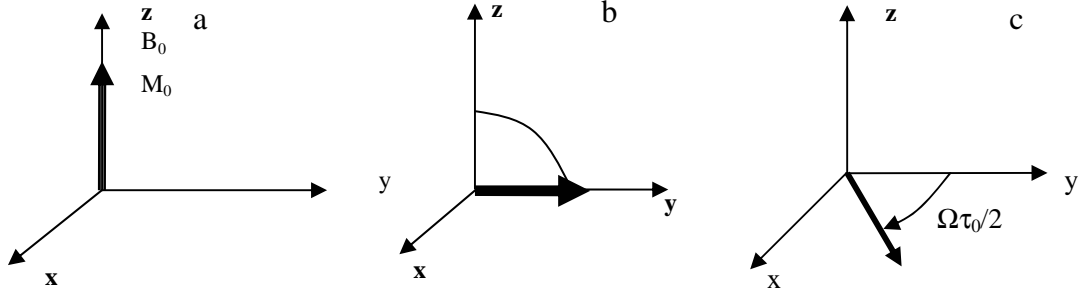


Fig A3.1(a) The magnetization vector of the system in thermal equilibrium state is aligned with the external magnetic field direction. (b) Magnetization is prepared in «y» direction by means of $(\pi/2)_x$ rf-pulse. (c) Evolution during $\tau_0/2$ period under linear Hamiltonian.

Step I Preparation. The magnetization is prepared in y-direction by applying the $(\pi/2)_x$ pulse. $M_y=M_0$ (Fig A3.1,a,b).

Step II Evolution time. The system evolves under the linear terms of the Hamiltonian (summarized as an offset frequency Ω) during the period $\tau_0/2$. The state of the magnetization can be described with $M_{\perp}(\tau_0/2)=M_0 \exp(-i\Omega \tau_0/2)$ that is equivalent to $(M_x=M_0 \sin(\Omega \tau_0/2), M_y=M_0 \cos(\Omega \tau_0/2), M_z=0)$ (Fig A3.1.c)

Step III Second (refocusing) pulse

1. $(\pi/2)_x$ the y-component is destroyed. The x-component is conserved. $M_x=M_0 \cos(\Omega \tau_0/2)$
2. $(\pi/2)_y$ the x-component is destroyed. The y-component is conserved. $M_y=M_0 \sin(\Omega \tau_0/2)$
3. $(\pi)_y$ the y-component is conserved, x-component changes the sign $M_x=M_0 \cos(-\Omega \tau_0/2)$

(Fig A3.2 (1),(2),(3))

Step IV. Refocusing Time The system continue to evolve after refocusing pulse under the influence of Hamiltonian during the time period exactly equal to the evolution period: $M_{\perp}(\tau_0)=M_{\perp}(\tau_0/2) \exp(-i\Omega \tau_0/2)$ forming the corresponding spin echoes:

$$S_1(\tau_0)=M_0 \cos(\Omega \tau_0/2) \cos(\Omega \tau_0/2), S_2(\tau_0)=-M_0 \sin(\Omega \tau_0/2) \cdot \sin(\Omega \tau_0/2), S_3(\tau_0)=M_0.$$

«Callaghan echo» is formed by combination of three echoes as: $S_{\beta}(\tau_0)=[S_2(\tau_0)-S_1(\tau_0)-S_3(\tau_0)]$. Combining eqn. (1,2,3) we obtain : $S_{\beta}(\tau_0)=[M_0(\sin^2(\Omega \tau_0/2) + \cos^2(\Omega \tau_0/2)-M_0)]=0$. That way, the Callaghan echo combination destroys completely the magnetization evolving under the linear terms of the Hamiltonian described by the offset of the resonance frequency (for example magnetic field inhomogeneity, chemical shift, etc).

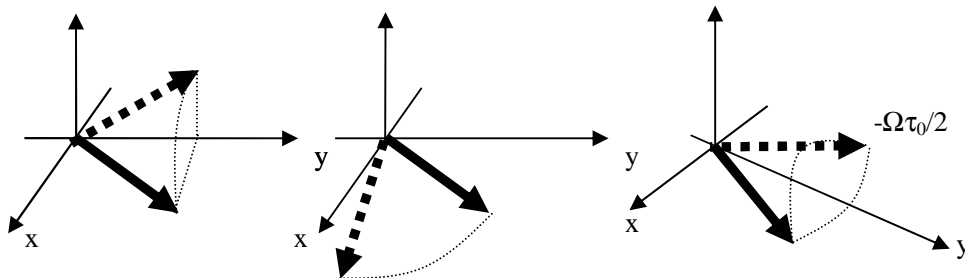


Fig 3A.3 Refocusing pulses (1) $(\pi/2)_y$ – (preserves x-component), (2) $(\pi/2)_x$ (preserves y-component) (3) π_y changes the sign of x-component, preserving y-component.

The role of the off-resonance offset and R.F. pulse imperfections.

Because of the signal compensation scheme the β -echo combination, it can be expected that it will be rather sensitive to the different experimental parameters imperfections which always takes place in practice.

There are two basic reasons of the experimental errors in the magnetization flip angle. First reason is the imperfections of the r.f-pulses produced by the experimental hardware. However, the role of these errors can be significantly reduced when using the appropriate phase cycle (for example **CYCLOPS**). Another reason arises from the resonance frequency offset leading to the tilting of the «effective» magnetic field direction (**Fig A3.3**) and therefore to the changing into the effective tilting angle produced by the r.f. pulse. This reason is especially important in our case because of the sufficiently wide spectrum of the ^{29}Si in polysiloxanes caused by *anisotropic chemical shift* distributions (anisotropy parameter $\Delta\sigma=48\text{ppm}$ leads to $\approx 3000\text{Hz}$ spectrum width at $H_0=9.4\text{T}$, therefore, the significant part of spins will generate the off-resonance NMR signal)

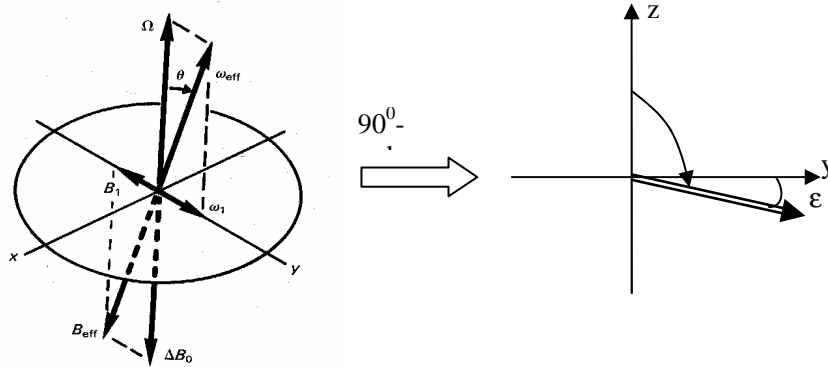


Fig A3.3. The resonance frequency offset leads to the changing of the effective field direction B_{eff} , and therefore altering the resulted magnetization flip angle.

If the magnetization tilting angles differs from the 90^0 for the “solid-echo” and “Hahn-echo-I” this leads to the non-complete destroying the “y” and “x” components of the magnetization respectively, after second pulse (see Fig A3.3). Therefore, despite of the theoretical expectation, after second evolution period and summation of echoes into the Callaghan combination the non-zero signal will be observed due to the non-compensated magnetization.

Due to the using of the cross-polarization for the initial excitation (see Chapter IV) the only error in second pulse of each echo becomes important. To calculate the resulting non-compensated signal the rotation matrix formalism can be used. The Cartesian matrix performing the rotation of the vector \mathbf{M} around all three axes, on arbitrary angle φ is given by:

$$R_z(\varphi) = \begin{bmatrix} \cos \varphi & -\sin \varphi & 0 \\ -\sin \varphi & \cos \varphi & 0 \\ 0 & 0 & 1 \end{bmatrix} \quad R_y(\varphi) = \begin{bmatrix} \cos \varphi & 0 & \sin \varphi \\ 0 & 1 & 0 \\ -\sin \varphi & 0 & \cos \varphi \end{bmatrix} \quad R_x(\varphi) = \begin{bmatrix} 1 & 0 & 0 \\ 0 & \cos \varphi & -\sin \varphi \\ 0 & \sin \varphi & \cos \varphi \end{bmatrix}$$

The resulted magnetization after the application of the r.f. pulses and two evolution periods will be described by the multiplication on corresponded matrices.

$$\mathbf{M}_1 = R_z(\Omega \tau_0 / 2) \cdot R_x(\pi / 2 + \varepsilon) \cdot R_z(\Omega \tau_0 / 2) \cdot \mathbf{M}$$

$$\mathbf{M}_2 = R_z(\Omega \tau_0 / 2) \cdot R_y(\pi / 2 + \varepsilon) \cdot R_z(\Omega \tau_0 / 2) \cdot \mathbf{M}$$

$$\mathbf{M}_3 = R_z(\Omega \tau_0 / 2) \cdot R_y(\pi + 2\varepsilon) \cdot R_z(\Omega \tau_0 / 2) \cdot \mathbf{M}$$

Where echoes values $M_{1,2,3}$ have the same sense as, S_2 and S_3 in previous section, and ε describes the error of the tilting angle due to the r.f. pulse imperfection. Starting from magnetization value \mathbf{M} just after the initial excitation i.e $\mathbf{M}=(0, M_0, 0)$ (see Fig A3.2) the following result can be obtained for the error signal of β -echo:

$$\begin{aligned} (S_{\text{err}}^{(\beta)})_y &= M_0 \cdot [\cos 2\Omega \tau_0 \cdot \sin^2(\varepsilon) - \sin^2(\varepsilon) - \sin(\varepsilon)] \rightarrow O(\varepsilon) \\ (S_{\text{err}}^{(\beta)})_x &= M_0 \cdot [-\sin 2\Omega \tau_0 \sin^2(\varepsilon) + \sin^2(\varepsilon)] \rightarrow O(\varepsilon^2) \end{aligned}$$

This means that the errors in the rf-pulses leads to the (i) generation of the additional component contributing to the echo amplitude S_y , which is proportional to the flip angle error, and (ii) appearing the imaginary component of echo which is equal to 0 in the ideal case and depends quadratic on error value. This allows one a two stage adjustment of the pulse length in experiment, making, at first, the imaginary component equal 0 during the coarse tuning, and then, for fine tuning, minimizing the real component for the echo time period $\tau_0=0$.

Zusammenfassung

Das entstehende Interesse an der Flüssigkristallinität von Polymeren gegen Ende der 70er Jahre des vorigen Jahrhunderts führte zu einem schnellen Fortschritt bei der Herstellung neuer Materialien mit sehr wertvollen Eigenschaften. Die eindrucksvollsten Ergebnisse wurden zunächst mit der Synthese von selbstverstärkenden Materialien (Terlon, Kevlar u. a.), die insbesondere in der Luft- und Raumfahrttechnik unverzichtbar wurden, erzielt. Die besonderen Eigenschaften von polymeren Flüssigkristallen (PLC) beruhen auf der Kombination der Merkmale, die für flüssigkristalline bzw. für makromolekulare Systeme typisch sind.

Eine spezielle Möglichkeit des molekularen Aufbaus ist in den sog. flüssigkristallinen Seitenkettenpolymeren realisiert. Dabei handelt es sich um PLC, die die mesogenen Einheiten in den Seitenketten enthalten. Die attraktiven Eigenschaften dieser Verbindungen entstehen aus der Kombination der für niedermolekulare Flüssigkristalle typischen anisotropen Eigenschaften (Seitenkette) mit der Fähigkeit von Makromolekülen (Hauptkette) zur Bildung von Filmen und Fasern. Das Phasenverhalten dieser Substanzen wird hauptsächlich durch die mesogenen Einheiten, in gewissem Maße aber auch durch das Rückgrat, festgelegt. Andere Merkmale werden im wesentlichen durch die Hauptkette bestimmt, wie zum Beispiel Glasübergang sowie viskose und elastische Eigenschaften. Auf molekularer Längenskala werden gegensätzliche Tendenzen erwartet: Während die mesogenen Seitenketten bestrebt sind, eine gewisse Orientierungsordnung aufrechtzuhalten, versuchen die Hauptketten, die Entropie zu maximieren, indem sie ungeordnete Knäuel bilden. Die reale molekulare Struktur und Dynamik sind das Resultat eines Kompromisses, der eine gewisse Orientierung der Hauptkettensegmente und eine Verlangsamung der Reorientierung des mesogenen Direktors in externen Feldern beinhaltet. Daher sind Fragen der molekularen Orientierung bei der Untersuchung von PLC von großer Bedeutung.

Der eigentliche Zweck der vorgestellten Arbeit ist die Erzielung von Erkenntnissen über die Hauptkettenorientierung und -dynamik. Als Untersuchungsgegenstand sind Polysiloxane mit mesogenen Seitenketten gewählt worden. In der NMR-Gruppe des Fachbereiches Physik der Martin-Luther Universität Halle wurden 1994 die ersten Untersuchungen über das Orientierungsverhalten der Seitenkettenpolymere begonnen. Dabei wurden Polysiloxan-Probenserien mit systematisch veränderten Strukturmerkmalen untersucht. Als Grundlage hierzu musste zuvor der Tensor der ^{29}Si -chemischen Verschiebung einschließlich seiner Ausrichtung im Molekül bestimmt werden, mit dessen Kenntnis der Orientierungsgrad der Hauptkettensegmente erst bestimmt werden konnte.

Eine vollständige und eindeutige Charakterisierung des Orientierungszustandes der Hauptkettensegmente erfordert jedoch eine Angabe über die *transversale Anisotropie* der molekularen Segmente. Diese kann nicht allein aus der eindimensionalen Orientierungsverteilungsfunktion gewonnen werden, die mit man Hilfe des axialsymmetrischen Tensors der chemischen Verschiebung erhalten hatte. Zusätzlich ist hierfür die Nutzung einer weiteren anisotropen NMR-Wechselwirkung erforderlich. Hier wurde die *direkte dipolare Wechselwirkung* verwendet, um die Orientierungsverteilung der Verbindungsvektoren benachbarter Si-Atome zu bestimmen. Diese Vektoren weisen in Segment-Längsrichtung. Wegen der geringen natürlichen Häufigkeit der ^{29}Si -Kerne (4.5%) ist jedoch die Nutzung der dipolaren Wechselwirkung aus zwei Gründen problematisch: (i) ist die Gesamt-Signalintensität gering, und (ii) ist die Wahrscheinlichkeit, daß zwei benachbarte Si-Atome beide einen ^{29}Si -Kern enthalten, sehr gering, was dazu führt, dass der überwältigende Teil des Signals von isolierten ^{29}Si -Spins stammt, das den schwachen Anteil der Spinpaare überdeckt. Dieses Problem kann durch die Implementierung spezieller NMR-Experimente und Auswertemethoden überwunden werden. Die folgenden Ziele wurden in der vorgestellten Arbeit angestrebt und erreicht:

1. Eine spezielle NMR-Methode, " β -Echo" genannt, wurde für die selektive Aufnahme derjenigen Signalkomponente verwendet, die von dipolar gekoppelten ^{29}Si -Paaren herrührt. Gleichzeitig unterdrückt dieses Verfahren das Signal der nichtgekoppelten ^{29}Si -Spins.
2. Mittels Zwei-Spin-Näherung wurde eine Beziehung zwischen der zeitlichen Entwicklung des β -Echos (β -Funktion) und der Stärke der dipolaren Wechselwirkung hergeleitet. Weiterhin liefert die Anisotropie der dipolaren Kopplung eine Verbindung zwischen der β -Funktion und der Orientierung des Si-Si-Vektors. Der Einfluß der Orientierungsverteilungsfunktion (ODF) der Si-Si-Vektoren auf

das Verhalten der β -Funktion wurde mit (i) Modell-ODFs und (ii) "modellfreien" ODFs überprüft, letztere beschrieben durch eine Legendre-Reihe. Die Empfindlichkeit der β -Funktion bezüglich der ODF-Parameter wurde durch eine Computersimulation geprüft.

3. Die Empfindlichkeit der β -Funktion bezüglich der ODF Parameter wurde durch das Verwenden ihrer Winkelabhängigkeit verbessert. Dabei wurden spezielle Methoden der Datenauswertung vorgeschlagen, um eine multiparametrische nichtlineare Anpassung zu vermeiden; die lineare Regression wurde im Falle mehrerer Anpassparameter vorgezogen.

4. Die selektive Analyse der Subspektren gestattet die Verwendung einparametrischer Fitmethoden, wodurch sich das ω_{OD} -Auswerteverfahren transparenter und exakter gestaltet. Nach unserer Kenntnis sind Fouriertransformation und Spektrenanalyse bislang nie in Verbindung mit der β -Funktion angewandt worden.

5. Die Rolle der transversalen NMR-Relaxation ist hinsichtlich zweier Aspekte untersucht worden: (i) Einfluss der transversalen Relaxationszeit T_2 auf die β -Funktion und (ii) Nutzung der transversalen Relaxation als Mittel für molekular-dynamische Untersuchung. Die Temperaturabhängigkeit von T_2 ist in einem breiten Bereich gemessen worden. Drei charakteristische Temperaturregionen des T_2 -Verhaltens wurden dabei gefunden. Die Analyse der Relaxationsdaten wurde im Rahmen der Anderson-Weiss Näherung ausgeführt, wobei die Reorientierung des Tensors der ^{29}Si -chemischen Verschiebung als primärer Relaxationsmechanismus angenommen wurde. Das unterschiedliche Verhalten der transversalen Relaxation in den drei Temperaturregionen konnte mit dem Modell der starken, exponentiellen bzw. schwachen Korrelation der molekularen Bewegung erklärt werden.

6. Um die dipolare Kopplungskonstante ω_{OD} abzuschätzen, sind Experimente an einer Polydomänen-Probe des Polysiloxans M4 ausgeführt worden. Der erhaltene Wert von ω_{OD} wurde verwendet, um die Daten der Experimente mit Monodomänen-Proben zu verarbeiten. Zusätzlich ist ω_{OD} verwendet worden, um den Bindungswinkel Si-O-Si am Sauerstoffatom festzustellen. Das erreichte Resultat stimmt gut mit quantenchemischen Berechnungen überein.

7. Die Experimente zur Orientierungsabhängigkeit der β -Funktion waren an den Monodomänen-Polysiloxanproben M4 und M6 erfolgt. Die Legendre-Koeffizienten der ODF wurden aus den β -Funktionen dreier charakteristischer Orientierungen ermittelt. Die Rekonstruktion der ODF mittels dieser Koeffizienten führte zu Abweichungen vom experimentellen Ergebnis, die 10% nicht überstiegen. Aus den Werten ergab sich, dass die Hauptkettensegmente in der Probe M6 vorzugsweise senkrecht zum lokalen Direktor (Seitenkette) ausgerichtet sind. Zwischen den Werten, die sich aus der Orientierungsabhängigkeit des ^{29}Si -Spektrums und denen, die sich aus der β -Funktion ergeben, besteht jedoch ein quantitativer Unterschied.

Die wesentliche Neuheit der dargestellten Arbeit ist nach unserer Kenntnis die Anwendung des β -Echos auf den Fall nicht angereicherter Spins geringer natürlicher Häufigkeit, wie ^{29}Si , wo zudem die schwache bilineare anisotrope Spin-Wechselwirkung durch eine starke lineare überdeckt wird. Es kann geschlussfolgert werden, dass das β -Echo eine wirkungsvolle Methode zur Gewinnung des NMR-Signals solcher Spins ist, die einer homonuklearen dipolaren Wechselwirkung unterliegen, indem das Signal der nicht-gekoppelten Spins abgetrennt wird. Die meisten Techniken mit ähnlicher Zielstellung basieren auf Doppelquanten(DQ)-Filtern (INADEQUATE, C7, DRAMA, usw.). Der Vorteil des β -Echos ist, daß eine Einquantenkohärenz benutzt wird und folglich DQ-Filter-Verluste vermieden werden. Gegenüber den meisten DQ-Methoden erfordert das β -Echo keine schnelle Probenrotation und kann für die Bestimmung der ODF mittels einer Winkelabhängigkeit verwendet werden.

Die Einfachheit der β -Echo-Impulsfolge erlaubt eine Anzahl unterschiedlicher Erweiterungen des Grundverfahrens. Insbesondere wurde die Kombination der β -Echo-Signalselektion mit einer weiteren Detektion der dipolaren Wechselwirkung durch eine Carr-Purcell-Echosequenz geprüft. Jedoch birgt diese Methode weitere experimentelle und theoretische Probleme in sich, die vor ihrer Anwendung gelöst werden müssen.

Abstract

The unique properties of the PLC material are connected with the orientation of the molecules in liquid crystalline state which combines the amorphous and liquid-crystal phase structural features. That way, the problems of the orientation structure are of great interest when studying the LC polymers.

One of the most interesting types of the PLC is side-chain LC polymers. Those are PLC which contains the mesogenic units in side chains. The attractive properties of these compounds are provided by the combination of the low-molecular LC anisotropy properties originated from the mesogenic units (side-chain) and the potential of persistent macromolecules (main-chain) in creating of the films and fibers. The phase behavior of these substances is mainly governed by the mesogenic units but influenced also by the backbone. Other properties, are determined essentially by the main chains, for instance glass transition, viscous and elastic properties. At molecular level opposite tendencies are expected: Whereas the mesogenic side chains generate some orientation order, the main chains try to maximize the entropy by forming random coils. The real molecular structure and dynamics are the result of a compromise which includes a certain orientation of the main-chain segments and a slowing-down of the reorientation of the mesogenic director in external fields.

The particular purpose of the presented work is the obtaining of knowledge about the role of main-chain orientation and dynamic. As an object of the investigation the side-chain polysiloxanes was chosen. In the NMR group of Martin-Luther University Halle the first studies on the orientation behavior of side-chain polymers was started in 1994. A series of mesogenic polysiloxanes samples were investigated. The information about the ^{29}Si chemical shift (CS) tensor axis orientation was obtained. With this knowledge it becomes possible to calculate the orientation degrees of main chain segments. For the unambiguous interpretation of the results, however, the suggestion about the transversal isotropy/anisotropy of the molecular segments is required which can not be done using the one-dimensional information provided by axial-symmetrical CS spin interaction. In order to get the supplementary information about the main-chain segment orientation another type of orientationally depended (anisotropic) NMR interaction is required. Therefore, the angular dependence of direct dipolar interaction was used to probe the orientation distribution of the vector which connects two Si atoms in main chain. This vector coincides with the main-chain alignment direction.

However, in the case of ^{29}Si NMR the sufficient difficulties are foreseen due to the low natural abundance of observable spins (4.5%). This makes the probing of dipolar interaction rather problematic for two reasons: (i) the low natural abundance of ^{29}Si nuclei gives considerably low signal sensitivity and (ii) the low probability that two neighbored Si are both ^{29}Si leads to overwhelming part of the signal arisen from isolated ^{29}Si which overlaps the weak spin-pair signal of interest. To overcome these problems one needs to implement the special ^{29}Si NMR techniques and data processing/interpretation methods. The following goals were aimed and achieved in the presented work:

The special NMR technique called “ β -echo” was used for the selective detection of the NMR signal from the coupled ^{29}Si spin pairs, with simultaneous suppression of the signal from isolated spins.

The relation between the β -echo time evolution (β -function) and the dipolar interaction intensity was found using two-spin approximation. Further, the anisotropy of dipolar coupling gave us the relation between the β -function and the orientation of Si-Si vector. The influence of the orientation distribution function (ODF) of the Si-Si vectors on the β -function behavior was checked using (i) Model ODF's and (ii) “model-free” ODF's represented by Legendre series. The sensitivity of the β -function to the ODF parameters was tested by the computer simulations. The sensitivity of the β -function to the ODF parameters was improved by using its angular dependence. The special methods of the information extraction from the several β -functions have

been proposed to avoid the multiparametrical non-linear fitting. The linear regression methods are preferable in the case when more than one parameter needs to be found from fitting.

The selective analysis of the subspectra allows one using the one-parametrical fitting that makes the ω_{OD} evaluation procedure more transparent and precise. In our knowledge, the method of Fourier transformation and spectrum analysis has been never applied so far in combination with β -function.

The role of transversal NMR relaxation has been investigated in two aspects: (i) influence of transversal relaxation time T_2 on the β -function and (ii) using the transversal relaxation as a tool for the molecular dynamic study. The temperature dependence of the T_2 was measured in wide temperature range. Three characteristic temperature regions of the T_2 behavior have been found. The analysis of the relaxation data was done in the frame of Anderson-Weiss approach supposing the ^{29}Si CS tensor axis reorientation as the primary relaxation mechanism. It was found that the behaviour of the transversal relaxation at various temperatures can be explained by the strong, exponential and weak correlations of the molecular motion.

The experiments on polydomain sample of polysiloxane M4 have been done in order to estimate the dipolar coupling constant ω_{OD} . The obtained value of ω_{OD} was used to process the data of the experiments with monodomain samples. In addition, the ω_{OD} was used to determine the angle at oxygen atom in Si-O-Si bond. The obtained result is well agreed with the quantum chemistry calculations.

The experiments on orientation dependence of the β -function were done on two monodomain polysiloxanes with different spacer lengths (4 and 6 methylene units), denoted as M4 and M6. The parameters of the ODF Legendre expansion were extracted from the 3 characteristic β -function orientation dependences. The ODF reconstruction error does not exceed 10%. The preferable orientation of the main-chain segments in the M6 sample was found orthogonal to the local director (side-chain). Also, some difference was established between the orientation of main chain obtained by from ^{29}Si spectrum angular dependence and from the β -function.

The sufficient novelty of the presented work, by our knowledge, is the application of β -echo for the case of non-enriched, low-abundant spins as ^{29}Si in the case when weak bilinear anisotropic spin interaction are masked by presence of the strong linear ones. It can be concluded that β -echo is an effective method of the detection of the NMR signal of the spins coupled via homonuclear dipolar interaction with separation it from the signal of non-coupled ones. Most of the similar techniques are based on double quantum (DQ) filtering (INADEQUATE, C7, DRAMA, etc). The advantage of the β -echo is that a single quantum coherence is detected and, therefore, the DQ filter losses are avoided. Contrary to the most of DQ-methods the β -echo does not require the sample MAS rotation and can be applied for the ODF estimation using the sample reorientation with respect to magnetic field.

The simplicity of the β -echo pulse sequence allows a number of different extensions of the basic experimental technique. Particularly, the combination of the β -echo signal selection with the further detection of dipolar interaction by the Carr-Purcell echo trend was tested. However, this method faces with more experimental and theoretical problems which have to be solved before its application in practice.

Acknowledgements

At first, I would like to express my appreciation and gratefulness to the head of the NMR group professor doctor Horst Schneider for his inspiration throughout this work and also for very good general supervising and encouragement.

Equally, my great appreciation is extended to Dr. Günter Hempel for his invaluable help and splendid scientific supervising on all stages of the project, wealthy suggestions in order to succeed this work and critical reading of the manuscript of this thesis.

I wish to express my heartfelt gratitude to Dr. Detlef Reichert, Dr. Manfred Knörger, Dr. Heike Menge for giving me valuable advises and encouragement, and to Ms. Karin Novak for all her help throughout the work and for making a nice working and outworking environment.

I am indebted to Dr. H. Siebert (University Freiburg) for synthesis the samples of polysiloxanes.

Deutsche Forschungsgemeinschaft (DFG) is greatly acknowledged for the financial support of the project.

My special «thank you» is going also to my current chief professor doctor Dieter Höpfel (Fachhochschule Karlsruhe) for his patience and providing me a possibility to complete this work and his great encouragement on the final stage.

During my stay in Halle, I have benefited from my colleagues who are also graduate students. I wish to thank them individually but there are many to be all listed. However, my special deep appreciation I would like do address to my former colleague Dr. Piyasiri Ekanayake who became a real friend of mine and from whom I was getting the priceless help and support during all this time. Many thanks to Dr. Ovidiu Pascui for his help with soft and hardware and a number of interesting discussions. Many thanks to Mihaela Aluas, Andrea Moldovan, Stephan Körner for providing a nice company for the working and leisure time.

I take this space to express my indebtedness to my parents, brother and sister, who always urged, encouraged and supported me to achieve high goals and who taught me the value of hard work.

Last and the most important thanks must go to Alexandra, my wife, who patiently endured my frequent absence from home and, inspired and supported me in my scientific achievements, for her encouragement only with which this work is completed.

Erklärung

Ich erkläre hiermit, dass die Dissertation selbständig verfasst wurde und nur die angegebenen Hilfsmittel benutzt wurden. Die Dissertation wurde noch an keiner anderen Universität oder Hochschule eingereicht.

Maxim Terekhov,



Karlsruhe, Mai. 2003